NMR of solid phosphorus and nitrogen compounds.

Lawrence Hale Merwin

NMR OF SOLID PHOSPHORUS AND NITROGEN COMPOUNDS

by

Lawrence Hale Merwin

B.A. (*summa cum laude*), Hamline University (1978)

M.Sc., University of East Anglia (1980)

A thesis submitted for the degree of
Doctor of Philosophy
of the University of Durham
October 1987

MEMORANDUM

The research presented in this thesis has been carried out in the Department of Chemistry of the University of Durham between October 1984 and October 1987. It is the original work of the author unless stated otherwise. None of this work has been submitted for any other degree.

<u>NMR of Solid Phosphorus and Nitrogen Compounds</u>

by

Lawrence Hale Merwin

ABSTRACT

The main thrust of this work is the determination of solid structure using the technique of solid-state nuclear magnetic resonance spectroscopy.

High-resolution ^{31}P NMR spectra have been obtained for a number of solid diphosphine disulphides under conditions of cross-polarization, high-power proton decoupling and magic-angle rotation. The results yield crystallographic information about the size of the asymmetric unit and are consistent with data from X-ray diffraction when known. In one case, evidence of morphological variation is obtained. Shielding tensor information was extracted from magic-angle spinning spectra wherever possible. Attempts to correlate tensor data with structural parameters met with little success.

Fifty-one solid phosphonic, aminophosphonic and phosphinic acid compounds have been studied using high-resolution ^{13}C, ^{31}P, ^{15}N and ^{23}Na NMR spectroscopy via the techniques noted above. Again, results yielded crystallographic information about the size of the asymmetric unit. Agreement was found with the limited amount of crystallographic information available. Additionally, ^{1}H CRAMPS results provided chemical shift information on the hydrogen-bonded acid protons. Comparison of these data with oxygen-oxygen bond lengths from known diffraction studies indicates a possible correlation between the ^{1}H shift and the oxygen-oxygen bond distance. Shielding tensor data was determined from static and slow-spinning MAS spectra. One empirical correlation was found. The asymmetry parameter was related to structural factors.

A number of methods are currently used to determine the principal components of the shielding tensor from slow-speed magic-angle spinning experiments. Two of these are examined and their limitations discussed. A computer program to simulate and fit spinning sideband spectra is presented. The advantages and disadvantages of such a program are examined and several examples given.

A survey of the literature of solid-state nitrogen NMR is presented. The experimental considerations of natural abundance nitrogen-15 NMR are examined. The viability of running nitrogen-15 at natural abundance and with reasonable utilization of spectrometer resources is discussed.

ACKNOWLEDGEMENTS

First and foremost I must thank my advisor, Professor Robin K. Harris, for being my "once and future" supervisor. I consider one of the most significant changing points in my life to be the day in 1977 that Dr. Cliff Creswell encouraged me to write to Robin regarding a Fulbright Scholarship. I have never regretted writing that letter.

Next, my appreciation must be expressed to Geoff Nesbitt and Barry Say who, each in their own unique way, taught me a great deal about the experimental side of NMR. The information learned from them could never be found in any book; I thank them for the time that they spent and the patient answering of endless questions.

I have been most privileged to share my three years here in Durham with Pete Jackson and Phil Wilkes. I could not have asked for better companions or colleagues - thanks boys!

Thanks, too, must go to the past and present members of the NMR research group and to the members of staff "up the hill" at the UDIRL. The laughter and discussions - NMR and otherwise - were always appreciated.

I should like to express my gratitude to those who have provided samples for this work. Specific thanks must go to Professor Gerhard Hägele and the members of his research group for providing the vast majority of compounds studied in this thesis.

I would also like to gratefully acknowledge the receipt of a fellowship from the University of Durham and an ORS award from the Committee of Vice Chancellors and Principals of the Universities of the United Kingdom.

Last, but certainly not least, I would like to thank my family for their support and love during the course of this endeavour. Very, very special thanks must go to my wife, Linda, and daughter, Laura, for the patience and encouragement that made the completion of this task possible.

TABLE OF CONTENTS

To My Dad

CHAPTER ONE - INTRODUCTION

In the past ten to fifteen years, advances in the techniques, understanding and instrumentation of solid-state nuclear magnetic resonance (NMR) have provided the scientific community with a wealth of information previously unobtainable from solids. As will be seen, present-day methods provide near liquid-like spectra for a wide range of solid compounds. From such spectra, information regarding the overall structure of a solid may be deduced. Furthermore, with the use of homonuclear decoupling techniques, detailed studies of hydrogen bonding in solids may be carried out. Finally, as a result of the fact that the anisotropic nature of the NMR interactions is retained in a number of the solid-state experiments, properties such as the anisotropic shielding may be characterized.

The ultimate aim of the work in this thesis is the elucidation of solid structure via the use of the techniques of solid-state NMR. The goals of this work may, thus, be seen to fall into two rather broad areas. The first area is the application of solid-state NMR to chemical systems which were previously uncharacterized by such methods. Here one wishes to first demonstrate the applicability of the technique by comparison with previously determined structural data from, say, diffraction studies. At that point, determinations made solely from NMR data may be made where diffraction studies are unavailable. The second area involves the extension of solid-state NMR both in terms of methodology and scope. The extension is seen to have two aspects, the results of which will ultimately be to increase the amount of data from which the experimentalist may draw pertinent conclusions. Firstly, an improved method of data analysis is demonstrated. The use of computerized simulation and fitting is shown to circumvent certain difficulties in the present techniques used for the determination of the principal components in the shielding tensor. Secondly, expansion is shown in terms of the use of nitrogen-15 at natural abundance. This nucleus, though somewhat neglected in the literature because of its low sensitivity, was shown to be a reasonable nucleus to observe given the present state of NMR instrumentation.

In the next chapter the theory of NMR as it applies to the solid-state will be discussed. The anisotropic nature of the NMR interactions will be emphasised, and the use of tensors to describe such interactions will be noted. The two main averaging techniques used in this work will be examined.

In Chapter Three, experimental considerations will be discussed. The various pulse sequences and techniques will be described from a practical standpoint.

Chapter Four deals with the extraction of shielding tensor values from spinning sideband spectra. A number of current methods of determining the principal tensor components will be examined and their limitations discussed. A computer program to simulate and fit spinning sideband spectra will be presented. The advantages and disadvantages of such a program will be examined. This program will subsequently be used in the remaining chapters to analyse spinning sideband spectra and to determine shielding tensor components. Suggestions for advanced versions of this program are proposed.

In Chapter Five, solid-state NMR techniques are applied to the study of the diphosphine disulphide compounds. These compounds had previously been well characterized by solution-state NMR. A number of crystal structures are known. The purpose of the present study was to compare the results obtained from solid-state and solution-state spectra and to determine the applicability of the former specifically with regard to solid structure.

The aim of Chapter Six is to extend the knowledge gained in the above study to a series of phosphonic, aminophosphonic and phosphinic acids. ^{13}C, ^{15}N, ^{23}Na and ^{31}P solid-state NMR are used to characterize the solid structure of these compounds. ^{1}H CRAMPS methods are used in an attempt to characterize the hydrogen-bonding structure in these acids.

Finally, the natural abundance nitrogen-15 NMR of solids is discussed in Chapter Seven. A survey of the solid-state nitrogen NMR literature is presented. Following this, the experimental considerations of nitrogen-15 NMR are examined. After a number of difficulties, the possibility of doing nitrogen-15 at natural abundance and with reasonable utilization of spectrometer resources is demonstrated.

CHAPTER TWO - SOLID-STATE NMR THEORY

2.1 Introduction

Anisotropy is defined[1] as "describing a property of a substance when that property depends on direction as revealed by measurement". In the study of NMR, the properties which govern the interactions of nuclear magnetic moments are all, in principle, anisotropic in nature. Furthermore, it is this fundamental fact of anisotropy which is the significant and overriding difference between nuclear magnetic resonance studies in the solution- and solid-state. In non-viscous solutions, the interactions are averaged by random, isotropic translational and rotational motion. The effect of such averaging may either be to remove the interaction as in the case of the direct dipole-dipole coupling, or to give an isotropic average as in the case of the very useful properties of the chemical shift and the indirect (scalar) coupling. These averaging processes have allowed the experimentalist to resolve the fine structure of solution-state spectra and are, in part, responsible for the success of NMR as an analytical tool. An additional consequence of the isotropic averaging process, however, is that the basic anisotropic nature of the interactions is lost with a concomitant decrease in information content. In contrast to the solution-state case, the NMR spectrum of a non-mobile solid is dominated by anisotropic interactions. The unfortunate effect of such dominance is to produce spectra of solid powders which are often of the order of tens of kHz wide and which show no fine structure whatsoever. In essence, the anisotropic nature of the information has been regained, but the informative fine structure evident in the solution-state spectrum has been lost in the process. The goal of solid-state NMR spectroscopy is, thus, to selectively remove or coherently average those anisotropic interactions which prevent such fine structure from being resolved, while at the same time leaving as much information as possible regarding the essential anisotropy of the remaining interactions of interest.

In discussing the interactions and the methods by which they might be averaged or removed, it is useful to subdivide the spins involved into the classes of "abundant" and "dilute". Abundant spins are those, such as ^{1}H and ^{19}F, which are present at 100% natural abundance. As one might expect, the spectra of these spins are dominated by coupling to other abundant spins. An example of a dilute spin is ^{13}C, which has a natural abundance of only 1.1%. Spectra of these nuclei are dominated by coupling to the abundant spins. Interactions between two dilute nuclei are generally weak because the chances of having more than one such nucleus in a particular molecule are small. For the case of nuclei such as ^{31}P, it is important to point out that an intermediate situation is found. While ^{31}P may be considered as abundant in terms of its isotopic constitution (100%), for the majority of the compounds in this thesis, it may be seen to be dilute in the sense of the overall populations of spins and the distance separating the individual phosphorus atoms. Considering specific chemical systems, it will be noted that the diphosphine disulphides are a marginal case in that there are direct P-P bonds. The phosphonic and phosphinic acids, on the other hand, are clearly a dilute case. Phosphorus-31 spectra may be obtained for both systems in the same manner as other dilute-spin nuclei, such as carbon-13, but also may contain information such as P-P scalar coupling which would not be evident for ^{13}C for the reason noted above. In the paragraphs below, phosphorus should be considered as a dilute spin unless otherwise noted.

For the work covered in this thesis, there are three methods of averaging which are used to narrow the solid-state spectra and reveal the information of interest. These methods are:

a) Heteronuclear, high-power, dipolar decoupling of the abundant spins (^{1}H). This technique is analogous to the decoupling technique used in solution-state NMR spectroscopy, though, of course, much higher power levels are required. It will remove the effects of heteronuclear (e.g ^{1}H-^{31}P) dipolar and scalar coupling.

b) Magic-angle spinning (MAS). As will be shown, macroscopic rotation of a powder sample about an axis oriented at 54° 44' to the B_o field will remove homonuclear, dilute-spin, dipolar coupling. It will also average the anisotropic chemical shielding to its isotropic value. It will be seen in Chapter 4 that under certain conditions this averaging will not be complete. In such cases, it is in principle possible to recover the principal components of the tensor which describes the anisotropic character of the chemical shielding.

c) Multiple-pulse techniques. For observing systems of abundant spins (i.e. ^1H) with large homonuclear dipolar couplings, it is clear that high-power decoupling methods are inappropriate. Further, although it is theoretically possible to remove these interactions with the use of magic-angle spinning, in practice this is not possible because of limitations in the rotation rates of current spinning systems. The homonuclear dipolar interaction may be as large as 40 kHz in some systems, while commonly available rotor systems can only achieve speeds of ca. 5 kHz. As the spinning speed must be of the order of the static bandwidth for a homogeneously broadened case (*vide infra*), it is evident that MAS will not be sufficient to obtain narrowing. Multiple-pulse techniques have been developed such that a series of pulses of differing phases act on the system of interest. In certain windows in the sequence, the magnetization behaves as if the effect of the homonuclear dipolar coupling were zero. The spectrum, at this point, will still be influenced by the anisotropic chemical shielding. If both MAS and multiple-pulse techniques are used simultaneously, the isotropic chemical shifts may be obtained directly from the spectrum.

In the following sections, the Hamiltonians affecting the NMR spectra of solids and methods of coherent averaging will be discussed. As stated above, the interactions represented by these Hamiltonians are all anisotropic in nature and, as such, they are represented by second-rank Cartesian tensors (except for the Zeeman and radio-frequency terms). In this text, tensors will be represented in bold type and underlined: $\underline{\boldsymbol{\sigma}}$; vector properties will be in bold type: $\mathbf{r}$; and operators will be indicated by circumflex: $\hat{H}$.

At this point, it will be useful to make a few comments regarding the tensors and the tensor representation of the interactions which they represent. First of all, a tensor may be defined as a matrix which relates two vectors. In the case of the NMR properties discussed here, the tensor is a 3×3 matrix or, more formally, a second-rank tensor. Now, as each of the internal Hamiltonians noted below results from a bilinear coupling of two vectors, they may all be represented by a purely general equation. (See, for example, Harris[2] or Haeberlen[3].) For a particular interaction, λ, the Hamiltonian may be represented:

$$\hbar^{-1}\hat{H}_\lambda = k_\lambda \mathbf{I}\cdot\underline{\mathbf{G}}_\lambda\cdot\mathbf{P}_\lambda \ ,$$

where $\underline{\mathbf{G}}_\lambda$ is the tensor describing the interaction, k_λ represents any constants associated with $\underline{\mathbf{G}}_\lambda$, $\mathbf{I}$ represents the nuclear spin and $\mathbf{P}_\lambda$ represents the vector property to which the spin is related. Tabulations of the $\underline{\mathbf{G}}_\lambda$, k_λ and $\mathbf{P}_\lambda$ may be found in the references noted directly above. To give an example, the shielding tensor Hamiltonian may be represented:

$$\hbar^{-1}\hat{H}_{CS} = \gamma\mathbf{I}\cdot\underline{\sigma}\cdot\mathbf{B}_o \ ,$$

where γ is the constant involved for the shielding tensor $\underline{\sigma}$, which relates the nuclear spin to the static magnetic field $\mathbf{B}_o$.

Now, given a suitable axis system in the molecule-fixed frame, the tensor may be put into a diagonal form:

$$\underline{\mathbf{R}} = \begin{matrix} R_{XX} & 0 & 0 \\ 0 & R_{YY} & 0 \\ 0 & 0 & R_{ZZ} \end{matrix}$$

This axis system is referred to as the principal axis system (PAS). The values of the diagonal components are known as the principal components of the tensor $\underline{\mathbf{R}}$.

Given this diagonal tensor, it is useful to define three additional properties which serve to further describe it. These three properties are the trace, the anisotropy and the asymmetry.

The trace of the tensor $\underline{\mathbf{R}}$ is defined as follows:

$$\mathrm{Tr}\underline{\mathbf{R}} = R_{XX} + R_{YY} + R_{ZZ}.$$

One of the properties of the trace of a tensor is that it is invariant to rotation of the reference frame. In fact, the quantity $1/3\mathrm{Tr}\underline{\mathbf{R}}$ is the isotropic average which is given the symbol $\bar{R}$. This is observed in solution for such interactions as the chemical shift and scalar coupling constant. It should be noted that both the dipolar and quadrupolar interactions are traceless and, thus, not observed directly for mobile liquids.

The second quantity which may be defined is that of the anisotropy, δ. (This should not be confused with the chemical shift symbol, which is given in this thesis as subscripted with the nucleus of interest, i.e. δ_P.) There are a number of definitions for the anisotropy. In this text, the definition of Haeberlen[3] will be used:

$$\delta = R_{ZZ} - 1/3\mathrm{Tr}\underline{\mathbf{R}}$$

In making this definition, it is assumed that R_{ZZ} is one of the extreme components. As such, a definition of the relative magnitude of the principal components is required. There are several conventions for this as well. Again following Haeberlen[3], the axes are labelled so that:

$$|R_{ZZ} - 1/3\mathrm{Tr}\underline{\mathbf{R}}| \geq |R_{XX} - 1/3\mathrm{Tr}\underline{\mathbf{R}}| \geq |R_{YY} - 1/3\mathrm{Tr}\underline{\mathbf{R}}| \ .$$

Finally, the asymmetry, η, is defined by the equation:

$$\eta = (R_{YY} - R_{XX})/\delta \ .$$

Given the above definitions, the value of η may lie between 0 and 1. For $\eta = 1$, the tensor is completely asymmetric (i.e. R_{YY} is midway between R_{XX} and R_{ZZ}), while for $\eta = 0$ the tensor is axially symmetric (i.e. $R_{XX} = R_{YY}$). The dipolar interaction, for example, is by nature axially symmetric about the distance vector which connects the two interacting dipoles.

Further aspects of the trace, anisotropy and asymmetry are revealed in Chapter 4, where they are explicitly used to describe the shielding tensor.

The discussion of the Hamiltonians and their associated tensors in this thesis is, of course, severely limited. The reader is referred to the monographs by Abragam[4], Haeberlen[3], Mehring[5], Slichter[6], and Gerstein and Dybowski[7] for rigorous treatments of the material in this chapter.

2.2 Nuclear Spin Hamiltonian

The nuclear spin Hamiltonian which describes the behaviour of a nuclear magnetic moment may be expressed as a sum of the Hamiltonians for a number of interactions. These interactions represent the coupling of the nuclear spin with physical features that are either integral to the solid system of which the spin is part or externally applied by the experimentalist. The Hamiltonian may be tabulated as:

$\hbar\hat{H} = \hbar\hat{H}_Z$ Zeeman
$+\hbar\hat{H}_{RF}$ Radio Frequency
$+\hbar\hat{H}_{CS}$ Chemical Shielding
$+\hbar\hat{H}_{SR}$ Spin Rotation
$+\hbar\hat{H}_Q$ Quadrupolar
$+\hbar\hat{H}_D$ Dipolar (direct) Spin-Spin Coupling
$+\hbar\hat{H}_J$ Indirect (scalar) Spin-Spin Coupling

Several of these Hamiltonians have little relevance to the work in this thesis and will not be discussed in detail. The Zeeman and radio frequency terms characterize the coupling of the nuclear spin to the externally applied static and radio frequency (RF) magnetic fields respectively. These so called "external" Hamiltonians allow the experiment to be performed but do not give information of molecular importance. The remaining Hamiltonians describe the interactions in the molecular framework and are, thus, referred to as "internal". The quadrupolar term describes the interaction of the nuclear spin with the electric field gradient for nuclei with spin > 1/2. There is no detailed work on quadrupolar nuclei in this thesis. The spin-rotation relationship defines the interaction of the nuclear spin with the magnetic moment associated with the overall angular momentum of the molecule. This interaction is quite weak and may be neglected for solids.

The remaining internal Hamiltonians are those which characterize the chemical shift and the direct (dipolar) and indirect (scalar) coupling. Each of these will be discussed in some detail.

2.3 The Dipolar Interaction

Between nuclear magnets there is a direct, through-space interaction which is analogous to the case of two macroscopic bar magnets. The energy, U, of this interaction may be given classically for two magnetic point dipoles $\boldsymbol{\mu}_1$ and $\boldsymbol{\mu}_2$ separated by a distance represented by the vector $\mathbf{r}$:

$$U = \left\{\frac{\boldsymbol{\mu}_1 \cdot \boldsymbol{\mu}_2}{r^3} - \frac{3(\boldsymbol{\mu}_1 \cdot \mathbf{r})(\boldsymbol{\mu}_2 \cdot \mathbf{r})}{r^5}\right\} \frac{\mu_o}{4\pi} ,$$

where μ_o is the permeability constant ($4\pi \times 10^{-7}$ kg m s^{-2} A^{-2}). The equation may be obtained in quantum mechanical form by substituting $\boldsymbol{\mu} = \gamma\hbar\hat{\mathbf{I}}$:

$$\hat{H}_D = \gamma_1 \gamma_2 \hbar^2 \left\{\frac{\hat{\mathbf{I}}_1 \cdot \hat{\mathbf{I}}_2}{r^3} - \frac{3(\hat{\mathbf{I}}_1 \cdot \mathbf{r})(\hat{\mathbf{I}}_2 \cdot \mathbf{r})}{r^5}\right\} \frac{\mu_o}{4\pi} ,$$

where γ_1 and γ_2 are the magnetogyric ratios of nuclei 1 and 2, and $\hbar$ is Planck's constant over 2π. It is usual[4] to expand this expression in terms of polar coordinates, giving the familiar alphabet expansion:

$$\hat{H}_D = r^{-3}\gamma_1\gamma_2\hbar^2[A + B + C + D + E + F](\mu_o/4\pi)$$

$$A = -\hat{I}_{1z}\hat{I}_{2z}(3\cos^2\theta - 1)$$

$$B = 1/4[\hat{I}_{1+}\hat{I}_{2-} + \hat{I}_{1-}\hat{I}_{2+}](3\cos^2\theta - 1)$$

$$C = -3/2[\hat{I}_{1z}\hat{I}_{2+} + \hat{I}_{1+}\hat{I}_{2z}](\sin\theta\ \cos\theta\ \exp(-i\phi))$$

$$D = -3/2[\hat{I}_{1z}\hat{I}_{2-} + \hat{I}_{1-}\hat{I}_{2z}](\sin\theta\ \cos\theta\ \exp(-i\phi))$$

$$E = -3/4[\hat{I}_{1+}\hat{I}_{2+}](\sin^2\theta\exp(-2i\phi))$$

$$F = -3/4[\hat{I}_{1-}\hat{I}_{2-}](\sin^2\theta\exp(2i\phi))$$

where θ represents the angle that the internuclear vector **r** makes with static magnetic field.

From this form of expansion, it is clear that each of the terms contains a spin part in square brackets and a geometrical part in parenthesis. This will become important when averaging techniques are discussed (*vide infra*). For the present, it is important to note that not all of the terms in the expansion need be considered. Those terms which are significant may be determined by examination of the effect of a particular term on the spin states.

The A term has essentially the form of two interacting dipoles and does not result in any spin transitions. Its overall effect is a small perturbation on the Zeeman levels. The B term, which is an energy-conserving transition for a pair of like spins (only), will be seen to allow the simultaneous reversal of two spins in opposite directions - the "flip-flop" transition. The term must be retained for homonuclear transitions but not for heteronuclear transitions, as the Zeeman energy of the $\alpha\beta$ and $\beta\alpha$ states in this latter case differ. The C and D terms alter one spin only. The E and F terms alter both spins up or both spins down simultaneously resulting in a double quantum transition. The effect of the last four terms, C, D, E and F is sufficiently small that there is no contribution to the energies of the states in first order.

Noting that the B term only contributes for homonuclear cases, the truncated secular dipolar Hamiltonian for unlike spins is given by:

$$\hat{H}_D = -\hbar^2(\mu_o/4\pi)\gamma_1\gamma_2 r^{-3}(3\cos^2\theta - 1)[\hat{I}_{1z}\hat{I}_{2z}] .$$

For like spins, the B term must be included, thus the equation is given by:

$$\hat{H}_D = -\hbar^2(\mu_o/4\pi)\gamma_1\gamma_2 r^{-3}(3\cos^2\theta - 1)[\hat{I}_{1z}\hat{I}_{2z} - 1/4(\hat{I}_{1+}\hat{I}_{2-} + \hat{I}_{1-}\hat{I}_{2+})].$$

In the discussion of the dipolar interaction, there is one very important point which must be understood. Although for simplicity's sake the interaction has been described for two isolated dipoles, the dipolar Hamiltonian in principle links each nucleus to all other nuclei in the sample which have magnetic moments. Using the shorthand notation described above, the dipolar Hamiltonian for a complete sample is given as:

$$\hbar^{-1}\hat{H} = \sum_{i<k} [\hbar(\mu_o/4\pi)\gamma_i\gamma_k r^{-3}]\ I_i\cdot\underline{D}^{ik}\cdot I_k$$

where i and k represent all pairs of nuclei in the sample and the inequality implies that each pair is only considered once. The resonances which arise from homonuclear interaction of this type are referred to as being homogeneously broadened.

For clarity, it is useful at this point to also define inhomogeneous broadening. For a nucleus which has, for example, chemical shielding (*vide infra*) as its dominant interaction, the powder spectrum is broad because each nucleus with a different orientation will have a slightly different resonance frequency. That is to say, the line arising from any specific nucleus will be sharp, but the whole resonance will be broad because it will be a superposition of all of these sharp resonances. Such a powder spectrum is said to be inhomogeneously broadened.

The significance of homogeneous versus inhomogeneous broadening may be found in comparing the speed of the averaging processes required to narrow a specific interaction. Quite straightforwardly, the averaging must be performed at a rate faster than that which the interaction can significantly change the system[7]. This rate is generally taken to be the inverse of the inherent linewidth from the interaction of interest. (Another way of expressing this is to say that the averaging must take place at a speed that is of the order of the inherent linewidth expressed in Hz.) For inhomogeneously broadened systems, the averaging may be slow compared to the overall bandwidth because it need only be fast compared to the inherent (sharp) linewidth of a single nucleus. This is the basis for the spinning sideband analysis methods described in Chapter 4. For homogeneously broadened systems, the situation is quite different. As will be seen from the equation above, the linewidth of each individual spin will be the linewidth of the whole spectrum. The averaging process in this case, <u>must</u> be of the order of the full static bandwidth. As this may be of the order of ca. 40 kHz for abundant protons, it is clear that a very fast averaging process is required.

2.4 Indirect Spin-Spin Coupling

The next internal Hamiltonian to consider is that for the indirect spin-spin coupling, which is also known as the scalar or J coupling. This describes the coupling of nuclear magnetic moments which is transmitted via the electrons of the molecular system, as opposed to direct coupling of the magnetic dipoles which is the mechanism for the dipolar interaction.

The full Hamiltonian which describes indirect spin-spin coupling is rather complex. It must contain several terms, as coupling involving electrons takes place via a number of interactions. In general, terms are required which describe: a) the dipolar interaction between the electrons and the nuclear spins; b) the interaction between the magnetic moments which arise from the electron orbital motion and the nuclear spin; and c) the Fermi contact term, which characterizes the electron-nucleus interaction when the electron is in the same region of space as the nucleus. The final term is required because calculation of (b) requires point dipoles and, therefore, fails as the electron-nucleus distance approaches zero. For the purposes of this thesis, however, it is not necessary to write out the full Hamiltonian. Rather, the shorthand description will suffice to illustrate the significant points. If $\underline{J}$ is the indirect coupling tensor, the Hamiltonian will have the form:

$$\hbar \hat{H}_J = \hbar \sum_{i<k} I_i \cdot \underline{J}^{ik} \cdot I_k$$

It will be seen immediately that the Hamiltonian is of identical form to that of the dipolar interaction, that is, a bilinear interaction of two spins. Only these two Hamiltonians are two-spin; all of the other internal Hamiltonians involve only a single spin. As will be seen, similarity in form will imply some similarity in action.

Considering the form of the interaction, several important points may be made. Firstly, the fact that the coupling is bilinear between spins indicates that scalar coupling may be an additional source of homogeneous broadening in solids. This coupling, which is no larger than ca. 150 Hz for compounds in this study, is quite small compared with the dipolar or chemical shielding interactions. However, Maricq and Waugh[8] have pointed out that where there is simultaneous occurrence of chemical shifts and dipolar coupling in an isolated pair of like spins, they may behave homogeneously. The main effect of this on the spectrum will be that the spinning sidebands in a MAS spectrum may not all be of the same shape. This is a direct result of the fact that the principal axis systems of the various interactions will have differing orientations in the molecular frame. It is pointed out that if there is a centre of inversion symmetry, the shift difference between the two nuclei will disappear because the shielding tensors will have the same orientation. In such a case, the system may be treated as inhomogeneous. This discussion will be seen to be especially relevant to the work in Chapter 5.

Secondly, similarity in form between the dipolar and scalar coupling implies that they will behave similarly under the processes which cause averaging. The implication, of course, is that any process which averages the dipolar interaction will also average any scalar coupling which may be present. This is certainly true for the isotropic motional processes in solution, and the same holds true for both magic-angle spinning and multiple pulse techniques. In solids, where the full tensorial nature of the interaction is realized, it should be pointed out that the averaging process is identical only for the anisotropic portion to the tensors of the two interactions. For scalar coupling, the averaging results in an isotropic value which is the trace of the tensor. In contrast, the isotropic part of the dipolar tensor does not exist, as the interaction is traceless. In addition, the dipolar interaction is axially symmetric whereas in general $\underline{J}$ is not.

2.5 The Shielding Hamiltonian

The next Hamiltonian of interest characterizes the chemical shift. The source of this shift is the shielding of the nucleus by the magnetic field resulting from the orbital motion of the surrounding electrons.

For a sample placed in a static magnetic field, B_o, a given nucleus, i, will experience a magnetic field, B_i, which is given by:

$$B_i = (\underline{1} - \underline{\sigma}_i)B_o \quad .$$

$\underline{\sigma}_i$ is the shielding tensor for the i^{th} spin. The fact that $\underline{\sigma}$ is a tensor is a direct result of the three dimensional nature of the electron density surrounding the nucleus. Further, it implies that the resonance frequency of the nucleus will depend on its orientation in the static magnetic field. As a result, powder patterns which arise from shielding anisotropy are inhomogeneously broadened.

This tensor, like all of the other internal interaction tensors, may be written in the diagonal form discussed in the introduction. In the PAS, the three tensor components are σ_{XX}, σ_{YY} and σ_{ZZ}. In the axially symmetric case, $\sigma_{XX} = \sigma_{YY}$, while for the completely asymmetric instance, all three components are required to describe the shielding.

In the shorthand form, the Hamiltonian may be written:

$$\hbar\hat{H}_{CS} = \hbar\sum_{i} \gamma_i \ \mathbf{I}_i\cdot\underline{\sigma}_i\cdot\mathbf{B}_o \quad .$$

The expansion of this Hamiltonian in a form which describes its behaviour under magic-angle spinning is detailed in Chapter 4. From the equations in that chapter, however, it is clear that the Hamiltonian has an isotropic part which is invariant to rotation, and an anisotropic part which gives rise to spinning sidebands in the MAS experiment. The isotropic part, $\bar{\sigma} = TR\underline{\sigma}/3$, is the shielding observed in solution.

2.6 Averaging Techniques in Solid-state NMR

In non-viscous liquids, the averaging of the interactions discussed above (and others) takes place through the random thermal motion of the molecules. In general, solution-state spectra with a great deal of fine structure may be obtained. Such spectra reveal important chemical shift and scalar coupling information. For the case of non-mobile solids, however, there are usually no isotropic averaging processes present. In order to obtain spectra of powdered solids which approach the resolution of solution-state spectra, averaging techniques must be applied by the spectroscopist. Two such techniques will be discussed here.

2.6.a Magic-Angle Rotation

The use of rapid macroscopic sample rotation in the NMR investigation of dipolar broadened solids was introduced by Andrew, Bradbury and Eades[9] in 1958. It was further recognised independently by both Andrew[10] and Lowe[11] that spinning the sample with the axis of rotation inclined at $\cos^{-1}(1/\sqrt{3})$ (54° 44') - the "magic" angle - to the static magnetic field would reduce dipole-dipole interactions to zero. Subsequently, Andrew and Eades[12] showed that magic-angle spinning (MAS) would also remove the broadening effects of the anisotropy in the shielding.

The theory of magic-angle spinning is most clearly seen if one examines the case of the dipolar interaction. It will be noted by inspection of the truncated dipolar Hamiltonians that both depend on the geometric term $(3\cos^2\theta - 1)$, where θ is the angle that the internuclear distance makes with the static magnetic field. Now, while it is clear that orienting a single spin-pair at the correct angle will result in the removal of the dipolar interaction, it is not immediately evident why this should work for a powder in which all values of θ are possible.

Given a powder which is rotated at an angle, β, to the static magnetic field, it is necessary to characterize the behaviour of the internuclear vector, $\mathbf{r}$, which will sweep out a conical path as the sample spins. Two other angles are necessary to characterize the situation: χ, the angle which the internuclear vector makes with the rotor axis and θ, the angle which the internuclear vector makes with the B_o field. It can be shown[2] that the average of the term $(3\cos^2\theta - 1)$ is given by:

$$\langle 3\cos^2\theta - 1\rangle = 1/2(3\cos^2\beta - 1)(3\cos^2\chi - 1)$$

It will be noted that the angles θ and χ will take on all possible values for a powder while, importantly, the angle β is under the control of the experimentalist. It is clear from the equation that if the angle $\beta = 54° 44'$ ($\cos^{-1}(1/\sqrt{3})$), the right side of the equality will be zero, and therefore, that $\langle 3\cos^2\theta - 1 \rangle$ will be zero for all initial vector orientations. Thus, the dipolar interaction will be removed for powdered samples. A similar argument may be made for the shielding as will be seen in Chapter 4.

It will be noted that in practice, generally attainable MAS speeds have an upper limit of ca. 5 kHz, though, recently, commercial probes capable of up to 15 kHz have been introduced. While such speeds are generally sufficient to average inhomogeneously broadened systems, homogeneously broadened spectra may be of the order of several tens of kHz and, thus, will not be averaged by magic-angle spinning. The reasons for this were discussed in section 2.3. The solution to this for the case of dilute spins, such as ^{13}C and ^{31}P, is the combined use of high-power proton decoupling and magic angle spinning[13] as described in the introduction to this chaper and in Chapter 3. For abundant spins, multiple-pulse techniques are required.

2.6.b Multiple-Pulse Techniques

As was pointed out in the introduction to this chapter, it is clear that high-power decoupling methods are inappropriate for the observation of systems of abundant spins (i.e. ^1H) which are broadened by large homonuclear dipolar couplings. Additionally, although it is theoretically possible to remove these interactions with the use of magic-angle spinning, as noted above, in practice this is not feasible because of limitations in the rates which current spinning systems can attain. To overcome these difficulties, a method of line narrowing was developed such that a series of pulses of differing phases act on the system of interest. In certain windows in the sequence, the magnetization behaves as if the effect of the homonuclear dipolar coupling were zero. Such methods are referred to generally as multiple-pulse techniques.

In discussing the theoretical basis for this method, it is useful to begin by examining the four-pulse cycle of Waugh, Huber and Haeberlen[14], generally known as the WAHUHA sequence after the initials of its developers. This cycle, which may be described by:

$$[\ 90^{\circ}_{x'} - 2\tau - 90^{\circ}_{-x'} - \tau - 90^{\circ}_{y'} - 2\tau - 90^{\circ}_{-y'} - \tau -\ ]$$

was the first successful multiple pulse sequence and is also the simplest.

Given that the magnetization **M** in the rotating frame is initially in the z' direction, the first pulse of the WAHUHA sequence will rotate **M** to the y' axis. After a period of 2τ, the second pulse will rotate **M** back to the z' axis where it will remain for a period τ. The third and fourth pulses will result in **M** remaining in the x' direction for 2τ and then being rotated back into the z' direction. After one complete cycle, **M** is again in the z' direction and has spent one third of the total time aligned along each of the three axes. This last statement has as an assumption the fact that the pulse times are negligibly short compared to τ. Furthermore, the time for the complete cycle (6τ) must be short for two reasons. Firstly, the time of the cycle must be significantly shorter than the spin-spin relaxation time, T_2, so as to avoid having the magnetization decay away during the experiment. Secondly, as was stated above, the averaging mechanism must take place at a rate faster than the interaction that one wishes to average. As linewidths for homogeneously broadened systems may be of the order of 40 kHz, cycle times of the order of 25 μs are generally required.

Now that the sequence has been described and some of its relevant properties noted, the mode of action may now be described. For this purpose, it is useful to rewrite the dipolar Hamiltonian in a way which emphasizes the geometrical and spin components. Given two point dipoles, $\boldsymbol{\mu}_i$ and $\boldsymbol{\mu}_j$, connected by an internuclear vector, **r**, which is inclined at an angle, θ, to the static magnetic field, the Hamiltonian may be written:[15]

$$\hat{H} = 2r^{-3}(3\cos^2\theta-1)[\boldsymbol{\mu}_i\cdot\boldsymbol{\mu}_j\ -3(\mu_z)_i(\mu_z)_j].$$

It is the effect of the pulse sequence on the spin term in square brackets that is of interest in this discussion. First of all, since $\boldsymbol{\mu}_i\cdot\boldsymbol{\mu}_j$ depends only on the relative orientation of the two dipoles, this term is invariant to any rotations of **M**. However, as the second term in the square brackets depends on the z component of μ, it must be averaged over the three orientations. As noted above, in the WAHUHA pulse sequence, **M** spends equal times along the x', y' and z' axes. The average is thus:

$$\langle(\mu_z)_i(\mu_z)_j\rangle = 1/3\{(\mu_{x'})_i(\mu_{x'})j + (\mu_{y'})_i(\mu_{y'})j + (\mu_{z'})_i(\mu_{z'})j\}$$

which is $= 1/3\{\boldsymbol{\mu}_i\cdot\boldsymbol{\mu}_j\}$

by definition of the scalar product. By insertion of this into the above Hamiltonian, the term in square brackets will be seen to be zero. Under such conditions, the dipolar Hamiltonian will average to zero. Although this explanation is at a rather naive level, it does provide a useful description of the effect of the WAHUHA sequence.

In practice, a series of cycles is used with single point sampling at an appropriate place in the cycle (usually while the magnetization is along the x' axis). A Fourier transform of the signal measured in successive cycles produces the usual frequency domain spectrum. It should be noted that although the signal decays with time, the T_2 constraint noted above becomes less important as this relaxation mechanism no longer includes the effects of the dipolar interaction.

Since the development of the WAHUHA sequence, a number of longer multiple-pulse sequences have been devised. These generally are used in order to reduce the effects of B_1 inhomogeneity and pulse-angle and timing errors. The latter can be a major source of error in the multiple-pulse type of experiments. In this work, the eight-pulse MREV-8 sequence[16] described in Chapter 3 was used.

Multiple-pulse sequences affect other internal interactions as well. The chemical shift, chemical shift anisotropy and heteronuclear scalar coupling are scaled by a factor which depends on the pulse sequence used. For the WAHUHA sequence, this scaling factor is approximately $1/\sqrt{3}$. Homonuclear scalar couplings are unaffected.

As the multiple-pulse sequence does not completely average the chemical shift anisotropy, the use of such sequences alone will not generally result in spectra in which the lines of chemically different species may be resolved. If, however, both multiple-pulse and magic angle methods are used simultaneously, the isotropic chemical shifts may be obtained directly from the spectrum. This technique, developed particularly by Gerstein and co-workers[17], has been given the mnemonic CRAMPS - combined rotation and multiple pulse spectroscopy. CRAMPS has a number of limitations to the resolution which it may yield; however, its overall usefulness in the examination of hydrogen-bonded protons will be shown in Chapter 6.

For a detailed description of multiple-pulse and CRAMPS techniques, the reader is referred to the monographs by Haeberlen[3] and Gerstein and Dybowski[7].

References

1. T. Collcott, Ed., "Dictionary of Science and Technology", W. & R. Chambers Ltd., Edinburgh (1971).

2. R.K. Harris, "Nuclear Magnetic Resonance Spectroscopy", Pitman Books Limited, London (1983).

3. U. Haeberlen, "High-resolution NMR in Solids: Selective Averaging", Academic Press, New York (1976).

4. A. Abragam, "The Principles of Nuclear Magnetism", Oxford University Press, Oxford (1961).

5. M. Mehring, "High-resolution NMR Spectroscopy in Solids", Springer-Verlag, Heidelberg (1976).

6. C.P. Slichter, "Principles of Magnetic Resonance", Springer-Verlag, Heidelberg (1980).

7. B.C. Gerstein and C.R. Dybowski, "Transient Techniques in NMR of Solids: An Introduction to Theory and Practice", Academic Press, Inc., New York (1985).

8. M.M. Maricq and J.S. Waugh, *J. Chem. Phys.* **70**, 3300 (1979).

9. E.R. Andrew, A. Bradbury and R.G. Eades, *Nature, London* **182**, 1659 (1958).

10. E.R. Andrew, *Arch. Sci., (Geneva)* **12**, 103 (1959).

11. I.J. Lowe, *Phys. Rev. Lett.* 2, 285 (1959).

12. E.R. Andrew and R.G. Eades, *Disc. Faraday Soc.* **34**, 38 (1962).

13. J. Schaefer and E.O. Stejskal, *J. Amer. Chem. Soc.* **98**, 1031 (1976).

14. J.S. Waugh, L.M. Huber and U. Haeberlen, *Phys. Rev. Lett.* **20**, 180 (1968).

15. T.C. Farrar and E.D. Becker, "Pulse and Fourier Transform NMR", Academic Press, New York (1971).

16. P. Mansfield, *J. Phys. C* **4**, 1444 (1971); W.K. Rhim, D.D. Elleman and R.W. Vaughan, *J. Chem. Phys.* **58**, 1772 (1973).

17. L.M. Ryan, R.E. Taylor, A.J. Paff and B.C. Gerstein, *Chem. Phys Lett.* **72**, 508 (1980).

CHAPTER THREE - EXPERIMENTAL CONSIDERATIONS

3.1 Spectrometer Systems

3.1.a Bruker CXP-200

The spectrometer used for the vast majority of the work in this thesis was a Bruker CXP-200. This instrument was equipped with an Aspect 2000 computer system and a 4.7 Tesla, super-conducting, wide bore magnet. The details of the CXP-200 have been well documented[1]. For all nuclei, except ^{1}H, dual channel probes of Bruker construction were used. Several aspects of these probes are discussed below. For ^{1}H CRAMPS work, a modified single-channel probe[2] was used.

It is important to note that during the course of this work two different sets of dual-channel CP/MAS probes were used. The spectra of the diphosphine disulphides were run using older probes which had Andrew-Beams[3] spinning systems; all of the later work (Chapters 5, 6 and 7) was done using newer, double-bearing[4] MAS probes.

There are several factors which the experimentalist must keep in mind here. Firstly, the Andrew-beams construction is generally less stable both in terms of angle and spinning speed than the double bearing system. This means that one must look very carefully at any spectra run with this system before doing sideband analysis. Unstable spinning will lead to greater linewidth in the spinning sidebands compared to the centreband. If this is the case, when measuring the intensity for sideband analysis, one must use integrated intensity rather than peak height. Additionally, because of the construction of the Andrew-Beams probes, the stator must be removed every time the sample is changed. As a result, it was necessary to set the angle for each sample. Moreover, the angle must be re-adjusted if the spinning speed is changed, even for the same sample. A small amount of KBr (*vide infra*) was included in the rotor for the purpose of accurately setting the angle.

The double-bearing (DB) probes provided a much more stable spinning system. As it is not necessary to move the stator to change samples, the angle remains fixed and was found not to vary to any detectable extent when checked on a daily basis over the period of a week. Spinning speeds for the DB-MAS system were generally found to remain stable to ±5 Hz for a well-packed sample. The drawbacks of the DB-MAS probes are that sample packing is critical and that the rotor must be absolutely full for stable spinning. Because of this latter constraint, it is difficult to run small samples if one does not wish to contaminate them with some filler to increase the volume sufficiently to properly pack the rotor.

3.1.b Other Spectrometer Systems

For the majority of the nitrogen-15 work and for several cases where a second field was deemed necessary, spectra were run on a Varian VXR-300 spectrometer. This instrument was equipped with a 7 Tesla, narrow bore, superconducting magnet. The probes used for MAS work were of double-bearing design and produced by Doty. Several additional comments regarding this spectrometer may be found in the last section of Chapter 7.

In several instances it was necessary to run solution-state spectra to confirm sample composition. These spectra were run using a Bruker AC-250 system. This spectrometer has a 5.3 Tesla, narrow bore, superconducting magnet. The spectra were obtained with the field locked to the resonance of a deuterium signal from the solvent.

3.2 Nuclei

3.2.a Relevant Properties

A number of nuclei have been used in this study. Their NMR-related properties are given in Table 3.1.

Table 3.1

NMR-Related Properties of Relevant Nuclei

	^{1}H	^{13}C	^{15}N	^{31}P	^{23}Na
Spin	1/2	1/2	1/2	1/2	3/2
Relative abundance (%)	99.9	1.11	0.37	100	100
Quadrupole moment (10^{28} Q/m^2)	-	-	-	-	0.10
Relative receptivity‡	1	1.7E-4	3.9E-6	6.7E-2	9.3E-2
NMR frequency Ξ^{+}/MHz	100.0	25.14	10.14	40.48	26.47

* Compared to ^{1}H.
$^{+}$The resonance frequency for a field in which the protons of TMS would resonate at exactly 100.00 MHz.

3.2.b Chemical Shift Referencing

For each of the nuclei in this study, the relevant chemical shift reference compound and mode of referencing is given below. Where a secondary reference is used, it is generally because the standard is a liquid. These liquid reference compounds cannot be used on a day-to-day basis because of the differing shimming considerations for solids and liquids.

The high-frequency-positive convention has been used in the reporting of all chemical shifts in this thesis.

3.2.b.1 Proton

Because of the scaling factors introduced by use of multiple-pulse sequences, it is necessary to use an internal standard for ^{1}H CRAMPS work[2]. After obtaining a spectrum of a clean sample, several grains of adamantane were added to the rotor. The shift of the sample is indirectly referenced to TMS by setting the resonance of adamantane at 1.7 ppm. It should be noted that the two proton shifts in adamantane are not resolved by this technique.

Chemical shift referencing in CRAMPS work is complicated by the scaling factors which are introduced by the pulse sequence as well as by the difficulties involved with broad linewidths and the phasing thereof. As such, proton shifts for CRAMPS results are only reported to an accuracy of ±0.5 ppm.

3.2.b.2 Carbon-13

Carbon-13 shifts have been referenced indirectly to TMS. This was done using the high-frequency resonance of adamantane as a secondary reference. The shift of the adamantane line was determined to be +38.5 ±0.1 ppm by replacement with TMS.

3.2.b.3 Nitrogen-15

Nitrogen-15 shifts have been referenced to the nitrate resonance of 20% enriched ammonium nitrate ($^{15}NO_3NH_4$) at 0.0 ppm. This is done by replacement of the sample with the reference.

3.2.b.4 Phosphorus-31

Phosphorus shifts have been indirectly referenced to 85% aqueous phosphoric acid (H_3PO_4). The secondary reference is "brushite" $CaHPO_4 \cdot 2H_2O$. The shift of brushite was determined to be 1.20 ±0.1 ppm by replacement with the standard.

3.2.b.5 Sodium-23

^{23}Na has been referenced to Na^+ at infinite dilution[5]. Solid NaCl, which has a shift of 7.1 ppm, was used as a secondary reference.

3.3 NMR Techniques and Pulse Sequences

The basic techniques of solid-state NMR have become generally well-known and will not be discussed here in great detail. The reader is referred to the monograph of Fyfe[6] for a comprehensive treatment of solid-state methodology and applications. A number of different pulse sequences have been used in this work. These are shown diagrammatically in Figure 3.1. The drawings are not to

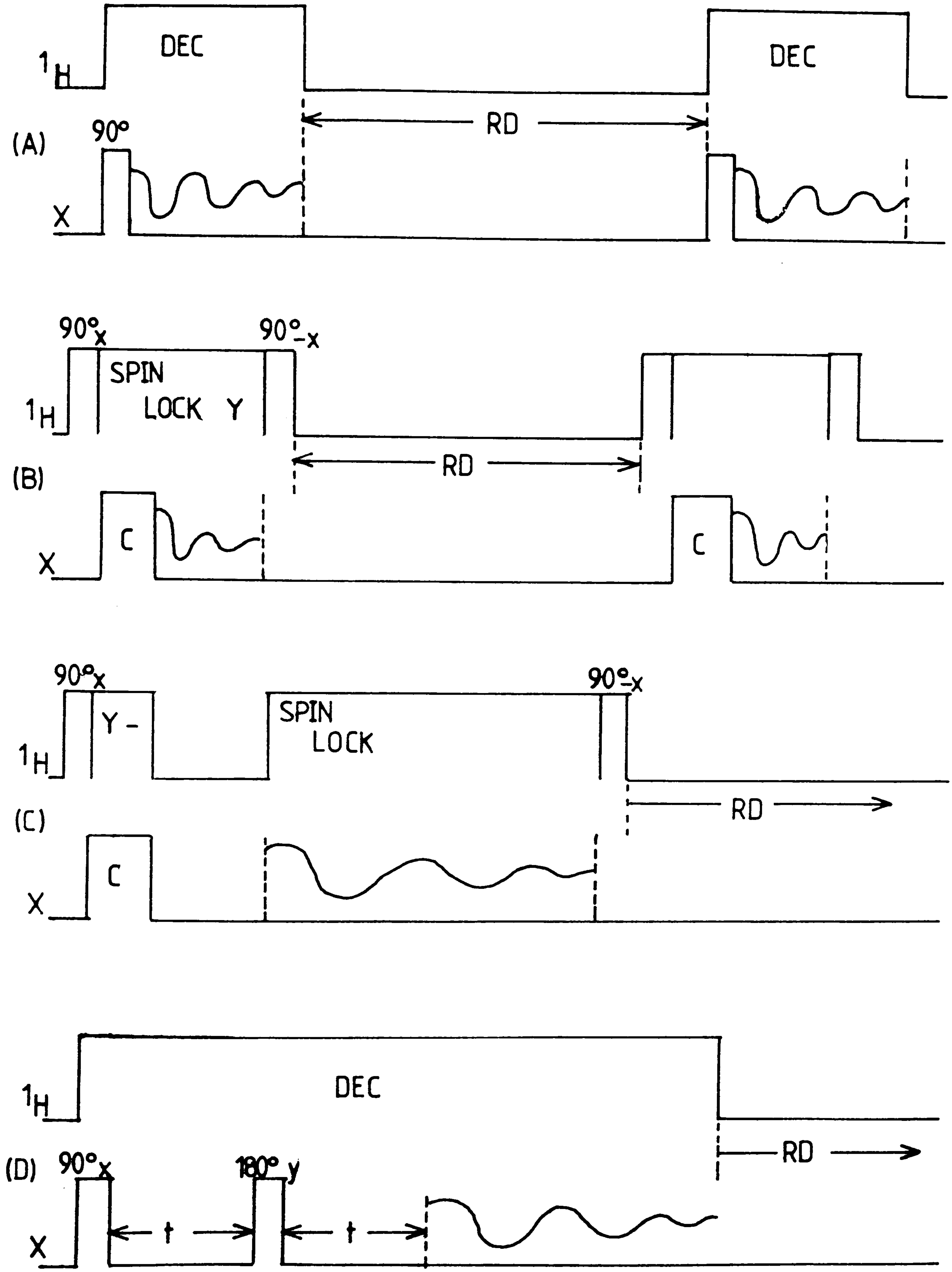

(A)
^1H
DEC
DEC
90°
RD
X
(B)
$90°_x$
$90°_{-x}$
SPIN
LOCK Y
^1H
RD
C
C
X
(C)
$90°_x$
Y -
SPIN
LOCK
$90°_{-x}$
^1H
RD
C
X
(D)
^1H
DEC
$90°_x$
$180°_y$
RD
t
t
X

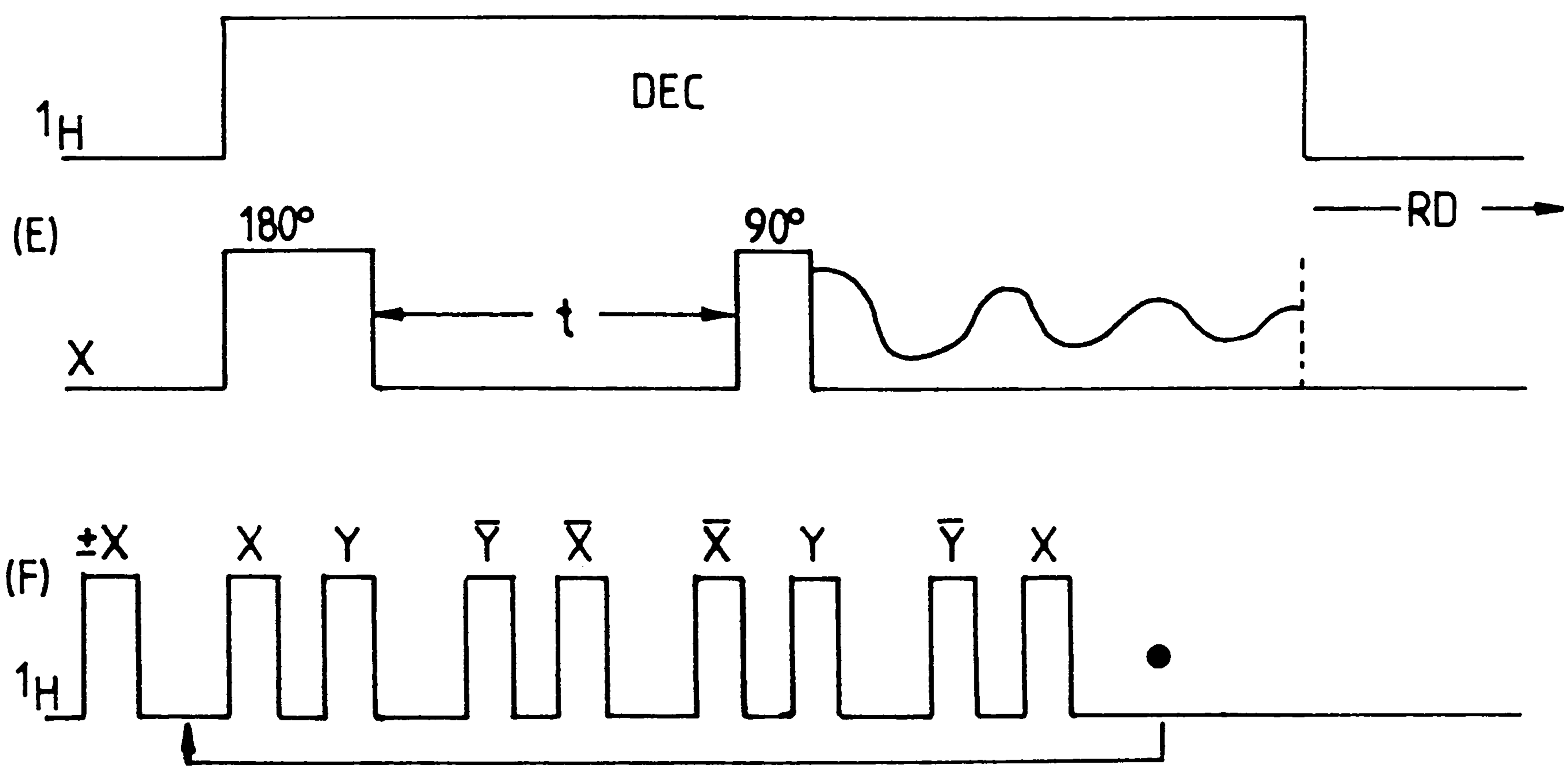

Figure 3.1: Pulse sequences used in this study.
(A) Single-pulse excitation. (B) Cross-polarization.
(C) Non-quaternary suppression. (D) Spin echo.
(E) Inversion-recovery. (F) MREV-8. Dec=decouple,
RD=recycle delay and C=cross-polarization contact
pulse. The drawings are not to scale.

scale as standard pulse durations are generally of the order of μs, and contact times for cross-polarization are generally ca. 1-10 ms, while recycle delays may be of the order of tens of seconds. For all pulse sequences, phase cycling is used in order to minimize instrumental artifacts.

3.3.a Single-Pulse Excitation (SPE)

Figure 3.1.A is the single-pulse sequence with high-power proton decoupling. This is analogous to its solution-state equivalent though, of course, much higher decoupling power is required. The instrument was generally set up with a 90° pulse duration of 4-5 μs. However, in practice, a shorter pulse duration (usually 1 μs) was used in the acquisition of spectra. This was done to take advantage of Ernst angle[7] considerations.

3.3.b Cross-Polarization and Magic-Angle Spinning

The techniques of cross-polarization[8] (CP) and magic-angle spinning[9,10] (MAS) were used for the vast majority of the ^{31}P and all of the ^{13}C and ^{15}N spectra in this thesis. The effect of cross-polarization is threefold[6]: Firstly, to remove heteronuclear dipolar and scalar coupling; secondly, to provide a sensitivity enhancement factor which is of the order of the ratio γ_H/γ_X; and, thirdly, to decrease recycle delay. It should be noted that in the latter case, it is $T_1(H)$ and not $T_1(X)$ that is the controlling factor. Magic-angle spinning was used to average the residual homonuclear dipolar interaction and the anisotropy in the shielding as described in Chapters 2 and 4.

Figure 3.1.B is the standard CP pulse sequence. It incorporates both spin-temperature inversion[11] and flip-back[12]. The purpose of the former is to remove instrumental artifacts, while that of the latter is to reduce recycle times. It should be noted that for technical reasons, flip-back was not implemented on

the VXR-300 spectrometer. The consequences of this are discussed in the last section of Chapter 7. On the CXP-200 the proton 90° pulse duration was usually 4 μs. Contact times were generally in the 0.1-10 ms range and were optimised for each sample.

In order to achieve cross-polarization, the so-called Hartmann-Hahn[13] condition must be met. In effect, the radio-frequency fields for the proton decoupler and observe (X) nucleus channels, B_{1H} and B_{1X} respectively, must be set such that the relationship $\gamma_H B_{1H} = \gamma_X B_{1X}$ is satisified. In practice the Hartmann-Hahn match is achieved by first setting a 90° pulse on the proton channel. The output of the X nucleus transmitter is then altered until a maximum FID is observed.

3.3.c Non-Quaternary Suppression

Figure 3.1.C is the non-quaternary suppression (NQS) pulse sequence. This method, also called dipolar dephasing, was devised by Opella and Frey[14] and is generally used to assist in assignment of resonances in solid-state spectra. It has found its greatest utilization in ^{13}C solid-state NMR, though it can be applied to any nucleus with directly bound protons. It is essentially a CP experiment with a "window" inserted into the decoupler channel. During the period of this window (usually 40 μs - 80 μs), the dipolar decoupling is removed, and the carbon spins will begin to dephase under the influence of the proton dipolar fields. Because of the $1/r^3$ relationship for the dipolar coupling, the spins of those nuclei with directly bound protons will dephase much more rapidly than those with no attached protons. Thus, the resulting spectrum will contain mainly lines from non-protonated carbons. For a particular site, however, it will be noted that if any mechanism exists which greatly averages the dipolar interaction at that site, the resonance for that nucleus will remain in the NQS spectrum. This is true for methyl carbons, for example, where rapid internal rotation partially averages the heteronuclear dipolar interaction.

3.3.d Spin Echo

Figure 3.1.D is the spin-echo sequence used to obtain static spectra. In the case of such spectra, the decay of the FID is rapid, and an appreciable amount of signal may be lost during the dead time after the RF pulse. With the echo sequence, the magnetization is refocused and the initial portion of the FID is recovered. The refocusing is effective because of the inhomogeneous nature of the static bandshape in most cases.

3.3.e Spin-Lattice Relaxation

Figure 3.1.E is the inversion-recovery (180°-τ-90°-acquisition) pulse sequence used for the T_1 measurements in this study. It is equivalent to the sequence used in solution-state NMR, though again, high-power proton decoupling must be used.

3.3.f ^1H CRAMPS

For systems with strong homonuclear dipolar interactions (e.g. ^1H), static linewidths may be of the order of 40 kHz. Noting that obtainable MAS speeds are only of the order of 5 kHz, it will be seen that the use of magic-angle spinning alone would be inadequate to average such interactions. If, however, a multiple-pulse sequence is used to remove the dipolar interaction, and at the same time MAS is used to average the shielding anisotropy, high resolution spectra will result. This technique[15,16,17] has the mnemonic CRAMPS - Combined Rotation and Multiple-Pulse Spectroscopy. The resulting spectra still have linewidths of the order of 100 Hz; however, as will be seen, this is sufficient to study hydrogen bonding in solid acids.

There are rigorous experimental considerations in using the CRAMPS technique. Radio-frequency (B_1) homogeneity must be high and probe ring-down times low. The single channel probe used for this work has been described by Nesbitt[2]. It consists of a narrow-diameter (ca. 7mm), flat wire coil with bundled resistors in the tuned circuit to decrease recovery time. A "broomstick"-type rotor with a small-volume (ca. 15 mm^3) spherical sample cavity was used.

Figure 3.1.F is the MREV-8 pulse sequence[18] used in the CRAMPS technique to acquire ^1H spectra. This sequence was part of UNIPAMPS.PPG, a general pulse program written at Durham[2] for multiple-pulse spectroscopy on the CXP-200. The mnemonic stands for UNIversal Phase Alternated Multiple Pulse Sequence. The advantage of the UNIPAMPS program is that it incorporates phase cycling to remove the effects of probe ringing and pulse breakthrough. For the CRAMPS spectra in this thesis, a pulse duration of 2 μs was used. Sampling was done twice per cycle, resulting in a dwell time of 24 μs. Spinning speeds of ca. 3.5 kHz were used.

For multiple-pulse sequences, is it is extremely important that pulse phase and amplitude errors be kept to an absolute mimimum. To this end, the method of Burum and Pearson[19] was generally followed to set-up the spectrometer. It is necessary to iteratively repeat the process several times before all of the pulse phases and amplitudes are set correctly. A glass sphere containing water was used as the tune-up sample.

3.3.g Setting the Magic Angle

The angle between the rotor and the B_o field was set to 54° 44' by observing the FID of the NMR transition of ^{79}Br in KBr and maximizing the number of spinning sidebands arising from the first order quadrupolar transition. This method can be used to set the magic-angle accurately to ± 0.1°[20].

VanderHart, Earl and Garroway[21] have shown that the linewidth which results from magic-angle mis-set may be calculated using the expression: $\nu_{½} = 0.5(3\cos^2\theta_{rot} - 1)\nu_{band}$, where $\nu_{½}$ is the linewidth of the resulting MAS centreband, θ_{rot} is the angle which the rotor axis makes with the static magnetic field, and ν_{band} is the static bandwidth. As typical compounds in this study have static bandwidths of the order of 12 kHz, a 0.1% error in setting the angle is calculated to result in MAS linewidths of ca. 29 Hz.

3.4 Spectra

All of the spectra in this thesis were obtained at room temperature. The abbreviations used to describe the experiment and the acquisition conditions are noted below. The centrebands of MAS spectra are indicated by a vertical arrow or line.

Techniques:

SPE = Single-pulse excitation
CP = Cross-polarization
MAS = Magic-angle spinning
NQS = Non-quaternary suppression
CRAMPS = Combined rotation and multiple pulse spectroscopy
Echo = Spin echo

Experimental Parameters:

RD = Recycle delay
NT = Number of transients
PD = 90° pulse duration
CT = Cross-polarization contact pulse duration
DA = NQS window duration
SF = Spectrometer frequency
SW = Spectrum width
δ_{x} = Chemical shift (in ppm)
ν_{r} = Spinning speed
$\nu_{1/2}$ = Half-height line width (in Hz)

3.5 Samples

3.5.a Diphosphine Disulphides, Phosphonic Acids and Phosphinic Acids

With the exceptions noted below, the majority of the samples examined in this work were obtained from the laboratory of Professor Gerhard Hägele, University of Düsseldorf, Düsseldorf, Federal Republic of Germany. The phosphonic and phosphinic acids had been freshly prepared and were used as received. The diphosphine disulphides were the result of synthetic work from several years ago. If the crystals were damp or discoloured, the compound was recrystallized from dry methanol/toluene.

Sample source other than that noted in the paragraph above:

Dr. M. Fild, Technical University of Braunschweig, Braunschweig, F.R.G.:

meso-methylphenyldiphosphine disulphide
meso- and rac-methylethyldiphosphine disulphide
tetramethylenediphosphine disulphide

Koch-Light Laboratories Inc.:

tetraethyldiphosphine disulphide

Ventrom GMBH:

tetra-n-butyldiphosphine disulphide

Aldrich Chemical Company Ltd.:

3-aminopropylphosphonic acid
2-aminoethylphosphonic acid

BDH Chemical Co. Ltd.:

benzenephosphonic acid

3.5.b Nitrogen-15 samples

Amersham UK Ltd.:

20% $^{15}NH_4{}^{15}NO_3$

95% $^{15}NH_4NO_3$

Glaxo Group Research Ltd.:

Cefuroxime E47 Ester

Aldrich Chemical Co. Ltd.:

glycine

ammonium nitrate

References

1. Bruker Spectrospin Ltd., "Pulse NMR Spectrometer CXP User's Manual".

2. G.J. Nesbitt, Ph.D. thesis, University of Durham (1986).

3. E.R. Andrew, A. Bradbury and R.G. Eades, *Nature, London* **182**, 1659 (1958).

4. Bruker Spectrospin Ltd., "NMR Probehead Series: MAS-DB".

5. G.J. Templemann and A.L. van Geet, *J. Amer. Chem. Soc.* **94**, 5578 (1972).

6. C.A. Fyfe, "Solid State NMR For Chemists", C.F.C. Press, Guelph (1983).

7. R.R. Ernst and W.A. Anderson, *Rev. Sci. Instr.* **37**, 93 (1966).

8. A. Pines, M.G. Gibby and J.S. Waugh, *J. Chem. Phys.* **59**, 569 (1973).

9. E.R. Andrew, *Progr. Nucl. Magn. Reson. Spectr.* **8**, 1 (1971).

10. J. Schaefer and E.O. Stejskal, *J. Amer. Chem. Soc.* **98**, 1031 (1976).

11. E.O. Stejskal and J. Schaefer, *J. Magn. Reson.* **18**, 560 (1975).

12. U. Haeberlen and N. Tegenfeld, *J. Magn. Reson.* **36**, 453 (1979).

13. S.R. Hartmann and E.L. Hahn, *Phys. Rev.* **128**, 2042 (1962).

14. S.J. Opella and M.H. Frey, *J. Amer. Chem. Soc.* **101**, 5854 (1979).

15. L.M. Ryan, R.E. Taylor, A.J. Paff and B.C. Gerstein, *Chem. Phys Lett.* **72**, 508 (1980).

16. L.M.Ryan, R.C. Wilson and B.C. Gerstein, *Chem. Phys Lett.* **52**, 341 (1977).

17. G. Scheler, U. Haubenreisser and H. Rosenberger, *J. Magn. Reson.* **44**, 134 (1981).

18. P. Mansfield, *J. Phys. C* **4**, 1444 (1971); W.K. Rhim, D.D. Elleman and R.W. Vaughan, *J. Chem. Phys.* **58**, 1772 (1973).

19. D.P. Burum and R.M. Pearson, "Bruker CXP Application Note (BII-1)".

20. J.S. Frye and G.E. Maciel, *J. Magn. Reson.* **48**, 125 (1982).

21. D.L. VanderHart, W.L. Earl and A.N. Garroway, *J. Magn. Reson.* **44**, 361 (1981).

CHAPTER FOUR - SHIELDING TENSOR ANALYSIS

4.1 Introduction

For a given nucleus, the exact resonance frequency in the NMR experiment is a function of its chemical environment. The effect of differing chemical environments is to change the electronic shielding around the nucleus and, thus, the resonance frequency. This is what is known as the chemical shift.

The shielding which causes the chemical shift is a tensor property as has been described in Chapter 2. In solution-state NMR, the tensor, $\underline{\sigma}$, is averaged by random isotropic motion. The shielding which is observed is simply the isotropic average of the tensor $\bar{\sigma} = 1/3\mathrm{Tr}\underline{\sigma} \equiv 1/3(\sigma_{11} + \sigma_{22} + \sigma_{33})$. In solid-state NMR, however, this tensor is not averaged, and it should be possible to obtain the three principal shielding tensor components.

In practice, there are a number of methods to obtain the shielding tensor information. NMR studies of single crystals provide the most informative means, as both the value of the tensor components and their orientation in the molecular frame may be determined.[1] This method is not satisfactory, of course, for materials which are not obtainable in crystalline form or if broadening from other interactions is present. Where the lack of crystallinity is the case, the tensors may be found from the powder spectrum either by measuring the breakpoints directly or by computerized simulation of the line shapes. This will only work, however, where there is only a single chemically and crystallographically distinct species in the material under examination. If more than one type of nucleus is present, overlap in the powder lines makes extraction of the tensor parameters quite difficult. A number of methods have been devised to overcome this difficulty. These include two-dimensional methods in which the powder spectrum is obtained in the second dimension[2,3], off-angle fast spinning[4], which scales the powder patterns sufficiently to avoid overlap, and slow speed magic-angle spinning followed by analysis of the pattern of the resulting spinning-sideband envelope[5,6]. Of these, the latter seems to be the most generally used.

To digress for a moment, it should be made clear that the powder methods noted above do not provide any information on the orientation of the tensor in the molecular frame; this information can only be obtained with absolute certainty from single crystal work. When tensor components are determined using one of the powder methods above, orientation must be inferred from either known single crystal studies or, more usually, from molecular geometry.

There are two well known methods for the analysis of slow magic-angle spinning spectra. These are the method of moments proposed by Maricq and Waugh[5] and the graphical method proposed by Herzfeld and Berger[6]. In this chapter, a short description of each of these methods and a discussion of the associated difficulties and errors are given.

Because of the problems with these methods for sideband analysis (*vide infra*), the most logical course of action seemed to be the computerized simulation and fitting of spinning sideband spectra. The use of simulation of a sideband manifold to accurately determine the tensor components was suggested in one of the original papers[5]; however, there have been few examples of this reported in the literature[5,7]. Further, the use of a simulation routine to actually fit a spinning sideband pattern has, it seems, only been reported by Ellis and co-workers[8,9]. Unfortunately, the computer program was not described in detail.

In this chapter, the extraction of shielding tensor data from static spectra will first be discussed followed by short descriptions of the moments and the graphical methods. The main body of the chapter will be concerned with the development and description of computer programs to simulate and fit spinning sideband spectra. Examples of the use of these programs will be given.

Finally, before beginning, it would seem prudent to explicitly state the conventions for the shielding tensor information which will be used in ths chapter and throughout this thesis. The convention which has been chosen is that of Haeberlen[10]. The isotropic shielding has already been given as:

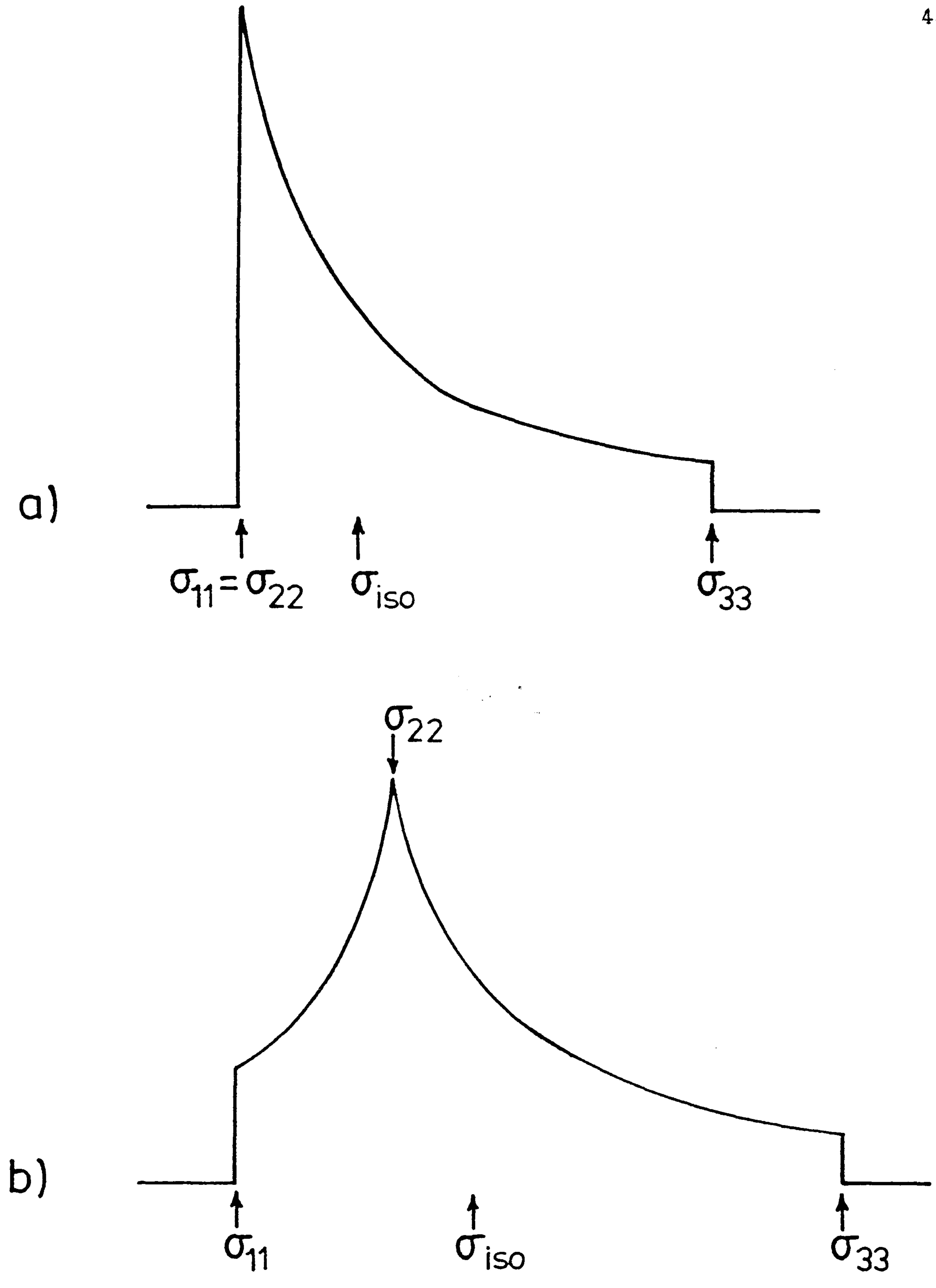

Figure 4.1: Representation of characteristic tensor powder patterns. (A) Axially symmetric. (B) General nonsymmetric.

$$\bar{\sigma} = 1/3\mathrm{Tr}\underline{\sigma} \equiv 1/3(\sigma_{11} + \sigma_{22} + \sigma_{33}). \qquad 4.1$$

The three tensors, σ_{11}, σ_{22} and σ_{33} are assigned as follows:

$$|\sigma_{33} - \bar{\sigma}| \geqslant |\sigma_{11} - \bar{\sigma}| \geqslant |\sigma_{22} - \bar{\sigma}|. \qquad 4.2$$

The anisotropy and asymmetry may be defined respectively as:

$$\delta = \sigma_{33} - \bar{\sigma} \qquad 4.3$$

and $\eta = (\sigma_{22} - \sigma_{11})/\delta.$ 4.4

It is clear that the symbol for the anisotropy may be confused with that used for the chemical shift. In this thesis, the chemical shift δ will always be subscripted with the atomic symbol for the nucleus of interest (e.g. δ_P).

4.2 Static Bandshape Analysis

If only one chemically distinct type of nucleus is present, and there are no complicating factors such as large dipolar coupling, the values of the shielding tensor can be determined from the static powder pattern. Figure 4.1 shows a general representation of the shape of an asymmetric and an axially symmetric tensor pattern. (There should actually be an infinity at the σ_{22} position of both patterns.) Of course, if real spectra were this well defined, one could read the tensor values directly from the spectrum; however, this is not the case. In actual spectra, the shapes are broadened by residual dipolar and scalar coupling, bulk magnetic susceptibility effects, and inhomogeneity in both the B_o and B_1 magnetic fields. As a result, static spectra have the appearance of Figures 4.2 and 4.3.

In order to extract the shielding tensor information from such a spectrum, it is necessary to fit it with a calculated lineshape. Several computer programs have been written to carry out this

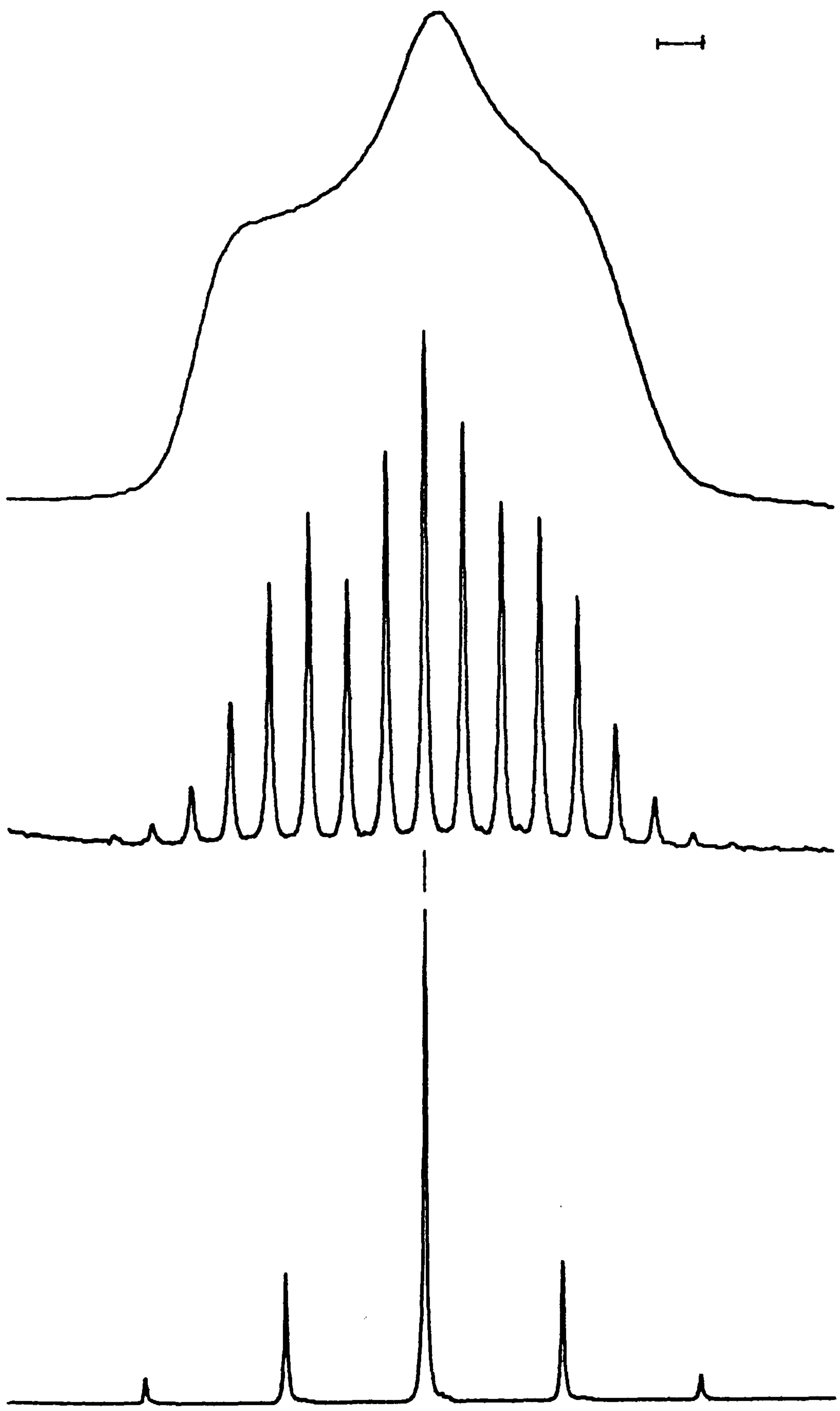

Figure 4.2: ^{31}P spectra of the disodium salt of 1,2-ethane-bisphosphonic acid (19). $[HO_3P\text{-}CH_2\text{-}CH_2\text{-}PO_3H]^{2-}$ $2Na^+ \cdot 4H_2O$.
Top: Echo; static; RD=45 s; PD=5 μs; NT=1038.
Centre: CP/MAS; RD=45 s; NT=80; CT=1 ms; ν_r=840 Hz.
Bottom: CP/MAS; RD=45 s; NT=48; CT=1 ms; ν_r=3004 Hz.
δ_P = 29.3 ppm. The bar represents 1 kHz.

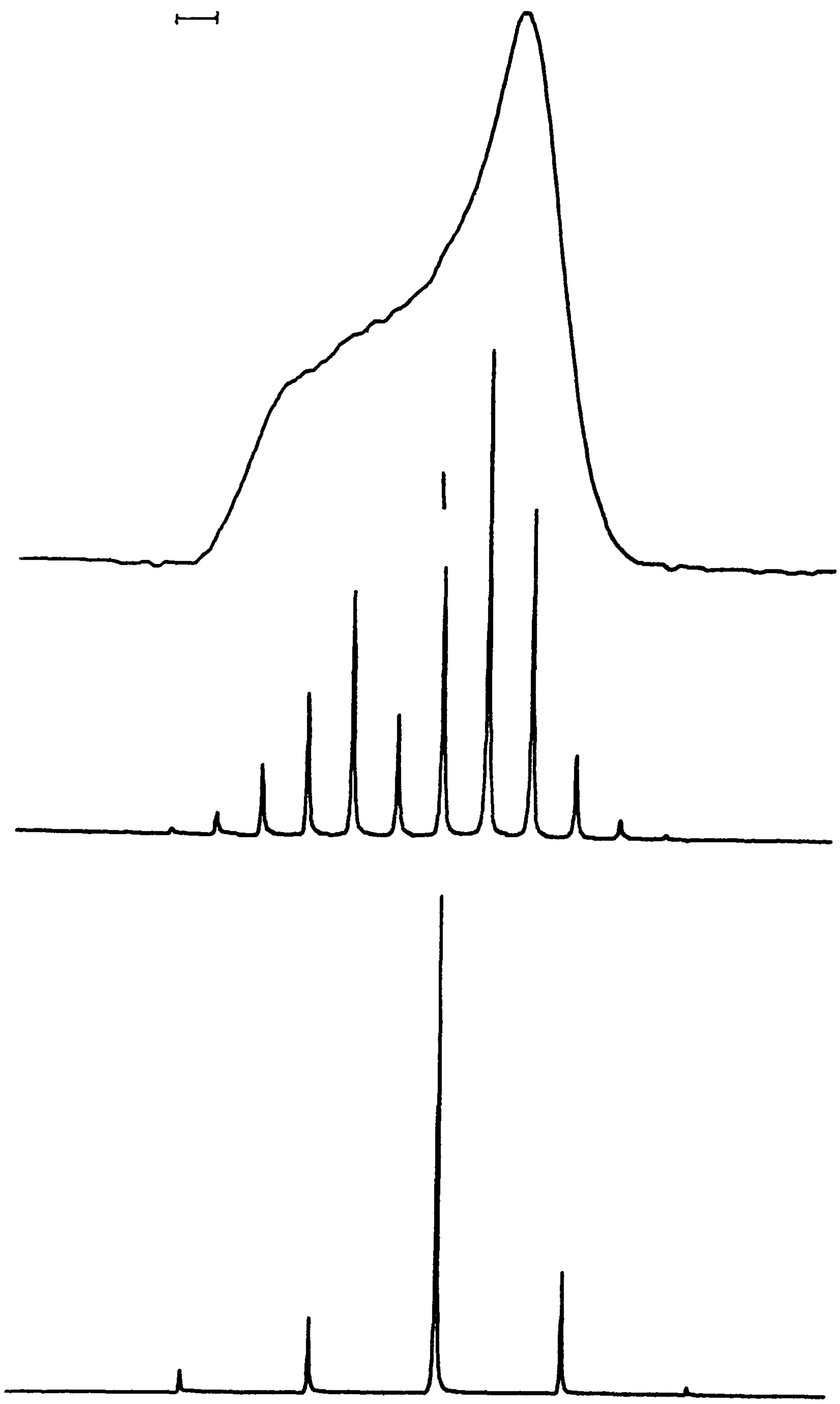

Figure 4.3: ^{31}P spectra of the tetrasodium salt of 1,2-ethane-bisphosphonic acid (20). $[O_3P-CH_2-CH_2-PO_3]^{4-}$ $4Na^+$.
Top: Echo; static; RD=45 s; PD=5 μs; NT=1040.
Centre: CP/MAS; RD=30 s; NT=100; CT=1 ms; ν_r=1060 Hz.
Bottom: CP/MAS; RD=45 s; NT=52; CT=1 ms; ν_r=3000 Hz.
δ_P = 24.8 ppm. The bar represents 1 kHz.

task[11,12]. In this work, the program written by Groombridge[12] was used.

The calculations of this program are based on the assumption that the broadening mechanisms in effect in a static powder spectrum are generally gaussian in nature. To simulate such a spectrum, the unbroadened powder pattern (similar to Figure 4.1) is first generated. This is then numerically convoluted with a gaussian function. The result is a spectrum which will resemble a real spectrum in that there is no discontinuity, and that the shoulders will be rounded. The program iterates over σ_{11}, σ_{22}, σ_{33} and the width of the gaussian function and uses a sum-of-squares difference criterion to describe the deviation between the experimental and calculated spectra. Minimization is carried out using a simplex routine (*vide infra*). An example of a fitted spectrum may be found in Figure 4.4. These type of fits generally give tensor values reproducable to ± 2 ppm.

The obvious limitation to this method is that it can only be used where a single chemically distinct type of nucleus is present. If more than one type of nucleus exists in the sample, each will have its own distinct powder pattern. The resulting superposition of these powder patterns will make the analysis of the spectrum quite difficult if not impossible. An example of such a spectrum which is the superposition of two such powder patterns may be seen in the top of Figure 4.5. The spectrum is complicated, and the positions of the shoulders and peaks which represent the various shielding tensor components are not immediately evident. The same figure also shows the advantage of the use of magic-angle rotation in the analysis of such systems. The two chemically distinct sites are clearly separated, each having its own well defined spinning-sideband manifold. The methods for extracting the tensor information from spinning sideband manifolds is the main emphasis in this chapter.

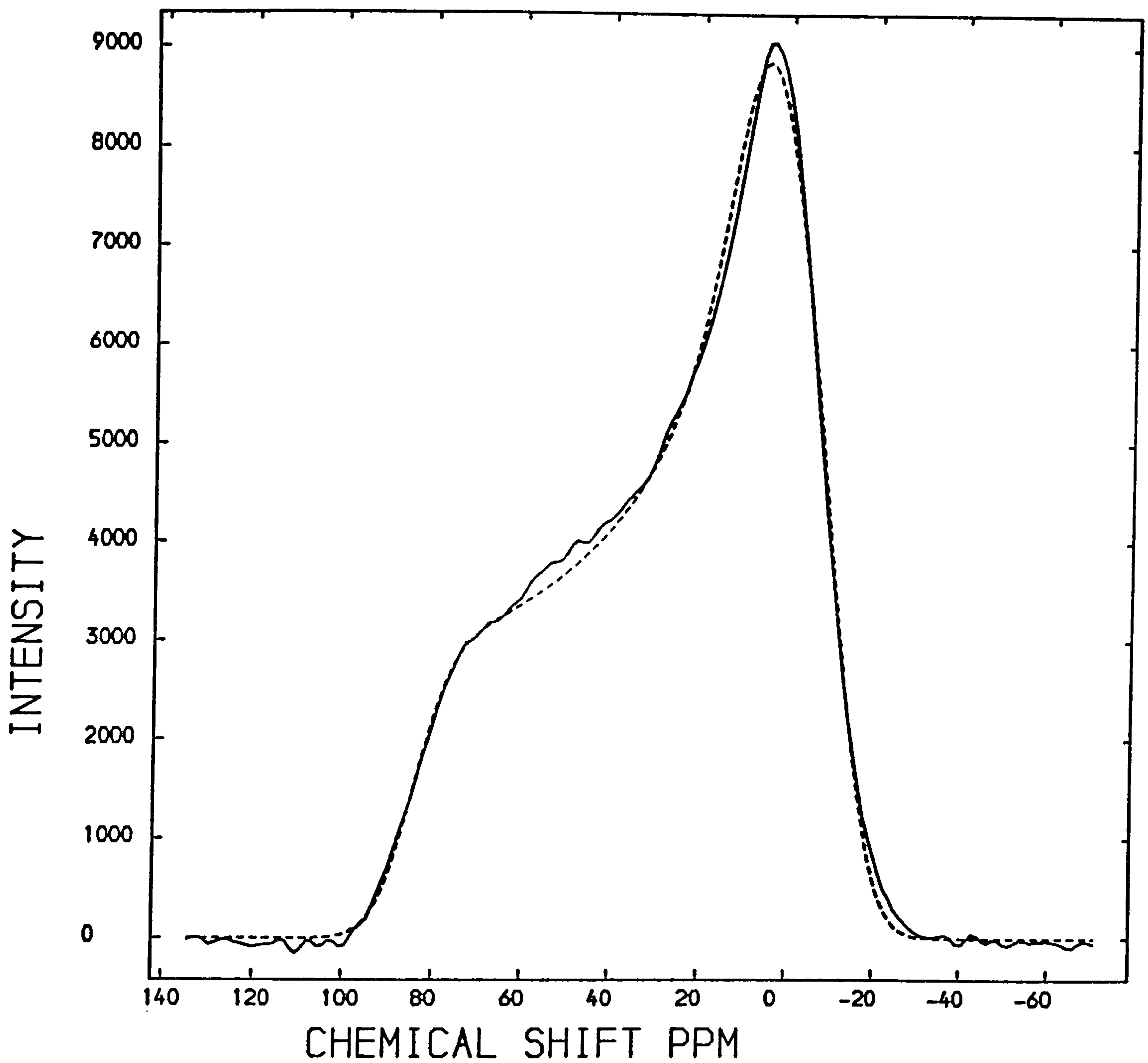

Figure 4.4: Example of the fit of a static powder spectrum using the computer program described in section 4.2. Tetrasodium salt of 1,2-ethanebisphosphonic acid (20). See Table 4.1 for results.

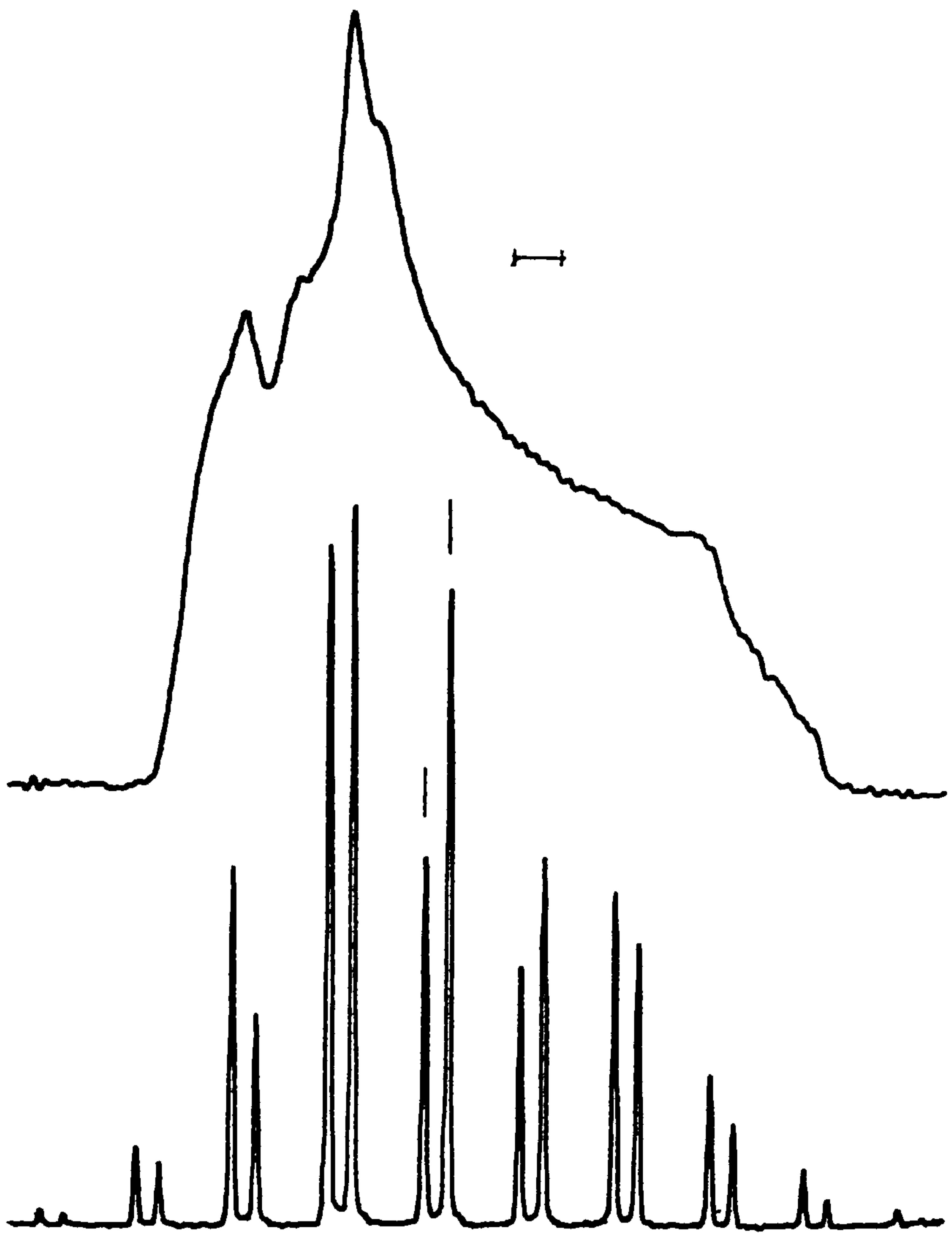

Figure 4.5: Example of a case where the tensor values cannot easily be determined from the static bandshape (top). However, the tensor components may be calculated for the two phosphorus sites (bottom) using the spinning sideband analysis methods described in the text. ^{31}P spectra of meso-methyl-1-menthyl diphosphine disulphide (**10**). Top: Echo; static; RD=15 s; PD=4 μs NT=132. Bottom: CP/MAS; RD=15 s; CT=1 ms; NT=48; ν_r=2290 Hz. δ_P = 48.1 and 41.0 ppm. The bar represents 1 kHz

4.3 Method of Moments

The first method for the determination of the shielding tensor values from a spinning sideband pattern is the moments analysis proposed by Maricq and Waugh[5]. The basis of this method is the fact that once the centreband is identified, the only information that one really needs to extract from the spinning-sideband pattern are the values of δ and η. Once these are determined, the principal tensor components may be easily found using the definitions noted above. The values of δ and η may be related to the shape of the spinning-sideband envelope by determining the second and third moments of that envelope.

The m^{th} moment of the normalized bandshape, $I(\omega)$, is defined as:

$$M_m = \int_{-\infty}^{\infty} I(\omega)\omega^m \, d\omega. \qquad 4.5$$

The zeroth moment may be seen to be the area under the bandshape, the first moment the mean value, the second the mean squared witdth, and so on. (In principle, the first moment may be used to identify the centreband.) It will be noted that this is a perfecly general equation concerning only the shape of the function. Furthermore, the moments may be calculated from first principles without having to determine the eigenstates of the total Hamiltonian[13]. Indeed, the moment method was first used to describe the static lineshape of dipolar broadened systems. The theoretical calculation of such systems is very difficult due to the fact that the solution of a many-bodied quantum mechanical problem is required. Van Vleck[14] determined expressions of the second and fourth moments as measures of the lineshapes of these systems. The second moment, in particular, has been used extensively in the study of molecular motion in solids.[15]

In the case where spinning-sidebands arise from averaging the powder spectrum by magic-angle spinning, the m^{th} moment is defined as:[5]

$$M_m = \nu_r^m \sum_{N=N-}^{N+} N^m A_N / \sum A_N \quad , \qquad 4.6$$

where A_N is the intensity of the N^{th} sideband, and ν_r is the spinning speed in frequency units. The convention of Maricq and Waugh[5] has been followed regarding the numbering of sidebands. They are numbered outwards from the centreband, which is band zero (e.g. ...-3,-2,-1,0,1,2,3,...). The above form of the equation is necessary because of the discrete nature of the sideband pattern. The denominator in the equation is simply a normalization factor.

Given that frequencies are measured from the isotropic average shift position and that the function is normalized to unit area, the lower order moments are given below:

$$M_0 = 1$$

$$M_1 = 0$$

$$M_2 = (\delta^2/15)(3 + \eta^2) \qquad 4.7$$

$$M_3 = (2\delta^3/35)(1 - \eta^2) \qquad 4.8$$

$$M_4 = (15/7)M_2 + 2\nu_r^2 M_2.$$

The first and second moments are the only independent moments. All higher order moments depend on the lower order moments as is shown for M_4.

It is important to note that the second and third moments are invariant to sample rotation. This is well known for the second moment for any motion in the lattice[16]. However, it is a special case for M_3 for rotation about the magic angle[5].

Given the equations for the second and third moments above, it is clear that a cubic solution in δ may be found. Experimentally, the procedure is to measure the intensities of the sidebands either using integrated intensities or simple peak heights. Then, the second and third moments are calculated using equation 4.6. The values for the moments are inserted into equations 4.7 and 4.8, and the cube roots of δ are found. The value of η is determined by inserting the value of δ back into one of the two moments equations. The values of the three shielding tensor components may then be calculated using the relationships:

$$\sigma_{11} = \bar{\sigma} - \tfrac{1}{2}\delta(1 + \eta) \qquad 4.9$$

$$\sigma_{22} = \bar{\sigma} - \tfrac{1}{2}\delta(1 - \eta) \qquad 4.10$$

$$\sigma_{33} = (\bar{\sigma} + \delta) \qquad 4.11$$

where $\bar{\sigma}$ is the isotropic value for the shielding, $\bar{\sigma} = 1/3\mathrm{Tr}\underline{\sigma}$. Also, remember that $\bar{\sigma} = -\delta_{x}$, where δ_{x} is the isotropic chemical shift.

It should be noted that as there may be up to three real solutions to a cubic equation, that there will be three values of δ. These three values of δ simply correspond to permutations of the three tensor components in the equations noted above.

The method of moments has several drawbacks to its use. First of all, an examination of equation 4.6 will immediately show a major source of errors. The moments are highly dependent on the intensity of the outer sidebands as the intensities are weighted by a factor, N^{m}, where m is the moment and N is the sideband number. These outer sidebands, which are critical to the moment calculation, are inherently difficult to measure accurately because of their weakness. Further, because of the source of errors noted above, excellent signal-to-noise is certainly indicated. While this may not be a problem for the phosphorus spectra of this study, obtaining the necessary s/n for a relatively insensitive nucleus, such as carbon-13, may be uneconomical in terms of spectrometer time. One must also be able to measure all of the spinning sidebands in the manifold[6]. This may not be possible where resonances overlap. Further, and of some importance, recent work by Clayden *et al.*[7] has shown the method of moments to give inconsistent results for nearly axial tensors. They report the method to be generally accurate for nonaxial tensors but encounter severe difficulties in the cases where the tensors were axial or near axial. The results of Clayden *et al.* support the general view of the method and are in agreement with the findings of this study (*vide infra*).

4.4 The Graphical Method

The second method devised for the determination of shielding tensor components from spinning sidebands is the graphical method of Herzfeld and Berger[6]. This method was devised in order to circumvent two of the difficulties in the method of moments; namely, the need to measure all of the sideband intensities and the need for measuring the outer, weak sidebands very accurately. The basis for this method is a complicated expression which is derived for the sideband intensities of magic-angle spinning spectra. This expression was evaluated over a large number of possible parameters, and a graphical method for extracting the required information was developed.

In the paper by Herzfeld and Berger, one is presented with five plots which were the result of the calculations noted above. These plots show a contour of the ratio $I_o/I_{\pm N}$ as a function of two parameters ρ and μ. I_o is the intensity of the centreband, and $I_{\pm N}$ is the intensity of the N^{th} sideband. The parameters ρ and μ are related to the tensor components by the following expressions:

$$\mu = (\gamma B_o)(\sigma_{33} - \sigma_{11})/\omega_r \qquad 4.11$$

$$\rho = (\sigma_{11} + \sigma_{33} - 2\sigma_{22})/(\sigma_{33} - \sigma_{11}) \qquad 4.12$$

The five plots presented are for the N = ±1 to N = ±5 sidebands, where N is the sideband number. One of these contour plots is shown in Figure 4.6.

In practice, what one does is to measure the intensity of each sideband in the spectrum of interest and then to calculate the intensity ratio, I_o/I_N. One then goes to the appropriate plot for each sideband number, N, and traces the contour line for the calculated intensity ratio, interpolating where necessary. At the end of the process, one will have a plot consisting of a series of contour lines for the various sideband intensity ratios. The main intersection of these contour lines gives the required value of ρ and μ. Such a plot, taken directly from reference [6], is given in the bottom of Figure 4.6. The intersection point, corresponding to $\mu \simeq 13$ and $\rho \simeq 0.4$, is indicated by a circle. An estimate of the error is given by the surrounding rectangle.

Once μ and ρ are determined, it is a straightforward process to determine the three shielding tensor components. Given that the isotropic chemical shift is known, the two equations above, when combined with the relationship $\bar{\sigma} = (\sigma_{11} + \sigma_{22} + \sigma_{33})/3$, give three equations in three unknowns which may be solved easily.

The main strengths of the graphical method are twofold and address the weakness of the method of moments directly. First of all, it will be seen that it is not necessary to use <u>all</u> of the sidebands to determine the tensor values. Indeed, there are only contour plots for $N = \pm 5$, so sidebands of higher order were neglected by Herzfeld and Berger in any case. The loss of a single intermediate sideband due to overlap will not invalidate the analysis as would be the case in the moments method. Secondly, the errors associated in measuring the outer sidebands in the moments method can generally be avoided. In principle, with the graphical method only two sidebands are necessary to define a crossing, though, of course, in practice the more sidebands one uses the more certain one can be of the result. Given a spectrum with a reasonable number of sidebands, the outer intensities need not be used or, as noted above, even come within the scope of the available contour plots.

Although the features noted above make the graphical method generally preferable to the method of moments, the graphical method still has a number of serious drawbacks. Firstly, and common in both methods, there is a lack of reproducibility when the tensors have near axial symmetry. It has been pointed out by Clayden *et al.*[7] that for near-axial symmetry, the ρ values of the contour plots approach ± 1, and that in this region the contours have a similar curvature. In such cases, a unique convergence is

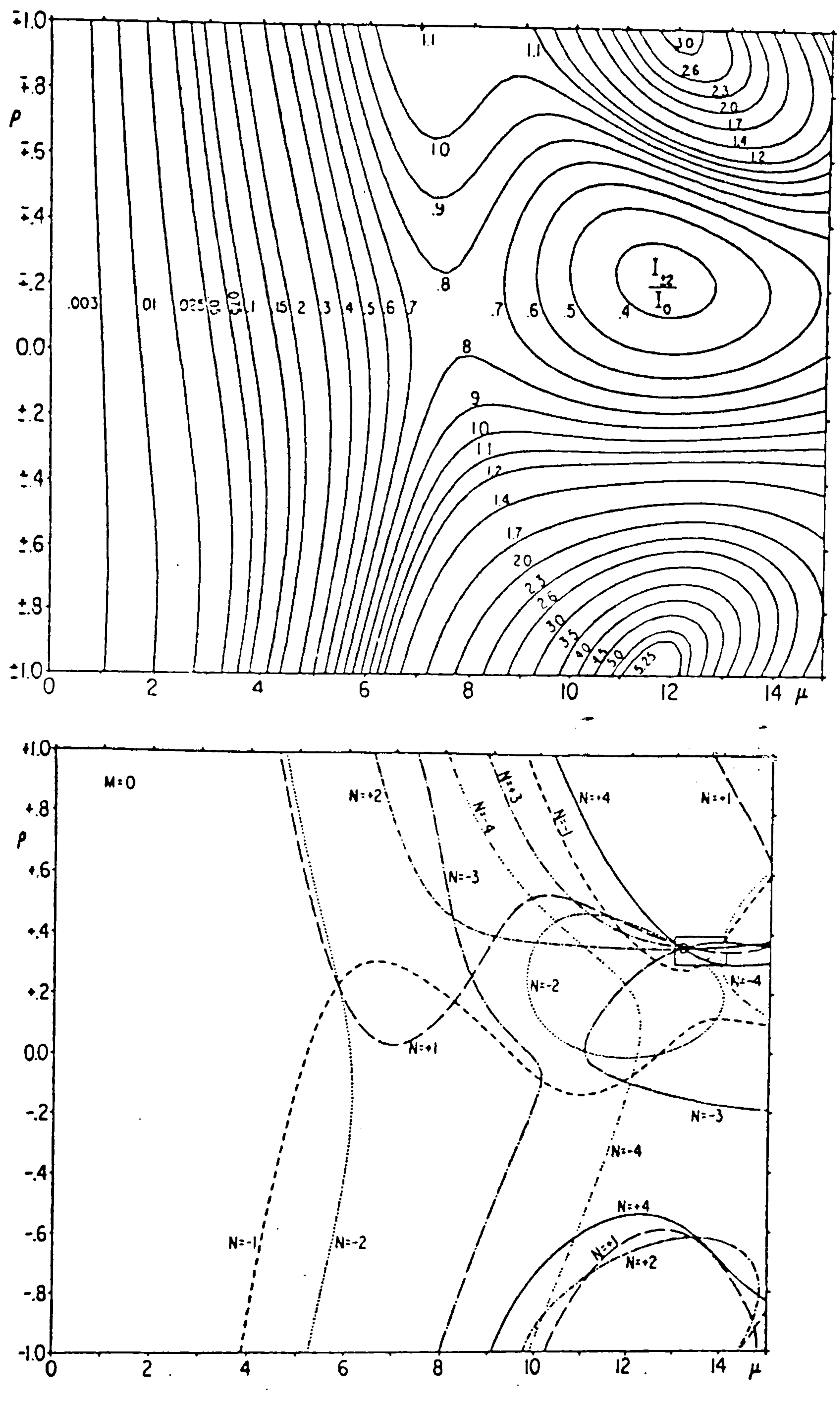

Figure 4.6: Top: example of a contour plot used in the graphical method. Bottom: resulting trace showing the crossing point (circle) and estimated error (rectangle). From reference 6.

difficult to pinpoint.

Secondly, the contour plots which are provided limit the analysis to a maximum of ten sidebands. For heavy metal nuclei, such as tin-119 and platinum-195, shielding anisotropies are very large and often give rise to upwards of thirty sidebands. In using the graphical method to analyse such a case, one would be using only a third of the available information. It would seem sensible to include as many of the sidebands in the calculations as is possible.

A third difficulty was found during the analysis of the data for Chapter 6 of this thesis. In a number of cases where the tensor pattern is clearly nonaxial, the combination of parameters placed the plots in the region where $\mu \leqslant 5$. In this region, all of the contour plots behave very similarly to that of the plot illustrated in the top of Figure 4.6. The resulting traces had many parallel or near-parallel lines in which there were regions of crossings rather than distinct points. In such traces it was very difficult to determine an exact crossing point.

Finally, there are often a number of crossing points from which to choose. One usually chooses the crossing point with the largest number of lines converging on it; however, it is sometimes necessary to calculate the tensor parameters for several points and then choose the set which makes the most sense in terms of the spectrum at hand.

4.5 Description of Spinning-Sideband Spectra

Given the overall limitations of the methods discussed so far for the determination of shielding tensor components, it was felt that a more reliable method should be found. The most obvious way seemed to be a computerized simulation and subsequent fitting of the experimental spectrum with a calculated spinning-sideband pattern. During the course of this work, a paper was published by Clayden *et al.*[7] which recounted the shortcomings which had been found in the moments and graphical methods. This work, then, went on to show the advantage of the use of simulations to evaluate whether the derived tensor components accurately represented the experiment and to further refine the estimate of the tensor components. The use of a computer program to actually fit a spinning-sideband spectrum has been noted by Ellis and co-workers[8,9]; however, no description of the program was given.

In order to simulate and fit a spinning-sideband spectrum, a mathematical description of such a spectrum is necessary. The complete derivation of the expression for the spectrum of a powder sample spinning at the magic angle has been given by several authors[5,6] and will not be repeated in detail here. A discussion of the resulting expresssions is, however, necessary for the understanding of the source of spinning sidebands and will be undertaken below. It should be noted that this author found the work of Munowitz and Griffin[17] to be particularly helpful in the understanding of this topic.

One will take as a beginning the Hamiltonian for a sample which contains a single type of chemically distinct nucleus, and which is rotating about the magic angle. In the absence of other interactions, this Hamiltonian will have the form (expression 23 in reference 5):

$$\hat{H} = \gamma B_o I_z[\bar{\sigma} + \delta\xi(t)], \qquad 4.14$$

where γ, B_o and I_z have their usual meanings, and where $\bar{\sigma}$ is the isotropic trace of the shielding tensor, δ is the shielding anisotropy and $\xi(t)$ contains the time-dependent relationships induced by the spinning of the sample. Before continuing, we must examine the form of $\xi(t)$ in more detail.

The derivation of the $\xi(t)$ term is a result of the operations necessary to translate the interactions from the laboratory frame into the frame of the principal axis system (PAS) of the tensor. Since we must also take into consideration the fact that the sample is in a rotor which is spinning at the magic angle, two separate transformations are necessary. The first transformation is from the laboratory frame to a rotor-fixed frame and the second from the rotor frame to the PAS. In the first transformation, only two angles are necessary due to the invariance of $\hat{H}$ to rotations about B_o. The two angles are θ, the angle between B_o and the rotor axis, and $\omega_r t$, the time (t) varying azimuth of the x axis of the rotor fixed frame with respect to B_o. (θ in this instance will be the magic angle; ω_r is the angular spinning speed.) The second transformation requires the usual Euler angles α, β and γ. Subsequent rotations of γ about z_r, β about y_r, and α about z_r map the rotor frame onto the PAS. (The subscript r refers to the rotor-fixed axis system.)

$\xi(t)$ has the form noted below[5,6]:

$$\xi(t) = C_1\cos(\omega_r t) + S_1\sin(\omega_r t) + C_2\cos(2\omega_r t) + S_2\sin(2\omega_r t) \qquad 4.15$$

where

$$C_1 = \tfrac{1}{2}\sin2\theta\sin\beta[\cos\beta(\eta\cos2\gamma - 3)\cos\alpha - \eta\sin2\gamma\sin\alpha]$$

$$S_1 = \tfrac{1}{2}\sin2\theta\sin\beta[\cos\beta(3 - \eta\cos2\gamma)\sin\alpha - \eta\sin2\gamma\cos\alpha]$$

$$C_2 = \tfrac{1}{2}\sin^2\theta\{[3/2\sin^2\beta + (\eta/2)\cos2\gamma(1 + \cos^2\beta)]\cos2\alpha - \eta\cos\beta\sin2\gamma\sin2\alpha\}$$

$$S_2 = \tfrac{1}{2}\sin^2\theta\{-[3/2\sin^2\beta + (\eta/2)\cos2\gamma(1 + \cos^2\beta)]\sin2\alpha - \eta\cos\beta\sin2\gamma\cos2\alpha\}.$$

All of the variables have been described in the text directly above except for η which is the asymmetry parameter mentioned previously in this chapter.

In order to develop a physical picture of the significance of $\xi(t)$ in expression 4.14, it is useful to recall the origins of a static powder spectrum. In a static powder, the precession frequency of a specific crystallite is dependent upon its orientation with respect to the static B_o field. This spatial dependence follows directly from the anisotropic nature of the shielding. The spectrum of the complete powder is simply a superposition of the contributions from all of the crystallites in the powder.

In the case of magic-angle spinning, a further time dependence is added to the spatial dependence noted above. This time dependence arises because the instantaneous precession frequency of a specific crystallite will change as the crystallite samples different orientations with respect to B_o during the course of its rotation. This is again a direct result of the anisotropic nature of the chemical shift. It will thus be seen to be necessary to evaluate the time integral of expression 4.17 to predict the behavior of such a crystallite.

Taking equation 4.14 and converting to frequency terms, the angular frequency of the k^{th} crystallite as a function of time will be:

$$\omega_k(t) = \omega_o\bar{\sigma} + \omega_o\delta\xi_k(t), \qquad 4.16$$

where ω_o is the larmor precession frequency. Now, if a specific crystallite accumulates a phase angle, ϕ, from its original orientation in a time, t, the required time integral is:

$$\phi_k(t) = \int_0^t \omega_k(t')dt' = \omega_o\bar{\sigma} + \omega_o\delta\eta\int_0^t \xi_k(t')dt' \qquad 4.17$$

Given that the free induction decay is represented by:

$$g(t) = \exp[\,i\phi_k(t)]$$

then the free induction decay of the spinning-sideband spectrum will be represented by:

$$g(t) = \exp(i\omega_o\bar{\sigma}t) \times \sum_k \exp[\,i\omega_o\delta\int_0^t \xi_k(t')dt'\,]. \qquad 4.18$$

The summation over all k is required to produce the complete spectrum. From the above spectrum, it is clear that each crystallite, k, will have its own spinning sideband pattern. This spectrum is, of course, a set of sidebands centred about the isotropic chemical shift. The shape of the spinning-sideband manifold is governed by that of the envelope of the static powder pattern and will approach it in the slow-spinning limit.

Returning to the concept of the phase angle, ϕ, aspects of the FID represented by the equation above can be described. At the beginning of the experiment, magnetization will be produced in the sample by one of the usual means. As the sample turns, however, this magnetization will dephase because of the fact that the different crystallites will experience continuously changing local fields resulting from the orientation dependence noted above. At the end of one rotor period, however, the total phase angle accumulated by any crystallite must be zero (everything will be back where it started from!) The magnetization will then be restored. The complete FID will thus be a characteristic series of rotational echos[5]. The intensity of sucessive echos will, of course, be governed by the normal T_1 and T_2 processes so that the FID will decay exponentially in the usual fashion. Additionally, the fact of the periodicity of these echos implies that all of the tensor information for the system is carried in one of these rotary echos. This is an important point for the simulation process in that it means that one need only sample the first echo (i.e. $t = 0$ to $t = 2\pi/\omega_r$ in equation 4.18 above) to get a complete description of the time averaging in the system.

To summarize the previous paragraph, all of the frequency and intensity information for the sideband envelope is contained in any one of the rotary echos. The full decay envelope of the train of echos will determine the linewidth of the sidebands.

At this point in the argument, both of the two main sources of the derivations of the sideband expressions resort to rather complicated Fourier and Bessel mathematics to describe the spinning sidebands themselves and the functions which govern their intensities. It is perhaps more useful here to try and describe a physical picture of what is going on as opposed to repeating the mathematics. It should be understood, though, that the exact shape of the spinning-sideband manifold is a complicated function of a number of variables as expressed in equations 4.14 and 4.15. There is no simple relationship from which one can calculate the intensities of a set of sidebands. One can, however, develop some understanding of spinning sidebands in relation to the static powder pattern and discuss the deviation of the sideband envelope from the powder pattern shape.

In the most simple vein, the production of spinning sidebands may be seen to be a straightforward modulation in the sense of audio or radio frequency electronics. For example, a 10 MHz carrier frequency modulated by a 1 kHz sine wave will have a centreband at 10 MHz and sidebands at 10.001MHz and 9.999MHz. In the case of NMR, one is dealing with a band of frequencies which is the static spectrum modulated with a single fixed frequency which is the spinning frequency. The resulting spectrum in such a case is simply a series of sidebands spaced at the spinning frequency having intensities which will resemble, in some manner, the shape of the envelope of the static spectrum.

The exact shape of the spinning sideband manifold will be a complicated function of expression 4.18 above. Given a finely divided powder which is spinning at the magic angle, the resulting spectrum will be dependent on the asymmetry, the anisotropy, the isotropic chemical shift and the spinning speed represented by η, δ, $\delta_{\times}$ and v_r respectively. For a particular sample, the first three of these parameters will be fixed for each of the chemically and crystallographically distinct environments within the sample. Given such a sample, the resulting sideband spectrum will vary as a function of v_r.

Looking first at the slow-spinning extreme, as $v_r \to 0$, the limit of the spinning-sideband manifold is, of course, the static spectrum. At the other extreme where $v_r \gg \Delta$, the static bandwidth, a single line at the isotropic chemical shift will result.

The intermediate case where $v_r \leqslant \Delta$, is much more complicated to explain than either of the two extremes. The spinning-sideband envelope will have the rough shape of the static spectrum but will not exactly mimic it. This may be seen by examining Figures 4.2

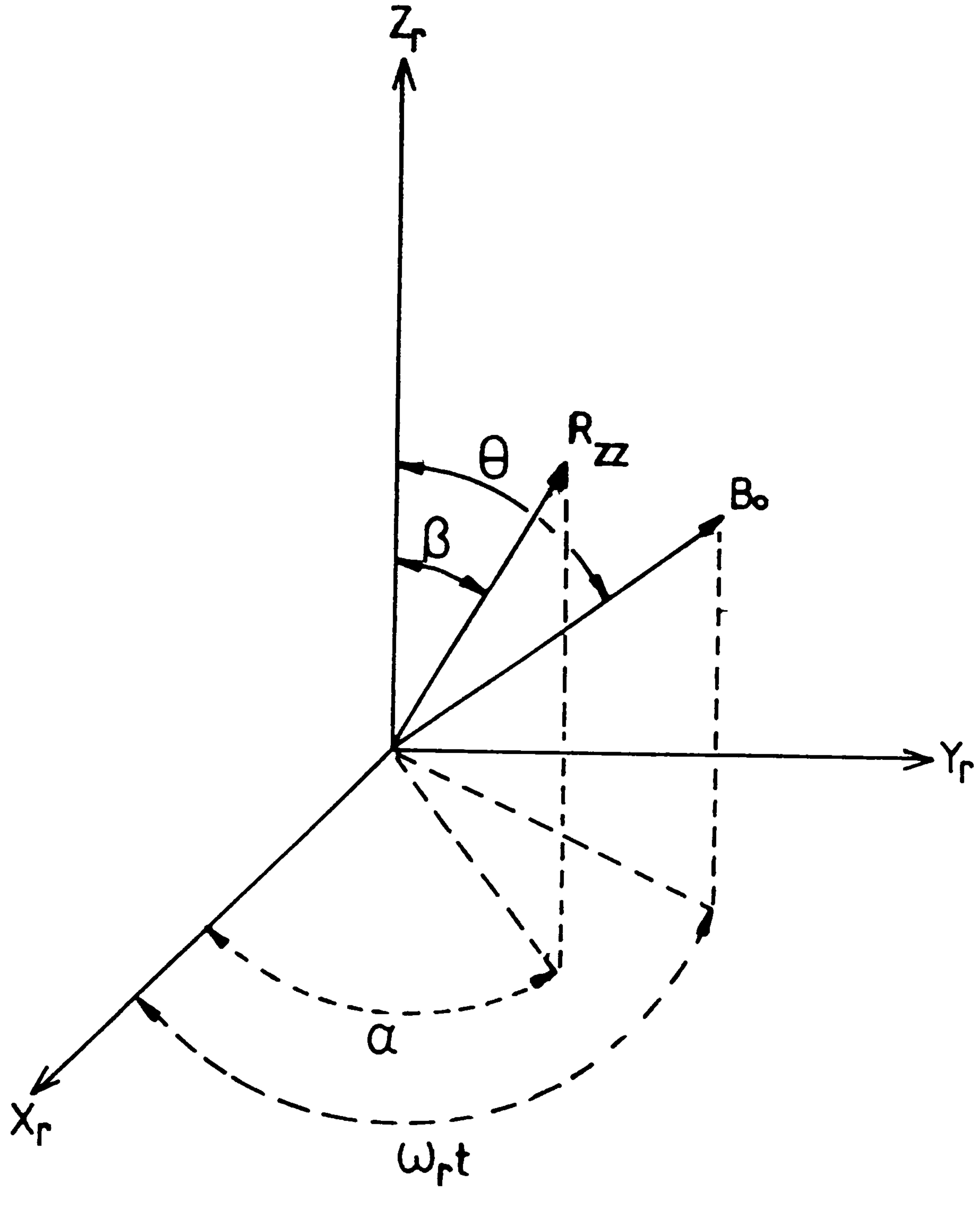

Figure 4.7: The orientation of the unique tensor axis R_{zz} and the static magnetic field B_o in a frame of reference fixed in the sample rotor. The Z_r axis is colinear with the rotor axis of rotation.

and 4.3. The fact that it does not exactly follow the static spectrum may be explained by resorting to two main arguments relating the static and spinning cases.

For both of these arguments, it is useful to use as a model a single crystallite in a powder. The orientation of this crystallite in the rotor will be defined by two angles, α and β, which refer to the position of the unique tensor axis in the rotor frame at the start of the experiment. (See Figure 4.7). β is defined as the angle between the z_r rotor axis (the axis of rotation) and the unique tensor axis r_{33}. The angle, α, will represent the projection of r_{33} in the rotor xy plane. The sum ($\alpha + \omega_r t$) will thus indicate the position of r_{33} with respect to the B_o field as a function of time.

For the first of the two arguments, one need only be concerned with the angle β. In the experiment, as the crystallite is rotated about the rotor axis which was stated to be at the magic angle, θ, it will cover angles ($\theta - \beta$) through to ($\theta + \beta$) with respect to B_o. It will thus have instantaneous frequencies which will sweep out only a portion of the full static bandwidth. This is illustrated in Figure 4.8.A. Of course, crystallites with a larger value of β will sweep out a larger portion of the static bandwidth. It may be seen that as a specific crystallite produces frequencies only within a given range, it cannot contribute intensity to sidebands which are outside of that range. It will, however, contribute intensity to all sidebands within its specific frequency range.

The result of this may be summarized as follows: 1) The intensity of a given sideband will be the sum of the intensities from all of the crystallites which sweep out frequency regions which contain the frequency of that sideband. 2) Not all crystallites will contribute to all sidebands.

The most straightforward example of this second point may be illustrated if one considers a crystallite oriented parallel to the magic angle (i.e. $\beta = 0$). Such a crystallite will give rise only to intensity at the centreband and nowhere else.

The consequences of this argument regarding the question of the deviation of the sideband envelope from the static bandshape

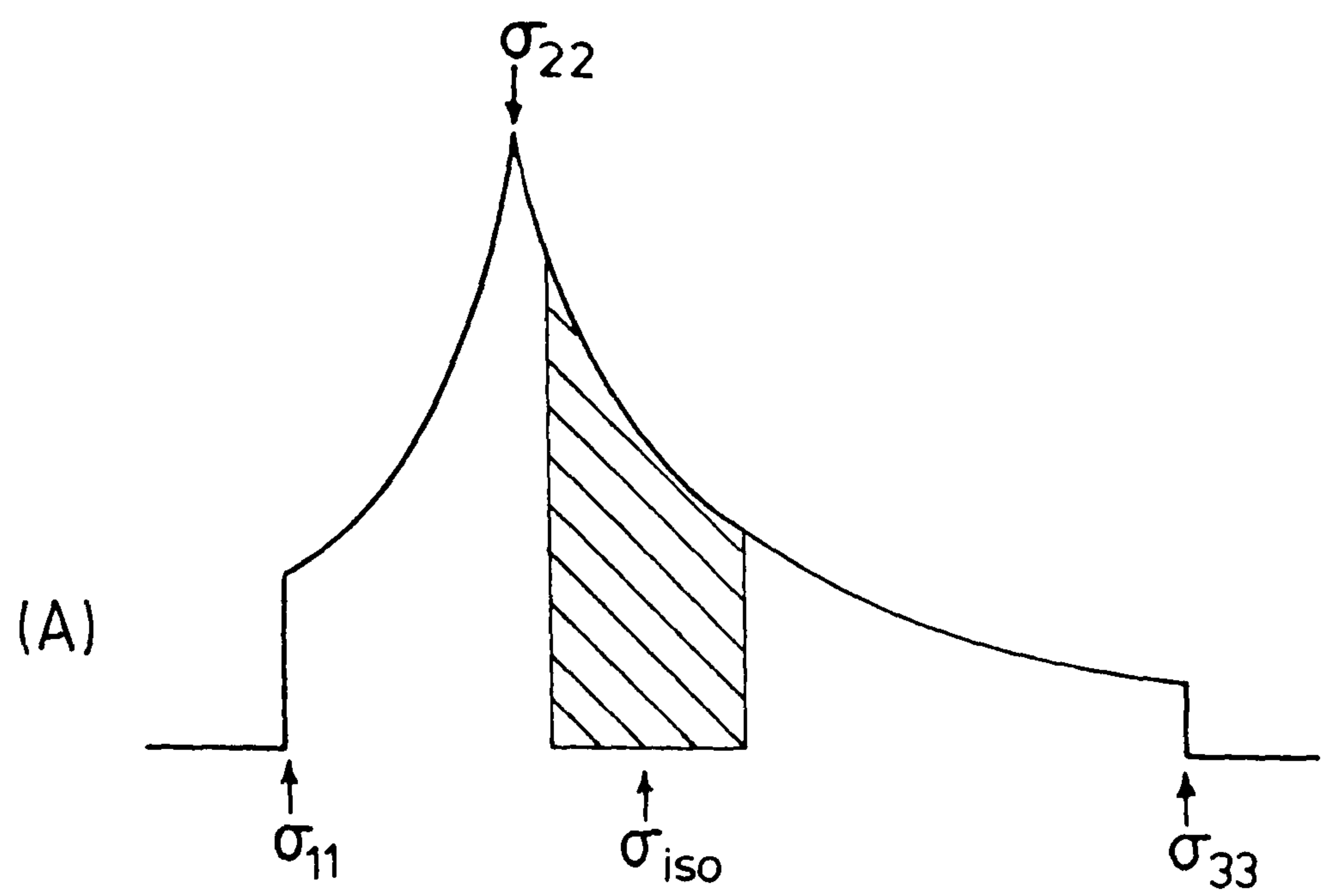

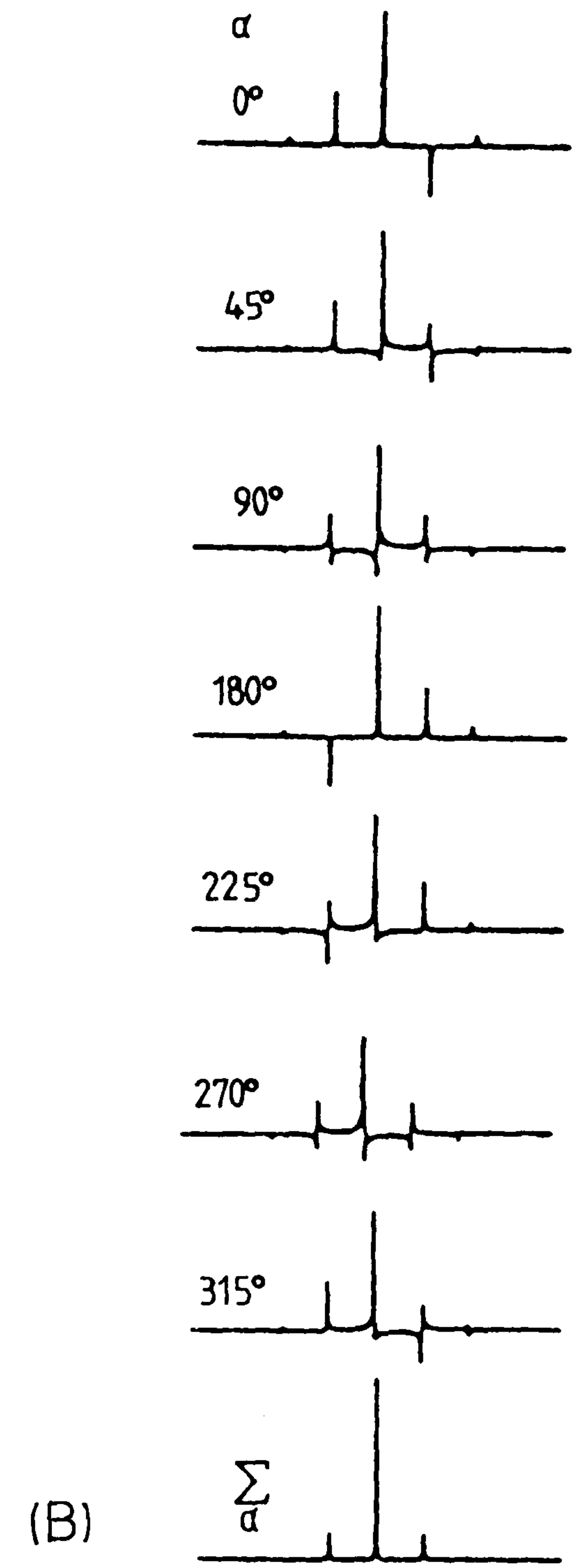

Figure 4.8: (A) Frequency region swept out by an arbitrary unique shielding tensor axis which makes an angle β with the rotor axis.
(B) Hypothetical calculated magic-angle spectra for an individual crystallite with initial tensor orientations α . The model chosen was an axially symmetric tensor and a spinning rate of 2.5 kHz. Note that the phases of the spinning sidebands depend on the initial orientation α, though a sum over all α produces a pure adsorption mode spectrum. 4.8.B was adapted from reference 17.

may be seen as follows. In a static powder pattern, the intensity at a given frequency is proportional to the number of crystallites which have a specific orientation in the powder. That is to say, there is a one-to-one correspondence between a specific orientation in the powder and a specific frequency in the spectrum. In contrast for the spinning case, it has been shown that there is a many-to-one relationship in that a number of crystallites having a spread of instantaneous frequency spectra can contribute to a sideband of specific frequency. One should not, thus, necessarily expect the static and spinning cases to give identical envelope shapes.

A second related factor governing the source of spinning sidebands may be seen by examining the results of Munowitz and Griffin[17]. (See Figure 4.8.B which was adapted from that reference.) Referring again to the model described above, attention is now centred on the angle, α, which describes the orientation of the r_{33} axis with respect to the B_o field. For an individual crystallite at a given β, the phase of the sidebands produced by that crystallite will be a function of the initial orientation α. Both adsorptive and dispersive components will be found depending on the value of α at the beginning of the experiment. Now, as may be seen from Figure 4.8.B, the sum over all values of α is a pure adsorption signal. In a rapidly rotating powder, this sum results from both asynchronous data acquisition and from the random α values found for all crystallites with orientation β.

The manner in which this causes the difference between the static and the spinning-sideband envelope is similar to the previous argument. In a static powder pattern, crystallites with identical orientation and having identical adsorption/dispersion characteristics will contribute to a specific frequency in the spectrum. In the spinning case, the intensity at a given frequency (sideband) will be governed by a multiplicity of crystallites with different orientations. Each of these crystallites will have differing adsorption/dispersion components which will add to give the final spectrum. Again, this spectrum will not be expected to exactly follow the static manifold.

4.6 Simulation of a Spinning-Sideband Spectrum

After that somewhat lengthy explanation, let me again return to the main purpose which is the simulation and fitting of spinning sideband spectra.

The necessary expression describing the spectrum of a powder sample spinning at the magic angle has been given as equation 4.18. For the purposes of computation, the initial exponential term may be dropped. This term only serves to give an overall offset to each spinning sideband which is equivalent to placing the centreband at the isotropic shift frequency . This may be done straightforwardly after the spectrum is generated, and elimination of this term speeds the simulation process. The sum on k is replaced by the sum over the Euler angles α, β and γ. Summing over these angles from 0 to π will give the required spatial averaging noted above. The resulting expression for the FID is given by:

$$g(t) = \sum_{\alpha}\sum_{\beta}\sum_{\gamma} \exp[\,i\omega_o\delta\int_0^t \xi(\alpha,\beta,\gamma,t')dt'\,]. \qquad 4.19$$

The complete expansion of this expression necessary for numerical evaluation is not given in any of the references. It may be found in Appendix 1.

The limits of the integral need only be 0 to $1/\nu_r$ as noted above. Further, sampling the number of points, N, which is equal to the number of expected sidebands (or the spectrum width divided by the spinning speed which amounts to the same thing) satisfies the Nyquist[18] criterion and simplifies peak picking in the following fitting routine. Such sampling is accomplished by evaluating the integral in equation 4.19 in $N(1/\nu_r)$ steps.

The resulting computer program for producing a stick-plot simulation of the intensities of a MAS spectrum may be found in Appendix 2. In general terms the program works as follows:

1) Input values of δ, η, $\bar{\sigma}$, ν_r, N, and ν_o. ν_o is the larmor frequency of the nucleus in question.

2) Generate the free induction decay by evaluating equation 4.19. For each value of α, β and γ, the integral of the last term in the equation is evaluated. Noting the relationship, $\exp[i\theta] = \cos\theta + i\sin\theta$, the sum of cos(g(t)) and sin(g(t)) for all possible α, β and γ will represent the real and imaginary components of the free induction decay respectively.

3) Normalize the FID and then perform the Fourier transform using Numerical Algorithms Group routine C06FCF[19]. This produces the frequency domain stick plot. The normalization is carried out to prevent overflow during the FT.

4) Normalize the intensities of the spinning sidebands. Output a listing of intensities and a plot of the spectrum.

The choice of a stick-plot spectrum was made mainly for reasons of speed. For the fitting routine, a large number of spectra must be calculated, and any unnecessary operations were eliminated. The general method for adding linewidth to the lines of the spectrum would simply make all spinning sidebands the same width and not add any new information to the system. The stick-plot spectrum gives the relative intensities of the sidebands, which is really all that is required.

One important consideration which has not yet been discussed is the number of orientations (NOR) through which the Euler angles (α, β and γ) must be stepped in order to insure the proper spatial averaging. This is important from the computational standpoint in that the ultimate number of orientations will be NOR^3. Clearly, it is important to use as small a number as possible to keep computer time to a minimum while still retaining accuracy of the computed

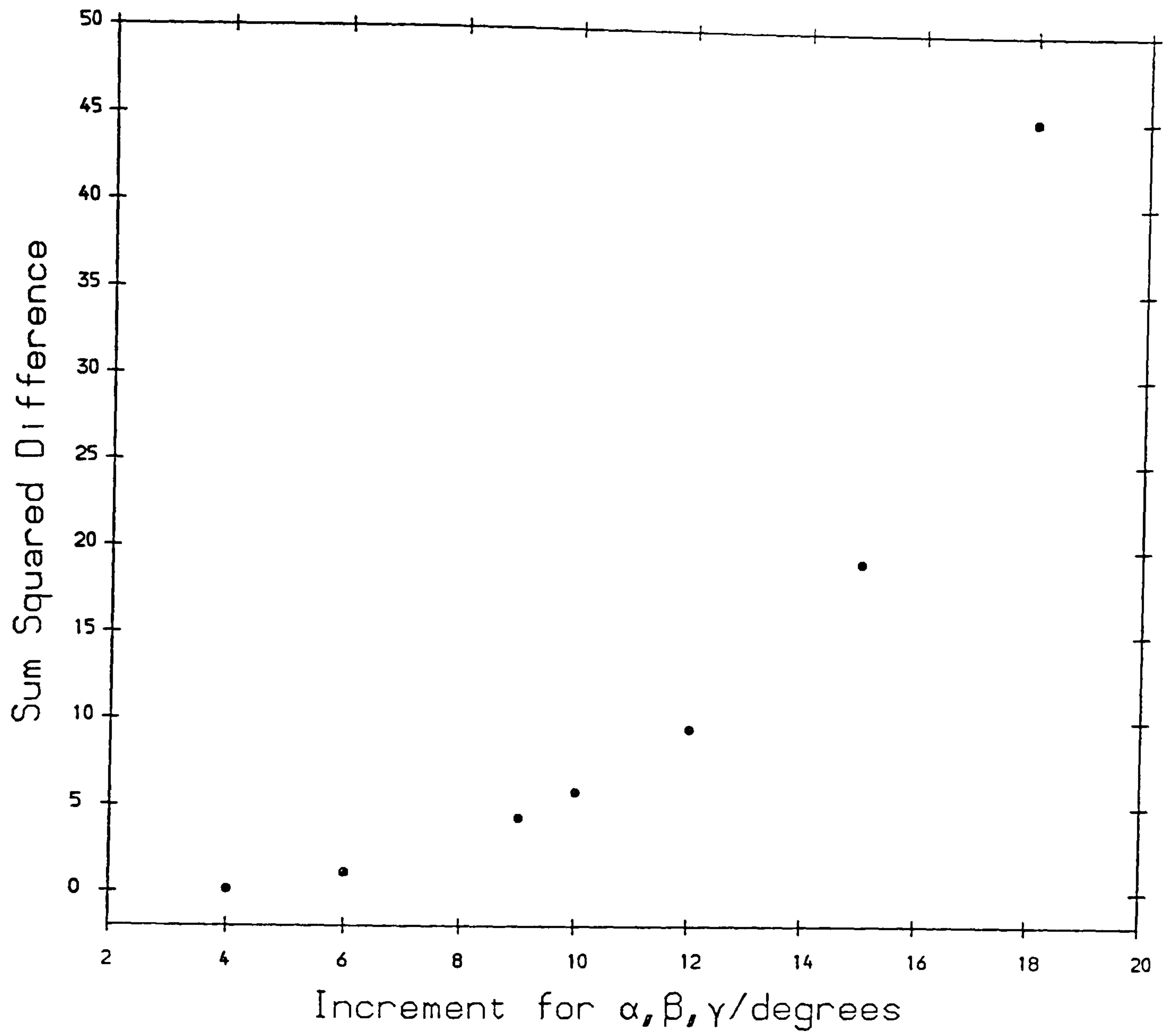

Figure 4.9: Convergence of the spinning-sideband simulation program as a function of the the size of the increment used to step the Euler angles.

result. Fortunately, NOR converges to a reasonable extent at 20 orientations. This amounts to stepping each of the angles in 9° increments. The convergence may be seen in Figure 4.9.

An example of this simulation program may be seen in Figure 4.10. Here a series of plots have been generated which demonstrate the appearance of spectra from $\eta = 0$ to $\eta = 1$ for a constant, moderate value of anisotropy for phosphorus, and a relatively slow spinning speed. Note that if the anisotropy were to be positive, the sidebands in a given spectrum would have the same intensity ratio but would be reflected through the centreband.

4.7 Spinning-Sideband Spectrum Fitting Program

Once the sideband simulation program has been set up, creating a program to iteratively fit a given experimental spectrum is straightforward. Given fixed values for the spinning speed and chemical shift, the anisotropy, δ, and asymmetry, η, will describe a spinning sideband spectrum. Starting from likely values of η and δ, an evaluation is made of the difference between the experimental and simulated spectrum. The fit is determined by varying δ and η until this difference reaches an absolute minimum. The FORTRAN 77 program which incorporates these features may be found in Appendix 3.

The criterion chosen to represent the difference between the experimental and simulated spectra is the sum of the squares of the difference between the intensities of the corresponding sidebands. There are a number of precedents in the literature for the use of this parameter in fitting static spectra[11,20]. If IC_n and IE_n represent the intensities of the n^{th} calculated and experimental sideband respectively, then the difference between the spectra may be represented by:

$$SSQ = \sum_{n} (IC_n - IE_n)^2 \qquad 4.20$$

Figure 4.10: Example of the simulation routine. A series of η values is shown for fixed values of δ and ν_r. The progression of the shape of the spinning-sideband envelope from axially symmetric through to completely asymmetric is illustrated.

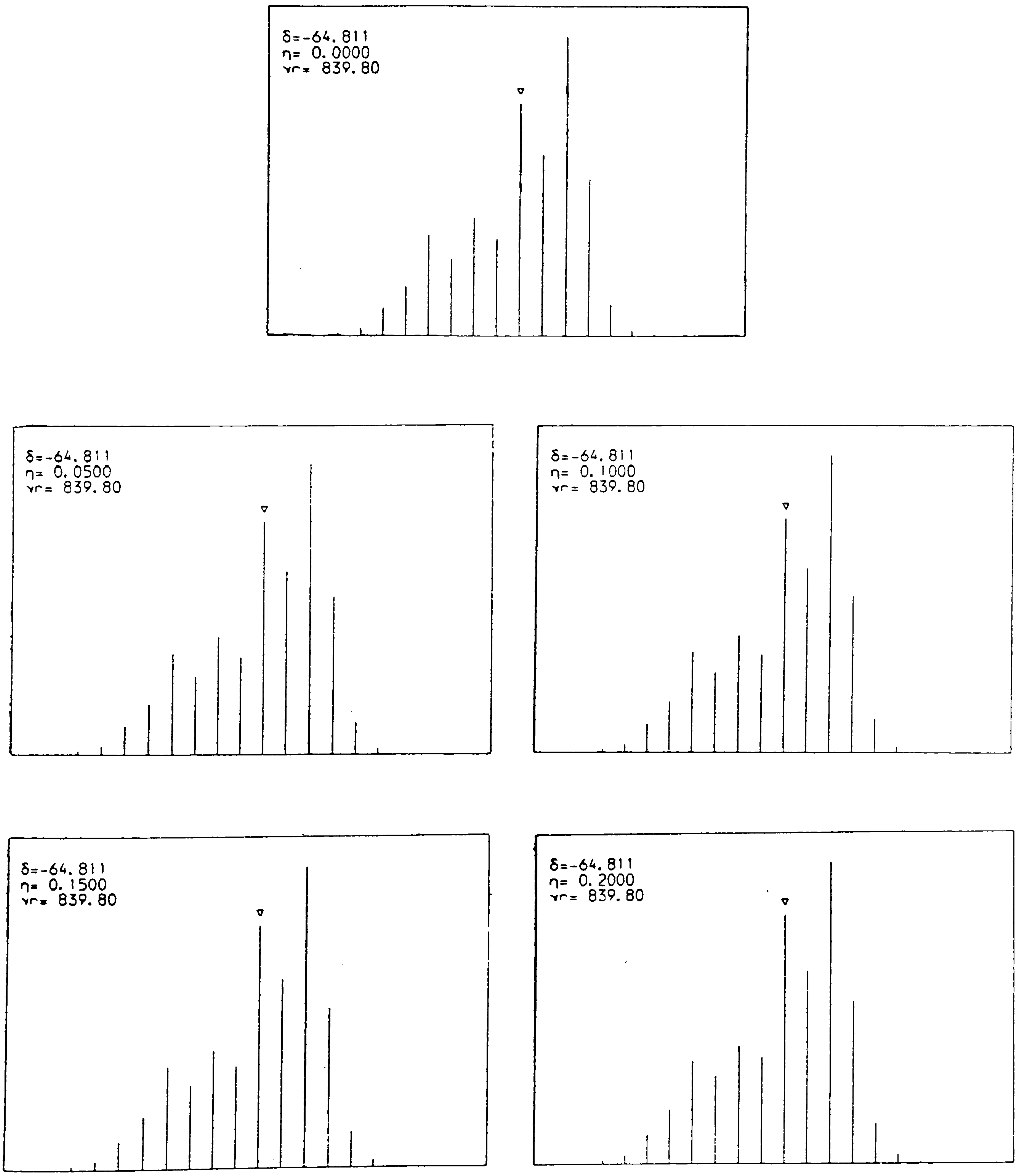

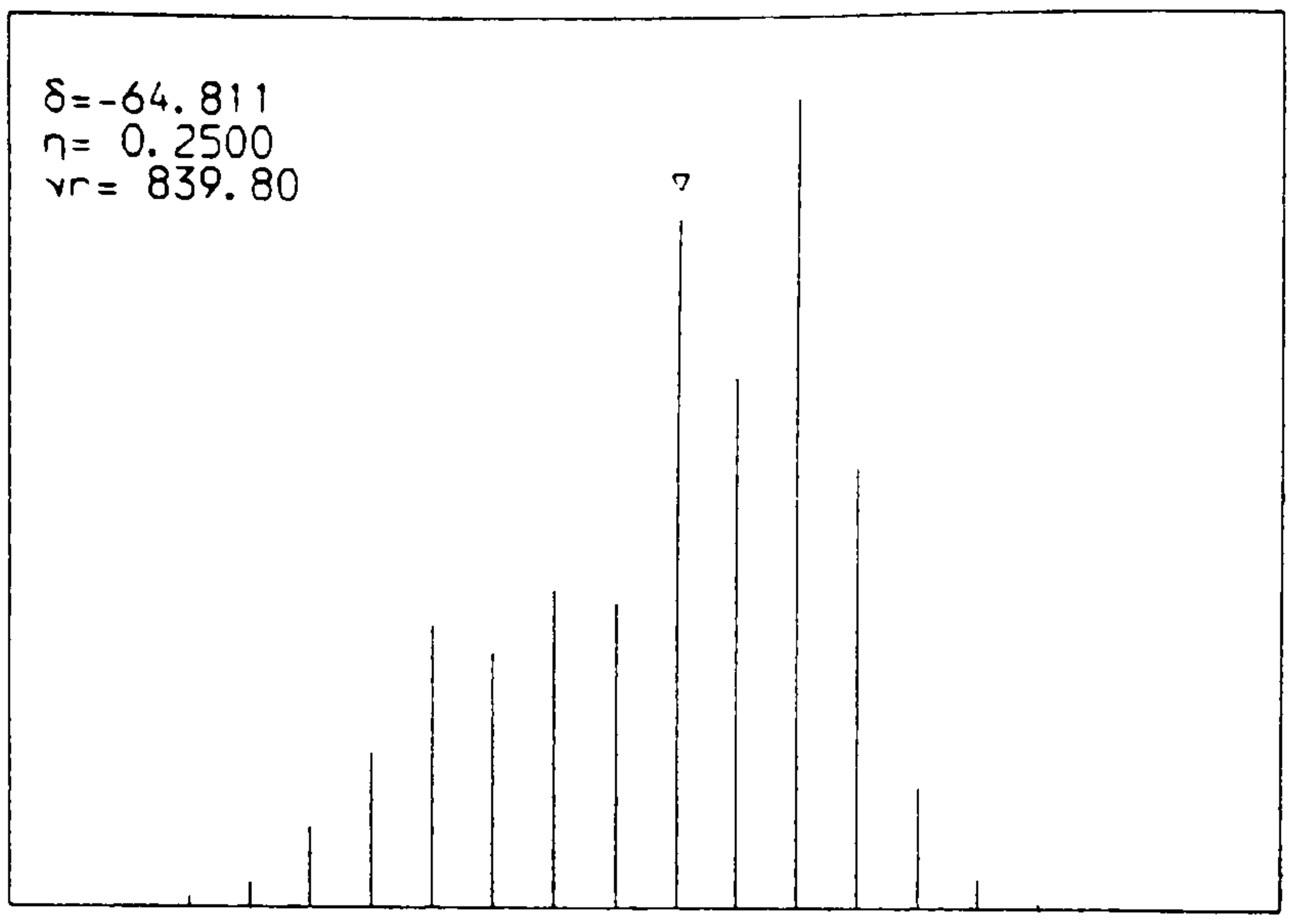
δ=-64.811
η= 0.2500
vr= 839.80

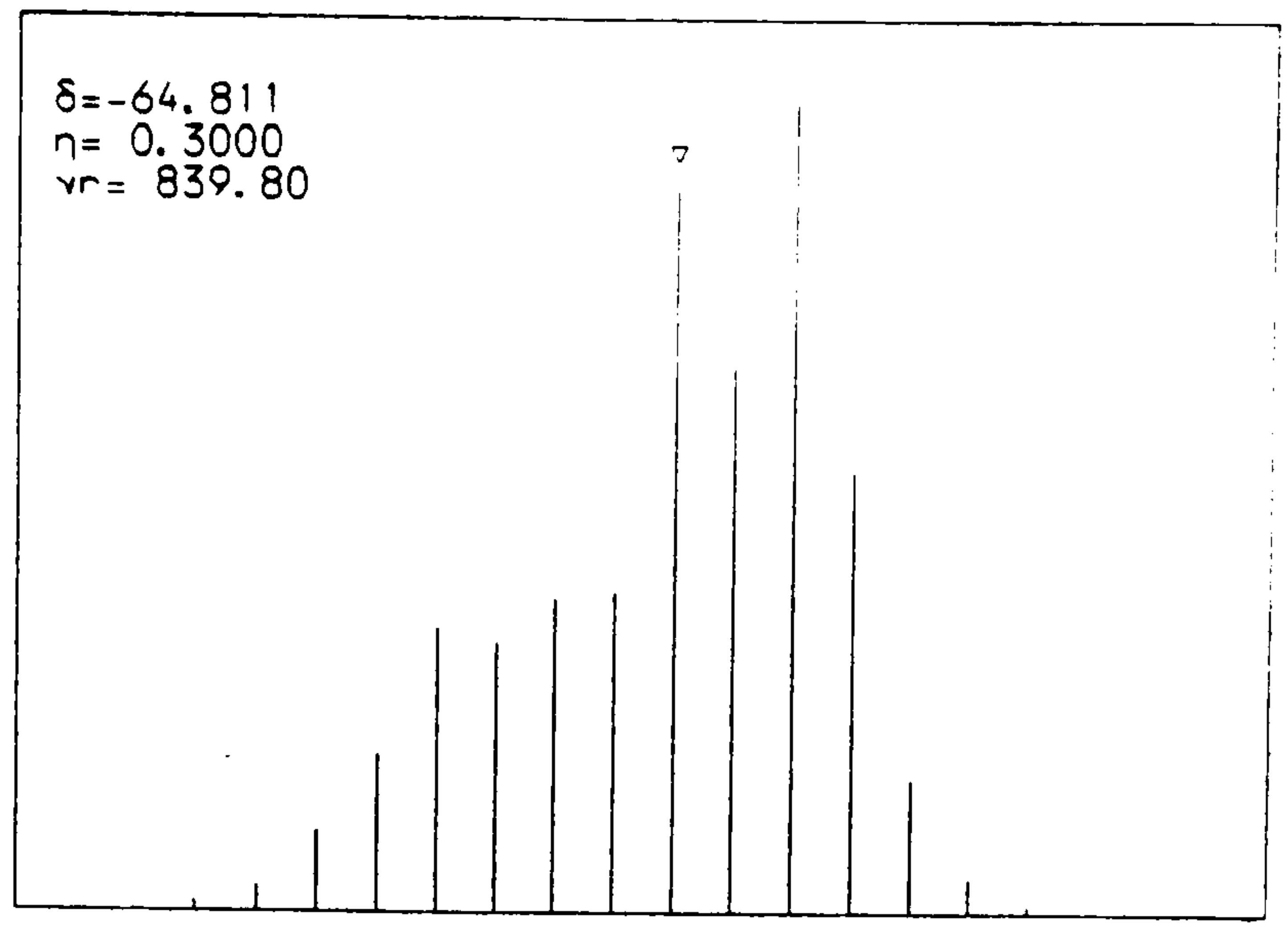
δ=-64.811
η= 0.3000
vr= 839.80

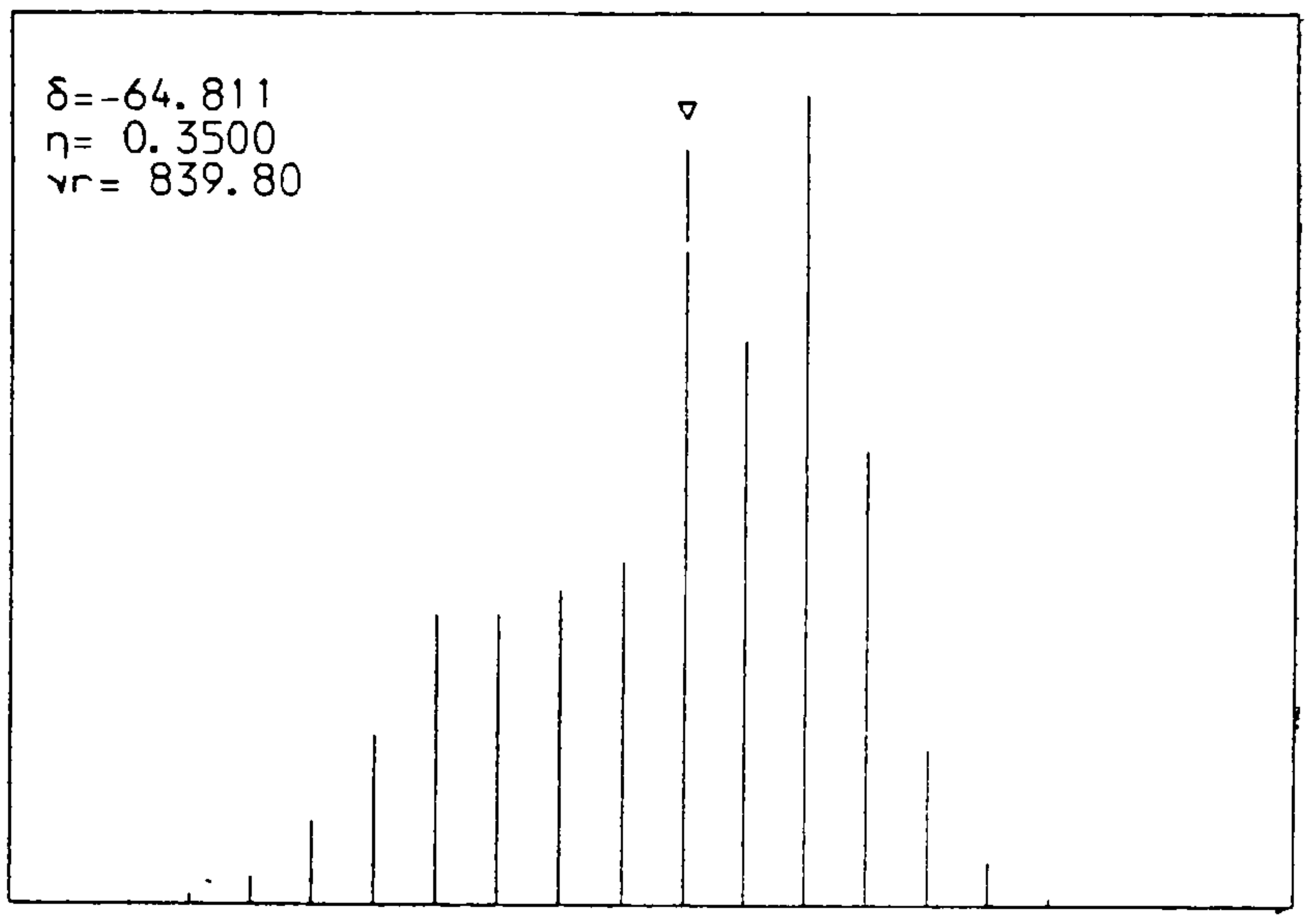
δ=-64.811
η= 0.3500
vr= 839.80

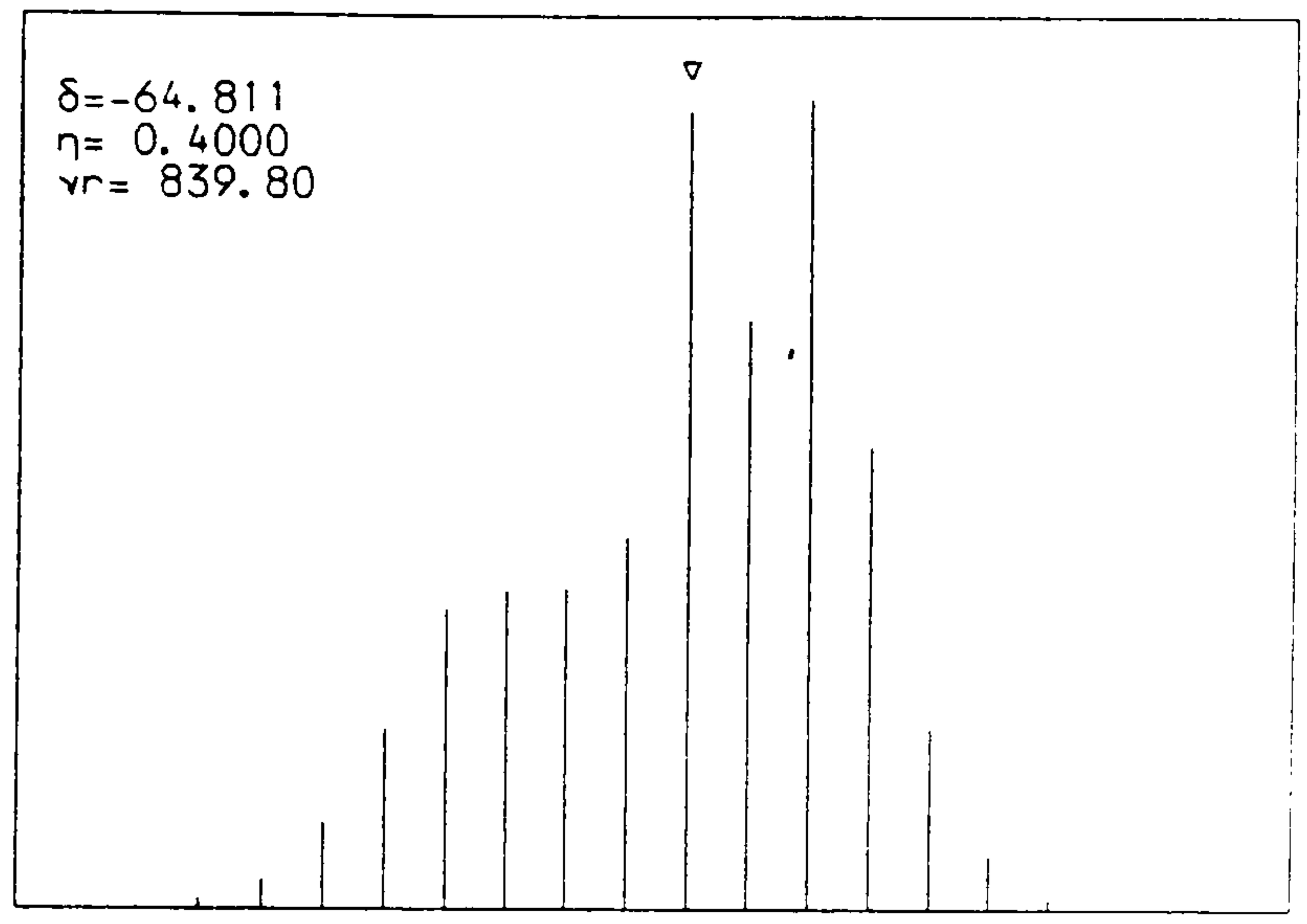
δ=-64.811
η= 0.4000
vr= 839.80

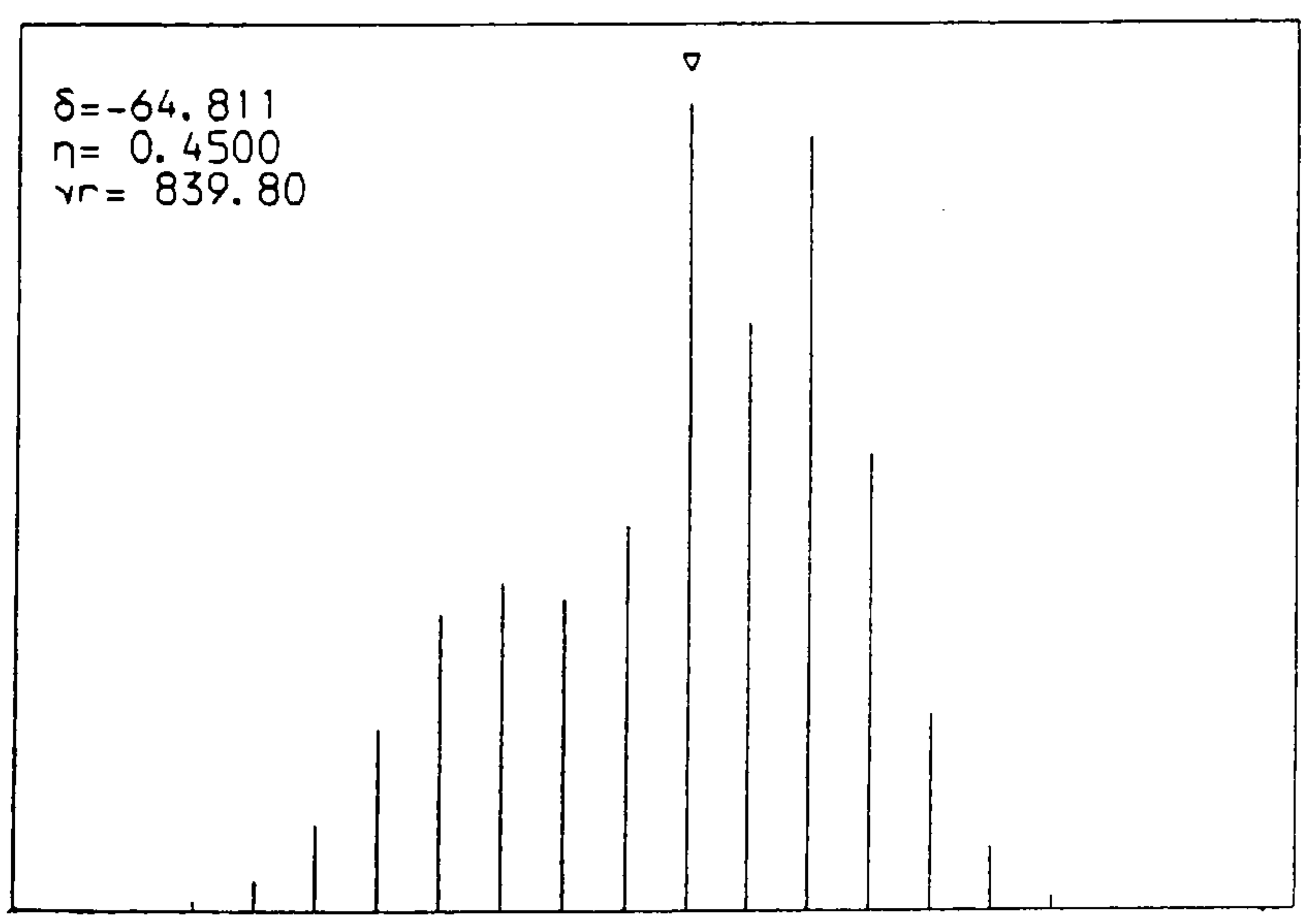
δ=-64.811
η= 0.4500
vr= 839.80

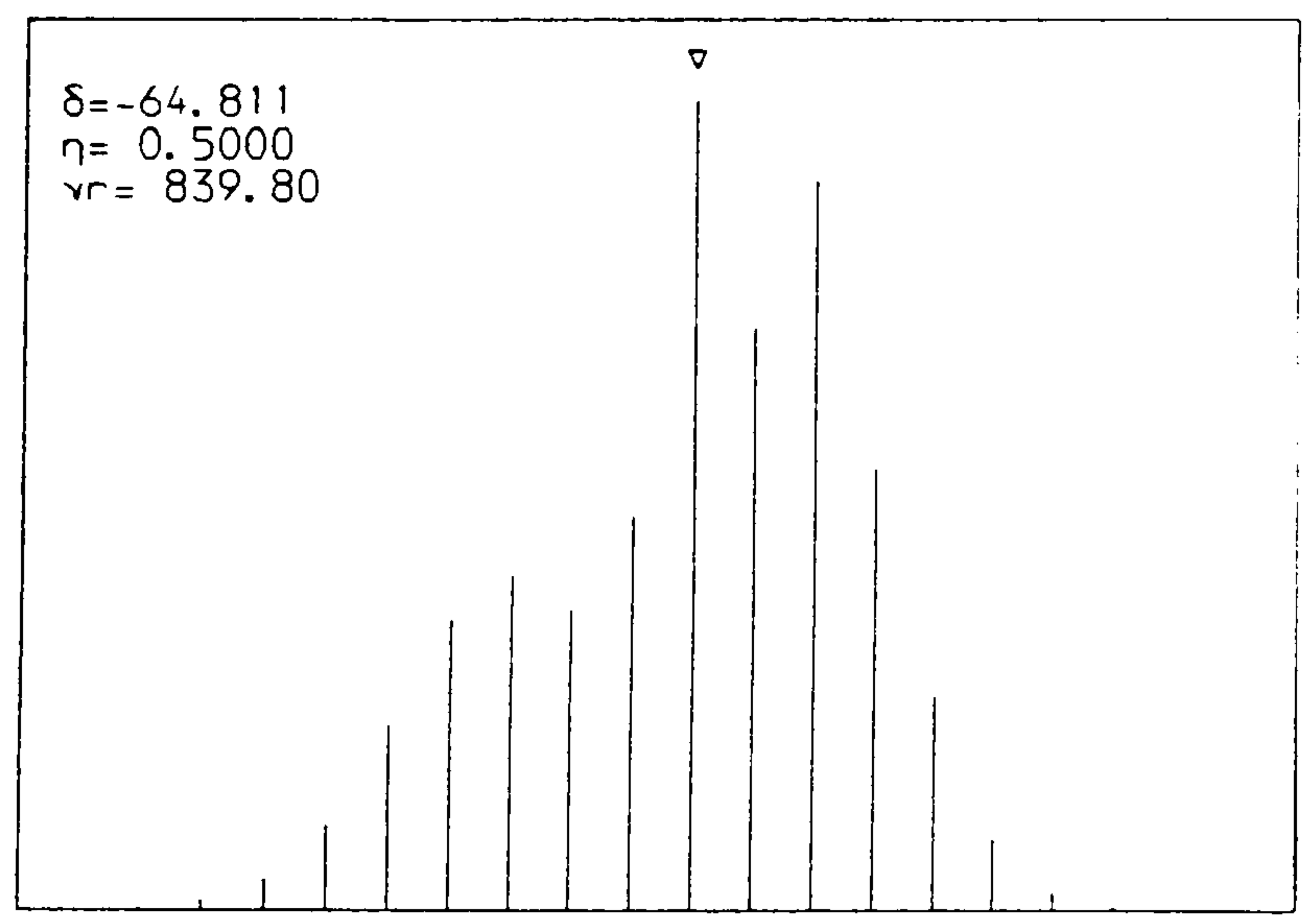
δ=-64.811
η= 0.5000
vr= 839.80

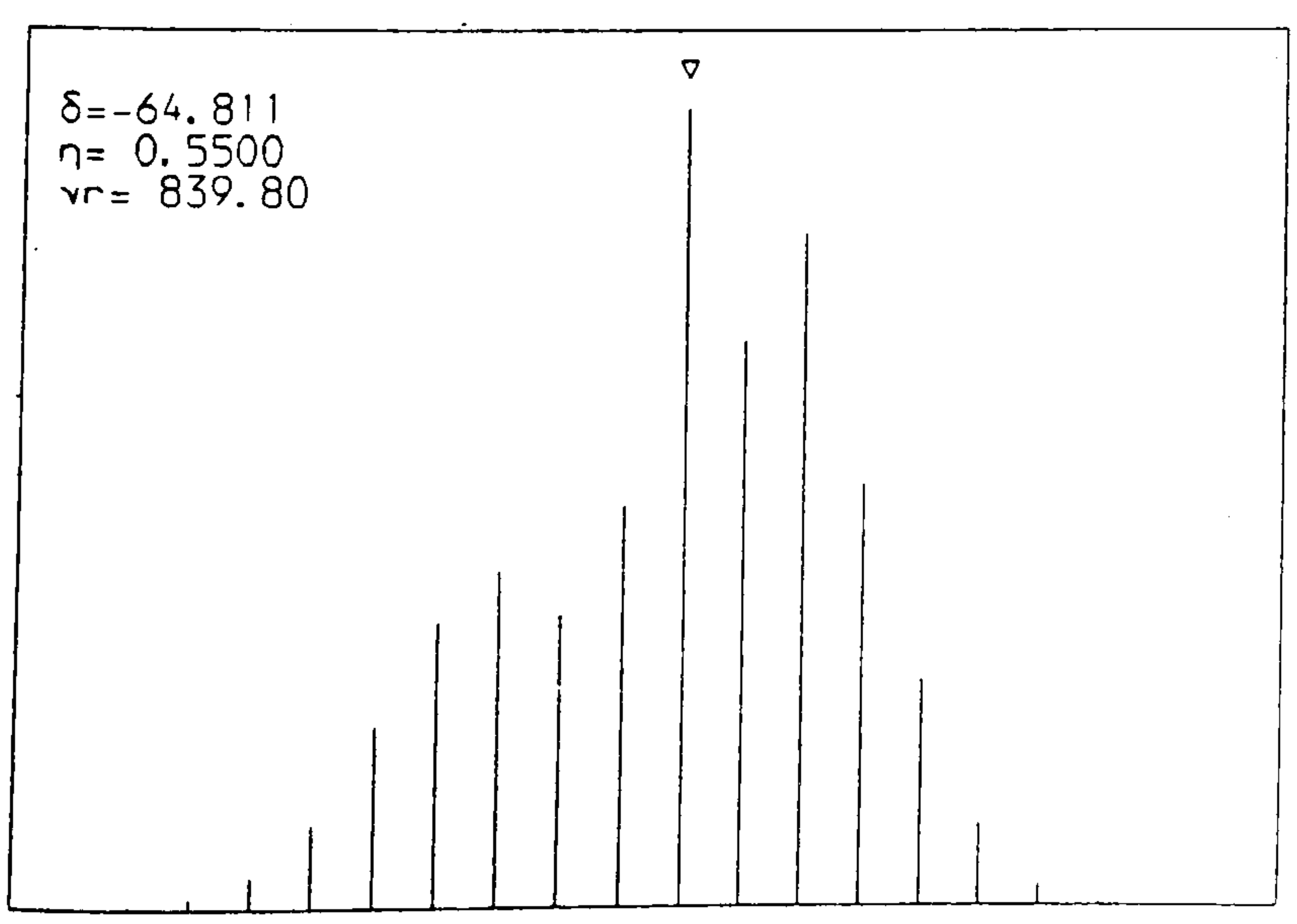
δ=-64.811
η= 0.5500
vr= 839.80

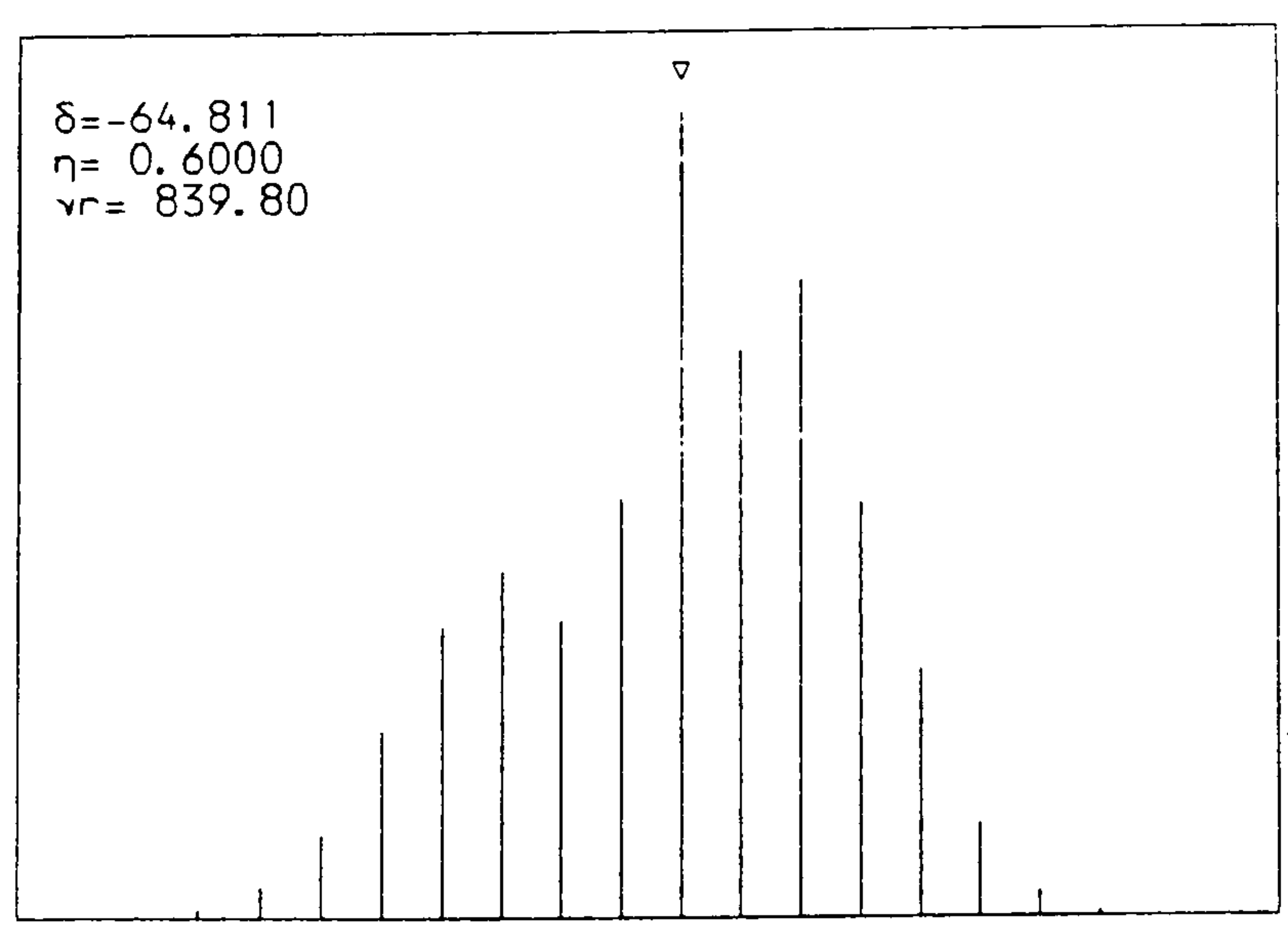
δ=-64.811
η= 0.6000
vr= 839.80

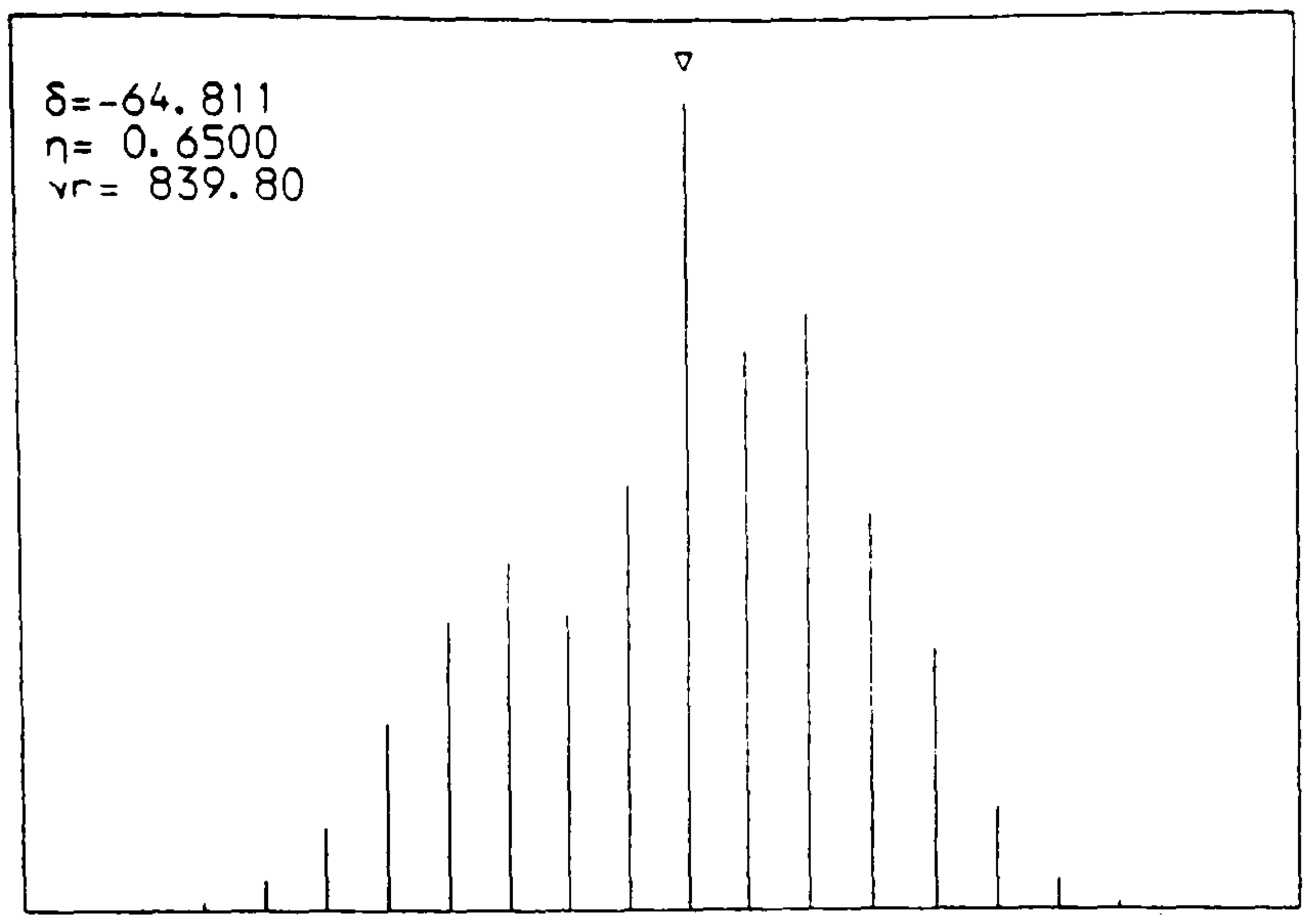
δ=-64.811
η= 0.6500
νr= 839.80

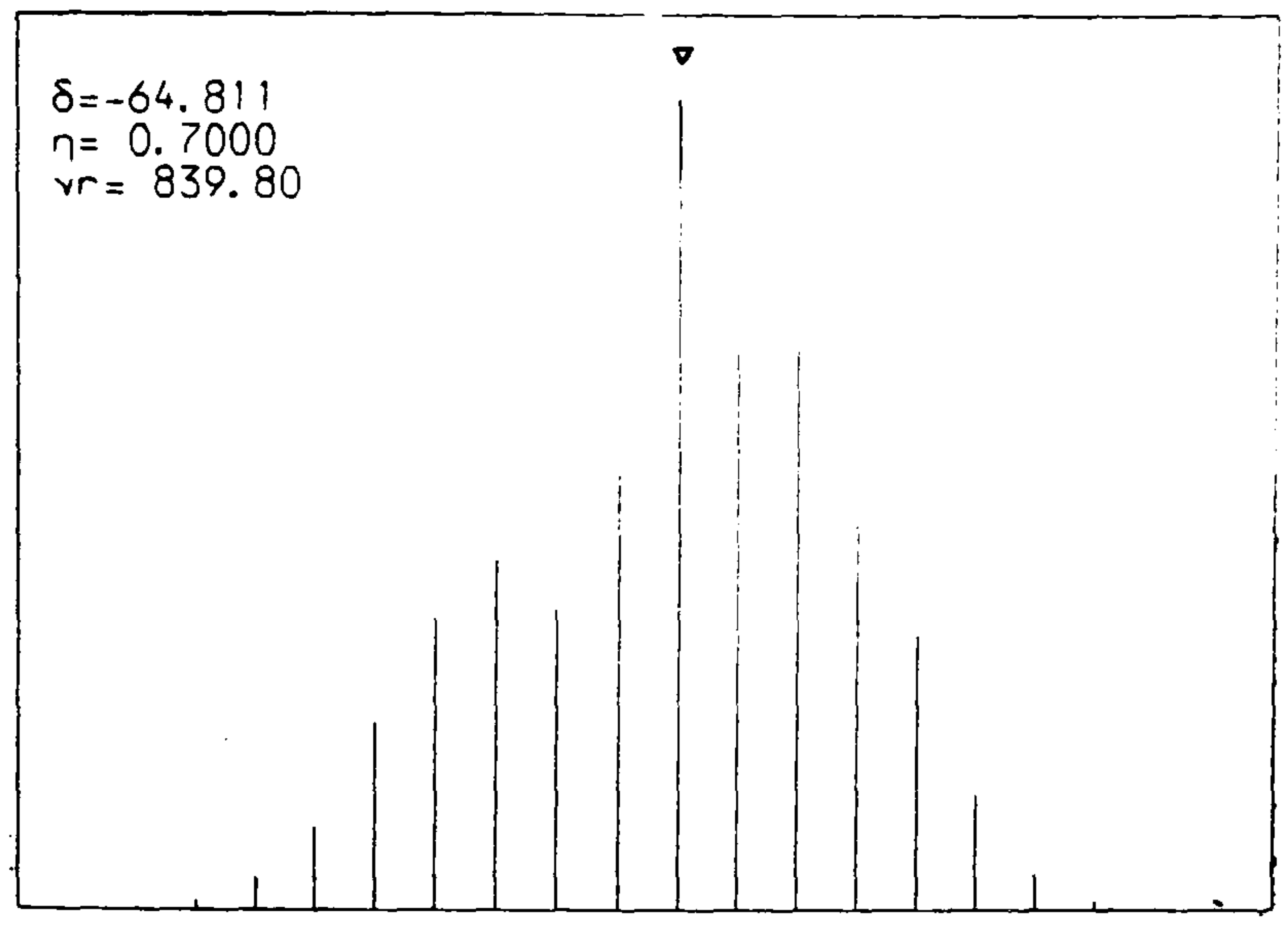
δ=-64.811
η= 0.7000
νr= 839.80

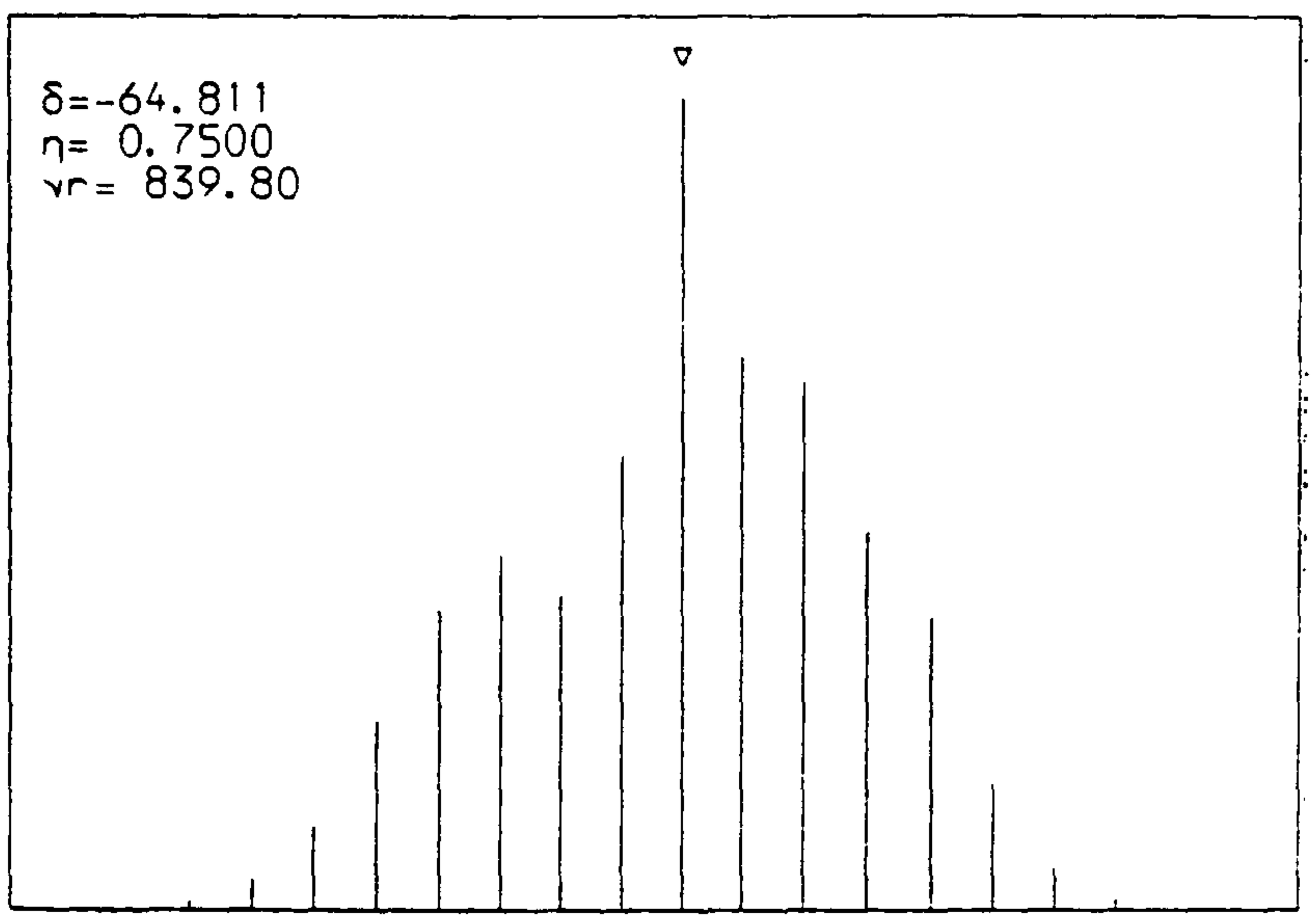
δ=-64.811
η= 0.7500
νr= 839.80

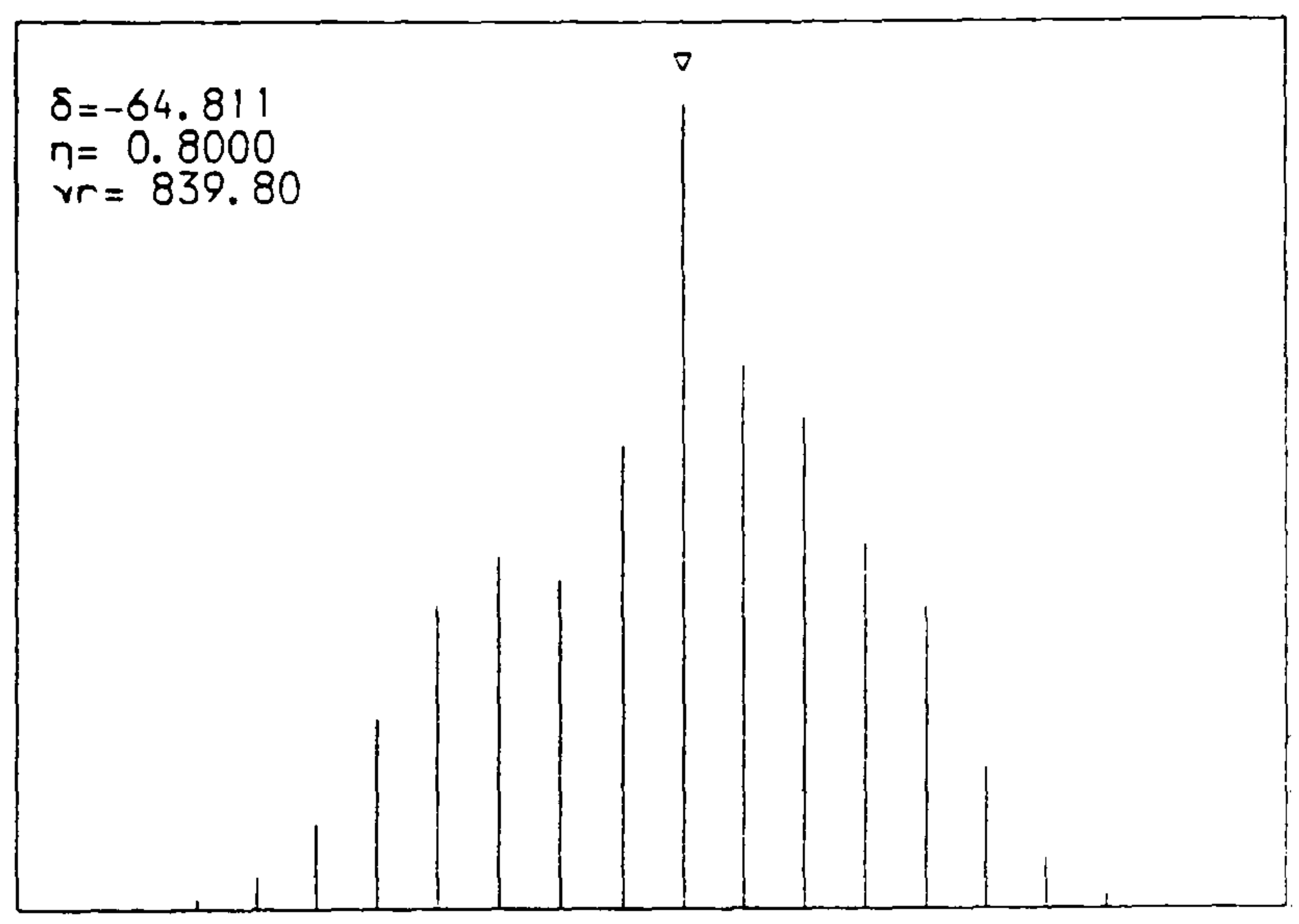
δ=-64.811
η= 0.8000
νr= 839.80

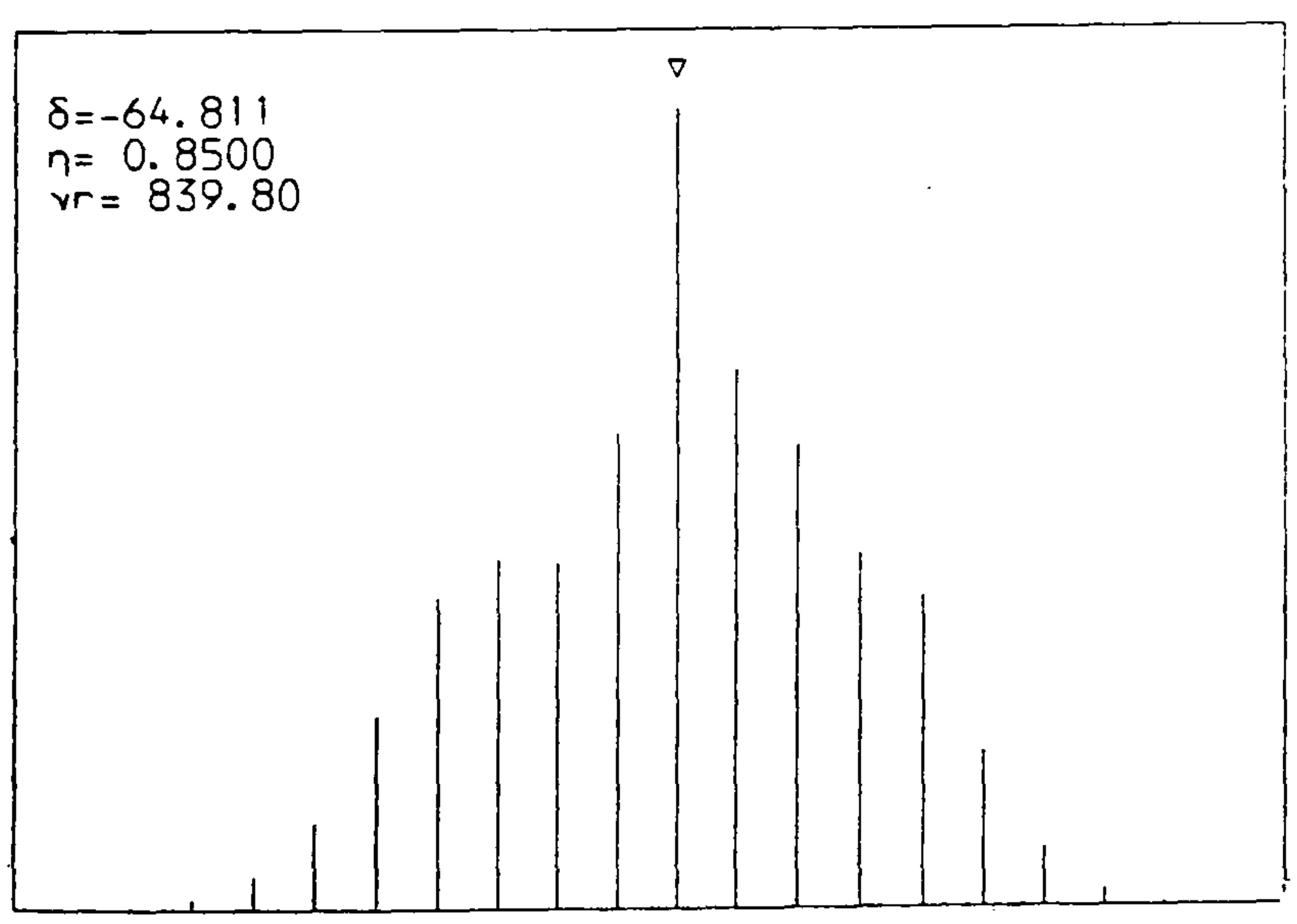
δ=-64.811
η= 0.8500
νr= 839.80

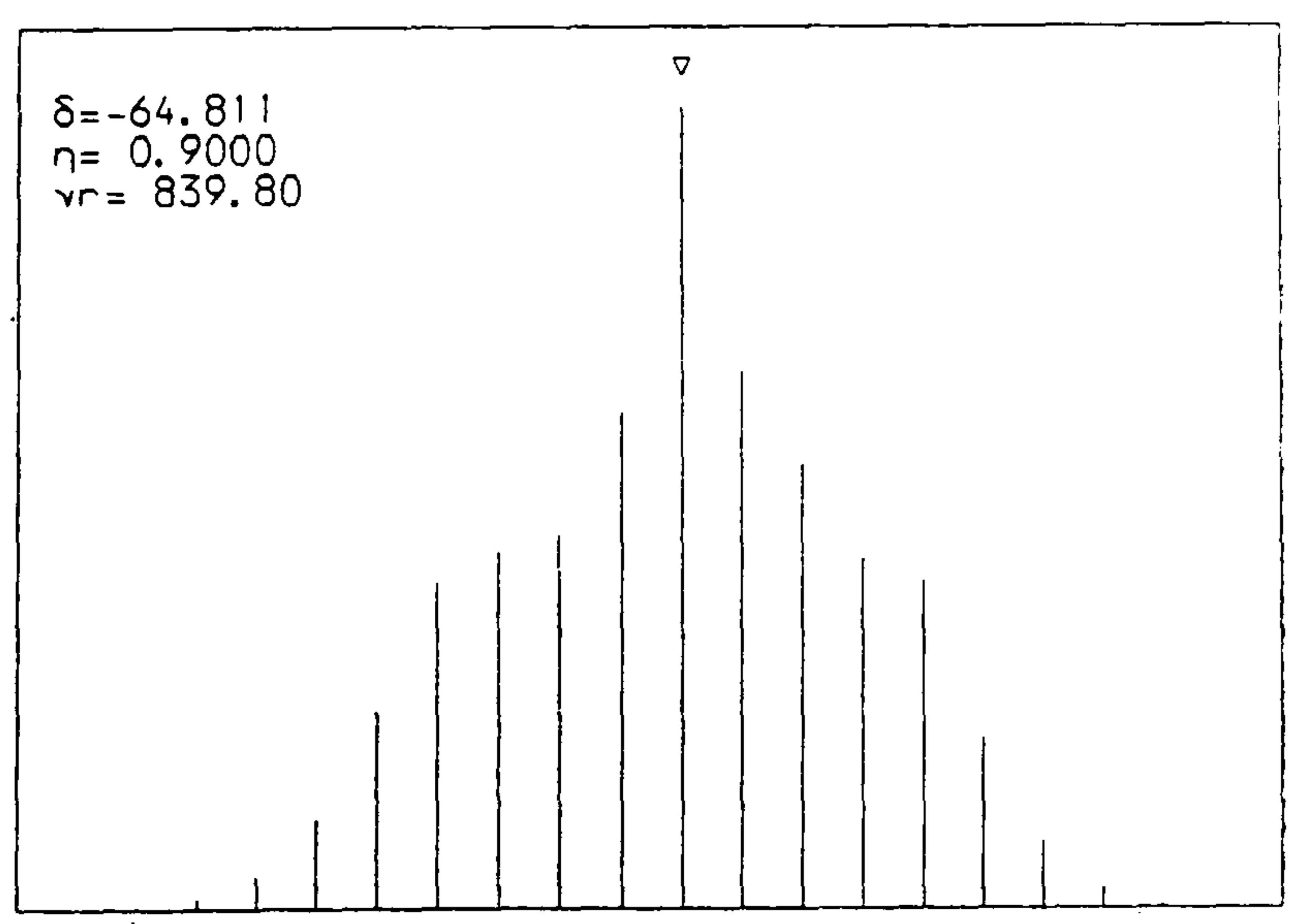
δ=-64.811
η= 0.9000
νr= 839.80

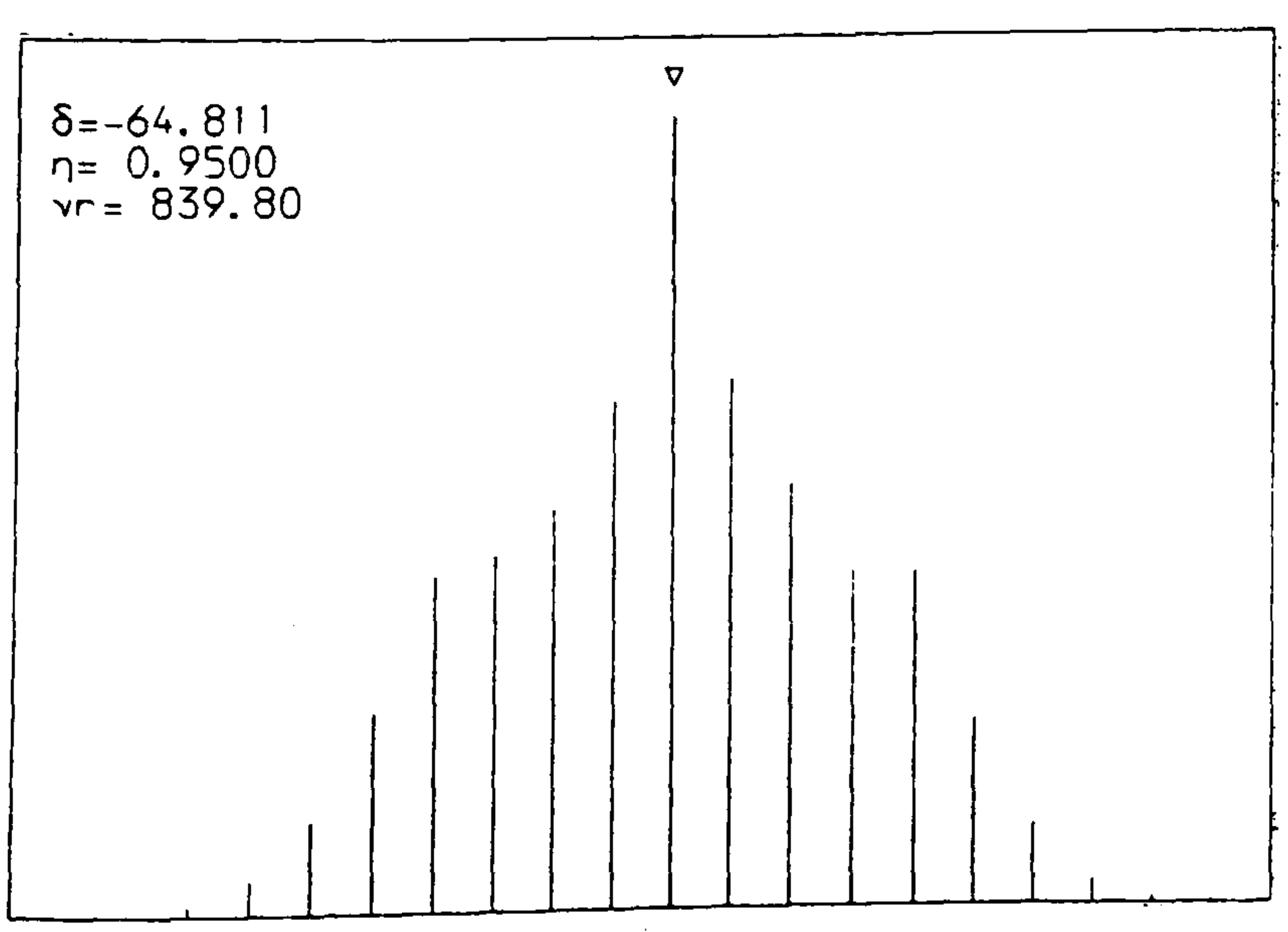
δ=-64.811
η= 0.9500
νr= 839.80

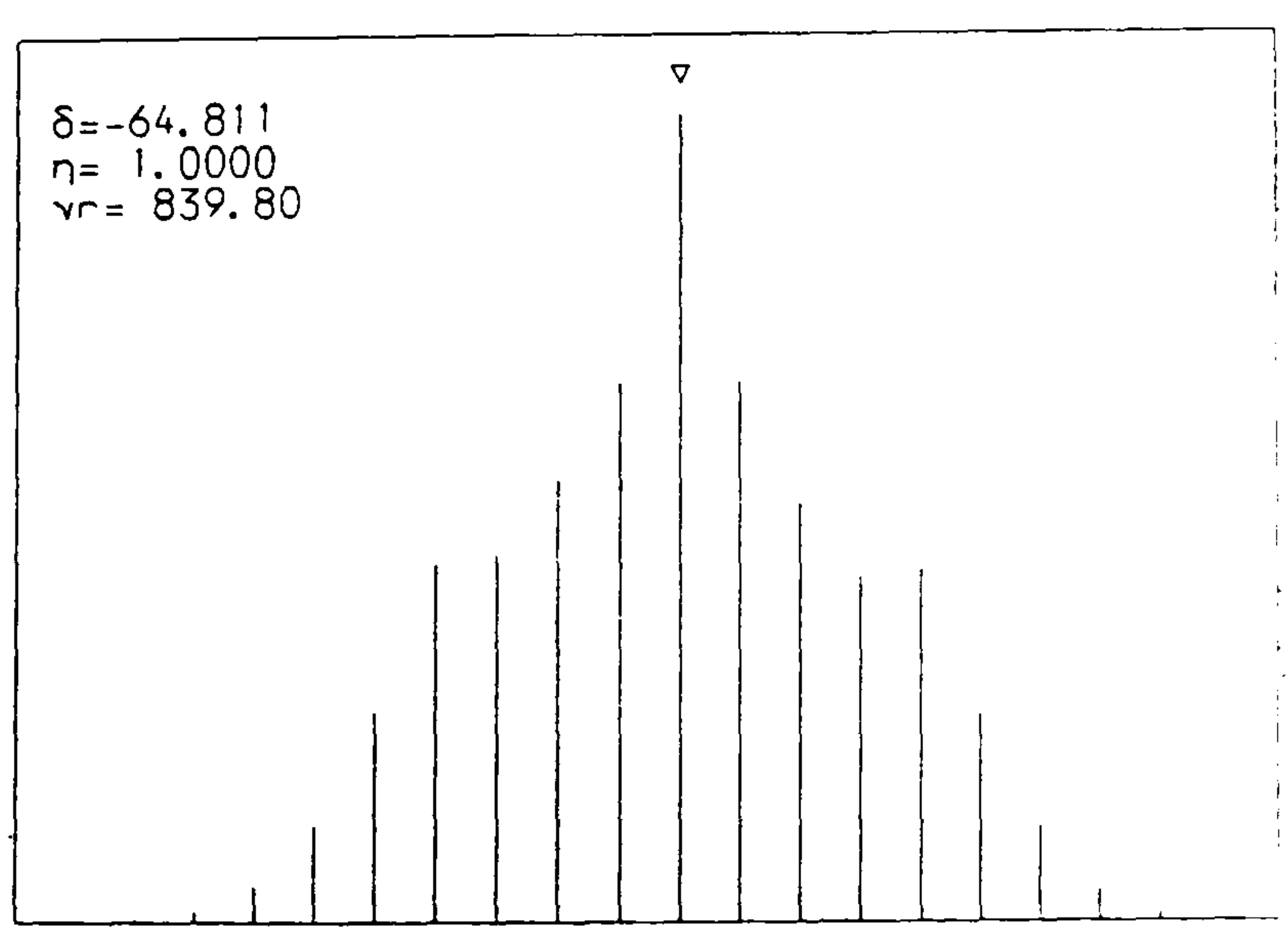
δ=-64.811
η= 1.0000
νr= 839.80

Both of the spectra must be normalized prior to this calculation.

The minimization routine chosen was Numerical Algorithms Group's program E04CCF which was available on the Durham mainframe. This routine is based on the simplex method[20,21]. Such methods are somewhat slow but are generally robust and are useful where functions may be noisy or have local minima.

The iterative routine of E04CCF will attempt to minimize SSQ in the following manner[21,22]: Given that there are two independent variables in this problem, a three dimensional space is established. A vertex in this space is represented by three variables, two of which are the independent variables, δ and η, and the third of which is the dependent variable SSQ. Given an initial guess for δ and η, the routine will calculate a simplex of three vertices. The vertex with the largest value of SSQ will be reflected through the midpoint of the other two vertices. The value of the dependent variable will be determined for this point and compared with the initial three vertices. The vertex with the largest value of the dependent variable in the new simplex is again reflected in a similar fashion. If a point is reached where no further progress can be made, the sides of the simplex are reduced and the process is repeated. The routine continues until the difference between values of SSQ within a simplex are smaller than a given tolerance. The tolerance used here was the value of the machine accuracy for double precision variables ($\approx 1\times10^{-14}$). If this criterion is not met, there is a maximum number of calculations after which the routine will stop.

The overall fitting program may be seen to work as follows:

1) ν_r, ν_o, the total number of sidebands, the number of sidebands to high and low frequency of the centreband, the intensity of each sideband, $\bar{\sigma}$ and initial values of η and δ are input. Further, the range of sidebands to be fitted may be specified.

2) The experimental spectrum is normalized. Sin and cos look-up tables are produced to speed the calculation process.

3) The sideband simulation routine described above is used to

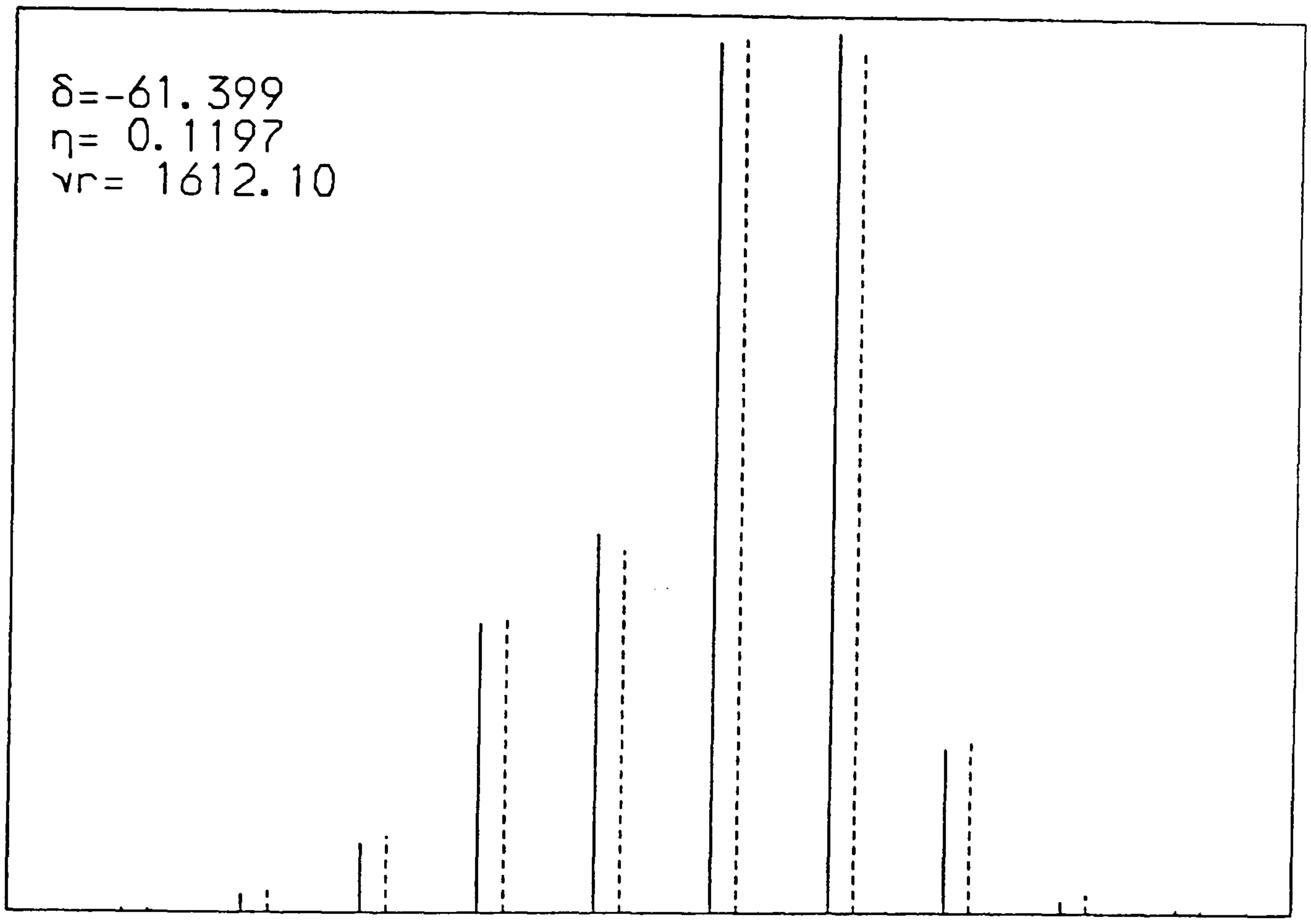

Figure 4.11: This stick-plot is an example of the plotted output of the spinning-sideband fitting program, SBFIT. The solid lines represent experimental spinning-sideband intensities, while the dashed lines represent the calculated sideband intensities corresponding to the parameters noted at the upper left corner of the plot.

calculate simulated spectra under the overall control of the E04CCF minimization routine. SSQ values are calculated from the frequency domain spectra. The parameters, δ and η are varied until a minimum in SSQ is found.

4) When the tolerance limit defined above is reached, the iteration stops. Values of η and δ corresponding to the smallest value of SSQ are printed out. Values for the three tensor components, σ_{11}, σ_{22}, and σ_{33}, are calculated and printed. The normalized experimental and simulated spectra are plotted in graphical form (See Figure 4.11) and printed in numerical form.

The largest drawback to the program as written is that it is quite slow. On the Durham mainframe, a fit will generally take from 500 to 700 CPU seconds. This is mainly a function of the sum over the Euler angles. A value of 20 orientations, corresponding to 9° increments, has been chosen as discussed above. This is the largest practical number of orientations usable considering the time limitations on the mainframe. Methods to speed the program, such as using sin and cos look-up tables, have been included where possible. For further discussion, see section 4.9 below.

4.8 Examples and Discussion

A comparison of typical results for the fitting routine and the method of moments may be found in Tables 4.1 and 4.2. It may be seen that the first of these is for a near axially symmetric case and the latter for an almost completely asymmetric case. The structures for the compounds may be found in Figures 4.2 and 4.3, and a detailed discussion regarding these compounds may be found in Chapter 6. The compounds were chosen because they contained a single type of chemically distinct phosphorus atom which was sufficiently distant from its nearest neighbors for residual dipolar interactions to be small. In such cases, static powder

Table 4.1
Shielding Tensor Data for
1,2-ethanebisphosphonic acid tetrasodium salt

Method	ν_r	δ	η	Tensor Components⁺ σ_{11}	σ_{22}	σ_{33}
Fit	1877.0	-65.7	0.214	15.1	1.03	-90.5
Fit	1066.0	-61.3	0.000	5.9	5.87	-86.1
Fit	2087.8	-64.5	0.236	15.1	-0.15	-89.3
Fit	1612.1*	-61.4	0.119	9.6	2.22	-86.2
Fit	1612.1**	-63.4	0.167	12.2	1.60	-88.2
Fit Average:		-63.3	0.147	11.6	2.11	-88.1
M•	1877.0	-56.8	0.571	19.83	-12.6	-81.6
M	1066.0	-58.3	0.360	14.89	-6.10	-83.2
M	2087.8	-59.0	0.333	14.47	-5.17	-83.8
M	1612.1*	-55.5	0.170	7.74	-1.88	-80.3
M	1612.1**	-55.8	0.502	17.10	-10.9	-80.7
Moments Average:		-57.1	0.387	14.83	-7.33	-81.9
Static:		-59.6	0.185	10.8	-0.51	-84.4

⁺ $\bar{\sigma}$ = -24.8 ppm. Units: δ, σ_{11}, σ_{22}, and σ_{33} are in ppm. ν_r is in Hz, and η is unitless. The tensor components for the static case are quoted to ±2 ppm. Errors for the fitted components are discussed in the text.
*NS=144 (see Figure 4.12 and discussion in text). Also this value used for Figure 4.13. **NS=4
•M=Method of moments.

spectra may be obtained and analysed for the tensor components by the means described earlier in this chapter.

Looking first at the axially symmetric case in Table 4.1, it may be seen that the values of the tensor components obtained from the fitting routine are both more precise and more accurate than the results from the moments calculation. The average absolute value error $((\sum_m|\sigma_{nn} - \sigma_{nn}(\text{static})|)/m)$ for the fitted components is 3.17 ppm as opposed to 4.86 ppm for the method of moments. Further, the largest single absolute value error for the fitted components was 6.1 ppm as opposed to 12.3 ppm for the moments method. Of particular interest are the results for ν_r = 1612.1. Two results are shown, one for a low number of transients and one

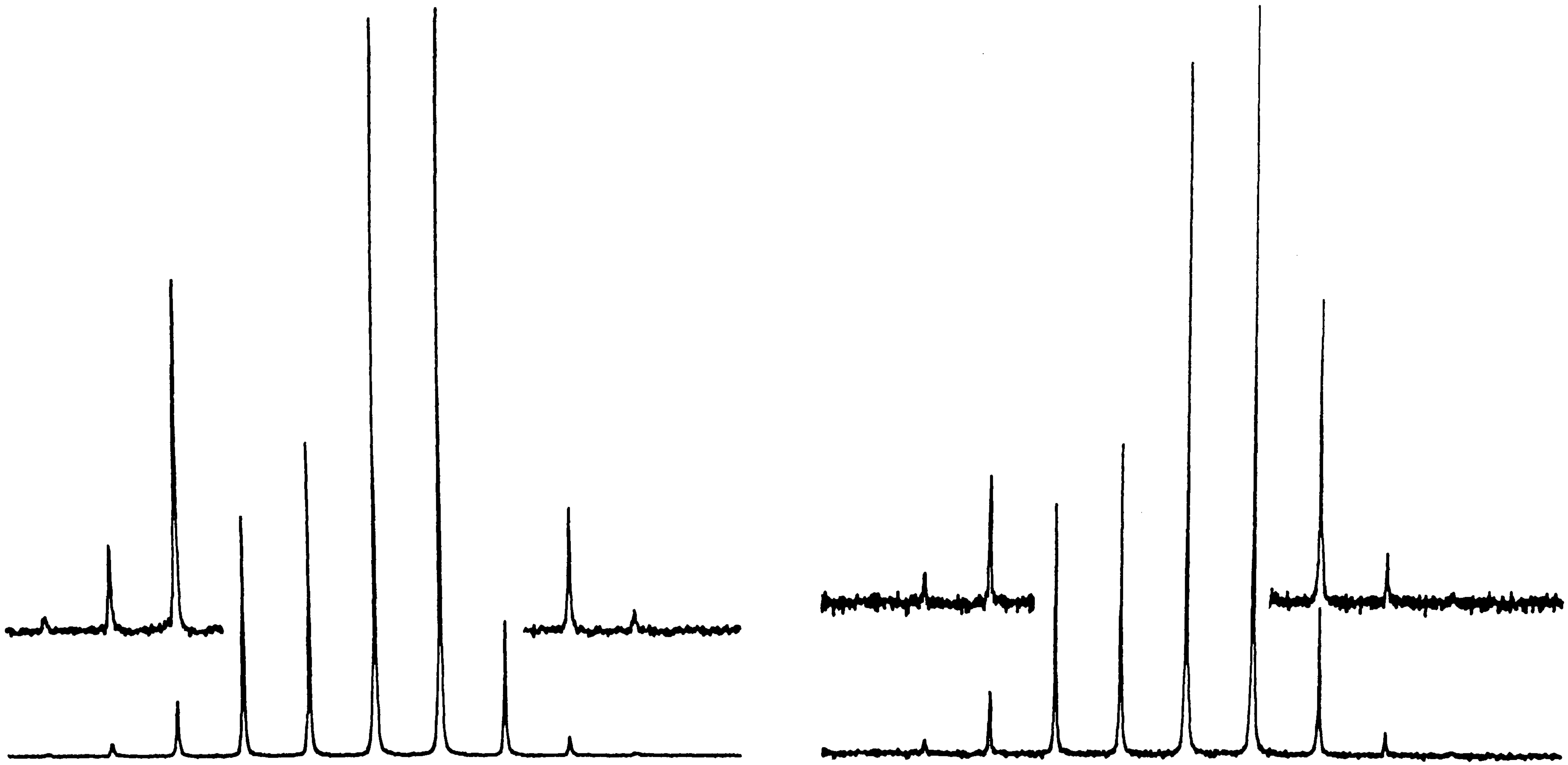

Figure 4.12 ^{31}P CP/MAS spectra of compound (20) (see Figure 4.3 for formula). RD=15 s; PD=4 μs; CT=1 ms; ν_r=1612.1 Hz. Left: NT=144; expansion = 5X. Right: NT=4; expansion = 2X. See Table 4.1 for isotropic shift and tensor components.

for a high number of transients (Figure 4.12). It is clear from comparison of these that the fitting method is much less sensitive to poor signal-to-noise than the method of moments.

Table 4.2
Shielding Tensor Data for
1,2-ethanebisphosphonic acid disodium salt

				Tensor Components⁺		
Method	ν_r	δ	η	σ_{11}	σ_{22}	σ_{33}
Fit	839.8	-64.8	0.847	30.5	-24.4	-94.2
Fit	3002.0	-66.5	0.869	32.8	-24.9	-95.8
Fit	1418.2*	-64.7	0.883	31.6	-25.5	-93.7
Fit	1418.2**	-64.4	0.871	31.0	-25.1	-93.7
Fit	1418.2***	-64.7	0.873	31.3	-25.2	-93.9
Fit Average:		-65.0	0.869	31.4	-25.0	-94.3
M‡	839.8	-60.7	0.844	26.7	-24.6	-90.0
M	3002.0	-58.4	0.980	29.5	-29.7	-87.7
M	1418.2*	-61.5	0.881	28.5	-25.6	-90.8
M	1418.2**	-61.1	0.730	23.7	-21.2	-90.4
M	1418.2***	-60.6	0.881	27.7	-25.6	-89.9
Moments Average:		-60.5	0.863	27.2	-25.4	-89.8
Static:		-61.3	0.857	27.6	-24.9	-90.6

⁺ $\bar{\sigma}$ = -29.3 ppm. Units: as defined in Table 4.1
*NS=4 **NS=8 ***NS=80, Also used for Figure 4.14.
‡M=Method of moments.

In the case of a highly asymmetric tensor (Table 4.2), the advantage of the computer fitting over moments methods is less clear. Indeed, the average absolute value error for the moments method (1.73 ppm) is smaller than that for the fitting routine (2.72 ppm). (Both of these values are smaller than the corresponding values for the axially symmetric case as would be expected from the discussion of errors in the moments method earlier in this chapter.) The generally poorer performance of the fitting routine in this region is most probably due to the use of insufficiently small increments of the Euler angles, α, β, and γ, in evaluating the equation above. While limitations on computer time prevent using significantly higher number of orientations to do a fit, simulation results seemed to indicate that the results were more sensitive to the size of the increment the closer one got to a completely asymmetric case. The most obvious solution to this will be to speed up the program somehow so that smaller increments of the Euler angles may be used (*vide infra*).

Judging from the results above, it would seem prudent to assign error bars of ±5 ppm to values for the shielding tensor components obtained from the fitting routine. The effect of the errors in σ_{11}, σ_{22}, and σ_{33} on the values of η and δ will depend on both the magnitude of the σ's and on the relative manner in which the errors affect each σ. However, reporting average values of δ to ±5 ppm and η to ±0.15 would seem reasonable from the data given.

It will be seen from the footnote to Table 4.1 that the tensor values for the static bandshape analysis are given to ± 2 ppm. This value was established both from recommendations of the authors of the static bandshape fitting program and from the reproducibility from analysis to analysis seen in the work done for this study. While it is clear that the static bandshape analysis method is more reproducible than the spinning-sideband fitting routine, it is not immediately evident which is the more accurate.

Having established the fitting program, it now seems reasonable to examine the behavior of the fit near the minimum. In principle, the best way to do this would be to establish a contour plot of the sum of squares difference (SSQ) between the real and experimental spectra as a function of η and δ. In practice, however, this would be very costly in terms of computer time. What has been done is to create plots of one of the variables versus SSQ with the other variable being fixed at the fit value. The resulting plots may be seen in Figures 4.13 and 4.14.

The most interesting feature of these plots may be seen in the graph of η vs SSQ for the near-axially symmetric case (Figure 4.13). It is clear that below η = 0.15 or so, the intensities of

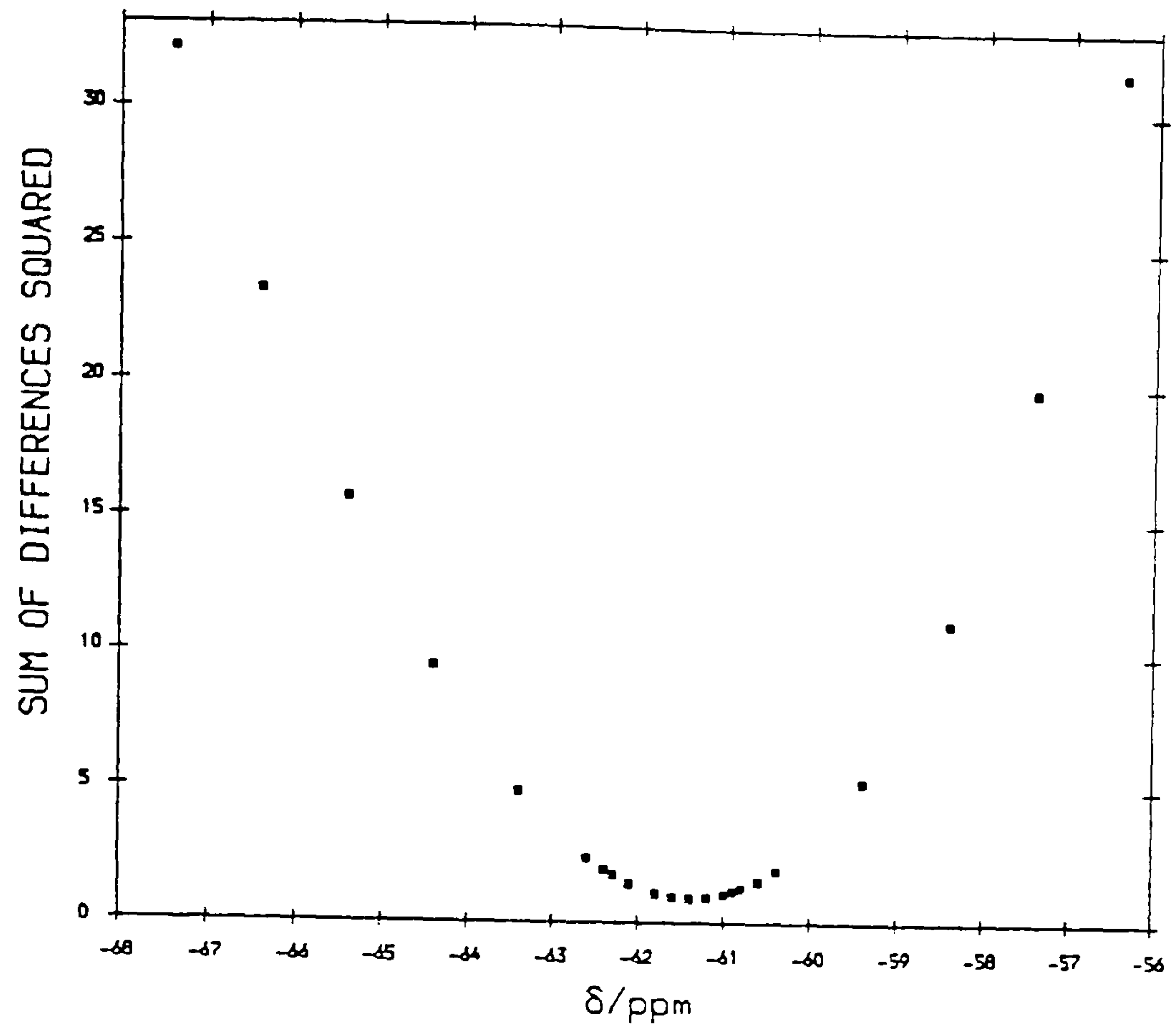

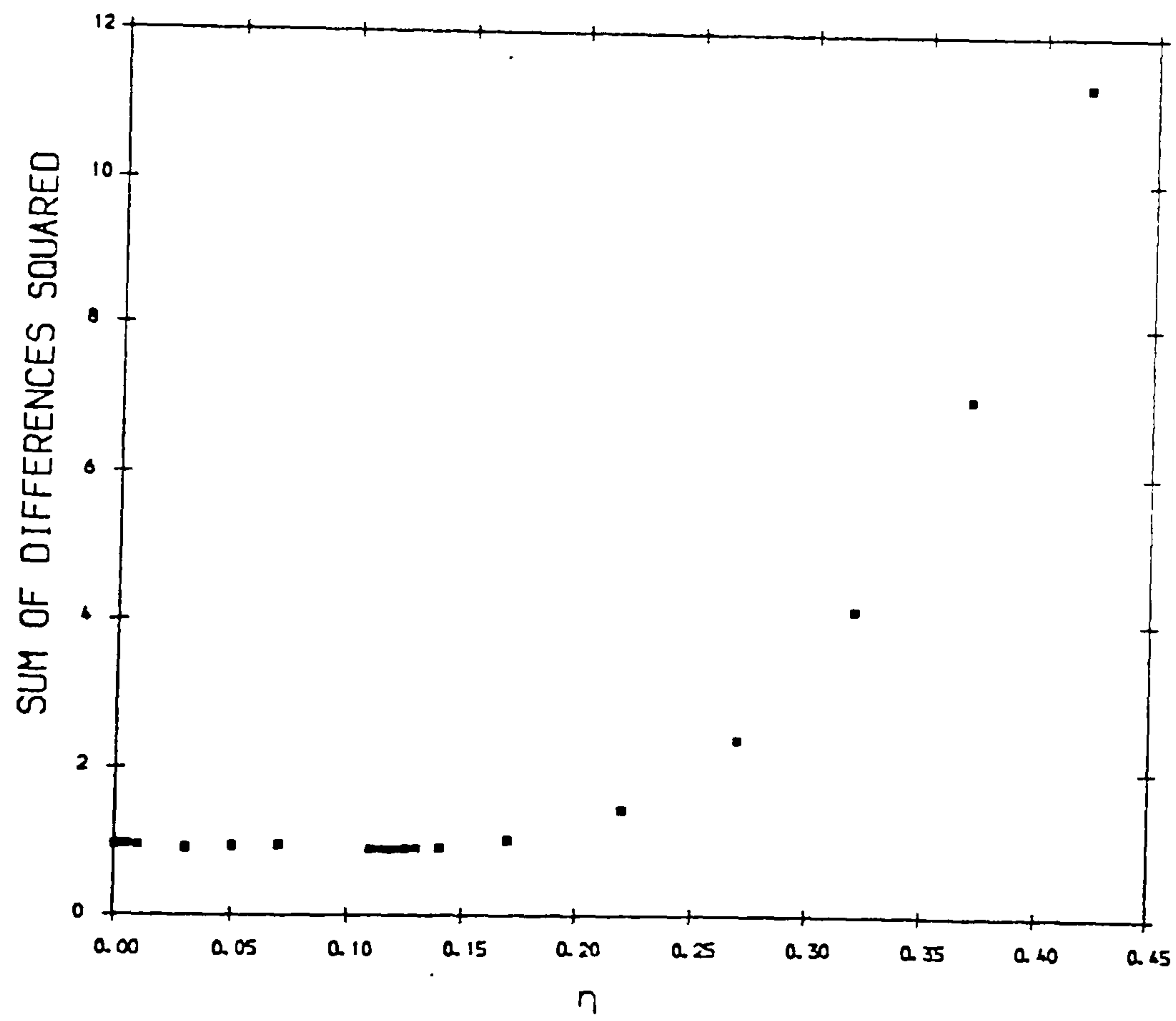

Figure 4.13: Behaviour of the fitting program for a near axially symmetric case. Top: sum squared difference as a function of δ while keeping η fixed at 0.119. Bottom: sum squared difference as a function of η while keeping δ fixed at −61.4 ppm. The difficulty in discriminating between a near-axial case and an axial case is illustrated in the lower graph. (See Table 4.1 and Figure 4.13 for further details.)

the simulated spectra change very little, and, thus, it is very difficult to determine a mimimum. (There is actually a shallow minimum here at $\eta = 0.12$, though it is difficult to see from this plot.) Such a result would indicate that actually discriminating between an axially symmetric case and a near-axially symmetric case may not be possible. This result is clearly in agreement with those of Clayden *et al.*[7] which indicate the same conclusion.

For the asymmetric example (Figure 4.14), there is a clear minimum for both variables. It may be noted that the minimum for η is somewhat broad at the bottom. This may be a contributing factor to the errors noted above for the fitting method near the completely asymmetric limit.

Table 4.3

Tensor Parameters and Sum Squared Difference For Sideband Fit Using a Variable Number of Sidebands For Fitting[+]

Sideband Range	δ	η	SSQ for Complete Spectrum
-1 to 1	-61.6	0.13	0.9512
-2 to 2	-61.4	0.12	0.9111
-3 to 3	-61.4	0.11	0.9048
-4 to 4	-61.4	0.11	0.9048
5 to 4	-61.4	0.11	0.9048

[+] For spectrum from Figure 4.12, NS = 144.

Finally, it was noted in the description of the program that the range of sidebands used for the SSQ criterion must be specified with the data. Table 4.3 shows the results of fitting with various numbers of sidebands. The SSQ value given in the table is for the complete spectrum. The fit was carried out using only the SSQ for the sideband range given. (Note that the range is specified by the number of the sideband. The centreband is 0 and sidebands to high frequency of the centreband are negative.) It is clear that even using only the -1 and +1 sidebands, results within

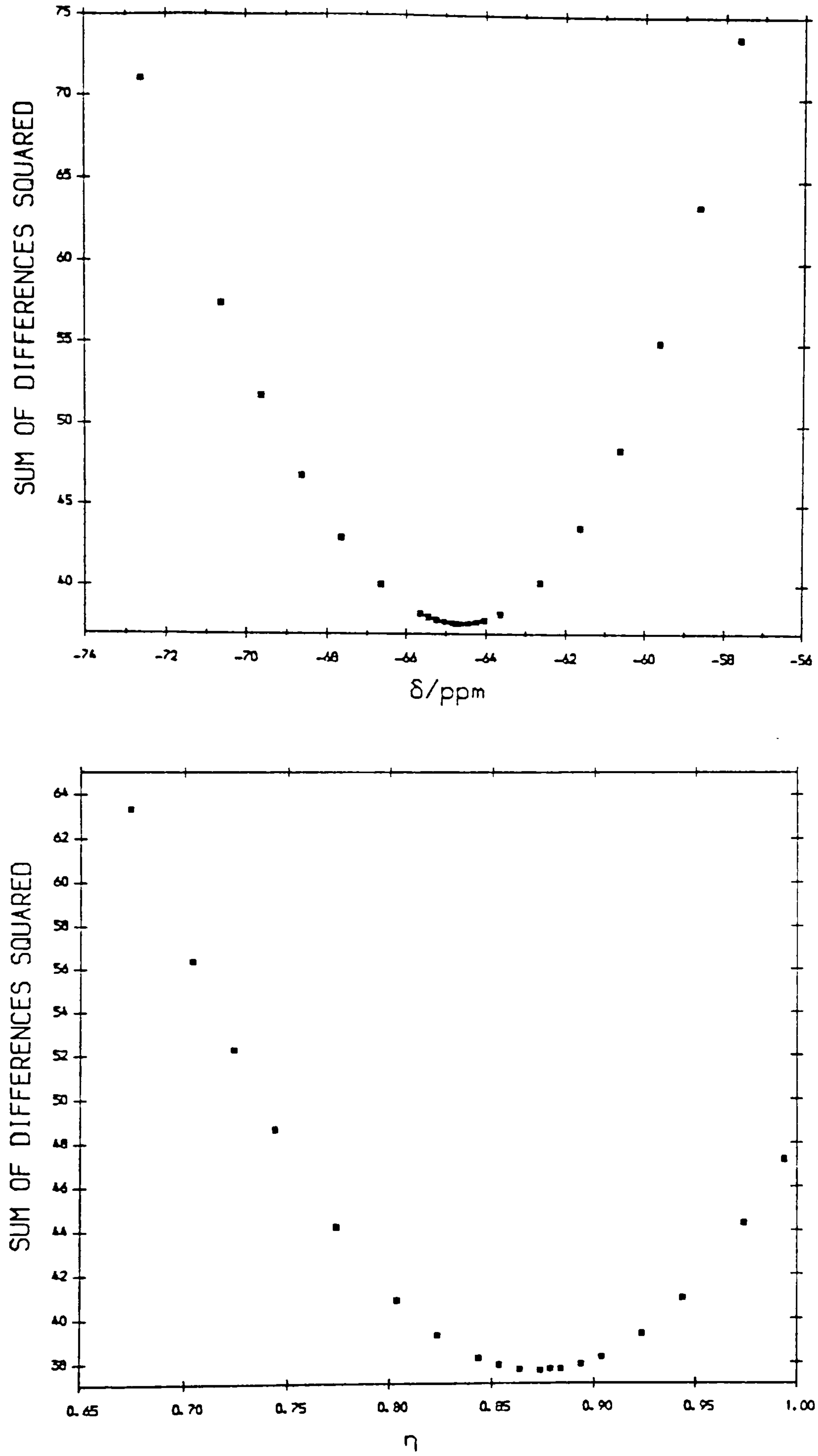

Figure 4.14: Behaviour of the fitting program for an asymmetric case. Top: sum squared difference as a function of δ while keeping η fixed at 0.873. Bottom: sum squared difference as a function of η while keeping δ fixed at -64.7 ppm. (See Table 4.2 for further details.)

the experimental error may be obtained. Slightly smaller errors are obtained, however, if more sidebands are included. One might expect the errors to increase if the outer, less accurately measured sidebands are used, but this does not appear to be the case here.

4.9 Recommendations for Further Work

The above results clearly show that the computer simulation method is applicable to the determination of shielding tensor components. In particular, it gives a distinct improvement in the determination of tensor components near the axially symmetric limit. The main drawback of the program may be considered generally one of time. Firstly, all fits are costly to run in that ca. 600 seconds of CPU time is required on a mainframe computer. Secondly, as a result of this limitation, a compromise choice for the size of the increments of the Euler angle in the calculation has had to be made. It is possible that this latter point limits the accuracy in the highly asymmetric cases. It is obvious that the program will be more more usable if run times can be made shorter.

One possible method for obtaining time savings is to do the fit in the time domain. In this manner, a Fourier transform need not be done for each FID generated. Further time savings are necessary in the evaluation over the Euler angles, as this is certainly the most time-consuming process in the program. It is not immediately clear how this can be done beyond the steps already taken.

References

1. W.S. Veeman, *Progr. NMR Spectrosc.* **16**, 193 (1985).

2. A. Bax, N.M. Szeverenyi and G.E. Maciel, *J. Magn. Reson.* **52**, 400 (1983).

3. A. Bax, N.M. Szeverenyi and G.E. Maciel, *J. Magn. Reson.* **54**, 147 (1983).

4. S.J. Opella and M.H. Frey, *J. Amer. Chem. Soc.* **101**, 5854 (1979).

5. M.M. Maricq and J.S. Waugh, *J. Chem. Phys.* **70**, 3300 (1979).

6. J. Herzfeld and A.E. Berger, *J. Chem. Phys.* **73**, 6021 (1980).

7. N.J. Clayden, C.M. Dobson, L. Lian and D.J. Smith, *J. Magn. Reson.* **69**, 476 (1986).

8. H.J. Jakobsen, P.D. Ellis, R.R. Inners and C.F. Jensen, *J. Amer. Chem. Soc.* **104**, 7442 (1982).

9. P.S. Marchetti, P.D. Ellis and R.G. Bryant, *J. Amer. Chem. Soc.* **107**, 8191 (1985).

10. U. Haeberlen, "High-resolution NMR in Solids: Selective Averaging", Academic Press, New York (1976).

11. P. D. Murphy and B.C. Gerstein, "Analysis and Computerized Fitting of the Lineshape of the NMR Powder Pattern", Iowa State University Report IS-4516 (1978).

12. C.J. Groombridge, Ph.D. thesis, University of East Anglia (1983).

13. A. Abragam, "The Principles of Nuclear Magnetism", Oxford University Press, Oxford (1961).

14. J.H. van Vleck, *Phys. Rev.* **74**, 1168 (1948).

15. C.P. Slichter, "Principles of Magnetic Resonance", Springer-Verlag, Heidelberg (1980).

16. I.V. Aleksandrov, "The Theory of Magnetic Resonance", Academic Press, New York (1966).

17. M.G. Munowitz and R.G. Griffin, *J. Chem. Phys.* **76**, 2848 (1982).

18. E. Fukushima and S.B.W. Roeder, "Experimental Pulse NMR", Addison-Wesley Publishing Co., Inc. (1981).

19. Numerical Algorithms Group, Fortran Library Manual Mark 10, Document C06FCF (1982).

20. D.W. Alderman, M.S. Solum and D.M. Grant, *J. Chem. Phys.* **84**, 3717 (1986).

21. M.S. Caceci and W.P. Cacheris, *Byte*, May, 340 (1984)

22. Numerical Algorithms Group, Fortran Library Manual Mark 10, Document E04CCF (1982).

CHAPTER FIVE - PHOSPHORUS-31 NMR STUDY OF SOLID DIPHOSPHINE DISULPHIDES

5.1 Introduction

In recent years, advances in the techniques and understanding of NMR spectroscopy of the solid-state have provided the chemist with a wealth of information previously unavailable from solids. Techniques such as magic-angle rotation,[1] cross-polarization,[2] high-power decoupling, and the combined use of these procedures[3] in many cases result in high-resolution spectra from nuclei such as ^{13}C and ^{31}P in solid systems. Where previously only broad, featureless resonances could be obtained, current techniques often result in the chemical shift and coupling constant information familiar from solution-state NMR spectra.

In addition to the usual data, NMR spectra of powdered solids may also provide information as to the overall (crystallographic) structure of the solid in question. By this it is not implied that exact atomic positions can be obtained as are determined from X-ray diffraction studies. However, it is often possible to deduce information regarding the unit cell and the size of the asymmetric unit purely from solid-state NMR data.

It is stressed here that for solid-state NMR, the term "equivalence" assumes a narrower definition than that used in conventional solution-state NMR. For two nuclei of a solid to be equivalent in the NMR sense implies not only symmetry of environment within the molecule, but also equivalence with respect to overall crystal geometry. Several of the examples below illustrate this point quite clearly.

The diphosphine disulphides (dithioxodi-λ^5-phosphanes) have been of interest for a number of years to both the solution-state NMR spectroscopist and the structural chemist. The interest of the former stemmed from the difficulties of spectral analysis for symmetrical spin systems[4,5,6] and from the relationship of coupling constants to conformation,[7,8] while that of the latter arose from questions of the electronic structure[9,10] and of internal rotation about the P-P bond.[11] Information on these matters has indeed been obtained, and as a consequence of such work there is a series of compounds, solid at room temperature, which has been well

TABLE 5.1
Phosphorus-31 NMR Data for
Symmetrical Diphosphine Disulphides, $[R^1R^2P(S)]_2$

	R_1R_2	Solid-State δ_P/ppm	$\Delta\nu_{1/2}$/Hz	$\|J_{PP}\|$/Hz	Solution-State δ_P/ppm	$\|J_{PP}\|$/Hz
(1)	Me_2	37.2 34.9	87 54	- -	35.07[12] 34.7[12] 35[14]	18.7[9]
(2)	Et_2	51.2	46	-	51.27[12] 49.4[15] 52.5[14]	53.5[12]
(3)	Pr^n_2	45.9	48	-	46.65[12]	53.2[12]
(4)	Bu^n_2	51.1 49.4	50	58	-	-
(5)	Ph_2	41.4 40.2	-	-	37.9[15]	-
(6)	MeEt (meso)	45.1	98	-	43.5[12]	37.5[12]
(7)	MeEt (rac)	45.0	175	-	44.0[12]	37.5[12]
(8)	$MeBu^t$ (rac)	54.8 51.2	-	109	59.39[16]	97[16] 103[9] 109[9] 118[6]
(9)	MePh (meso)	38.4	96	-	37.55[12] 37.0[14]	21[19]
(10)	Me-l-Men[a] (meso)	48.1 41.0	122 122	-	48.93[17]	55.5[17]
(11)	$EtBu^t$ (rac)	64.2 61.2	-	111	72.4[18]	-
(12)	$EtBu^t$ (meso+ rac)	63.6	-	-	65.3[18] (meso)	-
(13)	Pr^iBu^t (meso+ rac)	74.1 68.6	329 158	- -	74.76[17] (rac) 68.19[17] (meso)	-
(14)	compound (II)[b]	62.7	73	-	61.6[12]	-

Estimate of errors for solid-state values: δ_P ± 0.1 ppm; $\Delta\nu_{1/2}$ ± 10%; $|J|$ ± 10 Hz.

[a] Men = l-menthyl

[b] See next page.

characterised by solution-state NMR.[12] A number of these have had their crystal structures determined by X-ray diffraction.

Table 5.2
Known Crystal Structures
for Diphosphine Disulphides

R_1R_2	Space Group	Asymmetric Unit/molecules	Reference
(1) Me_2	C2/m	1 1/2	23
(2) Et_2	$P\bar{1}$	1/2	25
(5) Ph_2	$P2_1/c$	2 × 1/2†	29
(8) $MeBu^t$ (rac)	$P2_1$	1	13
(9) MePh (meso)	P_{bca}	1/2	24
(14) compound II	$P\bar{1}$	1/2	26

† the unit cell here consists of two half-molecules

Thus, this system formed an excellent basis for further study using the techniques of high-resolution solid-state NMR spectroscopy. The purpose of this present work was to compare the results of solid-state and solution-state spectra and to determine what additional information could be obtained from the former, specifically with regard to solid structure.

A list of the diphosphine disulphides studied may be found in Table 5.1. These materials are symmetric compounds, $[R^1R^2P(S)]_2$, all but one of which[13] have the *trans* structure (I) with respect to the S=P-P=S skeleton. One cyclic system (II) was also studied.

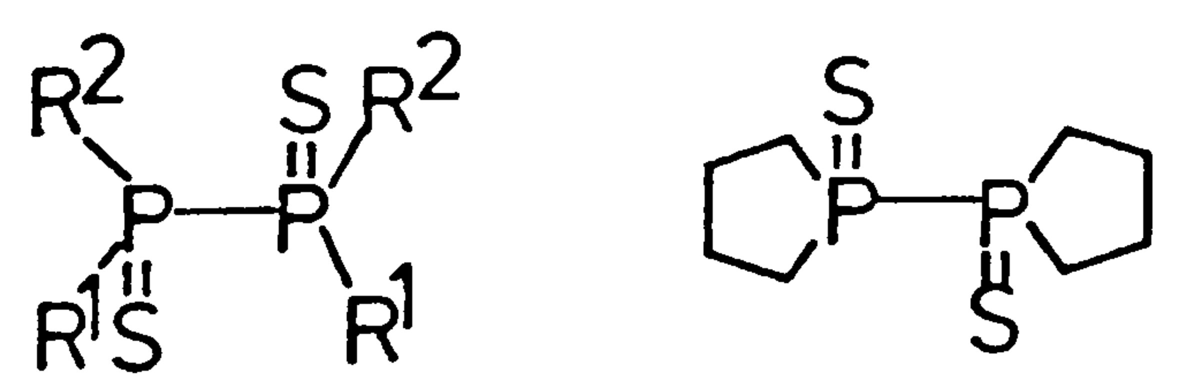

I II

R^1,R^2 = Me, Et, Pr^n, Pr^i, Bu^n, Bu^t, Menthyl, Phenyl.

When R^1 and R^2 are not identical the phosphorus atoms are chiral centres, and the compounds may exist as stereoisomers in the forms *meso* and racemic. In compounds such as *meso* P,P'-dimethyl-P,P'-bis-(l-menthyl)-diphosphine disulphide, it can be seen that in addition to the chirality of the phosphorus atoms, the C_3 carbon atoms of the l-menthyl groups are also chiral.

5.2 Isotropic Chemical Shift Considerations

The results of this study are summarized in Table 5.1. Literature values for the solution-state ^{31}P chemical shifts have been included where available. No solid-state NMR data were found in the literature apart from the results of Tutunjian and Waugh[20] for a single crystal sample of the tetraethyl compound (δ_P = 48.7 ppm).

In general, solid-state ^{31}P chemical shifts are comparable with those noted in solution. Differences can be attributed to solvent effects and small changes in bond length and angle between solution and solid.

As can be seen in Table 5.1, there is a general increase in phosphorus chemical shift with the size of the substituents. It is postulated that the bulkier substituents result in an increase in CPC bond angle and thus change the phosphorus hybridization. (The change in CPC angle for compound II should be seen to be due to ring strain rather than to substituent bulk.) This finding is in agreement with previously published solution-state results given in reference 12, where a more detailed explanation may be found.

A further trend in the isotropic chemical shift is illustrated in Figure 5.1 which is a plot of N_β versus the isotropic shift for the alkyl-substituted diphosphine disulphides. N_β is the number of carbon atoms β to the phosphorus. This empirical parameter is indicative of general deshielding effects[21,22] and has been used for these compounds to discuss chemical shifts in the solution state[12]. In general, there is a good correlation between this parameter and the isotropic shift in both the solution- and solid-state.

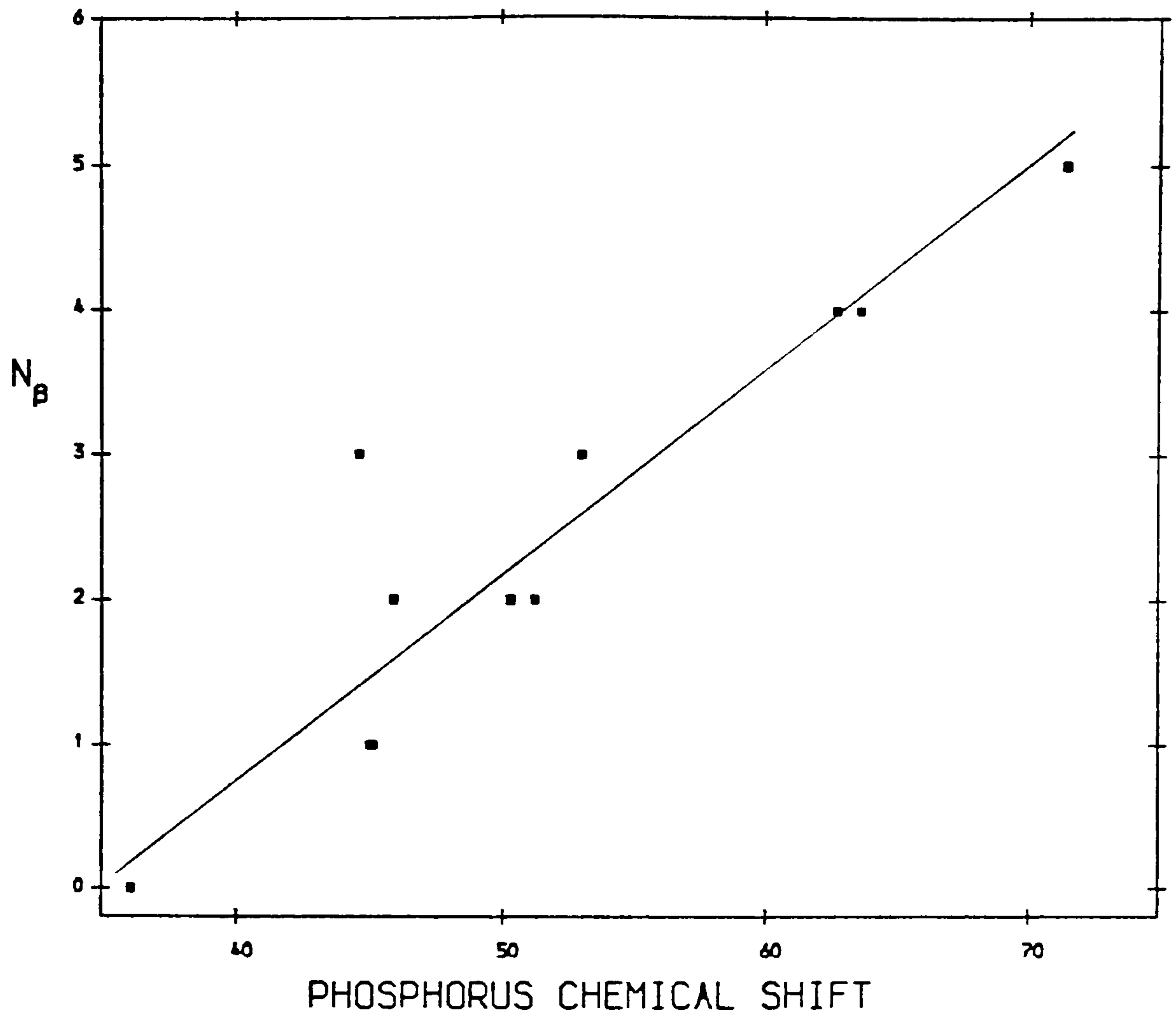

Figure 5.1: A plot of N_β versus phosphorus chemical shift (ppm) for the alkyl-substituted diphosphine disulphides. N_β is defined as the number of carbon atoms β to the phosphorus.

5.3 Crystallographic Considerations

We shall begin with the spectrum of tetramethyldiphosphine disulphide, $[Me_2P(S)]_2$, (Figure 5.2). Although this is not the simplest case, it illustrates well the type of crystallographic information available. The centreband spectrum of this compound consists of two resonances. The high-frequency peak is at δ_P= 37.2 ppm and has a half-height width of 87 Hz. The low-frequency peak has a shift of 34.9 ppm and a width of 54 Hz. The two lines have relative intensities integrated over their respective spinning sideband manifolds of 2:1. Measurement of spin-lattice relaxation times using eleven τ values gave T_1 = 30.1 ± 1 seconds for both resonances. This implies that the difference in line-widths is real and not due to differing relaxation characteristics.

This spectrum may be understood in relation to the X-ray diffraction crystal structure reported by Lee and Goodacre.[23] This report shows the unit cell of $[Me_2P(S)]_2$ (space group C2/m) to contain six molecules, all in the *trans* configuration, which occupy two different sets of special positions. Two molecules per unit cell occupy the special position 2(a) with inversion symmetry 2/m. The phosphorus atoms in these centrosymmetric molecules are thus completely equivalent and do not show direct P-P J-coupling. The narrow peak at 34.9 ppm may probably be assigned to the molecules of this symmetry.

The remaining four molecules in the unit cell occupy special positions 4(i) with symmetry m. In these, the phosphorus atoms are not equivalent thus giving rise to an AB spin system with P-P coupling, in principle, affecting the spectrum. It is postulated that the width of the line at 37.3 ppm arises from the AB pattern with both the chemical shift difference and the splitting due to coupling unresolved. The increase in linewidth of 33 Hz over the other centreband is consistent with this interpretation. The value of J_{PP} reported for this compound in solution is 18.7 Hz.[9] It should also be noted that the 4:2 ratio of molecules at m sites compared to those at centrosymmetric 2/m sites agrees with the 2:1 intensity ratio in the spectrum.

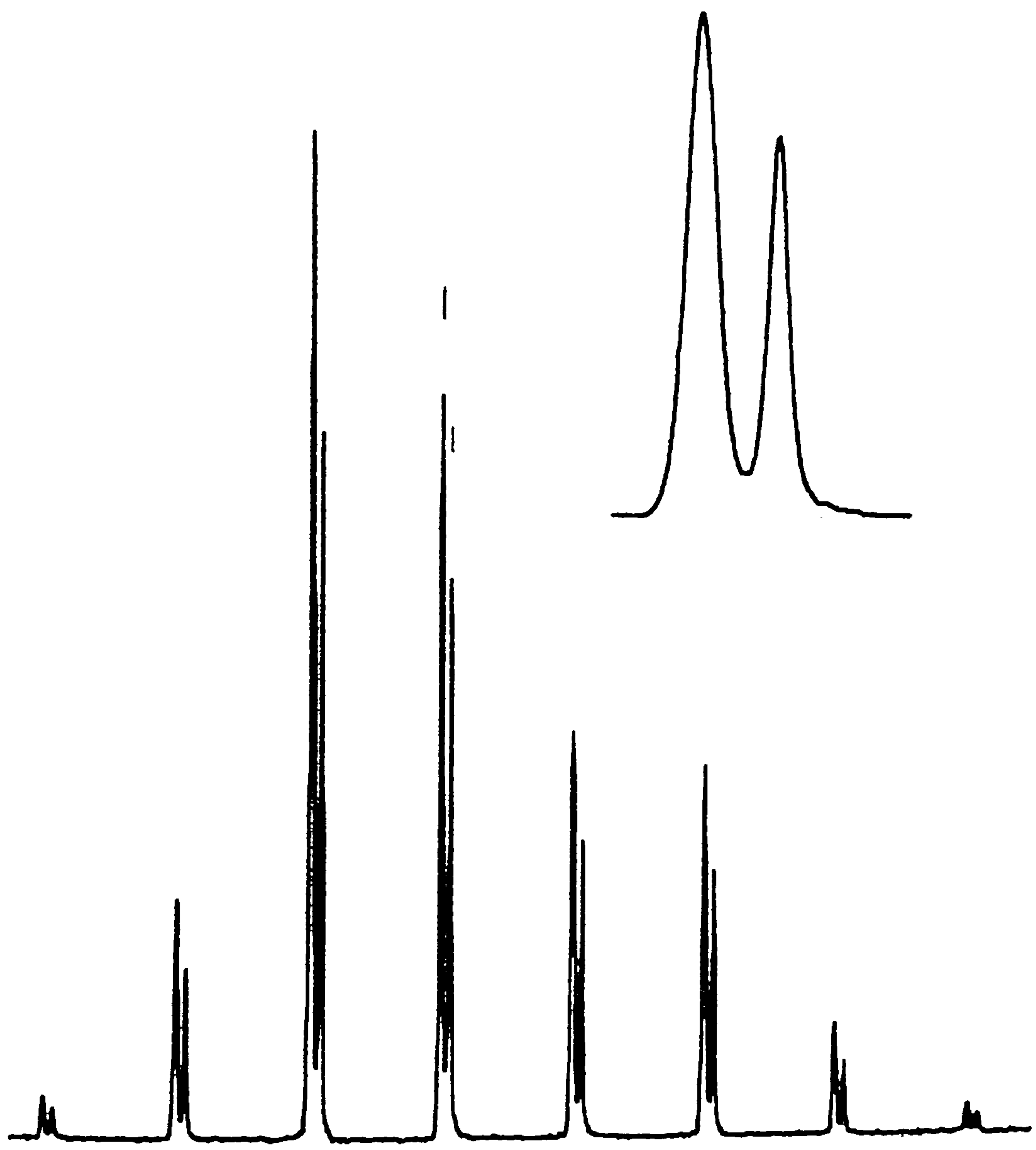

Figure 5.2: ^{31}P CP/MAS spectrum of tetramethyldiphosphine-disulphide and expanded centreband. $[Me_2P(S)]_2$ (1). RD=20 s; PD=5 μs; CT=0.25 ms; NT=32; SF=81.014 MHz; ν_r=2950 Hz.
δ_P = 37.2, 34.9 ppm
$\nu_{½}$ = 87 54 Hz

The simplest cases we have examined are those of meso-$[MePhP(S)]_2$, $[Et_2P(S)]_2$, and compound (II). Each of these has a spectrum (e.g. Figure 5.3) in which the centreband is a single, relatively narrow line (half-height width less than 100 Hz). Such a spectrum implies that all phosphorus atoms within the crystal lattice are equivalent in the sense defined above. This conclusion is consistent with the fact that for all three of these compounds, X-ray diffraction studies have shown[24,25,26] the unit cell to contain a single molecule with the asymmetric unit being half of the molecule.

The spectra of meso-$[MeEtP(S)]_2$ and $[Pr^n{}_2P(S)]_2$ also show a centreband which is a single narrow line. Although there are no corroborating X-ray data, the NMR result is strongly suggestive of an asymmetric unit which consists of a half a molecule.

For the compound rac-$[MeEtP(S)]_2$, the data are somewhat more ambiguous. The centreband is again a single line; however, the linewidth (ca. 150 Hz) is bigger than one would expect for a single type of crystallographically-equivalent phosphorus nucleus. Although there are a number of possible explanations, it is postulated that the rac-$[MeEtP(S)]_2$ contains an asymmetric unit which consists of either a whole molecule or two half molecules. It may be noted that $|J_{PP}|$ is expected to increase as the size of alkyl-substituents in a diphosphine disulphide increases.

The case of a single-molecule asymmetric unit with strongly-coupled phosphorus environments is found for the compound rac-$[MeBu^tP(S)]_2$. The centreband of the spectrum (Figure 5.4) of this material appears to consist of two bands of two peaks each. The separations of the two peaks within the high and low frequency bands are 113 and 105 Hz respectively. One may view these two bands as AB doublets of two coupled phosphorus environments. The result is consistent with reported $|J_{PP}|$ values of 97 Hz,[16] 103 Hz,[8] 109 Hz,[8] or 118 Hz[6] obtained by various methods for this compound in the solution state. The larger chemical shift difference and $|J_{PP}|$ for rac-$[MeBu^tP(S)]_2$ as compared to previous compounds is caused by the increase in substituent size as has been discussed by Aime *et al.*[12] A recent X-ray diffraction crystal

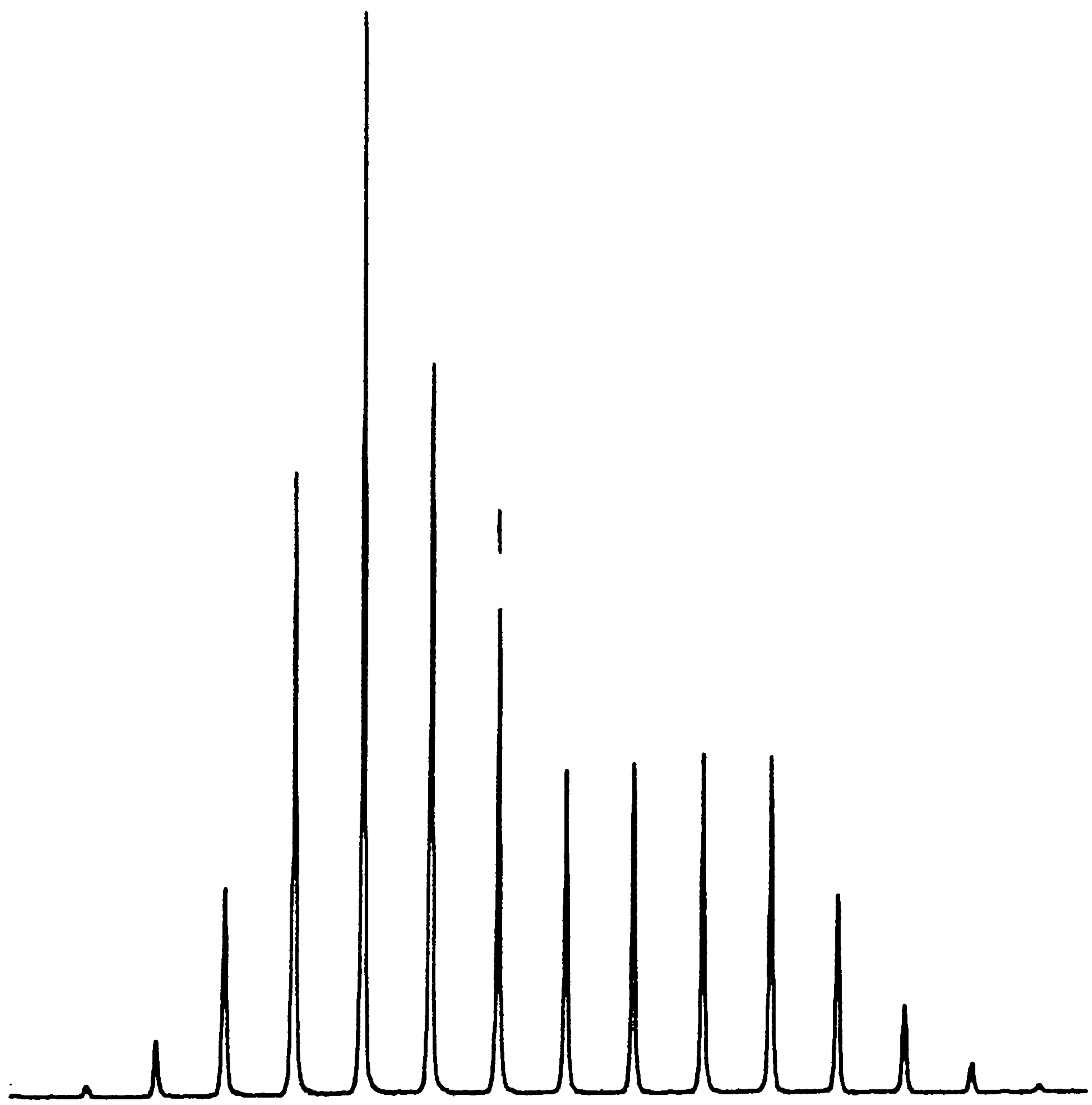

Figure 5.3: ^{31}P CP/MAS spectrum of tetraethyldiphosphine-disulphide. $[Et_2P(S)]_2$ (2). RD=6 s; PD=4 μs; CT=1.0 ms; NT=32; SF=81.014 MHz; ν_r=1380 Hz. δ_P = 51.2 ppm; $\nu_{½}$ = 68 Hz

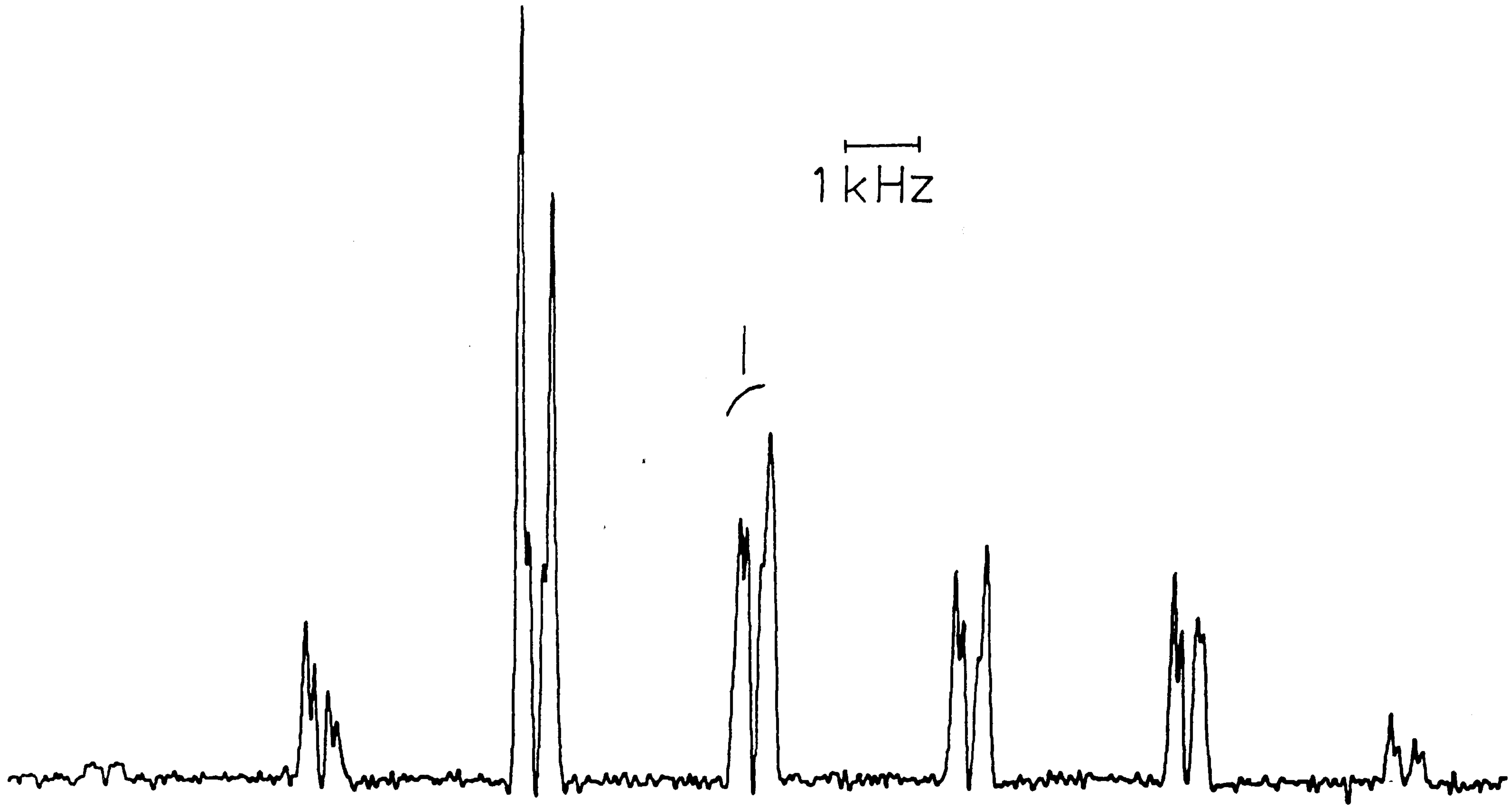

Figure 5.4: ^{31}P CP/MAS spectrum of rac-[MeBu^{t}P(S)]$_2$ (8). Resolution enhanced. RD=15 s; PD=5 μs; CT=1 ms; NT=32; ν_r=2.8 kHz; SF=81.014; δ_P = 54.8 and 51.2 ppm; $|J_{PP}|$=109 Hz.

study of this molecule by Wunderlich and Wussow[13] has indicated that the unit cell (space group $P2_1$) contains one type of molecule in which the phosphorus atoms are not related by symmetry (the asymmetric unit is a complete molecule). Thus, two coupled phosphorus environments are indicated supporting the analysis above.

A similar system is that of the meso and racemic isomers of $[EtBu^tP(S)]_2$. The spectrum of the racemic compound shows an AB-type pattern comparable to that of rac-$[MeBu^tP(S)]_2$. For the rac-$[EtBu^tP(S)]_2$, δ_P = 64.2 ppm and 61.2 ppm and $|J_{PP}|$ = 111 Hz.

For the meso- + rac-$[EtBu^tP(S)]_2$, (the separate meso compound was not available), the situation is somewhat more complicated by differing crystal morphologies found for different samples. The first spectrum taken for this mixture showed a centreband of a single narrow line (δ_P = 63.6 ppm) with a distinct broadening at the base (Figure 5.5A). As the chemical shift of the narrow line corresponded to the reported solution-state value for the meso compound, and the width of the broadened area at the base of the line was equivalent to the width of the centreband of the solid-stateracemic isomer, an assignment of a simple superposition of centrebands is proposed. (Although the meso and racemic forms were later determined by solution-state $^{31}P\{^1H\}$ NMR to be present in similar concentrations, the meso peak is a sharper resonance and thus rises above the broad component from the racemic isomer.)

Spectra taken of a second sample of this material show (Figure 5.5B) a completely different centreband structure. This centreband structure has the appearance of two AB patterns, one within the other. The outer AB pattern has δ_P = 67.5 and 61.0 ppm and a $|J_{PP}|$ of 95 Hz; for the inner pattern δ_P = 65.2 and 63.2 ppm and the $|J_{PP}|$ is 89 Hz. It would seem that this centreband arises from crystals which have a different morphology from those giving rise to Figure 5.5A. One possible explanation is that Figure 5.5B reflects crystals involving incorporation of meso and d,l forms into the same unit cell with each of the AB patterns directly corresponding to one of these forms. This analysis would imply intramolecular P-P coupling; the magnitude of the $|J_{PP}|$ apparent in

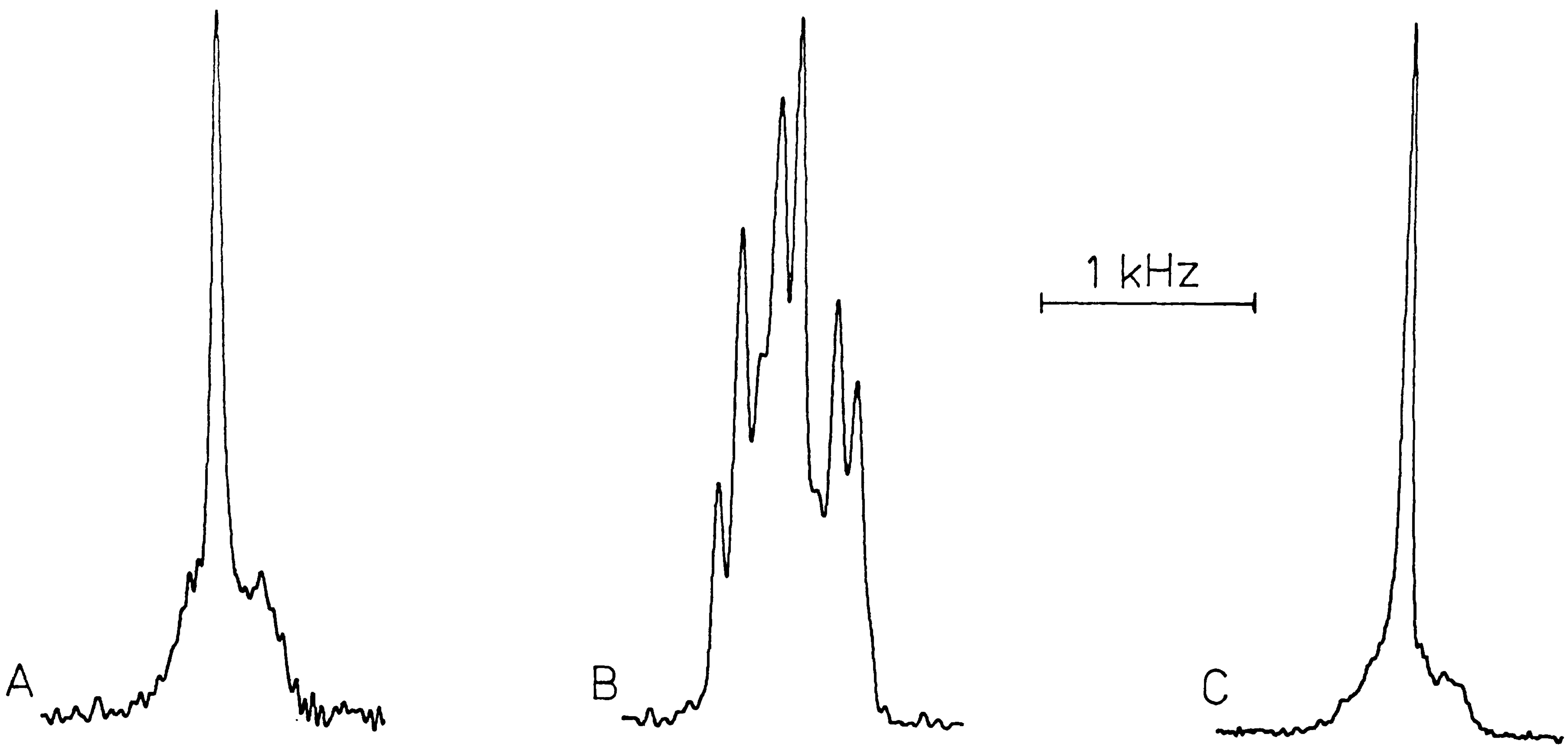

Figure 5.5: Centreband CP/MAS ^{31}P spectra of meso+rac-[EtBu^{t}P(S)]$_2$ (12). (A) Original centreband showing the narrow component of the meso form superimposed over the broad component from the racemic isomer. NT=64. (B) Centreband of a second sample of this compound showing the two AB patterns proposed as evidence of variation in morphology. NT=120. (C) Spectrum of the second sample after recrystallization. NT=72. See text for further details. SF=81.0141; RD=20s; CT=1 ms; ν_r=2.5 kHz

the spectra of this sample is very similar to the intramolecular $|J_{PP}|$ values of other compounds in this study. The solution-state spectrum of this sample showed it to contain similar amounts of the meso and racemic isomers. Solid-state spectra taken of the powder obtained after recrystallization of this solution gave a centreband (Figure 5.5C) similar to that of the first sample which, we believe, strengthens our argument for different crystal morphology.

It should be noted that for both rac-$[MeBu^tP(S)]_2$ and rac-$[EtBu^tP(S)]_2$ the detailed distribution of spinning sideband intensities is unusual (e.g. Figure 5.4). The relative intensities of the lines in the AB subspectra do not have the appearance of a usual AB spectrum. It is felt that this may be due to anisotropy in the scalar coupling. Such effects have been discussed by Zilm and Grant[27] and by Harris, Packer and Thayer[28]. Unfortunately, the resolution in these spectra is not sufficient for a clear analysis. Attempts to improve the resolution by running at a higher field were unsuccessful.

An excellent example of an AB pattern from a solid compound may be noted in the spectrum of $[Bu^n{}_2P(S)]_2$. As can be seen in Figure 5.6, the AB spectrum is clearly resolved. The centrebands have a δ_P of 51.1 ppm and 49.4 ppm with a $|J_{PP}|$ of 57.5 Hz. The solid-state NMR data are strongly indicative of an asymmetric unit consisting of a single molecule.

The situation of a unit cell containing two centrosymmetric but non-equivalent molecules is found for the compound $[Ph_2P(S)]_2$. The centreband spectrum consists of two partially resolved resonances of 144 Hz total width. The width of each of the resonances, if resolved, would be ca. 80 Hz. This observation is in agreement with the X-ray diffraction crystal structure reported by Blake, Howie and McQuillan[29]. The data show the unit cell to be of space group $P2_1/c$ and to contain two different half-molecules. Each of the two resonances, therefore, represents one of the non-congruent phosphorus molecules within the unit cell. The fact that the phosphorus atoms within the individual molecules are equivalent accounts for each of the lines being reasonably narrow. What has not yet been fully explained in this case is the apparent

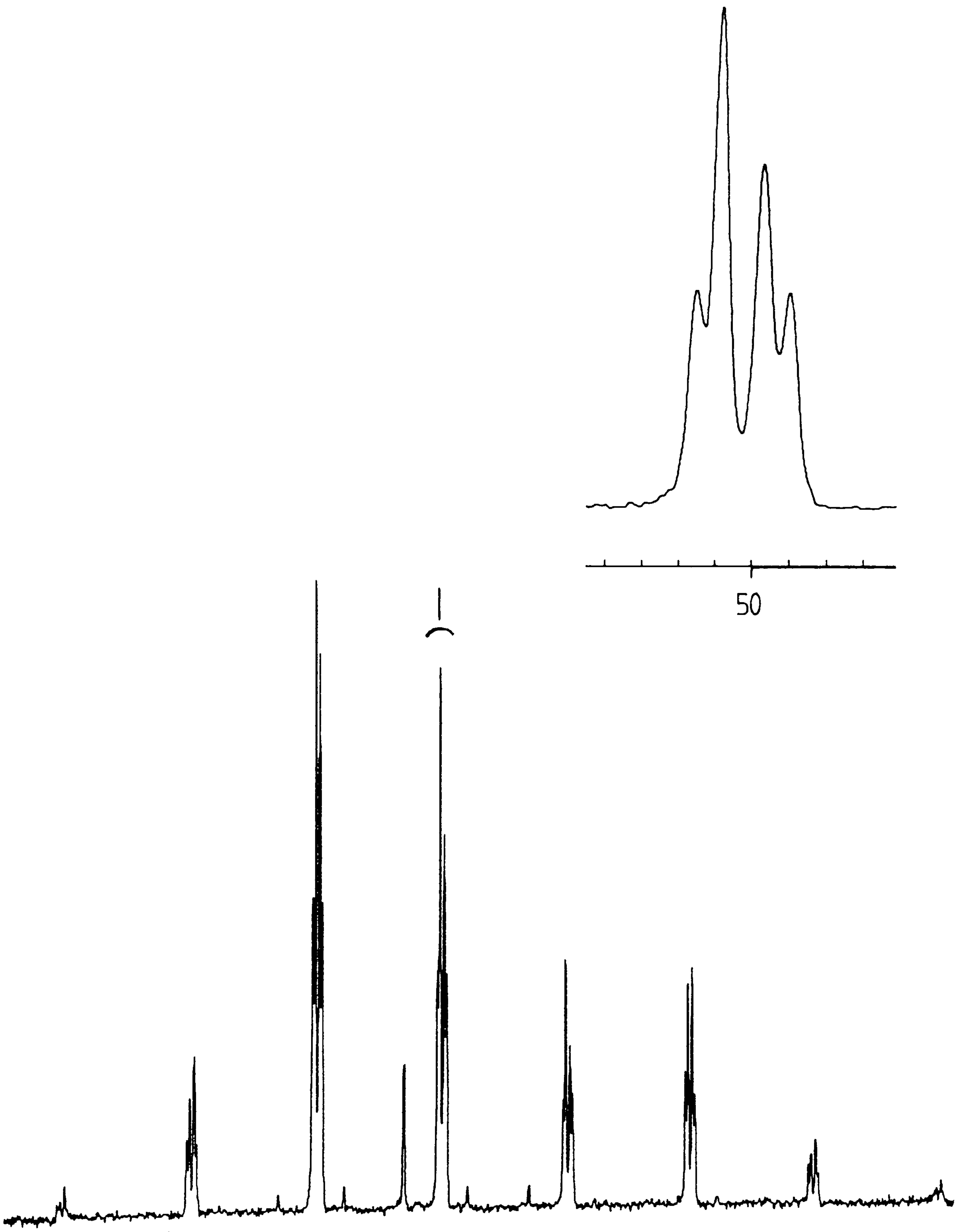

Figure 5.6: ^{31}P CP/MAS spectrum of $[Bu^{n}_{2}P(S)]_{2}$ (4) and expanded centreband. SF=81.014 MHz; RD=60 s; PD=5 μs; CT=1 ms; ν_r=2629 Hz; NT=12. δ_P = 51.1 and 49.4 ppm. $|J_{PP}|$=58 Hz. The scale divisions represent 1 ppm

difference in intensity between the two resonances integrated over the spinning sideband manifolds. From the crystallographic data noted above, the ratio of the peaks should clearly be 1:1; however, the ratio of the high-frequency to low-frequency peaks is closer to 2:3. The difference is almost certainly a relaxation phenomenon, since the ratio approaches unity as the recycle delay between pulses is increased. However, it is not at all apparent why there should be such a difference between two similar molecules.

The next example to consider here is that of meso-$[Me(l\text{-}Menthyl)P(S)]_2$. As noted above, because the menthyl group is itself chiral, this molecule contains four chiral centres. The centreband spectrum consists of two resonances at 48.1 and 41.0 ppm each with a linewidth of ca. 122 Hz. A possible explanation for this spectrum may be found by comparison of the solid- and solution-state data. The solution-state spectrum is that of an AB pattern with δ_P = 48.93 and 43.44 ppm and a $|J_{PP}|$ of 55 Hz.[17] This suggests that the solid spectrum results from a single molecule in the unit cell with the phosphorus atoms unrelated by symmetry thus giving a similar spectrum but with the AB coupling unresolved. This analysis is not unambiguous, however, as a similar spectrum could possibly result from a crystal structure containing two asymmetric molecules per unit cell. As yet, crystals stable under X-ray bombardment have not been obtained.

The last system to be discussed is that of the meso + racemic mixture of $[Pr^iBu^tP(S)]_2$. The centreband spectrum consists of a broad band at δ_P = 74.1 ppm and a somewhat narrower band at δ_P = 68.6 ppm. It has been postulated that the broad band is a superposition of the P-P coupled resonances from the racemic form of the molecule. If this is indeed the case, the narrower peak would correspond to the meso form. This suggestion is confirmed by previous solution-state work, which shows the racemic and meso forms to have a δ_P of 75.2 and 68.6 ppm respectively.[18] Unfortunately, it has not been possible to separate the isomers. There is also not sufficient information to draw any conclusions about the crystal structure involved.

5.4 Scalar Coupling Considerations (PP AND PC)

One of the most disappointing aspects of this study was the general inability to obtain scalar coupling information. Such information has proven very valuable in solution-state studies of the conformation of these compounds[16,11] and of the related diphosphines[7,8]. In this study, there were only three phosphorus-phosphorus coupling constants resolved (Table 5.1). Furthermore, no coupling information whatsoever was resolved in the carbon spectra. For both ^{13}C and ^{31}P, high-field studies on the VXR-300 did not give resolution that was significantly better.

For both nuclei, it is the case that resolution was not sufficiently good to resolve the coupling that was present. For phosphorus, the narrowest line resolved in this study was ca. 46 Hz wide. As may be seen in Table 5.1, solution-state studies have found $|J_{PP}|$ values to range from 18.7 to 118 Hz. However, they are generally 55 Hz or below and thus too small to be resolved. It may be noted that one of the three exceptions is the only case where $|J_{PP}|$ in solution was larger than 100 Hz.

Residual linewidths in solid-state NMR may be seen mainly to arise from chemical shift dispersion and anisotropic bulk magnetic susceptibility effects as well as such factors as insufficient decoupling fields and magic angle mis-set. A discussion of residual linewidths in solid-state ^{31}P spectra has recently been published by Hemminga *et al.*[30]

Figure 5.7 is the ^{13}C spectrum of $[Bu^n_2P(S)]_2$. It is the best resolved of all of the ^{13}C spectra attempted for these compounds. As can be seen, there is no resolution whatsoever for the α-carbon at ca. 29 ppm and clearly insufficient resolution for the β- and γ-carbons (25-26 ppm). In this spectrum, it seems obvious that there are two types of inequivalent n-butyl groups in the molecule as evidenced by the two well-resolved, narrow methyl group resonances. The resonances of these two groups overlap and the P-C coupling, which is generally of the order of 30-50 Hz for the diphosphine disulphides[12], has remained unresolved.

As was stated, the tetra-n-butyl case was the best ^{13}C

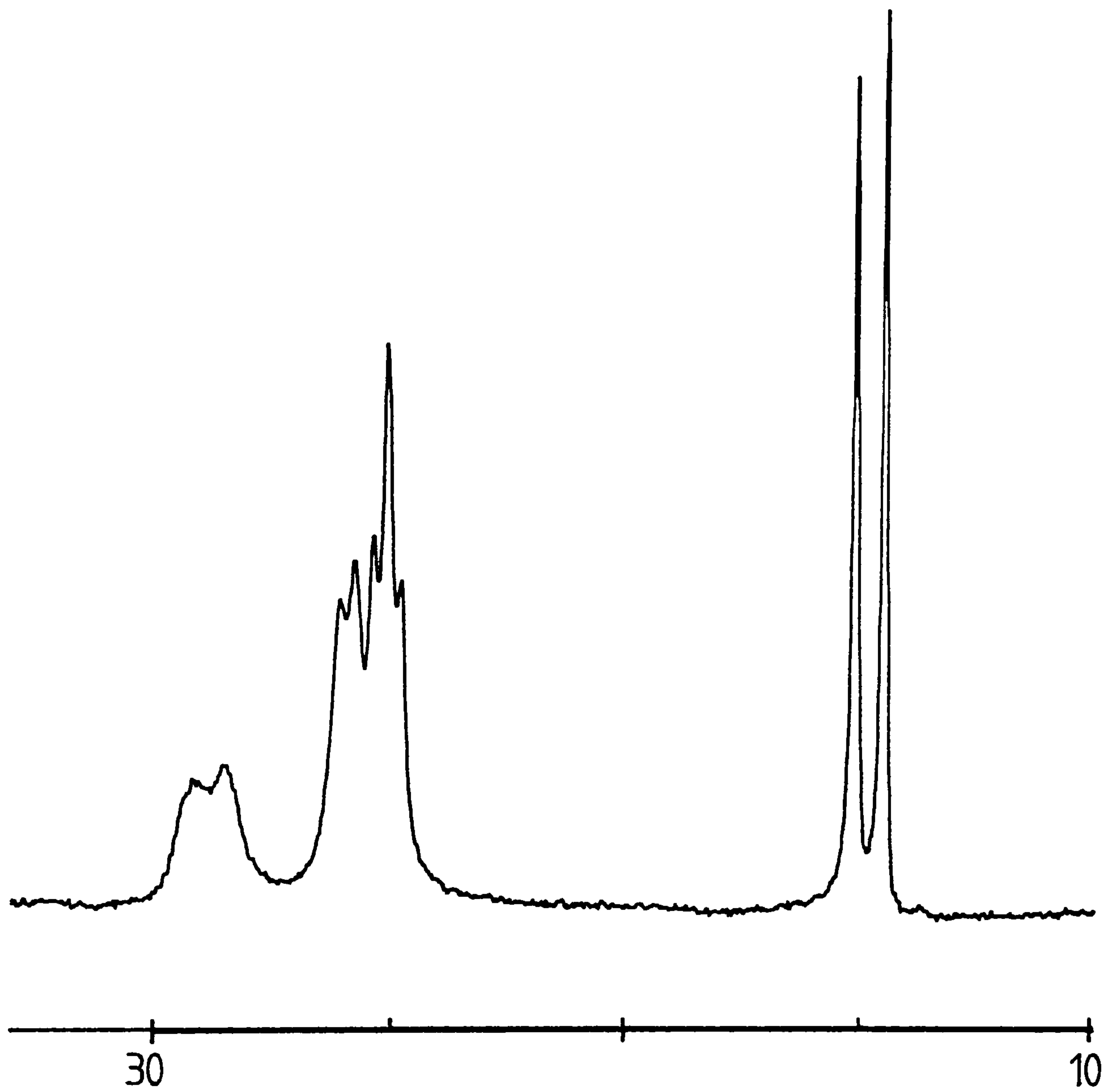

Figure 5.7: ^{13}C CP/MAS spectrum of $[Bu^n{}_2P(S)]_2$ (4).
SF=50.3227 MHz; RD=30 s; PD=5 μs; CT=3 ms; ν_r=2626 Hz; NT=100.
Scale = 5ppm per small division. δ_C = 26.1, 25.8, 25.4, 25.1, 24.8, 15.0 and 14.4 ppm. $\nu_{1/2}$ for the methyl group resonances (15.0 and 14.4 ppm) 7 Hz.

spectrum obtained in this study. For the most part, the spectra were less-well resolved than this and did not provide sufficient detail to even give unambiguous assignment of the size of the asymmetric unit. These limitations can generally be seen to be a result of relatively small P-C coupling constants combined with ^{13}C linewidths in solids which are generally larger (ca. 5 Hz for mobile methyl groups to ca. 40 Hz for other groups) than in the solution-state. Again, a discussion of ^{13}C solid-state linewidths is available in the literature[31].

5.5 Shielding Tensor Considerations

5.5.a Introduction

In the literature of the solid-state ^{31}P NMR of condensed phosphates, there are a number of studies relating the components of the shielding tensor to various structural characteristics of the compounds concerned. Phosphate resonances generally occur within a relatively small isotropic chemical shift range[32], and, therefore, additional parameters are required to assist in the characterization of these materials. Given the fact that such studies have provided useful correlations (*vide infra*), it was decided to investigate whether shielding information could also provide similar information for the diphosphine disulphides. After a limited survey of the shielding tensor literature for phosphorus, diphosphine disulphide results from this study and from the literature will be presented and discussed.

As was noted, a number of solid-state studies have been carried out on condensed phosphate systems. Since this thesis is not directly concerned with phosphates, the literature presented here was generally chosen to be representative of the information available from the analysis of phosphate shielding tensors rather than being a comprehensive review. A more complete review of the phosphate literature may be found in reference[33]. It should also be noted that the literature survey is equally applicable to the phosphonic and phosphinic acid compounds in the next chapter.

One of the initial correlation studies was done by Grimmer[34]. In this work, the shielding anisotropy of solid phosphate and POX_3 compounds with C_{3v} symmetry was studied. A correlation between the anisotropy and the P-O bond length along the threefold symmetry axis was found. The relationship is expressed as $\Delta\sigma = -1585r_{P-O} + 2553$, where $\Delta\sigma$ is expressed in ppm and r_{P-O} in Angstroms. This correlation was further related to the π-bond character of the P-O bonds.

Oldfield and co-workers[35] have reported a study of the effect of structure and cation on ^{31}P chemical shifts and chemical shift anisotropies for orthophosphates. Correlations were drawn between the isotropic chemical shift and the electronegativity of the cation. A linear correspondence was found between the P-O bond length and the anisotropy. This resulted in an expression similar to that given by Grimmer. A somewhat better correlation was found between the anisotropy and the deviation of the O-P-O bond angle from that of a perfect tetrahedron (109° 28'). The equation given is of the form: $\Delta\sigma = 30.90(\sum_n|109.5-\theta_{O-P-O}|/n)-1.22$. This latter expression gave a correlation constant of 0.99 as opposed to 0.93 for the bond distance expression. In this work, no attempt was made to theoretically explain these empirical relationships.

The Brown and Shannon bond-strength parameter[36] has been correlated to the isotropic chemical shift for a number of phosphates in a paper by Cheetham *et al*[37]. Further, the anisotropy in the ^{31}P shielding was found to be related to the size of the range of the P-O bond strengths at oxygen. That is to say, in a phosphate in which there are several different types of phosphate unit, that unit which has the largest range of bond strengths at oxygen is also that which has the largest anisotropy. As such, the anisotropy information may be used to correlate NMR data with X-ray structures. It is pointed out in the paper that the relationship is inconclusive where the values of the anisotropy are close, and that further study is necessary to determine the general applicability of the approach.

Moving now to organophosphorus compounds, there has been one single-crystal NMR study of the diphosphine disulphides. Tutunjian and Waugh[20] report the study of a single crystal of tetraethyl-diphosphine disulphide. This study is, for the most part, concerned with the spin-spin coupling tensor; however, the shielding tensor eigenvalues and eigenvectors are also reported. The results of this work will be discussed below. It should be noted that three figures, which were to relate the directions of the principal components to the molecule-fixed frame, seem to have been omitted from this work.

Finally, Dutasta *et al.*[38] have used four organophosphorus compounds to investigate the effect of O-P-O bond angle on the anisotropy and asymmetry of the ^{31}P shielding tensors. The systems chosen were four cyclic organophosphorus compounds each containing the $O_2P(S)CH_3$ group. In this fashion, the phosphorus had the same chemical environment in all of the compounds. The size of the ring, which attached to the two oxygens, was used to vary the O-P-O bond angle. The study showed a good linear correlation between the asymmetry parameter and the intracyclic O-P-O bond angle, α. The relationship is given as $\Delta\eta/\Delta\alpha = -6.9$. Through symmetry arguments, the direction of the σ_{33} component is assigned to be close to the P=S bond orientation.

5.5.b Shielding Tensor Results and Discussion

For the spectra of the diphosphine disulphide compounds in which the resonances were sufficiently resolved, calculations of the principal components of the chemical shielding tensors were done. Initial calculations were made using the method of moments analysis of Maricq and Waugh. In all cases, the results were further refined using the sideband fitting routine SBFIT. (Both of these methods have been described in detail in Chapter 4.) The results of these calculations and the results from the literature are reported in Table 5.3

Table 5.3
Shielding Tensor Data: Diphosphine Disulphides

Compound	σ_{iso}	δ	η	σ_{11}	σ_{22}	σ_{33}
	Shielding Tensor Components†					
(1) Me_2	-37.2	108	0.09	-96	-86	71
	-34.9	106	0.12	-94	-81	71
(2) Et_2	-51.2	115	0.07	-113	-105	64
(2) Et_2**	-48.7	107	0.08	-106.6	-98.2	58.8
(3) $Pr^n{}_2$	-45.9	115	0.04	-106	-101	69
(5) Ph_2	-41.4	120	0.05	-105	-98	78
	-40.2	120	0.17	-110	-89	80
(6) MeEt (meso)	-45.1	108	0.35	-118	-80	63
(7) MeEt (rac)	-45.0	106	0.31	-114	-82	61
(9) MePh (meso)	-38.4	113	0.21	-101	-88	74
(10) Me-l-Men (meso)	-48.1	120	0.27	-124	-92	71
	-41.0	96	0.50	-113	-65	55
(14) compound II	-62.7	80	0.67	-130	-76	17

† All data (except η) are in ppm with respect to 85% aqueous H_3PO_4. The tensor components are quoted to ±5 ppm and η to ±0.15.
**Results from reference (20). Error ±1 ppm.

The anisotropy values for the diphosphine disulphides are all positive and range from 80 to 126 ppm. The spread is smaller than that reported for the inorganic phosphates, the magnitude of which cover from approximately 69 to 156 ppm[32,33]. The smaller overall range for the compounds in this study can generally be attributed to several factors. Firstly, all of the diphosphine disulphides in Table 5.3 for which crystal structures are reported have the same overall *trans* configuration[13]. In this series there are no major substituent or conformational changes which would radically alter the shielding environment. Secondly, the hydration, protonation, and cation charge and electronegativity factors which have a significant effect in the inorganic phosphates are not present in the diphosphine disulphides.

The fact that all of the anisotropy values are positive implies that the largest tensor component (in the chosen convention - see Chapter 4) is one of relative shielding rather than deshielding. This seems straightforward if one makes the assumption that the results reported by Tutunjian and Waugh[20] for the tetraethyl compound are applicable across the full range of compounds discussed here. Their single-crystal study has shown the σ_{33} tensor (which is the largest of the three) to be approximately co-linear with the P=S bond direction and to be a shielding effect. One may also look to the work of Dutasta *et al.*[38] in which symmetry arguments are used to assign the maximum shielding direction, σ_{33}, as co-linear with the P=S bond in the cyclic derivatives of $O_2P(S)CH_3$. Again, positive anisotropies are noted.

The asymmetry values reported for the diphosphine disulphides range from 0.0 to 0.67; that is, from axially symmetric to moderately asymmetric. It may be seen that the symmetrical compounds are generally close to axially symmetric, while the compounds for which $R_1 \neq R_2$ have increasing values for the asymmetry parameter. This trend for the asymmetric compounds may be explained by overall molecular symmetry considerations and by the differing shielding effects and P-C bond lengths of the various substituents.

While the trend of increasing values of the asymmetry parameter with molecular asymmetry seems to be generally straightforward, it is not immediately evident why the symmetrical compounds should have axial symmetry. One may naively expect axial symmetry where the three phosphorus σ bonds are all to oxygen, for example, but not in the case where bonding to more than one type of atom is concerned.

Taking, for example, $[Et_2P(S)]_2$, it may be seen from the results reported here and in the literature[20] that this compound has essentially axial shielding symmetry. Given that the σ_{33} axis lies along the P=S bond[20], the fact that the asymmetry is only 0.07 implies virtually cylindrical shielding perpendicular to that axis. Such cylindrical shielding would further imply rather similar electron density characteristics in the three σ bonds which are contained within this cylinder. Two of these σ bonds are to carbon ($\simeq$ 1.83Å) and one is to phosphorus (2.22Å). At first examination, it is not clear why these bonds should have such similar electron density characteristics; however, given these results, it seems likely that they do. It has been suggested[40] that this result is not as unreasonable as it initially seems if viewed from an electronegativity and electron-donating perspectve. While carbon is seen to be slightly more electronegative than phosphorus, the electron-donating ability of the overall ethyl group may compensate for this difference. Thus, the electron density along the three bonds at the phosphorus is generally similar to within the small value of the asymmetry parameter given.

Moving to possible empirical relationships described for other phosphorus compounds in the literature discussed above, it was found that there were very few, if any, good correlations between the shielding tensor values listed in Table 5.3 and any of various physical parameters. Attempts to correlate δ, n, σ_{11}, σ_{22}, or σ_{33} with such parameters as N_R; P-C, P-S, and P-P bond distances; CPP, CPC and SPC bond angles; sum of the deviation of the bond angles from the tetrahedral angle (109.5°); P-S bond strength; and a number of others were all generally unsuccessful. A number of specific correlations might have been expected from a straight-forward examination of the literature. Several of these will be briefly noted. Further, there are a number of possible explanations for the apparent lack of correlation between the tensor data and the molecular structural features. The remainder of the chapter will be concerned with these.

A number of possible areas of correlation were indicated either by solution-state results or by results in the literature for other classes of compounds (above). Although unsucessful, these included:

a) A correlation might have been expected between the σ_{33} tensor and the P=S bond distance. Tutunjian and Waugh[20] have shown the σ_{33} tensor axis to be co-linear with the P=S bond. Further, Grimmer[34] has shown direct correlation between the P=O bond distance and the shielding anisotropy. One might thus expect a direct relationship between the P=S bond distance and the size of either the anisotropy or the σ_{33} tensor.

b) Given that a reasonably good correspondence was found between N_B and the isotropic chemical shift, one might also have expected a strong correlation between N_B and one of the tensor components (probably either σ_{11} or σ_{22}).

c) Finally, a correspondence of the CPC or SPC bond angles with the asymmetry might have been expected. The paper by Dutasta *et al.*[38] described above showed good correlation between the asymmetry and the O-P-O bond angles in the compounds considered. No similar correspondence was found in this study.

There are a number of possible explanations for the lack of meaningful correlations noted here. The first main area of discussion contains a number of points and is concerned in the loose sense with errors and the size of the data set. The second relates a more fundamental problem regarding the nature of the internal interactions present. Each area will be discussed in turn.

The first possible explanation for the lack of correspondence may be considered, generally, to be a statistical one. Of the fourteen diphosphine disulphides in this study, only nine gave spectra for which sideband analysis seemed reasonable. The remaining spectra contained broad or poorly resolved bands which precluded any accurate analysis. Further, of the nine compounds analysed, only five have known crystal structures. Therefore, it will be seen that the set of data upon which one must draw conclusions is quite small. This fact, combined with the error bars of ±5 ppm involved in the determination of the tensor components, generally indicates the difficulties involved in any correlation study of this sort.

The single major source of error in this study is most probably in the calculation of the shielding tensor components from the spinning sideband pattern. The general difficulties involved for these calculations have been considered at length in Chapter 4.

Even though the fitting routine was used, the errors in this work are most certainly larger than those reported for the compounds used as examples in that chapter. This is because the diphosphine disulphide work was done on the earlier and less-stable Andrew-Beams rotor system. Errors resulting from spinning-speed drift and angle mis-set are more likely than for the double-bearing probe system (see Chapter 3). It was generally not possible to repeat these experiments on the newer probe system as sample quantities were small and not amenable to spinning on the double-bearing system. In addition, one could not circumvent this problem by running static spectra as there are direct P-P bonds in these compounds and the static spectra would thus contain components from direct dipolar coupling.

A smaller, but possibly still significant source of error, may be in the bond lengths quoted in the X-ray crystal structures of these compounds. Grimmer has pointed out[34,41] that a change in P-O bond distance of 0.0005 Å can result in a change of approximately 1 ppm in the phosphorus anisotropy. Several of the crystal structures of the diphosphine disulphides date from the 1960's. P=S distances in these papers are quoted with errors from ±0.002Å to ±0.005Å. If a similar relationship to that quoted by Grimmer holds, this could represent an additional uncertainty of up to ±10 ppm. The difficulty in finding a correspondence between σ_{33} and the P=S bond distance may thus arise from errors in both the NMR and X-ray data.

Correlations with the parameter, N_{β}, may be problematic for several reasons. Firstly, only seven of the compounds in Table 5.3 are alkyl-substituted and thus available for this correlation. Further, such parameters, although generally useful, may always be liable to exception. The solution-state study of the diphosphine disulphides by Aime *et al.*[12] noted that the tetra-n-propyl compound fell well to the left of the line. This fact was ascribed to further γ-shielding effects. Such scatter in N_{β}, caused by additional steric and shielding effects, when combined with the errors in the tensor components and the small data set, again make correlation studies difficult.

A second significant source of errors that must be considered is the effect on the MAS spectrum of the various internal interactions which are present. It should be remembered that the diphosphine disulphide system consists of directly bonded, abundant nuclei. Therefore, in principle, the system is homogeneous, though the spin pairs are to some extent isolated (See section 2.4). If the static spectrum is first considered, it is clear that its form will result from shielding anisotropy, P-P dipolar coupling and, in a number of cases, P-P scalar coupling as well. All of these affect the MAS spectrum to varying extents. The presence of such interactions implies that the tensor components derived from the spinning sideband analysis will not be purely the result of the shielding interaction, but will be some sort of average of shielding and dipolar tensors. Since the static pattern for the dipolar interaction alone would consist of two subspectra, symmetrical about the centre, it is likely that the results of spinning sideband analysis will approximate to the shielding tensor components, at least when the dipolar term is relatively small. However, the existence of dipolar as well as shielding interactions implies that, strictly speaking, it will not be possible to fit the sideband pattern to the model presented in Chapter 4. Although Maricq and Waugh[42] discuss the general aspects of an isolated spin pair affected by both shielding and dipolar interactions, no suitable theory for the analysis of this type of homonuclear coupled case appears to exist. Fortunately, the errors which result in the shielding tensor values are probably small given that the shielding anisotropy, which is ca. 9 kHz, is much larger than the P-P dipolar coupling, which is calculated to be of the order of 3 kHz.

It is suggested for future work that there may be two methods to determine the extent that the dipolar interaction affects the MAS spectra of the diphosphine disulphides. Firstly, a simulation of the spinning-sideband pattern could be done which takes account of both shielding and dipolar contributions. This would probably be unambiguous for at least the tetraethyldiphosphine disulphide case, where the orientation of the shielding and dipolar axes are known. The second alternative would be the use of phosphorus CRAMPS techniques to remove the dipolar interaction. The use of CRAMPS techniques may add additional sources of error to the sideband calculations, though, in the form of scaling factor errors and variation in the efficiency in the removal of the dipolar interaction with offset from the carrier[43].

References

1. E.R. Andrew, *Progr. Nucl. Magn. Reson. Spectr.* **8**, 1 (1971).

2. A. Pines, M.G. Gibby and J.S. Waugh, *J. Chem. Phys.* **59**, 569 (1973).

3. J. Schaefer and E.O. Stejskal, *J. Amer. Chem. Soc.* **98**, 1031 (1976).

4. R.K. Harris, *Canad. J. Chem.* **42** 236 (1964).

5. P. Diehl, R.K. Harris and R.G. Jones, *Progr. Nucl. Magn. Reson. Spectr.* **3**, 1 (1967).

6. G. Hägele, R.K. Harris and J.M. Nichols, *J. Chem. Soc., Dalton Trans.*, 79 (1973).

7. R.K. Harris, E.M. McVicker and M. Fild, *J. Chem. Soc., Chem. Commun.*, 886 (1975).

8. H.C.E. McFarlane and W. McFarlane, *J. Chem. Soc., Chem. Commun.*, 582 (1975).

9. R.K. Harris and R.G. Hayter, *Canad. J. Chem.* **42**, 2282 (1964).

10. J.D. Lee, *J. Inorg. Nucl. Chem.* **32**, 3209 (1970).

11. S. Aime, R.K. Harris, E.M. McVicker and M. Fild, *J. Chem. Soc., Chem. Commun.*, 426 (1974).

12. S. Aime, R.K. Harris, E.M. McVicker and M. Fild, *J. Chem. Soc., Dalton Trans.*, 2144 (1976).

13. H. Wunderlich and H-G. Wussow, *Z. Naturforsch* **39b**, 1581 (1984).

14. K. Moedritzer, L. Maier and L.D.C. Groenweghe, *J. Chem. and Eng. Data* **7**, 307 (1962).

15. E. Fluck and K. Issleib, *Chem. Ber.* **98**, 2674 (1975).

16. G. Hägele, G. Tossing, W. Kuckelhaus, J. Seega and R.K. Harris, *J. Chem. Soc., Dalton Trans.*, 2803 (1984).

17. G. Tossing, Ph.D. thesis, University of Düsseldorf (1983).

18. G. Hägele, private communication.

19. E.G. Finer, M.Sc. thesis, University of East Anglia (1966).

20. P.N. Tutunjian and J.S. Waugh *J. Chem. Phys* **76**, 1223 (1982).

21. D.M. Grant and E.G. Paul. *J. Amer. Chem. Soc.* **86**, 2984 (1964).

22. L.D. Quin and J.J. Breen, *Org. Magn. Reson.* **5**, 17 (1973).

23. J.D. Lee and G.W. Goodacre, *Acta Cryst.* **B27**, 302 (1971).

24. P.J. Wheatly. *J. Chem. Soc.*, 523 (1960).

25. S.N. Dutta and M.M. Woolfson, *Acta Cryst.* **14**, 178 (1961).

26. J.D. Lee and G.W. Goodacre, *Acta Cryst.* **B25**, 2127 (1969).

27. K.W. Zilm and D.M. Grant, *J. Amer. Chem. Soc.* **103**, 2913 (1981).

28. R.K. Harris, K.J. Packer and A.M. Thayer, *J. Magn. Reson.* **62**, 284 (1985).

29. A.J. Blake, R.A. Howie and G.P. McQuillan, *Acta Cryst.* **B37**, 966 (1981).

30. M.A. Hemminga, P.A. de Jager, J. Krüse and R.M.J.N. Lamerichs, *J. Magn. Reson.* **71**, 446 (1987).

31. D.L. VanderHart, W.L. Earl and A.N. Garroway, *J. Magn. Reson.* **44**, 361 (1981).

32. T.M. Duncan and D.C. Douglass, *Chem. Phys.* **87**, 339 (1984).

33. P. Wilkes, Ph.D. thesis, University of Durham (1987).

34. A.R. Grimmer, *Spectrochemica Acta*, **34A**, 941 (1978).

35. G.L. Turner, K.A. Smith, R.J. Kirkpatrick and E. Oldfield, *J. Magn. Reson.* **70**, 408 (1986).

36. I.D. Brown and R.D. Shannon, *Acta Cryst.* **A29**, 266 (1973).

37. A.K. Cheetham, N.J. Clayden, C.M. Dobson and R.J.B. Jakeman, *J. Chem. Soc., Chem. Commun.*, 195 (1986).

38. J.P. Dutasta, J.P. Robert and L. Wiesenfeld, *Chem. Phys Lett.* **77**, 336 (1981).

39. L. Griffiths, A. Root, R.K. Harris, K.J. Packer, A.M. Chippendale and F.R. Tromans, *J. Chem. Soc., Dalton Trans.*, 2247 (1986).

40. K.B. Dillon, private communication.

41. A.R. Grimmer, private communication.

42. M.M. Maricq and J.S. Waugh, *J. Chem. Phys.* **70**, 3300 (1979).

43. U. Haeberlen, "High-resolution NMR in Solids: Selective Averaging", Academic Press, New York (1976).

CHAPTER SIX - MULTINUCLEAR MAGNETIC RESONANCE STUDY OF SOLID PHOSPHONIC AND PHOSPHINIC ACIDS

6.1 Introduction

This chapter details the results obtained in a study of a series of phosphonic and phosphinic acid derivatives by solid-state nuclear magnetic resonance spectroscopy. The work had two main goals. The first aim was to characterize the solid structure of these compounds by the use of ^{31}P, ^{13}C and ^{15}N CP/MAS NMR. The second goal was to determine the applicability of ^{1}H CRAMPS techniques in the characterization of the hydrogen bonding present in these materials.

The main interest in studying these two systems may be found in the examination of the chelation properties of the phosphonic acids. A number of gem-diphosphonates have been found to have effective alkaline-earth ion sequestration properties[1]. HEDP (24), in particular, has been demonstrated to be an effective inhibitor of calcium hydroxyapatite crystal growth *in vitro* and to inhibit pathological calcification *in vivo*[2]. Furthermore, oligophosphonate complexes of tecnetium-99 and indium-133 have found application in modern *in vivo* diagnostic techniques[3]. Importantly, the form of the phosphonate ligand has been conclusively shown to influence the organ specificity of the technique. As the structure and hydrogen bonding of such phosphonic and phosphinic acid complexes will certainly have an important influence on their properties, it was felt that this could be a useful area of investigation.

A list of compounds studied may be found in Tables 6.1 and 6.6. These are generally derivatives of the hypothetical phosphonic (I) and phosphinic (II) acids, the acid groups having the forms noted below. In this study R, will be for the most part methyl, although several phenyl phosphinic acids are included.

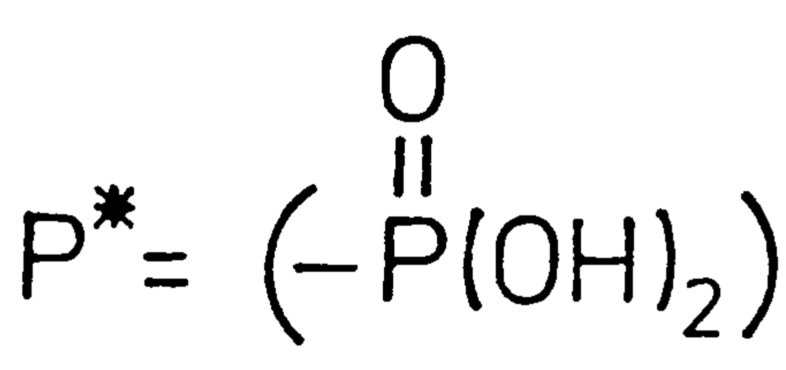

I

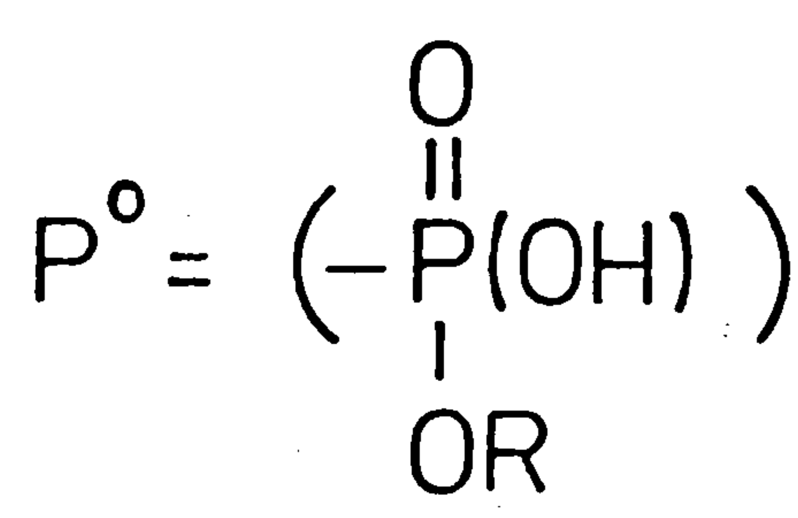

II

A wide range of compounds was examined in this study, and there are many different ways in which they could have been arranged for discussion. In order to simplify the presentation, the compounds have been divided into three main categories: 1) phosphonic acids; 2) amino phosphonic acids; and 3) phosphinic acids. Within each group, the materials have been arranged roughly in order of a) increasing organic backbone length, and b) number of phosphorus acid groups. Note that compounds (30)-(32) and similar compounds have been named as the derivatives of ethane phosphonic acid.

6.2 Results and Discussion

The following sections contain a detailed, compound-by-compound discussion of the materials in this study. While this may not be the most elegant manner in which to relate a set of results, this method of organisation was dictated by the reasonably large number of compounds examined. While this diverse group was not particularly amenable to overall generalities, a number of subsets have produced data which are instructive and informative. As such, it was considered better to include more information than less. To assist the reader, a large number of tables have been included. Following these sections, there are general discussions of chemical shift and shielding considerations as well as a discussion of the ^{1}H CRAMPS results. The proton results are given in Tables 6.2 and 6.7.

^{13}C spectra were run for all of the compounds in this chapter; however, in many cases the resolution of the solid-state MAS technique was not sufficient to resolve the various lines in the spectrum. This is considered to be a result of the small relative chemical shift range occupied by carbons bonded to phosphonic or phosphinic acids (e.g. di- or tri- acids on an ethane or propane hydrocarbon backbone), combined with the moderate-to-large P-C scalar couplings and a solid-state ^{13}C residual linewidth of ca. 20-30 Hz. Only data from those ^{13}C spectra which have provided useful information are included in this discussion and in the results of Table 6.5. Where carbon results are omitted, it may be assumed that the spectrum of that particular compound did not show fine structure.

Where necessary, nitrogen-15 spectra of the aminophosphonic acids were run. The results are presented in the discussion as well as in Table 6.4. The nitrogen results gave useful confirmation of the size of the asymmetric unit. For several of the compounds, such information was not available from the carbon spectrum. The nitrogen shifts were generally in the amine range, as would be expected.

6.2.a Phosphonic Acids

(15) P*-CH_2-P* Methylenediphosphonic acid

The ^{31}P spectrum of this compound shows two broad, partially resolved singlets with a total linewidth of ca. 280 Hz. This linewidth seems rather large in comparison with other phosphonic acids. Two X-ray crystal structures of this compound have been published[4,5]. Both of these report a single molecule per unit cell with the two phosphorus atoms being inequivalent. Each of the two resonances most likely arises from one of the phosphorus atoms in the molecule. P-P scalar coupling is certainly present though not resolved. Geminal couplings for phosphonic acids are generally of the order of less than 10 Hz[3] so geminal P-P scalar coupling alone is probably not responsible for the large linewidths present in the spectrum. Such broadening in the NMR of solids can result from a number of factors; however, in this instance, the particular source is not clear.

The CRAMPS spectrum of this material shows two types of hydrogen bonded acid protons at 11.9 and 10.3 ppm with an approximate intensity ratio of 3:1. The correspondence with the X-ray crystal structure is noted in Table 6.11 and Figure 6.16. The reader is directed to section 6.5 for details.

Table 6.1: Solid-State ^{31}P CP/MAS
Data for Phosphonic Acids P*= -P(O)(OH)$_2$

	Compound	δ_P/ppm	$\lvert J_{PP}\rvert$/Hz	$\lvert J_{PC}\rvert$/Hz
(15)	P*-CH$_2$-P*	26.2 24.7	-	-
(16)	P*-CH$_2$-P* Na$_2$ salt	22.3 14.4	-	-
(17)	HOOC-CH$_2$-P*	17.1	-	-
(18)	P*-CH$_2$-CH$_2$-P*	32.7	-	-
(19)	P*-CH$_2$-CH$_2$-P* Na$_2$ salt •4H$_2$O	29.3	-	-
(20)	P*-CH$_2$-CH$_2$-P* Na4 salt	24.8	-	-
(21)	P*-CH$_2$-CH-P*$_2$	28.7 19.9	-	-
(22)	P*$_2$-CH-CH-P*$_2$ [(NH$_2$)$_3$C]$^+_6$salt •6H$_2$O	19.9 18.3	-	-
(23)	P*$_2$-CH-CH-P*$_2$ anhydride Na$_5$ salt •11H$_2$O	19.3 16.1	-	-
(24)	CH$_3$-C(P*)$_2$-OH •1H$_2$O (HEDP)	25.3[d] 18.7[d]	51.8	154
(25)	HEDP Na$_2$ salt •4H$_2$O	23.8 22.5	-	151
(26)	HEDP Na$_3$ salt •6H$_2$O	27.8 18.4	-	148
(27)	HEDP Na$_4$ salt	27.8 22.2 20.9 18.4	-	-
(28)	HEDP Ca$_2$ salt	23.1 19.2	-	138
(29)	Ø-CH(P*)-CH$_2$(P*)	32.3 (broad)	-	-
(30)	CH$_3$-CH(P*)-CH(P*)$_2$ •1 Aniline	28.7 25.6[d] 12.9[d]	55.9	-
(31)	Bu^t-CH(P*)-CH(P*)$_2$ •3 Aniline	24.8 20.6[u] 17.7[u]	-	-
(32)	Ø-CH(P*)-CH(P*)$_2$	26.7[d] 21.5 20.0[d]	63	-
(33)	P*$_2$-CH-CH$_2$-CH-P*$_2$	29.3 26.2 24.1 21.4	-	-

[continued]

Solid-State ^{31}P NMR Data for Phosphonic Acids (continued)

Compound	δ_P/ppm	$\lvert J_{PP}\rvert$/Hz	$\lvert J_{CP}\rvert$/Hz
(34) $CH_2(P^*)-CH(P^*)-CH(P^*)(P^*)$ •3 Aniline •$7H_2O$	37.2^d 29.6 18.0 12.7^d	63	–
(35) 1-phenyl-trans-1,4-tetralin-bisphosphonic acid$^+$	37.5 36.5		
(36) 1-phenyl-cis-1,4-tetralin-bisphosphonic acid$^+$	35.1 31.7	–	143
(37) Compound III	4.9 -0.5	–	–
(38) $C_6H_5-P^*$	21.0	–	–
	<u>Aminophosphonic Acids</u>		
(39) $H_2N-CH_2-P^*$	18.3	–	–
(40) $H_2N-CH_2-CH_2-P^*$	19.1	–	–
(41) $H_2N-CH_2-CH_2-CH_2-P^*$	25.2	–	–
(42) $(CH_3)_2N-C(P^*)(P^*)-H$	9.1 2.0	–	–
(43) $H_2N-CH_2-CH_2-C(P^*)(P^*)-OH$	15.9 12.8	–	158
(44) $H_2N-CH_2-CH_2-C(P^*)(P^*)-OH$ Na_2 salt	broad, unresolved band 25-17 ppm	–	–
(45) $N(CH_2-P^*)_3$	12.1	–	–
(46) Compound IV (AHP)	17.8 8.4	–	–
(47) AHP Na_2 salt	28.1 23.9	–	–
(48) $(P^*-CH_2-)_2N-CH_2-CH_2-N(-CH_2-P^*)_2$	10.3 9.4 5.5	–	–

Ø = phenyl. d = doublet. u = probable unresolved doublet.
Estimated errors: δ_P ± 0.1 ppm; $\lvert J\rvert$ ± 10 Hz.
$^+$See Figure 6.8 for structure.

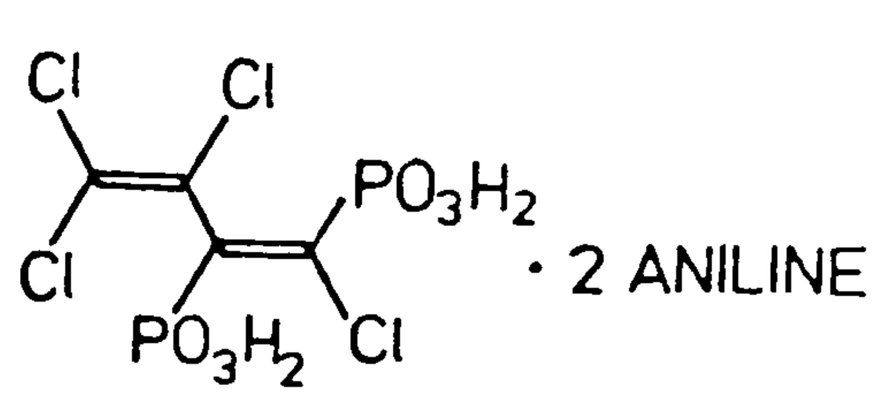

III

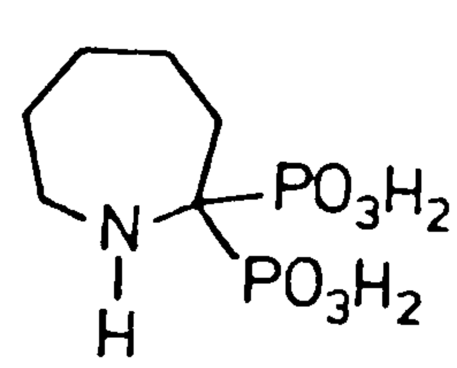

IV

(**16**) P*-CH_2-P* Na_2 salt Methylenediphosphonic acid disodium salt

The spectrum of this salt shows two singlets with an intensity ratio integrated over the spinning sideband manifold of 1.7:1. The singlet at high frequency has a pronounced shoulder at ca. 20.8 ppm. Linewidths for both main resonances are ca. 70 Hz. The naive explanation for this spectrum is that each line results from one phosphorus in the molecule. On salt formation, one line has a shift similar to that of the acid (**15**), and the other has a relatively larger crystallographic shift. This, however, does not explain either the discrepancy in intensity ratio or the shoulder on the high frequency peak. The shift of the high frequency peak is significantly different from that of the acid, so it is unlikely that either discrepancy is due to the presence of the acid. One possible source of impurity would be the presence of crystals of the tetrasodium salt. Since it is unlikely that solution state NMR would reveal such an impurity, an analytical determination of the Na/P ratio was done. The results of this, however, were not conclusive.

The CRAMPS spectrum of this compound indicates a single type of hydrogen bond present. This bond shows a higher shift (i.e. is stronger/shorter) than either bond in the acid (**15**).

A ^{23}Na MAS spectrum of this compound was also run. It showed the sodium environment to be highly asymmetric. (See compounds **19** and **20**).

(**17**) HOOC-CH_2-P* Carboxymethylphosphonic acid

This carboxylic - phosphonic diacid gives a single line phosphorus spectrum indicative of a single-molecule asymmetric unit. The ^{31}P chemical shift for this compound is ca.7 ppm to low frequency of that for the analogous diphosphinic acid (**15**). This shift is most probably due to a combination of effects from the carboxylic acid group and the hydrogen bonding present in the crystal lattice.

The CRAMPS spectrum shows three resonances in the hydrogen

Table 6.2: Solid-State ^1H CRAMPS Data for Phosphonic Acids $P^* = -P(O)(OH)_2$

	Compound	δ_H/ppm of Hydrogen Bonded Acid Protons	Approximate Integral
(15)	$P^*-CH_2-P^*$	11.9 10.3	3:1
(16)	$P^*-CH_2-P^*$ Na_2 salt	14.8	
(17)	$HOOC-CH_2-P^*$	13.5 12.4 8.7	1:1:1
(18)	$P^*-CH_2-CH_2-P^*$	–	
(19)	$P^*-CH_2-CH_2-P^*$ Na_2 salt $\bullet 4H_2O$	–	
(20)	$P^*-CH_2-CH_2-P^*$ Na4 salt	–	
(21)	$P^*-CH_2-CH-P^*_2$	11.6 10.9	1:1
(22)	$P^*_2-CH-CH-P^*_2$ $[(NH_2)_3C]^+_6$ salt $\bullet 6H_2O$	14.4	
(23)	$P^*_2-CH-CH-P^*_2$ anhydride Na_5 salt $\bullet 11H_2O$	17.2	
(24)	$CH_3-\underset{P^*}{\overset{P^*}{C}}-OH$ $\bullet 1H_2O$ (HEDP)	14.5 11.0	2:3$^+$
(25)	HEDP Na_2 salt $\bullet 4H_2O$	11.9	
(26)	HEDP Na_3 salt $\bullet 6H_2O$	12.6	
(27)	HEDP Na_4 salt	–	
(28)	HEDP Ca_2 salt	–	
(29)	$\varnothing-\overset{P^*}{CH}-\overset{P^*}{CH_2}$	11.5	
(30)	$CH_3-\overset{P^*}{CH}-\underset{P^*}{\overset{P^*}{CH}}$ $\bullet 1$ Aniline	10.6	
(31)	$Bu^t-\overset{P^*}{CH}-\underset{P^*}{\overset{P^*}{CH}}$ $\bullet 3$ Aniline	17.5 12.5	1:1
(32)	$\varnothing-\overset{P^*}{CH}-\underset{P^*}{\overset{P^*}{CH}}$	15.9 10.3	1:1
(33)	$P^*_2-CH-CH_2-CH-P^*_2$	11.4 9.4	3:1

[continued]

Solid-State ^{1}H CRAMPS Data for Phosphonic Acids (continued)

Compound	δ_H/ppm of Hydrogen Bonded Acid Protons	Approximate Integral
(34) P* P* P* $CH_2-CH-CH$ •3 Aniline •$7H_2O$ P*	16.0 11.8	1:7
(35) 1-phenyl-trans-1,4-tetralin-bisphosphonic acid	10.9	
(36) 1-phenyl-cis-1,4-tetralin-bisphosphonic acid	12.1	
(37) Compound III	11.8	
(38) $C_6H_5-P^*$	11.9	
	Aminophosphonic Acids	
(39) $H_2N-CH_2-P^*$	11.9	
(40) $H_2N-CH_2-CH_2-P^*$	12.4	
(41) $H_2N-CH_2-CH_2-CH_2-P^*$	12.2	
(42) P* $(CH_3)_2N-C-H$ P*	16.9 12.8 11.1	1:1:1
(43) P* $H_2N-CH_2-CH_2-C-OH$ P*	13.3 8.2	1:1
(44) P* $H_2N-CH_2-CH_2-C-OH$ Na_2 salt P*	-	
(45) $N(CH_2-P^*)_3$	16.3 12.5	1:4
(46) AHP	16.3 11.4	1:1
(47) AHP Na_2 salt	14.4	
(48) $(P^*-CH_2-)_2N-CH_2-CH_2-N(-CH_2-P^*)_2$	13.9 (broad)	

[+]The integral of 3 includes the hydroxyl proton.
Estimated error: $\delta_H \pm 0.5$ ppm.

bonding region, concomitant with the number of hydrogen atoms available for bonding. The shifts are indicative of two hydrogen bonds of moderate strength and one rather weak bond.

(**18**) P*-CH_2-CH_2-P* Ethane-1,2-bisphosphonic Acid

The ^{31}P spectrum of (**18**) (Figure 6.1) is a single line with a chemical shift of 32.7 ppm and a half-height width of 61 Hz. The single phosphorus environment is suggestive of an asymmetric unit consisting of a single, centrosymmetric molecule. This is confirmed by the crystal structure of Peterson et al[5]. The X-ray data show the molecule to be of space group $P2_1/c$ with a centre of inversion symmetry at the midpoint of the C-C bond.

The phosphorus T_1 of this compound was determined to be greater than 900 seconds. This seems reasonable, as the crystal structure has shown a strongly hydrogen-bonded system. Thus, a highly rigid lattice is probable.

For reasons which are not completely understood, attempts to obtain CRAMPS spectra of this compound were unsuccessful.

(**19**) P*-CH_2-CH_2-P* Na_2 salt $\cdot 4H_2O$

(**20**) P*-CH_2-CH_2-P* Na_4 salt

The phosphorus spectra of compounds (**19**) and (**20**) (Figure 6.1) are both single narrow lines with shifts of 29.3 and 24.8 ppm respectively. The retention of only a single type of phosphorus environment is interesting in that it implies either that the sodium salts are added symmetrically, or that there is a large degree of motion in these salts. In addition, even if the sodium ions are adding symmetrically, it is noteworthy that the addition of these atoms does not produce distortions in the lattice which render the two phosphorus atoms in the molecule inequivalent.

It should be noted that the ^{31}P shift decreases as one moves from the acid through the disodium salt to the tetrasodium salt (δ_P = 32.7, 29.3 and 24.8 ppm respectively). This trend agrees

Missing pages are unavailable

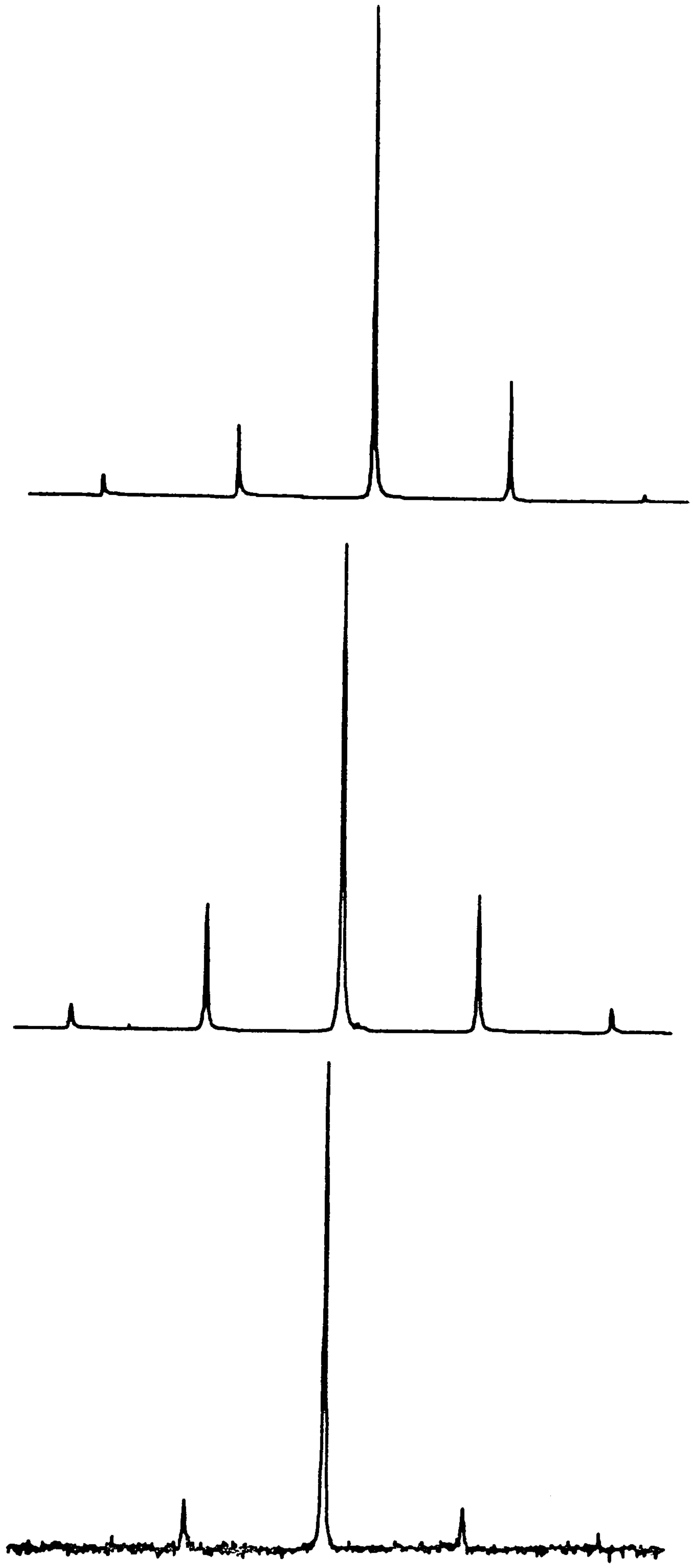

Figure 6.1: ^{31}P CP/MAS spectra of the derivatives of 1,2-ethane bisphosphonic acid plotted with aligned scales. Top: Tetrasodium salt (**20**) RD=30 s; PD=5 μs; CT=1 ms; NT=32; ν_r=2997 Hz; $\nu_{1/2}$=35 Hz; δ_P =24.8 ppm. Middle: disodium salt tetrahydrate (**19**) RD=45 s; PD=5 μs; CT=1 ms; NT=48; ν_r=3004 Hz; $\nu_{1/2}$=53 Hz; δ_P = 29.3 ppm. Bottom: acid (**18**) RD=30 s; PD=4 μs; CT=1 ms; NT=64; ν_r=3083 Hz; $\nu_{1/2}$=61 Hz; δ_P = 32.7 ppm.

Table 6.3: Known X-ray Crystal Structure Data for Phosphonic Acids

	Compound	Space Group	Asymmetric Unit/molecules	Ref.
(15)	P*-CH_2-P*	$P2_1/c$	1	4,5
(18)	P*-CH_2-CH_2-P*	$P2_1/c$	1/2	5
(22)	P*$_2$-CH-CH-P*$_2$ $[(NH_2)_3C]^+{}_6$ salt •$6H_2O$	†	1/2	10
(23)	P*$_2$-CH-CH-P*$_2$ anhydride Na_5 salt •$11H_2O$	†	1/2	10
(24)	P* CH_3-C-OH •$1H_2O$ (HEDP) P*	$P2_1/c$	1	11
(25)	HEDP Na_2 salt •$4H_2O$	$P2_1/c$	1	14
(38)	C_6H_5-P*	P*bca*	1	18
	Aminophosphonic Acids			
(39)	H_2N-CH_2-P*	P*bca*	1	19
(40)	H_2N-CH_2-CH_2-P*	P*bca*	1	20
(41)	H_2N-CH_2-CH_2-CH_2-P*	P*na*2_1	1	21
(45)	N(CH_2-P*)$_3$	$P2_1/c$	1	22

† Preliminary work from reference 10. Molecular diagrams and bond distances were provided but not the full results of the structural analysis.

with the results obtained by Moedritzer and Irani[7] for these compounds in the solution state (δ_P = 27.4, 23.3, and 22.4 ppm). Possible causes for this increase in shielding may include a differing charge at the phosphorus nucleus or a change in the P-O bond distances.

As can be seen from the slow spinning spectra of these samples (Figures 4.2 and 4.3), the shielding tensor patterns for the two salts are quite different. The disodium salt has an essentially asymmetric pattern, while that of the tetrasodium salt is axially symmetric. It is felt that the pattern of the disodium salt arises because there will be at least one oxygen on each phosphorus still involved in hydrogen bonding. This would both limit motion and create inequivalences in the oxygens which would lead to an asymmetric shielding environment. The axial symmetry for the tetrasodium salt implies equivalence of the three oxygens. Such equivalence may arise from bond fluctionality on the NMR timescale, from electronic equivalence of the oxygens or from rapid rotation about the C_3 axis.

The sodium-23 spectra of these two compounds shed additional light onto the considerations here; however, first a short digression into the theory of the NMR study of quadrupolar nuclei is necessary. Nuclei with spin > 1/2 possess a nuclear electric quadrupole moment which interacts with the electric field gradient at the nucleus. For such nuclei, the spectrum will depend on the relative contributions of the Zeeman and quadrupolar interactions and upon the symmetry of the site of the nucleus in question[8]. The latter point is important in that for a cubic site, the electric field gradient goes to zero, and, as a result, the coupling term vanishes. For ^{23}Na in a cubic environment, the first order quadrupole interaction gives rise to a relatively sharp central line (corresponding to the +1/2, -1/2 transition) and to two broad absorptions from the satellite transitions (3/2, 1/2 and -1/2, -3/2). Under such conditions, MAS will further sharpen the central transition and break-up the satellite transitions into a number of sidebands. If the site symmetry is lower than cubic, the quadrupolar coupling will be larger. The resulting NMR spectrum

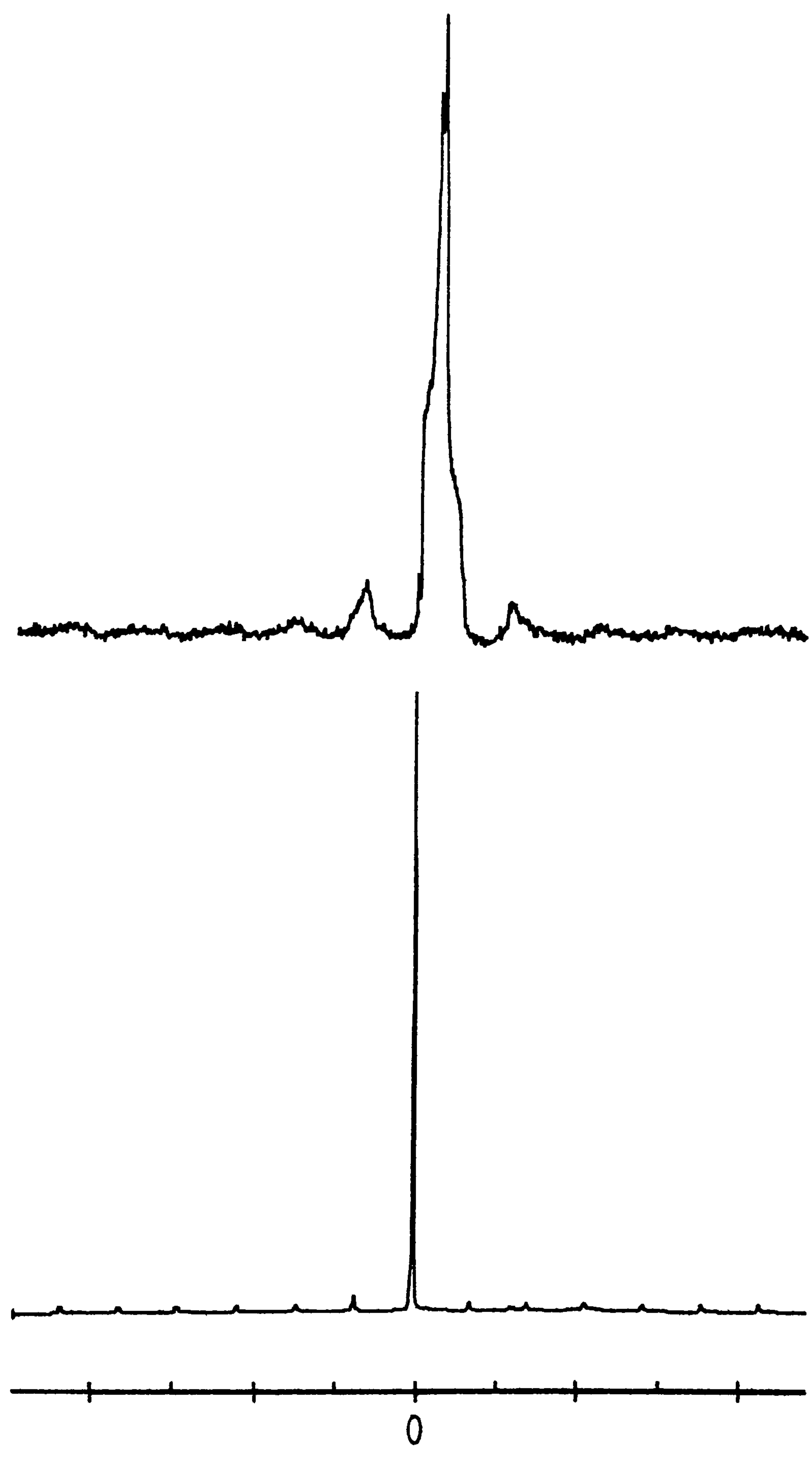

Figure 6.2: ^{23}Na SPE spectra of the sodium salts of 1,2-ethanebisphosphonic acid. Top: disodium salt tetrahydrate (**19**), ν_r=4.6 kHz; RD=4 s; δ_{Na} of singularities in the centreband are -21.7 and -26.8 ppm. Bottom: tetrasodium salt (**20**), ν_r=3.6 kHz; RD=5 s; PD=2 μs; δ_{Na} = 2.5 ppm. Scale: 0 = 0.0 ppm, small division equals 5kHz.

will still have a strong central transition; however, this will be broadened and show additional structure due to second order quadrupolar effects. These effects will not be averaged by MAS.

Moving now to the sodium-23 MAS spectra of compounds (19) and (20), Figure 6.2 shows a significant contrast between the two materials. The ^{23}Na spectrum of the disodium salt shows a broad centreband indicative of an asymmetric environment. For the tetrasodium salt, the ^{23}Na centreband is quite narrow with a spinning sideband manifold greater than 125 kHz wide. For this to be the case, the sodium would have to be in a highly symmetric or a highly mobile environment. This supports the above analysis of the shielding tensor patterns.

(21) $P^{*}-CH_2-CH-P^{*}_2$ Ethane-1,1,2-trisphosphonic acid

The ^{31}P spectrum consists of two singlets at 28.7 and 19.9 ppm which have an integrated intensity of ca. 2.6:1. The origin of this unusual intensity distribution is at present uncertain. A solution-state spectrum of this sample showed a triplet and a doublet in a ratio of 1:2 and no impurities.

(22) $P^{*}_2-CH-CH-P^{*}_2$ $[(NH_2)_3C]^{+}_6$ salt $\cdot 6H_2O$
Ethane-1,1,2,2-tetraphosphonic acid hexaguanidinium salt hexahydrate

The centreband ^{31}P spectrum of this compound consists of two partially resolved resonances. The half-height width of the band is 317 Hz, suggesting further inequivalences or unresolved coupling. The crystal structure of this material has been provided by Hägele[10]. This X-ray structure shows there to be a plane of symmetry passing through the midpoint of the C-C bond. There are, thus, two crystallographically different types of phosphorus in the molecule. However, the width of the band seems somewhat large to be accounted for simply by P-P scalar coupling.

The CRAMPS spectrum of this material shows a single type of moderately strong hydrogen bond (14.4 ppm). The crystal structure data at hand suggests two bridging hydrogen bonds in the molecule, but bond distances are not indicated. It would be very useful in correlating bond distance to ^1H chemical shift if these distances were available.

(23) P^*_2-CH-CH-P^*_2 anhydride •$11H_2O$
Ethane-1,1,2,2-tetraphosphonic acid anhydride pentasodium salt •$11H_2O$

The ^{31}P spectrum of (23) consists of a broad, pyramidally shaped band at 19.3 ppm and a second, rather less broad band at 16.1 ppm. The half height widths of these are 270 and 160 Hz respectively, though the integral is 1:1. Again, the molecular structure[10] (shown below) indicates an asymmetric unit of half of

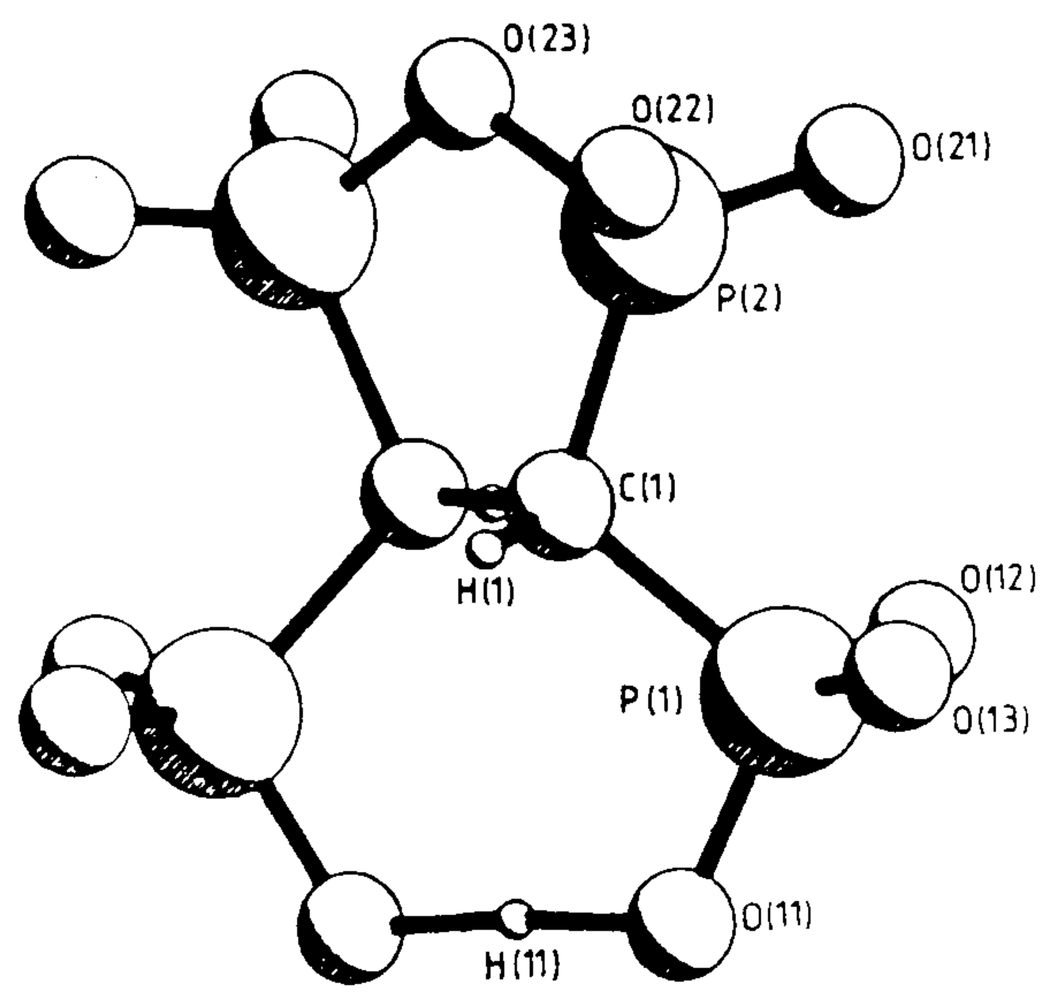

the molecule. A plane of symmetry passes through the bridging oxygen and the midpoint of the C-C bond. As in (22) above, two types of coupled phosphorus environment are suggested by the NMR, in agreement with the X-ray results. The P-P scalar coupling is unresolved.

The CRAMPS spectrum of this compound indicates a very strong hydrogen bond with a shift of 17.2 ppm. The crystal structure shows the only hydrogen bond in the system to be an intramolecular bridge ($r_{O...O}$ = 2.439 Å) opposite to the anhydride link.

(24) $CH_3-\underset{P*}{\overset{P*}{C}}-OH \cdot 1H_2O$ (HEDP) Ethane-1-hydroxy-1,1-diphosphonic acid monohydrate

The phosphorus spectrum of HEDP (**24**) and its di- tri- and tetrasodium salts (**25, 26** and **27**) may be seen in Figure 6.3.

The phosphorus CP/MAS spectrum of (**24**) shows two AX doublets with shifts of 25.3 and 18.7 ppm and a $|J_{PP}|$ of 52 Hz. The ^{13}C spectrum (Figure 6.4) consists of a single line in the methyl region and a triplet at 70.1 ppm with $|J_{PC}|$ of 154 Hz. The indicated crystal structure is one of a single-molecule asymmetric unit with inequivalent phosphorus atoms within the molecule. In this case, of course, the triplet in the carbon spectrum is actually an unresolved doublet of doublets. This assignment is confirmed by the X-ray crystal structure of Uchtman and Gloss[11] (single complete molecule per asymmetric unit with phosphorus atoms unrelated by symmetry; space group $P2_1/c$).

The CRAMPS results for this molecule show two different types of hydrogen bonding with ^1H shifts of 14.5 and 11.0 ppm. The lines have an approximate intensity ratio of 2:4. These show a general correspondence to the hydrogen bonds noted in the crystal structure; however, exact correlation (*vide infra*) is made difficult by inaccuracies in both the X-ray and CRAMPS technique as well as fluctuation in bonding distances due to motion of the hydrogen-bonded water molecules.

(25) HEDP Na_2 salt $\cdot 4H_2O$

The ^{31}P spectrum of the disodium salt of HEDP consists of two broad, overlapping singlets at 23.8 and 22.5 ppm. Both resonances show only moderate crystallographic shifts from those for the acid form. The P-P scalar coupling for this compound is unresolved, as it is for all of the HEDP salts. The broadening which limits resolution most probably arises from one or both of two causes. Firstly, there may be distortion of the crystal lattice by the presence of the sodium. Secondly, it may be the case that the

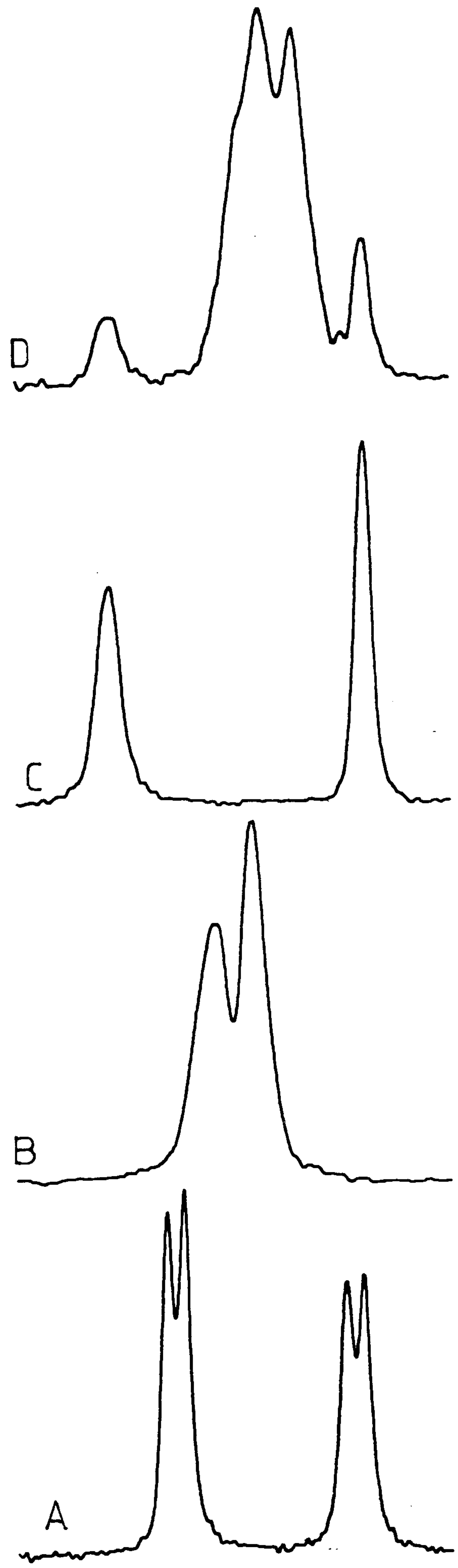

Figure 6.3: ^{31}P CP/MAS spectra of the derivatives of HEDP. SF=81.014 MHz. (A) HEDP (**24**), RD=10 s; PD=4 µs; CT=5 ms; v_r=3055 Hz; NT=112; $v_{1/2}$ = 89 and 95 Hz. (B) HEDP disodium salt tetrahydrate (**25**), RD=5 s; PD=4 µs; CT=1 ms; v_r=3360 Hz; NT=80. (C) HEDP trisodium salt hexahydrate (**26**), RD=15 s; PD=4 µs; CT=1 ms; v_r=2675 Hz; NT=64; $v_{1/2}$ = 83 and 56 Hz. (D) HEDP tetrasodium salt(**27**), RD=15 s; PD=4 µs; CT=1 ms; v_r=2945 Hz; NT=100.

dipolar coupling to quadrupolar ^{23}Na is not completely removed by MAS. Such effects for sodium phosphates have been reported by several authors[12,13]. The ^{13}C spectrum indicates that there is still a single molecule in the asymmetric unit, as there is still only a single methyl resonance. This is confirmed by the X-ray crystal structure of Barnett and Strickland[14]. The $|J_{PC}|$ is 151 Hz. The CRAMPS results here show a single type of moderately strong hydrogen bond. The ^{23}Na spectrum is indicative of sodium in an environment of low symmetry.

(26) HEDP Na_3 salt $\cdot 6H_2O$

In this spectrum, the phosphorus shifts of 27.8 and 18.4 ppm show only small displacements from those of the acid. Again, no P-P scalar coupling is resolved.

The ^{13}C spectrum is still indicative of a single-molecule asymmetric unit. The $|J_{PC}|$ here is 148 Hz. The CRAMPS results indicate a single type of reasonably strong hydrogen bond. The ^{23}Na spectrum shows the sodium to be in an enviromnment of low symmetry.

(27) HEDP Na_4 salt

This compound is clearly shown by solid-state NMR to be impure, of mixed crystal composition, or both. The outer resonances of the centreband (27.8 and 18.4 ppm) almost certainly arise from the trisodium salt as can be clearly seen from the stacked plot of the HEDP series (Figure 6.3). The remaining centreband shows at least three unresolved resonances. In the carbon spectrum, three resonances are resolved in the C-2 methyl region. One of these resonances (21.6 ppm) can be attributed to the trisodium salt impurity. Whether the two remaining methyl resonances are due to a two-molecule asymmetric unit, or whether the presence of the trisodium salt is indicative of further impurities which would give rise to these resonances has yet to be determined.

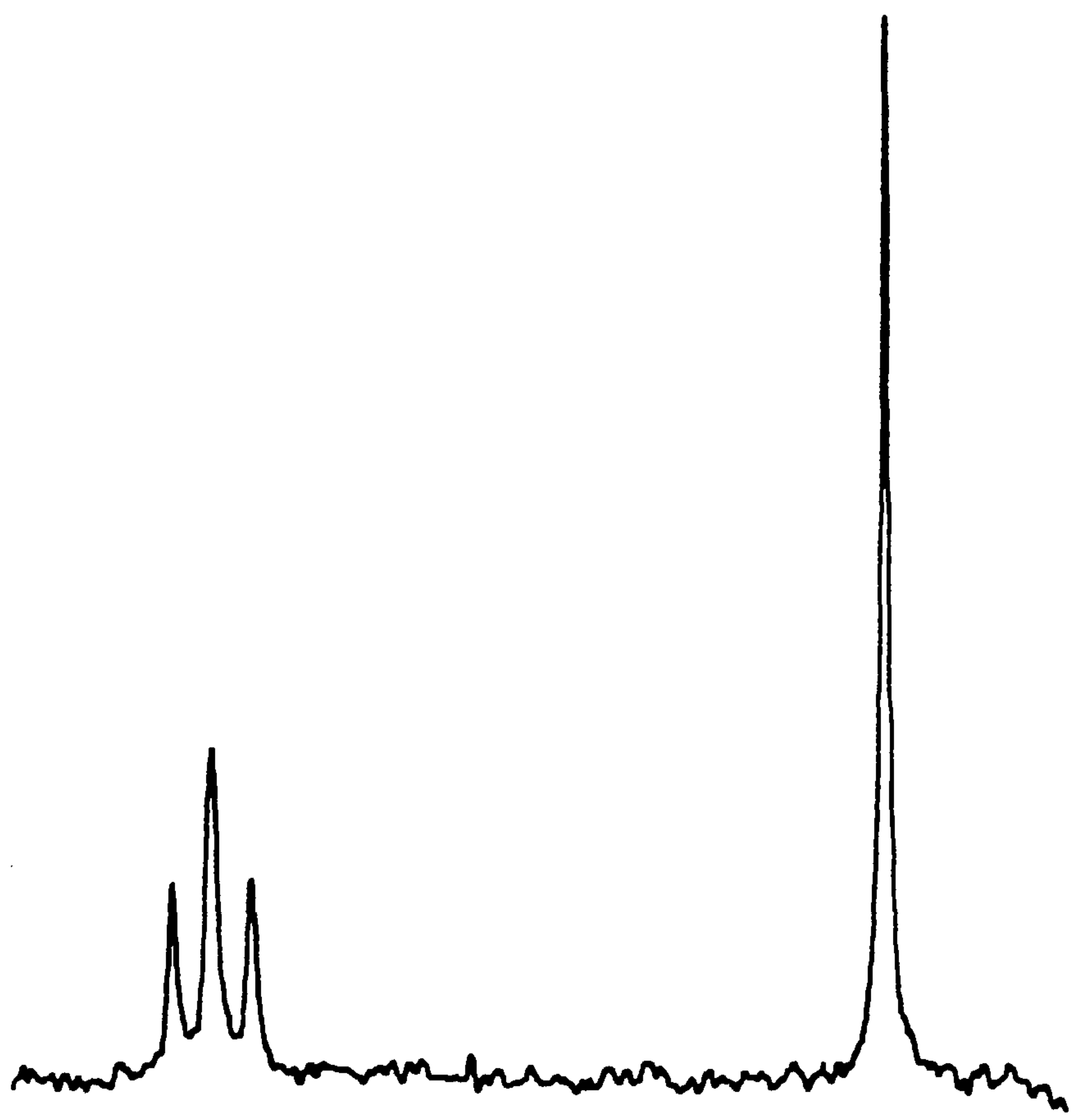

Figure 6.4: ^{13}C CP/MAS spectrum of HEDP (24) SF=50.3227 MHz; RD = 10 s; PD = 4 μs; CT = 5 ms; ν_r = 2920 Hz; NT = 254. δ_C = 70.1 and 17.1 ppm. $|J_{PC}|$ = 154 Hz. For line at 17.1 ppm the $\nu_{1/2}$ = 34 Hz.

(28) HEDP Ca_2 salt

The dicalcium salt is the last in the HEDP series. Again, the ^{31}P spectrum consists of two singlets (23.1 and 19.2 ppm) with P-P scalar coupling unresolved. The difference in shifts between the acid form and the dicalcium salt are rather small, indicating very little crystallographic distortion on salt formation. The single methyl resonance in the carbon spectrum maintains the trend of a single-molecule asymmetric unit containing phosphorus atoms unrelated by symmetry. The $|J_{PC}|$ is 138 Hz.

General Comments on the HEDP series:

a) It should be noted that, unlike the sodium salts of methylene diphosphonic acid and ethane-1,2-bisphosphonic acid, the ^{31}P chemical shifts for the sodium salts of HEDP do not show a simple trend as protons are subsequently replaced by sodium ions. There are probably a number of reasons for this including: 1) the effect of the hydroxyl group; 2) a more complicated hydrogen bonding structure; and 3) chemical shift changes due to crystallographic distortions overshadowing other factors which affect the phosphorus shift.

b) For the HEDP series of acid, disodium salt, trisodium salt and tetrasodium salt, there appears to be a monotonic relationship between the C-1 chemical shift and the $|J_{PC}|$. This trend would seem to indicate increasing s character of the P-C bond upon sucessive deprotonation steps. This is indicated by the fact that the coupling is increasing linearly with the shielding[15].

c) As shown by sample (27), solid-state NMR can clearly show impurities or variations in salt formations which may not be revealed in the solution-state spectrum.

```
      P* P*
(29) Ø-CH-CH2    1-Phenyl-ethane-1,2-bisphosphonic acid
```

The phosphorus spectrum of this sample is a single broad line which has symmetric shoulders that give the appearance of unresolved P-P scalar coupling. It is interesting to note that this appearance seems more noticeable in the sidebands than the centreband. A single molecule unit cell is postulated. Supporting this, the ^{13}C NQS results show a single resonance for the phenyl group C-1 carbon. Solution-state results[16] for this compound have shown that the conformation of the phosphorus groups has an important effect on the $^{3}J_{PP}$ value. For the trans and gauche conformations, the P-P coupling is 69.4 Hz and 31.3 Hz respectively. As these couplings are unresolved in the solid-state, no conclusions may be drawn for this compound. However, it will be seen that these results may assist in the analysis of the spectra below. The CRAMPS spectrum shows a single, relatively weak type of hydrogen bond.

```
          P* P*
(30) CH3-CH-CH   •1 Aniline     Monoanilinium salt of 1-methyl-
            P*                  ethane-1,2,2-trisphosphonic acid

          P* P*
(31) But-CH-CH   •3 Aniline   Trisanilinium salt of 1-t-butyl-
            P*                ethane-1,2,2-trisphosphonic acid

       P* P*
(32) Ø-CH-CH                  1-Phenyl-ethane-1,2,2-trisphosphonic
          P*                  acid
```

It is useful to begin by examining the ^{31}P spectrum of (32) which may be found in Figure 6.5. This compound gives a ^{31}P spectrum of a singlet and two AB doublets, one of which is not completely resolved from the singlet. The shifts are noted on the spectrum and in Table 6.1. Comparison with solution-state data[3] allows the assignment of the highest frequency doublet to the P attached to the C-1 carbon. The $|J_{PP}|$ of 63 Hz is thus a vicinal coupling, which may be compared to the solution state value ($^{3}J_{PP}$ = 51.1 Hz). The solution-state study showed the gauche $^{3}J_{PP}$

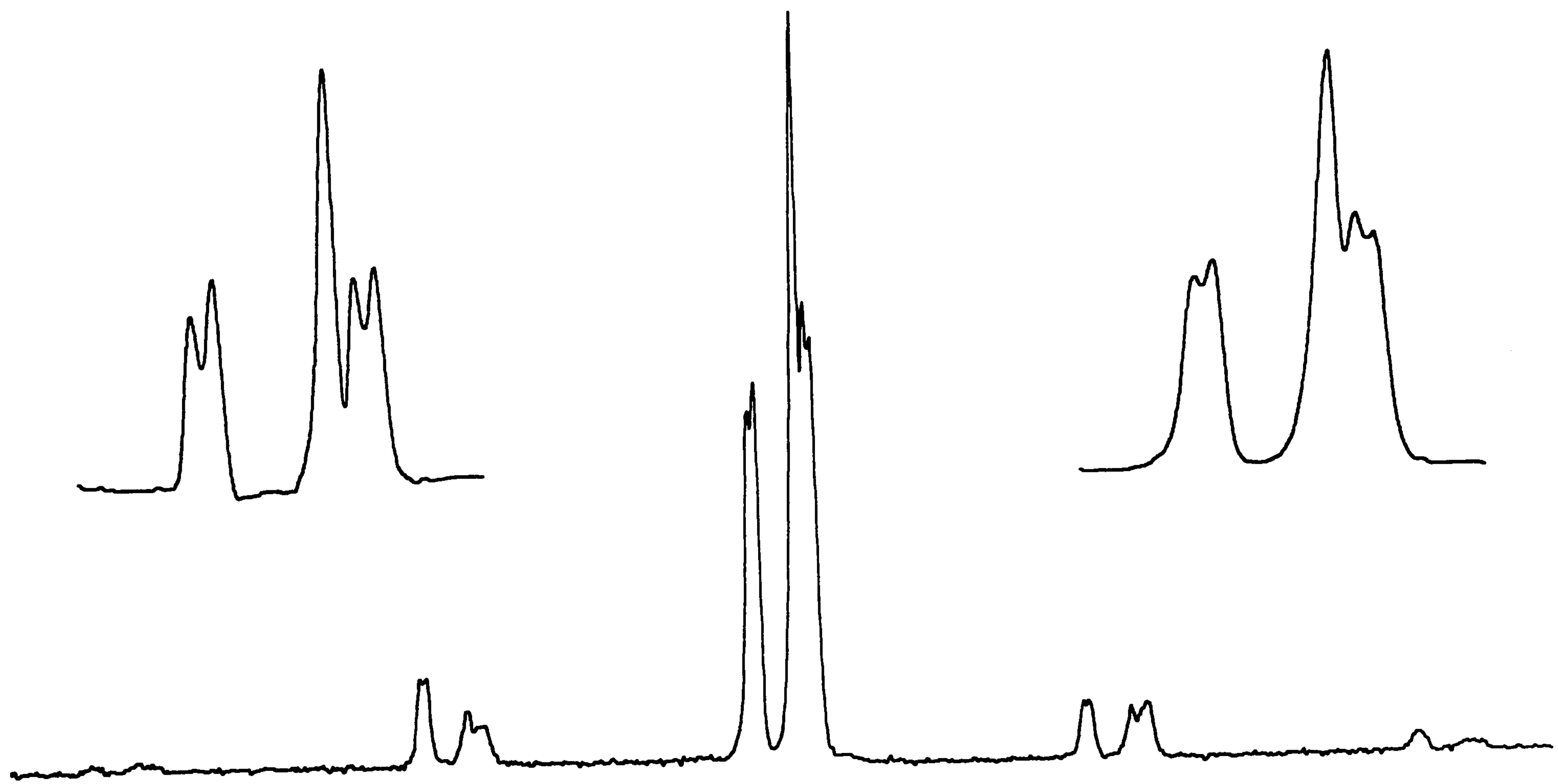

Figure 6.5: ^{31}P CP/MAS spectrum of compound (32) with centreband expanded (right) and resolution enhanced (left). SF=81.014; RD=10 s; PD=4μs; CT=5 ms; ν_r=3160 Hz; NT=404. δ_P = 26.7, 21.5 and 20.0 ppm. $|J_{PP}|$ = 63 Hz.

to be 17.1 Hz and the geminal P-P coupling to be ~0.0 Hz. The gauche $^3J_{PP}$ is far too small to be resolved here, as the linewidths involved in ^{31}P CP/MAS work are generally greater than 40 Hz.

It has been proposed[17] from solution-state titration studies of ethane-1,2-bisphosphonic acid that the magnitude of the coupling constant is indicative of the conformation of the vicinal phosphorus groups. A minimum $|^3J_{PP}|$ of 50.9 Hz in the titration curve of the ethane-bisphosphonic acid was related to a gauche configuration of the two phosphorus atoms, while a $^3J_{PP}$ of 75.0 Hz was related to a trans configuration. Further solution-state work reported by Fischer[16] has extended this correlation to 1-phenyl-ethane-1,2-bisphosphonic acid ((29) above). In this case, the $^3J_{PP}$ values for the gauche and trans conformations were 31.3 and 69.4 Hz respectively. While from such studies one is tempted to draw conclusions regarding the structure of compound (32) in the solid state, it is questionable whether differences in the solution-state data are significant for the solid-state. As there are no diffraction studies which could assist the assignment, no decisive conclusions may be drawn.

Samples (30) and (31) show a very similar pattern to that of compound (32), though in both cases the singlet has become the highest frequency line in the centreband. This can be seen as a result of both substituent and crystallographic effects. In compound (31), the P-P scalar coupling is unresolved; however, it is clear from the integration (1:1:1) that this is a similar case. A rough judgment from the linewidths suggest that the $^3J_{PP}$ must be less than 50 Hz. For compound (30), the coupling is resolved and found to be 56 Hz. For the latter case, it is again tempting to draw the conclusion of a trans configuration from comparison with the solution-state data above; however, one could not be absolutely sure of this without confirmation by X-ray crystal structure.

For all three of these compounds, the carbon spectrum confirmed a single-molecule asymmetric unit. The CRAMPS results show that compound (30) has a single type of weak hydrogen bond. The phenyl derivative (32) has one strong and one weak bond, while sample (31) shows two types of hydrogen bond, one of which is quite

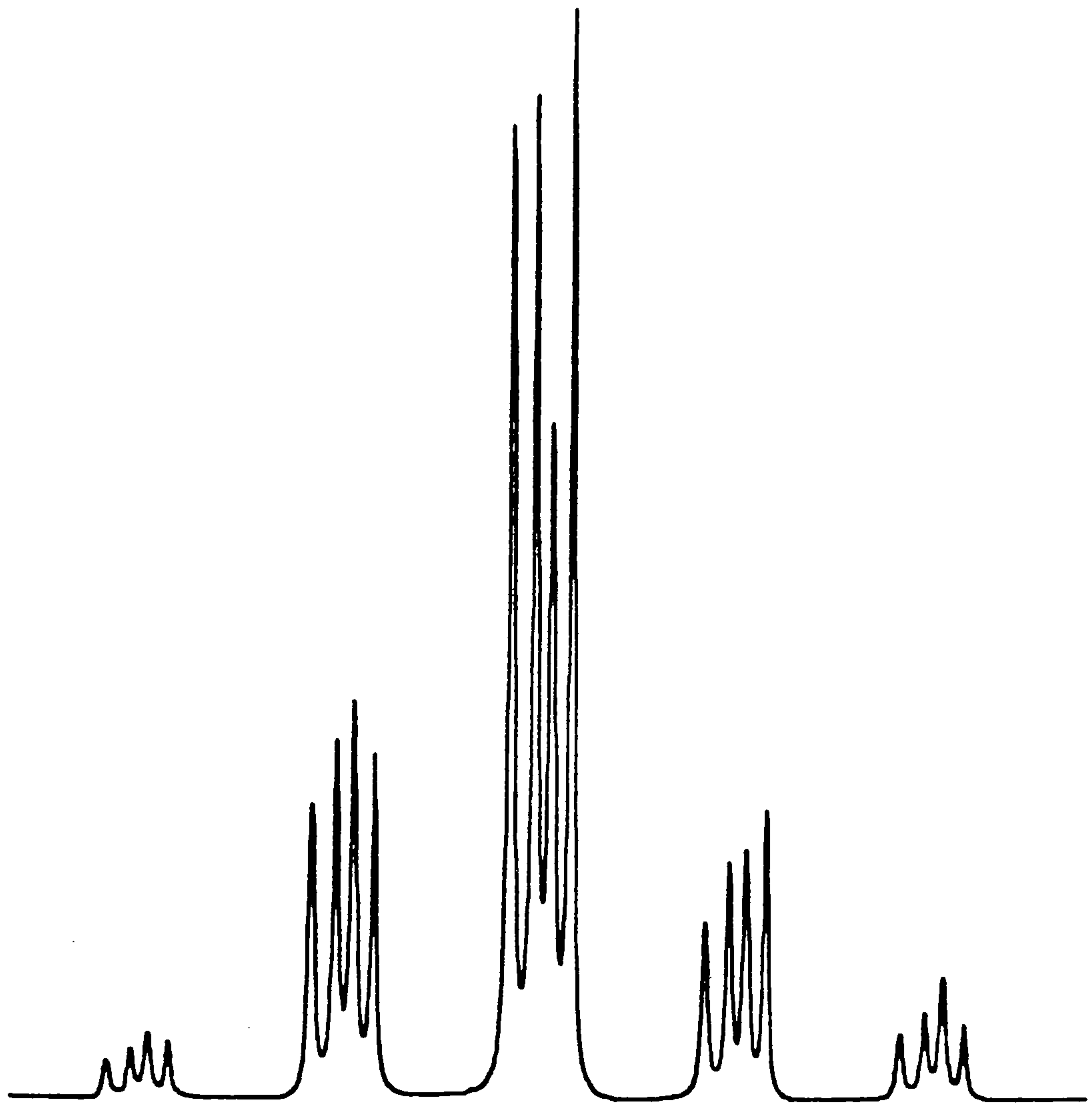

Figure 6.6: ^{31}P CP/MAS spectrum of compound (33), 1,1,3,3-propanetetraphosphonic acid. SF=81.014 MHz; RD=10 s; PD=4 μs; CT=1 ms; v_r=2097 Hz; NT=60.

δ_P (ppm)	$v_{1/2}$ (Hz)
29.3	75
26.2	73
24.1	70
21.4	58

strong. The strong hydrogen bonding in the latter two compounds may be indicative of intramolecular bridging.

(33) P^*_2-CH-CH_2-CH-P^*_2 Propane-1,1,3,3-tetraphosphonic acid

The centreband of this spectrum consists of four reasonably narrow singlets ranging in chemical shifts from 29.3 to 21.4 ppm. It is most likely the case that the origin of these lines is a single-molecule asymmetric unit with none of the phosphorus atoms related by symmetry. It has been shown in solution-state work[3,16,17] that geminal couplings are small, and $^4J_{PP}$ would be small as well, so it is not unreasonable that no splittings are seen in the spectrum. Attempts to prove this by CP/MAS ^{13}C NMR were not sucessful. The carbon resonance was broad and unresolved, most probably due to P-C scalar coupling. The CRAMPS spectrum of this sample showed there to be two types of reasonably weak hydrogen bonds.

$$\begin{array}{l} \quad\;\; P^* \quad\; P^* \;\; P^* \\ (34)\; CH_2\text{-}CH\text{-}CH \\ \qquad\qquad\quad\;\; P^* \end{array}$$
•3 Aniline •$7H_2O$ Trisanilinium salt of propane-1,1,2,3-tetraphosphonic acid heptahydrate

The ^{31}P spectrum of sample (34) shows two singlets within two doublets. The shifts may be found in Table 6.1. The results suggest a single molecule asymmetric unit. This spectrum has several unusual features. First, although one $|J_{PP}|$ of 64 Hz is resolved, one would expect at least two or maybe three such couplings to be present. Second, the AB doublets have odd intensities. This may be due to unresolved vicinal P-P scalar couplings or to small, unresolved geminal couplings. In any case, it would seem likely that the apparent "lack" of coupling data here (i.e. several couplings must all be comparatively small) is indicative of the conformation of the molecule. The answer to this may be contained in the discussion of compounds (30) - (32) above. As the gauche conformation $^3J_{PP}$ for compound (32) was 17.1 Hz, it might seem that with the exception of the one trans pair, all of the remaining phosphorus atoms may be in a mutually gauche

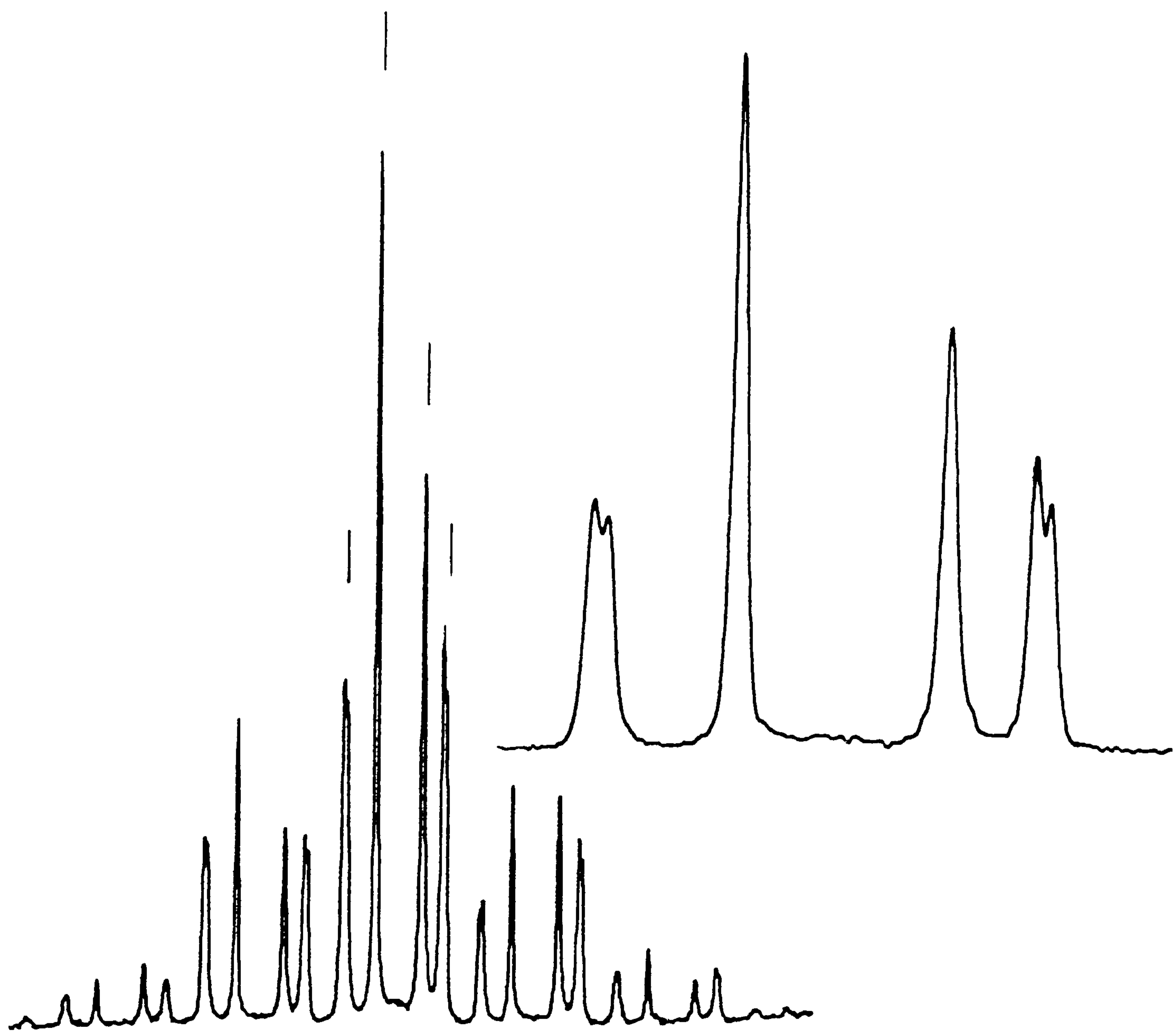

Figure 6.7: Compound **34**: ^{31}P CP/MAS spectrum and resolution enhanced centreband. SF=81.0141 MHz; RD=5 s; PD=4 μs; CT=5ms; ν_r=2742 Hz; NT=318. δ_P = 37.2, 29.6, 18.0 and 12.7 ppm. $|J_{PP}|$ = 63 Hz.

arrangement. It would be useful to have a ^{31}P solution-state study of this and related compounds done to determine the values of P-P scalar coupling.

The CRAMPS data here suggest two types of hydrogen bonding present, one type strong and one reasonably weak.

(35) 1-Phenyl-trans-1,4-tetralin-bisphosphonic acid

(36) 1-Phenyl-cis-1,4-tetralin-bisphosphonic acid

See Figures 6.8 to 6.10. for spectra and molecular structure.

Considering the cis compound first, the spectral assignment is straightforward. There are two resonances, one from each of the two phosphorus atoms in the molecule. No P-P scalar coupling is seen, but this would not be expected, as in solution the $|J_{PP}|$ is only 5 Hz. A single-molecule asymmetric unit is confirmed by the carbon NQS spectrum which clearly shows the four non-protonated carbons in the molecule. The J_{PC} for the C-1 carbon of the tetralin is found to be 143 Hz. This compares with 125.9 Hz from the solution state[6].

The CRAMPS spectrum of this material clearly shows the acid, aromatic, and aliphatic protons. A single type of hydrogen bond is found at 12.1 ppm. This is only a slightly stronger hydrogen bond than that found in the the trans compound (10.9 ppm), and it is far weaker than the strong bonds found in other compounds (ca. 17 ppm for compounds (23) and (31)). While one might have expected a strong intramolecular hydrogen bond in this cis compound, it is clear that the phosphonic acid groups are separated by the tetralin ring to such an extent that strong intramolecular hydrogen bonding cannot occur.

The assignment of the trans compound (35) is much less straightforward. As can be seen, there are two partially resolved resonances in the phosphorus spectrum; the intensities of which are not equivalent. There is not sufficient resolution for integration. The ^{13}C NQS spectrum, which was so clear for the cis case, does not shed any conclusive evidence. The spectrum seems to

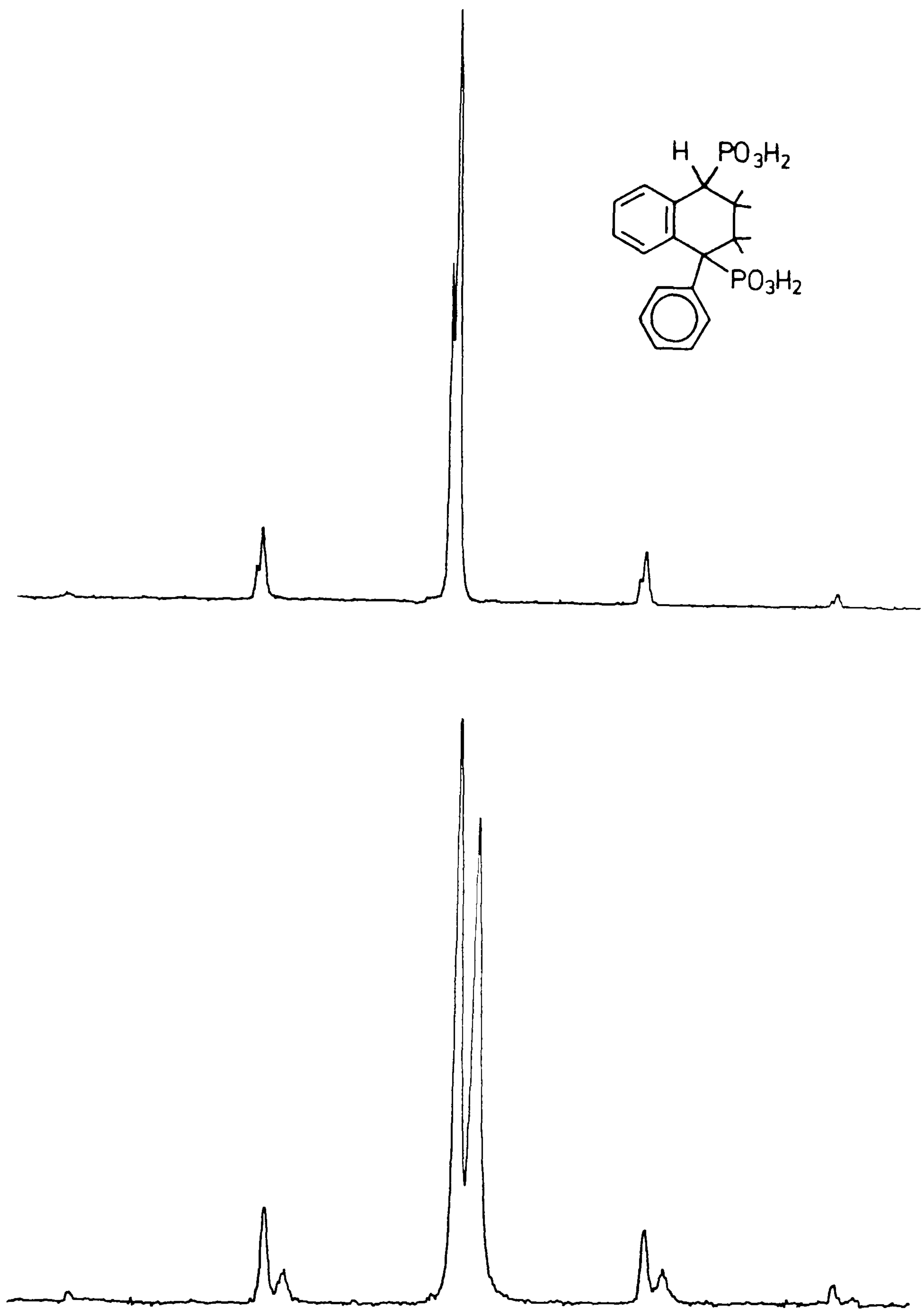

Figure 6.8: ^{31}P CP/MAS spectra of trans and cis 1-phenyl-1,4-tetralinbisphosphonic acid. Top: trans compound (**35**), SF=81.014 MHz; RD=60 s; PD=5 μs; CT=1 ms; ν_r=2698; NT=24. δ_P = 37.5 and 36.5 ppm. Bottom: cis compound (**36**), RD=45 s; PD=5 μs; CT=1 ms; ν_r=2698; NT=24. δ_P = 35.1 and 31.7 ppm.

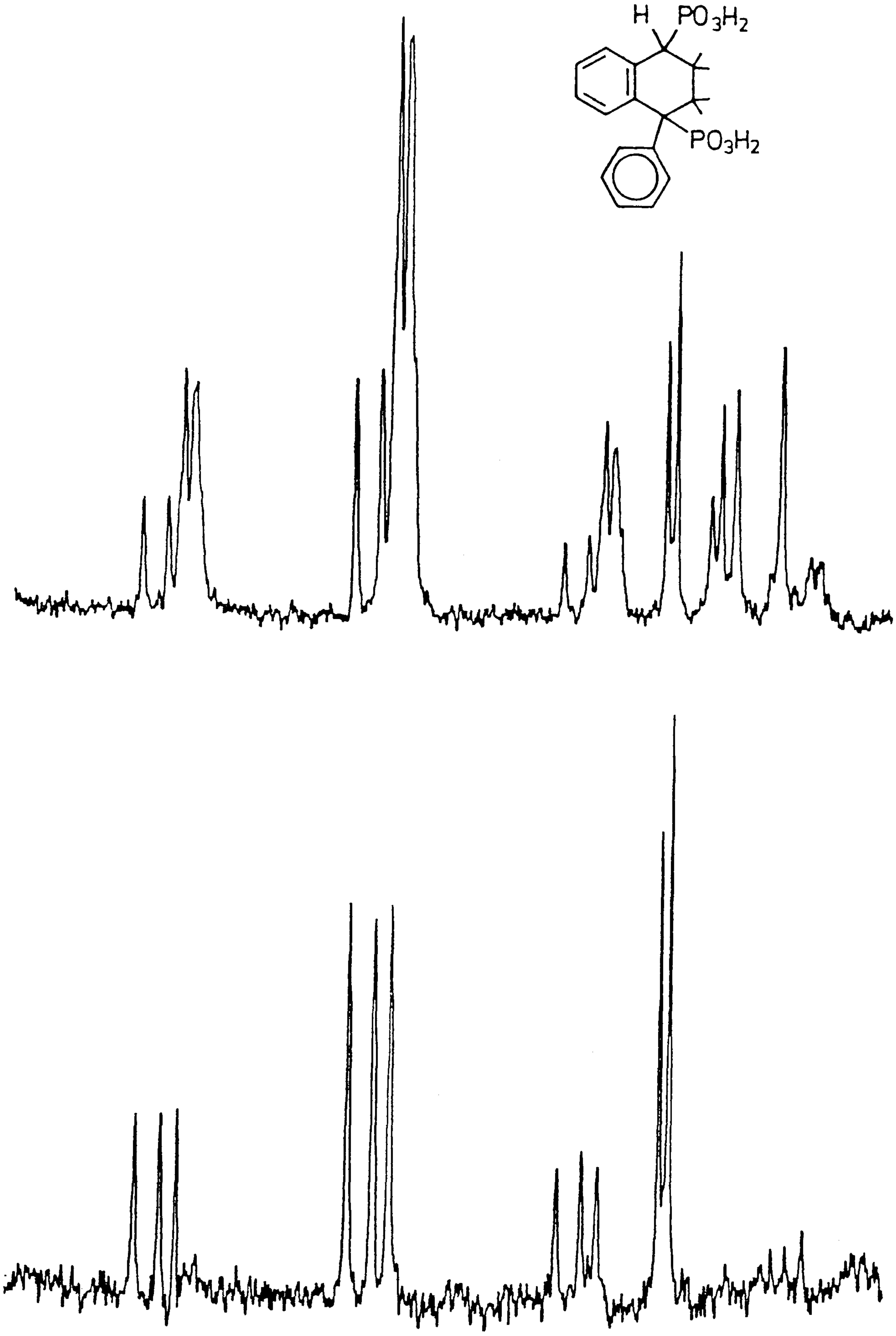

Figure 6.9: ^{13}C spectra of compound (**36**), 1-phenyl-cis-1,4-tetralinbisphosphonic acid SF=50.3227. Top: CP/MAS; RD=10 s; PD=5 μs; CT=5 ms; ν_r= 3081 Hz; NT=900. Bottom: NQS/MAS; RD=10 s; PD=5 μs; CT=5 ms; DA=40 μs; ν_r= 3081 Hz. δ_C = (a) 143.3, (b) 135.9, (c) 131.3 and (d) 50.3 ppm. (d) is split by coupling to phosphorus $|J_{PC}|$ = 143 Hz.

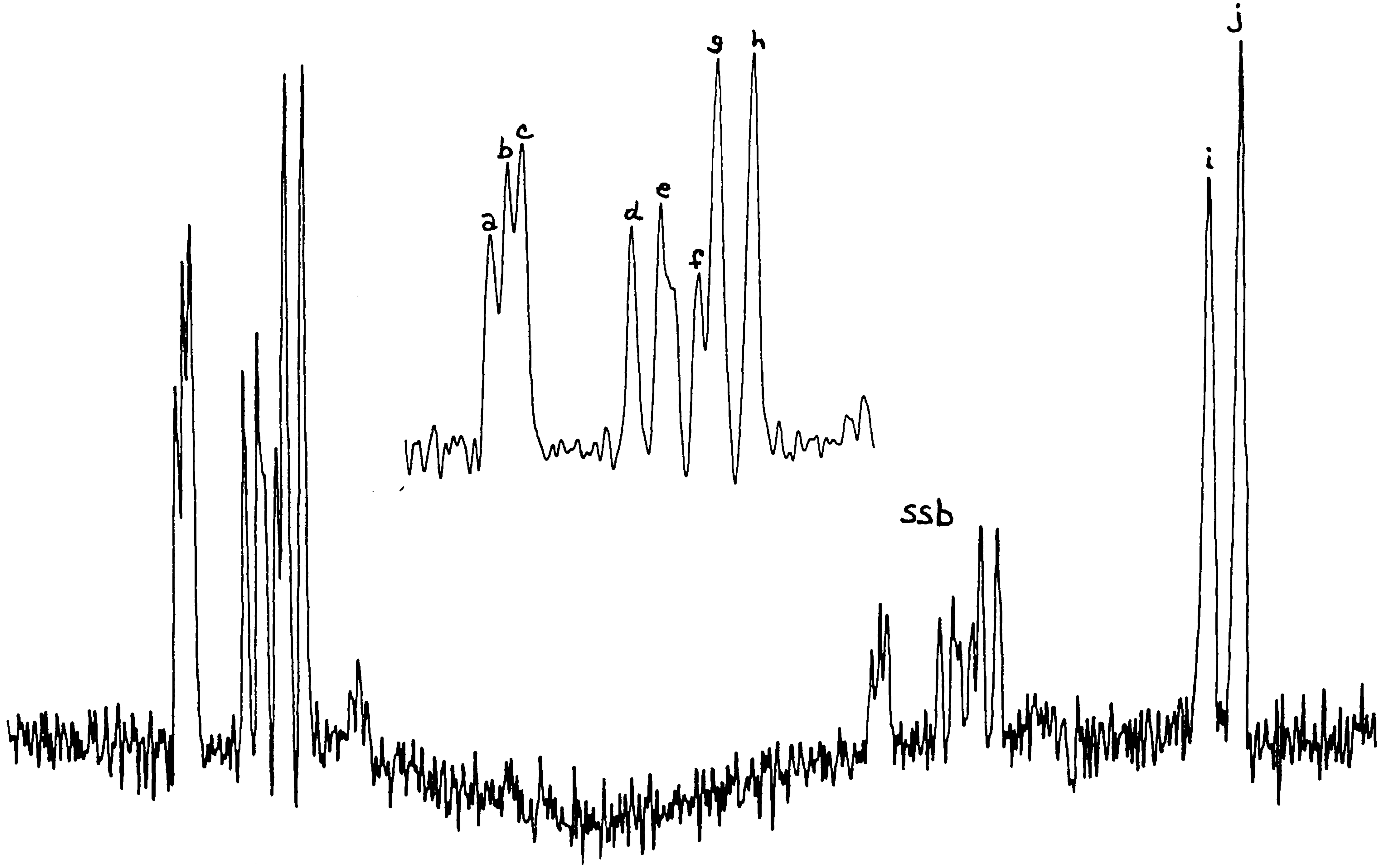

Figure 6.10: ^{13}C NQS/MAS spectrum of compound (35), 1-phenyl-trans-1,4-tetralinbisphosphonic acid. SF=50.3227. The inset region is an expansion of the aromatic region to the left. RD=120 s; PD=4 μs; CT=1 ms; DA=40 μs; ν_r=3112 Hz; NT=6604. δ_C = (a) 143.2, (b) 142.5, (c) 141.9, (d) 137.2, (e) 136.0, (f) 134.1 (g) 133.6, (h) 132.0, (i) 51.8 and (j) 49.0 ppm.

suggest two or perhaps three different crystallographic sites. It has been suggested that the line multiplicity in the region of the "quaternary" carbons, which are common to both rings of the tetralin, is due to some unusual coupling effects; however, this is unlikely in that the P-C scalar coupling for these carbons in solution state is only 6-8 Hz. This is far below the linewidths and separations involved here. The sample has been checked by solution-state NMR and found to be pure.

(37) Compound III: 1,1,2,4-tetrachloro-1,3-butanediene-3,4-bisphosphonic acid

The ^{31}P spectrum of this material consists of two rather broad singlets with J-coupling unresolved. The phosphorus chemical shifts of 5.0 and -0.5 ppm correspond reasonably closely to the solution state values obtained for this compound of 2.4 and 0.2 ppm. The differences in shift can be attributed to solvent and crystallographic effects. The asymmetric unit is most probably a single molecule, though this could not be confirmed by carbon-13 CP/MAS NMR because of interference due to coupling to the quadrupolar chlorine.

In this spectrum, both the linewidths and integrated intensity are unusual. The linewidths are 142 and 211 Hz for the high and low frequency peaks respectively. As the solution-state $|J_{PP}|$ is only 45 Hz, this probably does not completely account for the linewidths present. The intensity ratio of the two resonances integrated over the spinning sideband manifolds is about 1.6:1, which is not necessarily reasonable either. A solution-state spectrum showed the sample to be pure. One possible explanation for the discrepancies is quadrupolar effects from the chlorines. The results from the 7 Tesla spectrum, however, did not show any significant reduction in linewidths which would be expected if the broadening was the result of quadrupolar effects.

The CRAMPS spectrum of this material showed a single type of hydrogen bond present of moderate strength.

(38) C_6H_5-P* Benzene phosphonic acid

Solid benzene phosphonic acid has a ^{31}P spectrum of a single narrow line. The analysis of a single-molecule asymmetric unit is confirmed by the crystal structure published by Weakley[18] (space group: P_{bca}). CRAMPS results indicate a single type of moderate-to-strong hydrogen bond.

6.2.b Aminophosphonic Acids

(39) H_2N-CH_2-P* Amino-methylphosphonic acid

(40) H_2N-CH_2-CH_2-P* 2-Amino-ethanephosphonic acid

(41) H_2N-CH_2-CH_2-CH_2-P* 3-Amino-propanephosphonic acid

As one might expect, the phosphorus spectra of compounds (39) (Figure 6.11), (40) and (41) are remarkably similar. They all consists of a centreband which is a single narrow line. The static bandshape/spinning sideband patterns of all three show an almost completely asymmetric shielding tensor. A single molecule asymmetric unit for all three compounds is confirmed by the corresponding published crystal structures[19,20,21]. These crystal structures show all three molecules to exist in the zwitterionic form. The ^{31}P chemical shifts for the three compounds increase with increasing chain length.

In each of the three compounds, a single type of acid hydrogen bond is present which agrees with the available x-ray data.

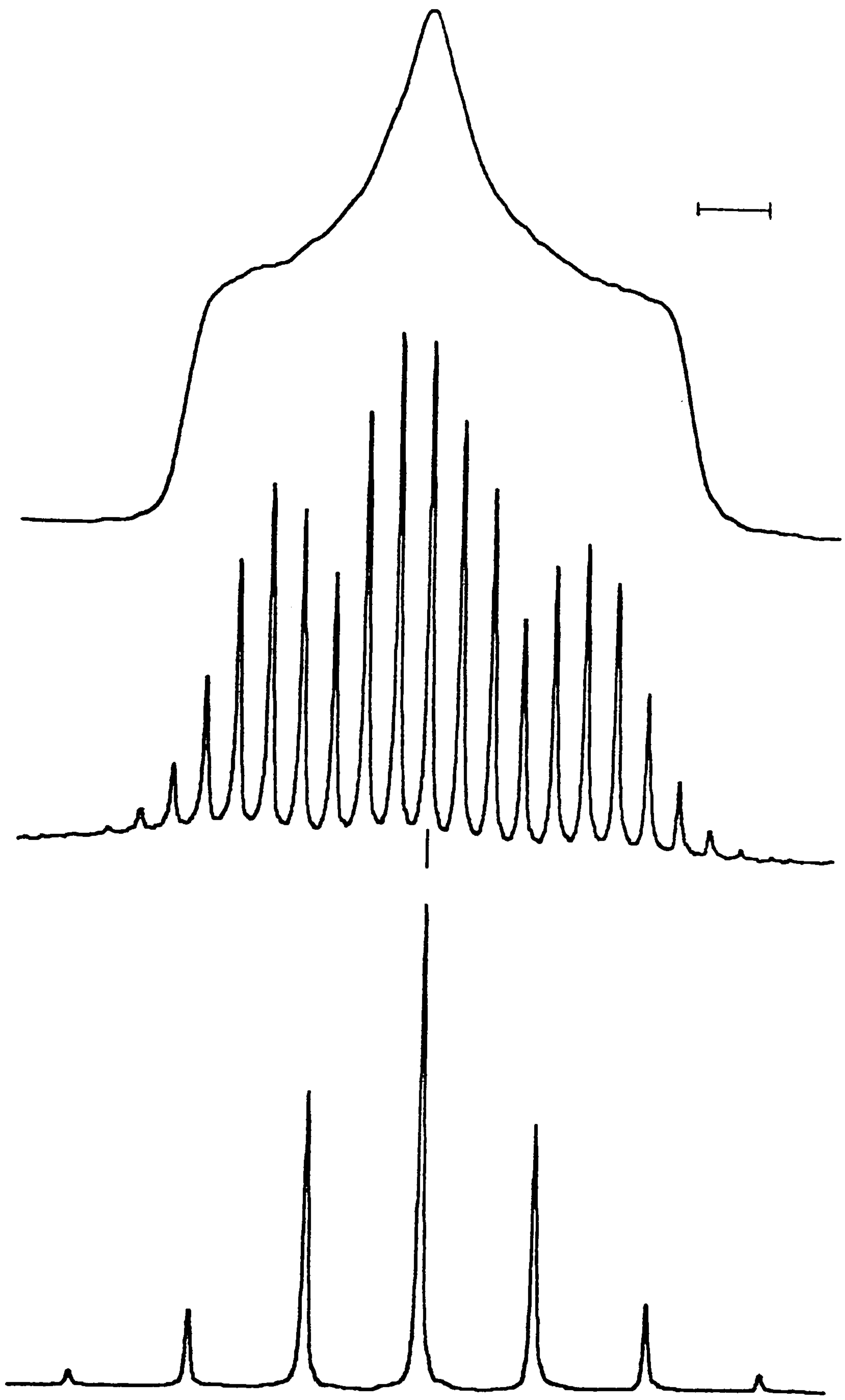

Figure 6.11: ^{31}P spectra of aminomethanephosphonic acid (**39**). SF=81.014. Top: Echo; static; PD=5 μs, RD=15 s; NT=360. Middle: CP/MAS; RD=15 s; PD=5 μs; CT=1 ms, ν_r=813 Hz. Bottom: CP/MAS; RD=15 s; PD=5 μs; CT=1 ms, ν_r=2950 Hz. δ_P = 18.3 ppm. The bar represents 2 kHz.

Table 6.4: Solid-State ^{15}N NMR Data for Selected Aminophosphonic Acids $P^* = -P(O)(OH)_2$

Compound	δ_N/ppm
(40) $H_2N\text{-}CH_2\text{-}CH_2\text{-}P^*$	-342.6
(42) $(CH_3)_2N\text{-}\overset{P^*}{\underset{P^*}{C}}\text{-}H$	-335.7
(43) $H_2N\text{-}CH_2\text{-}CH_2\text{-}\overset{P^*}{\underset{P^*}{C}}\text{-}OH$	-343.5
(44) $H_2N\text{-}CH_2\text{-}CH_2\text{-}\overset{P^*}{\underset{P^*}{C}}\text{-}OH$ Na_2 salt	-338 to -342 (broad, unresolved)
(45) $N(CH_2\text{-}P^*)_3$	-330.8
(46) AHP	-318 to -328 (broad, unresolved)
(47) AHP Na_2 salt	-330.5

Estimated error: $\delta_N \pm 0.1$ ppm.

(42) $(CH_3)_2N\text{-}\overset{P^*}{\underset{P^*}{C}}\text{-}H$ N,N-Dimethylaminomethanediphosphonic acid

The ^{31}P spectrum of compound (42) consists of two singlets at 9.1 and 2.0 ppm, each with a half-height linewidth of 65 Hz. The supposition of a single molecule asymmetric unit with the phosphorus atoms unrelated by symmetry is confirmed by ^{15}N CP/MAS spectroscopy. The nitrogen spectrum (Figure 7.5) consists of a single line at -335.7 ppm. The nitrogen chemical shift indicates the presence of a zwitterion. The CRAMPS results show three different types of acid group hydrogen bonding present, one of which is quite strong (16.9 ppm).

(43) $H_2N\text{-}CH_2\text{-}CH_2\text{-}\overset{P*}{\underset{P*}{C}}\text{-}OH$ 3-Amino-1-hydroxy-propane-1,1-diphosphonic acid

Sample (**43**) has a centreband ^{31}P spectrum of two narrow, but incompletely resolved singlets. The shifts of these singlets are 15.9 and 12.8 ppm and each has a linewidth of ca. 111 Hz. Again, as with several analogous compounds ((**28**), (**42**), (**52**)), the P-P scalar coupling is too small to be resolved. The ^{15}N CP/MAS spectrum (Figure 7.5), which is a single narrow line at -343.6 ppm, suggests a single-molecule asymmetric unit with phosphorus atoms unrelated by symmetry. This is supported by the ^{13}C spectrum which shows a single line for the central methylene resonance. The J_{PC} for this sample is 158 Hz.

The CRAMPS spectrum is indicative of two types of hydrogen bonding present in the crystal, one at 8.2 ppm, which is quite weak, and the other at 13.3 ppm, which can be considered moderate to strong.

(**44**) $H_2N\text{-}CH_2\text{-}CH_2\text{-}\overset{P*}{\underset{P*}{C}}\text{-}OH$ Na_2 salt [disodium salt of (43)]

Both the ^{31}P and ^{13}C spectra of this disodium salt simply show broad, unresolved bands. It may be speculated that the salt formation has disrupted the crystalline structure of the acid leaving an amorphous material in which there is a relatively wide range of phosphorus and carbon environments.

(**45**) $N(CH_2\text{-}P*)_3$ Nitrilomethylenetriphosphonic acid

The phosphorus spectrum of this sample consists of a single line at 12.1 ppm with a half-height linewidth of ca. 140 Hz. The ^{15}N spectrum is also a single line with a δ_N of -330.8 ppm. Both of these spectra point to a single molecule asymmetric unit with all three phosphorus atoms related by symmetry. This is confirmed by the crystal structure published by Daly and Wheatley[22] (space group: $P2_1/c$).

The CRAMPS spectrum of this material shows two types of hydrogen bonding at 16.3 and 12.5 ppm present in a ratio of 1:4. This result is also corroborated by the crystal structure which indicates five O-H-O hydrogen bonds, one which is quite strong (2.458 Å), and four others which are of moderate strength (2.532 - 2.602 Å). A further discussion of the proton results for this compound may be found in section 6.5

(46) Compound IV: Azacycloheptane-2,2-diphosphonic acid (AHP)

(47) AHP Na_2 salt

The ^{31}P spectrum of both of these samples has a centreband of two singlets. In the disodium salt, these singlets are only partially resolved. However, in the acid form there is baseline separation. There is no P-P scalar coupling evident in the spectrum of either compound. It has been noted above, however, that geminal couplings may be small in relation to the solid-state linewidths. As in the case of the methylene- and ethane-diphosphonic acids, there is a shift to low frequency upon neutralization.

(48) $(P^*\text{-}CH_2\text{-})_2N\text{-}CH_2\text{-}CH_2\text{-}N(\text{-}CH_2\text{-}P^*)_2$ Ethylenediamine-tetramethylenephosphonic acid

This compound, which is the phosphonic acid equivalent to EDTA, has a rather unusual ^{31}P spectrum. The centreband consists of two main resonances. The high frequency line is composed of two resonances which are only just resolved. The integrated intensity of the two main resonances is 3:1. This suggests a single-molecule asymmetric unit in which three of the phosphonic acid groups are reasonably similar (but <u>not</u> equivalent), and one which is significantly different. One might suppose that this could be caused by variation in the hydrogen bonding structure.

Table 6.5: Solid-State ^{13}C CP/MAS Data for Selected Phosphonic and Phosphinic Acids[+]

Compound	δ_C/ppm	$\lvert J_{PC}\rvert$/Hz
(24) CH_3-C(P*)(P*)-OH •$1H_2O$ (HEDP)	C-1 70.1‡ C-2 17.1	154
(25) HEDP Na_2 salt •$4H_2O$	C-1 70.8‡ C-2 19.2	151
(26) HEDP Na_3 salt •$6H_2O$	C-1 71.7‡ C-2 21.6	148
(27) HEDP Na_4 salt	C-1 broad C-2 28.8, 24.1, 21.6	
(28) HEDP Ca_2 salt	C-1 72.5 C-2 19.7	138
(30) CH_3-CH(P*)-CH(P*)(P*) •1 Aniline	C-3 12.5	
(31) Bu^t-CH(P*)-CH(P*)(P*) •3 Aniline	34.5[Q] 28.4[M]	
(43) H_2N-CH_2-CH_2-C(P*)(P*)-OH	C-1 72.9‡ C-2 32.3 C-3 35.7	
(46) AHP	C-1 62.6‡	135.4
Phosphinic Acids[@]		
(52) CH_3-C(P•)(P•)-OH	C-2 17.2, 16.6	
(53) Bu^t-CH(P•)-CH(P•)(P•)	35.5[Q] 29.8[M]	

Estimated errors: δ_C ± 0.1 ppm; $\lvert J\rvert$ ± 10 Hz.

[+] For tetralinbisphosphonic acid derivatives see spectra.

‡ = deceptively simple triplet.

Q = NQS result: quaternary carbon of Bu^t group.

M = NQS result: methyl group of Bu^t group.

[@] All methylphosphinic acids.

The ^1H CRAMPS spectrum of this compound is still under some question. There appear to be three resonances in the hydrogen bonding region at 14.8, 13.9 and 12.9 ppm. Although this is not unreasonable, the proximity of these resonances is at the limit of resolution of the CRAMPS technique. Until the results are confirmed, the most that can be said with confidence is that there is a broad region of hydrogen bonding present in the CRAMPS spectrum centred at about 13.9 ppm. This region represents bonding of moderate to strong character.

6.2.c Phosphinic Acids

(**49**) $P^{\circ}-CH_2-CH_2-P^{\circ}$ Ethane-P,P'-dimethyl-1,2-bisphosphinic acid

The ^{31}P centreband of compound (**49**) (Figure 6.12) consists of two partially resolved singlets with shifts of 61.9 and 60.8 ppm. The lines are very narrow (33 Hz each) and do not display any evidence of P-P scalar coupling. Two different environments of equal integrated intensity are indicated. This could indicate a unit cell containing a single type of asymmetric molecule or a unit cell containing two different types of molecule, each with the two phosphorus atoms related by symmetry. (Note that the phosphonic acid analog (**18**) of this compound contained a single-molecule asymmetric unit with the phosphorus atoms related by a centre of inversion symmetry.)

An attempt was made to clarify this situation using carbon-13 CP/MAS NMR. However, this was unsuccessful. The ^{13}C spectrum was a broad band, complicated by P-C scalar coupling which remained generally unresolved in the linewidths obtainable by present techniques.

The phosphorus T_1 of this compound was examined using the inversion-recovery technique and found to be ca. 48 seconds. It will be noted that this is at least an order of magnitude less than for the analogous phosphonic acid. One explanation for the lower T_1 of the phosphinic acid may be the presence of the highly mobile

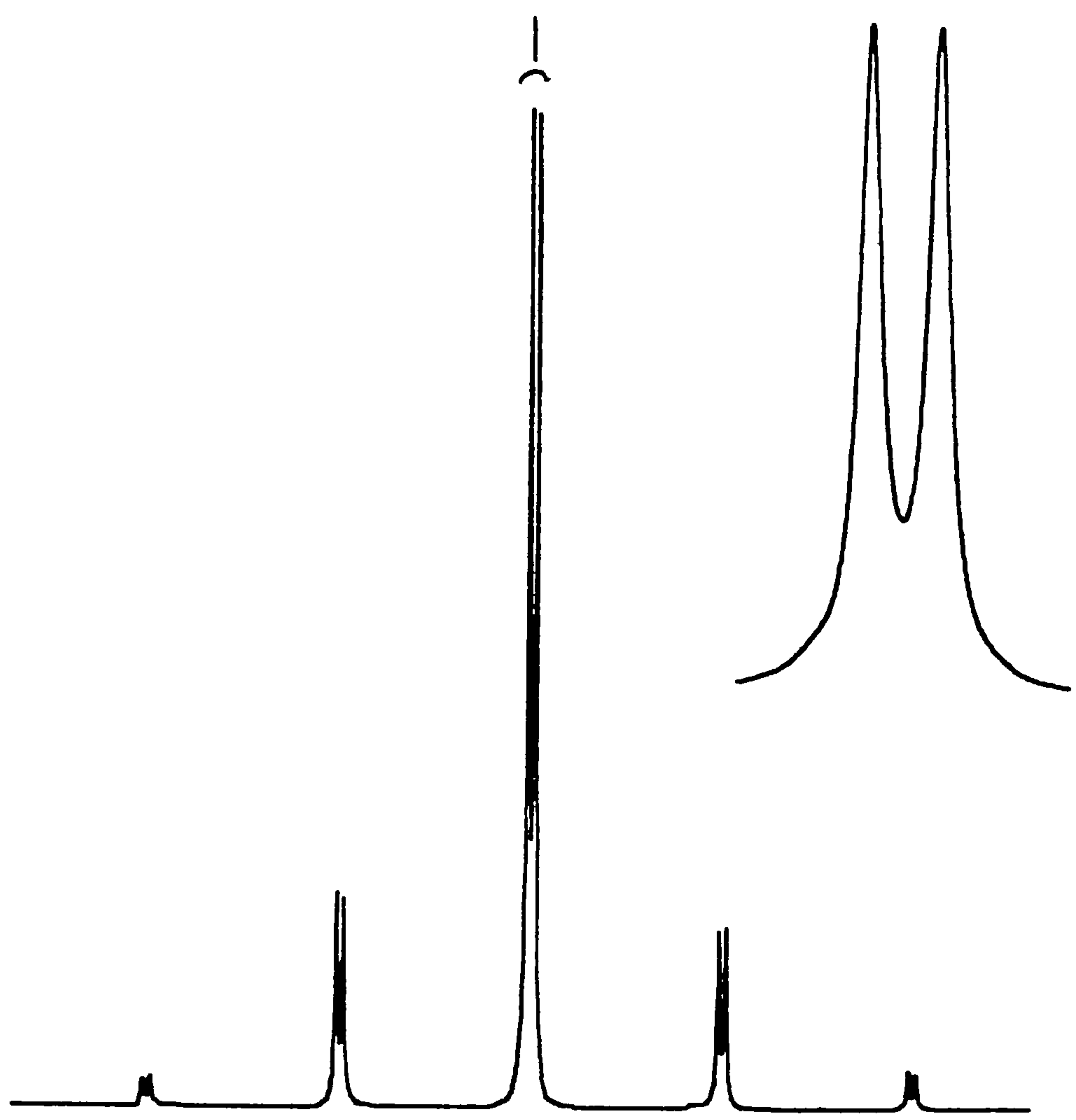

Figure 6.12: ^{31}P CP/MAS spectrum and expanded centreband of ethane-P,P'-dimethyl-1,2-bisphosphinic acid, (**49**). SF=81.014 MHz. RD=10 s; PD=4 μs; CT=1 ms. v_r=2370 Hz; NT=96. δ_P = 61.9 and 60.8 ppm. $v_{½}$ = 33 and 33 Hz.

Table 6.6: Solid-State ^{31}P CP/MAS Data for Phosphinic Acids $P^\circ = -\underset{R}{P}(O)(OH)$

R	Compound	δ_P/ppm	$\lvert J_{PP}\rvert$/Hz	$\lvert J_{PC}\rvert$/Hz
(49) CH_3	$P^\circ-CH_2-CH_2-P^\circ$	61.9 60.8	-	-
(50) CH_3	$P^\circ-CH_2-CH-P^\circ_2$	54.4 52.8 39.0	-	-
(51) CH_3	$P^\circ_2-CH-CH-P^\circ_2$	54.3 39.9 39.0	-	-
(52) CH_3	$CH_3-\overset{P^\circ}{\underset{P^\circ}{C}}-OH$	53.2 46.4	-	-
(53) CH_3	$Bu^t-\overset{P^\circ}{CH}-\overset{P^\circ}{\underset{P^\circ}{CH}}$	61.3 47.5^u 45.8^u	-	-
(54) CH_3	$Ø-\overset{P^\circ}{CH}-\overset{P^\circ}{\underset{P^\circ}{CH}}$	58.0 50.5 48.1 46.1	-	-
(55) Ø	$P^\circ-CH_2-CH_2-P^\circ$	44.0	-	-

Ø = phenyl u = probable unresolved doublet
Estimated error: δ_P ± 0.1 ppm.

methyl group. Another probability is that there is more motion in the lattice as a whole because there is less hydrogen bonding in the phosphinic acids.

The ^1H CRAMPS spectrum of this material showed a single proton resonance in the hydrogen bonding region indicative of a moderately strong (14.1 ppm) bond.

(50) $P^\circ-CH_2-CH-P^\circ_2$ Ethane-P,P',P''-trimethyl-1,1,2-trisphosphinic acid

The centreband phosphorus spectrum consists of three resonances at shifts of 54.4, 52.8 and 39.0 ppm. The first two lines are incompletely resolved. The most likely assignment is one in which the geminal phosphorus atoms are represented by the two resonances at high frequency. An attempt to confirm this by running a ^{13}C spectrum was met by the usual problem of insufficient resolution. The ^{1}H CRAMPS spectrum of this material has two acid proton resonances with shifts indicative of moderately strong H-bonding.

Table 6.7: Solid-State ^{1}H CRAMPS Data for Phosphinic Acids

	R	Compound	δ_H/ppm of Hydrogen Bonded Acid Proton		Approximate Integral
(49)	CH_3	P°-CH_2-CH_2-P°	14.1		
(50)	CH_3	P°-CH_2-CH-P°$_2$	14.7	13.7	1:1
(51)	CH_3	P°$_2$-CH-CH-P°$_2$	15.2	13.6	1:1
(52)	CH_3	P° CH_3-C-OH P°	12.3		
(53)	CH_3	P° P° Bu^t-CH-CH P°	15.3		
(54)	CH_3	P° P° Ø-CH-CH P°	14.1		
(55)	Ø	P°-CH_2-CH_2-P°	15.8		

Estimated error: $\delta_H \pm 0.5$ ppm.
Ø = phenyl.

(51) P°$_2$-CH-CH-P°$_2$ Ethane-P,P',P'',P'''-tetramethyl-1,1,2,2-tetrakisphosphinic acid

The ^{31}P centreband spectrum of this material contains three resonances with chemical shifts of 53.3, 39.9 and 39.0 ppm; the two lines to low frequency are only partially resolved. The ratio of

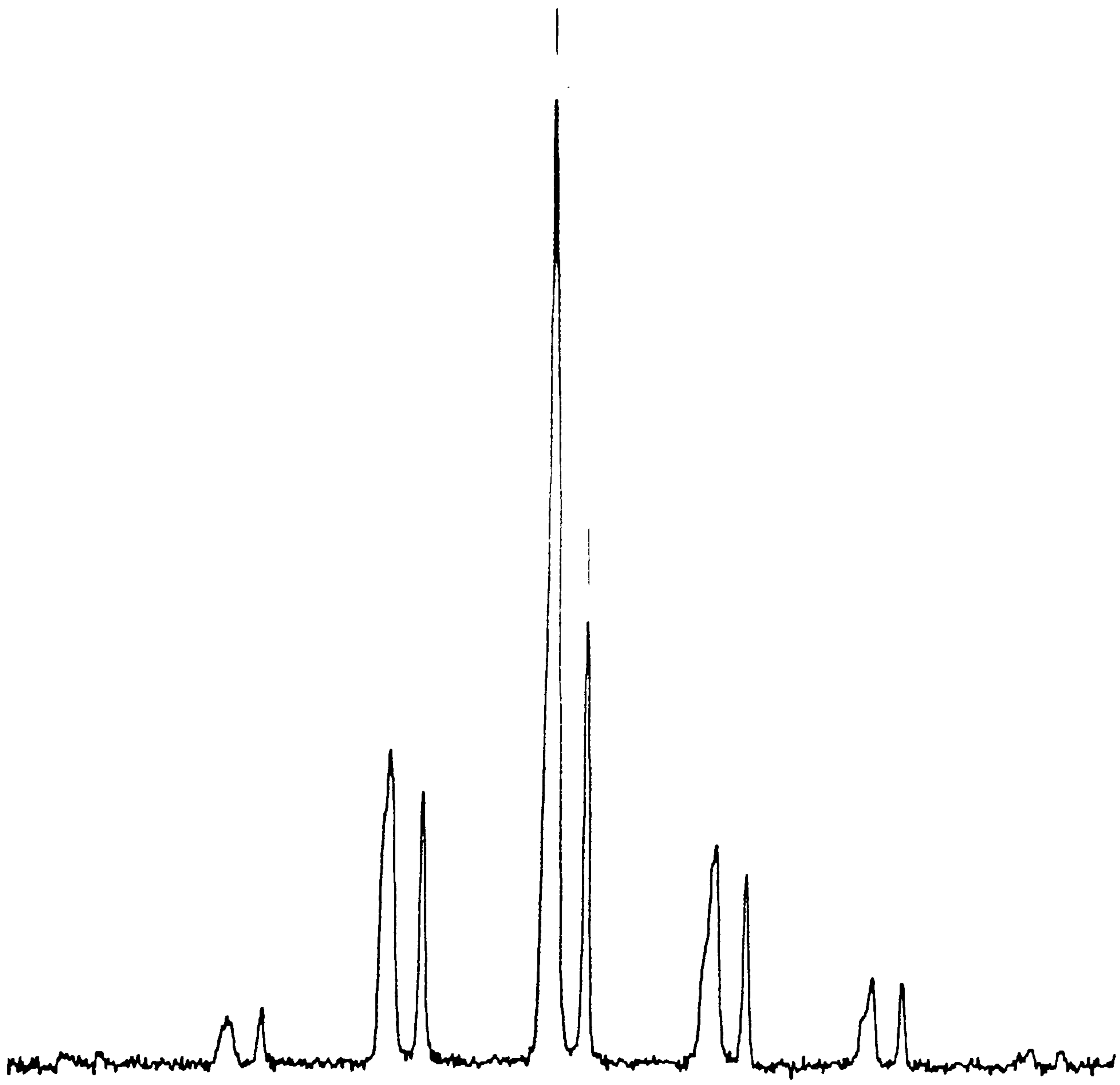

Figure 6.13 ^{31}P SPE/MAS spectrum of compound (**52**). RD=240 s; PD=4 μs; ν_r=2630 Hz; NT=24; SF=81.014 MHz. The ratio of the two resonances integrated over the spinning sideband manifolds is 3:1.

δ_P (ppm)	$\nu_{1/2}$ (Hz)
53.2	180
46.4	95

the high-frequency resonance to the two partially resolved low-frequency resonances is 1:1. In looking at the molecular structure, it is not clear why there should be three phosphorus environments. The most likely explanation for this is accidental equivalence in the case of the high frequency line. The ^{1}H data for this compound also show two reasonably strong hydrogen bonds.

$$\text{(52)}\quad CH_3-\overset{\displaystyle P^{\bullet}}{\underset{\displaystyle P^{\bullet}}{C}}-OH$$

1-Hydroxyethane-P,P'-dimethyl-diphosphinic acid

With regard to the crystallographic information revealed, the ^{31}P and ^{13}C spectra of compound (52) (Figures 6.13 and 6.14) are probably the most interesting of all the phosphinic acid spectra. The ^{31}P centreband consists of two singlets, the high frequency one of which is significantly broader than the other. The intensity ratio integrated over the spinning sideband manifolds is 3:1. The ^{13}C spectrum is broad and unresolved in the C-1 region, and the phosphinic acid methyl groups are broadened by P-C scalar coupling and are not resolved; however, there are <u>two</u> backbone methyl group resonances. These two methyl resonances would seem to indicate two crystallographically different kinds of molecule in the unit cell. Given that this is the case, the explanation for the phosphorus spectrum is straightforward. In the unit cell, one of the two types of molecule has phosphorus atoms which are significantly different. This would account for the low frequency singlet of integral one and also for one-third of the integral of the broad resonance. The remaining two-thirds of the integral of the high frequency line must then come from the second type of molecule in the unit cell. In this molecule the two phosphorus atoms are either related by symmetry, or, at the very least, similar enough to have a very small chemical shift difference. Although no other certain cases of such a "mixed" unit cell have been observed in the present study, an example of this in the diphosphine disulphide series, which was confirmed by existing X-ray data, may be found in Chapter 5.

The proton CRAMPS results for (52) show only a single type of

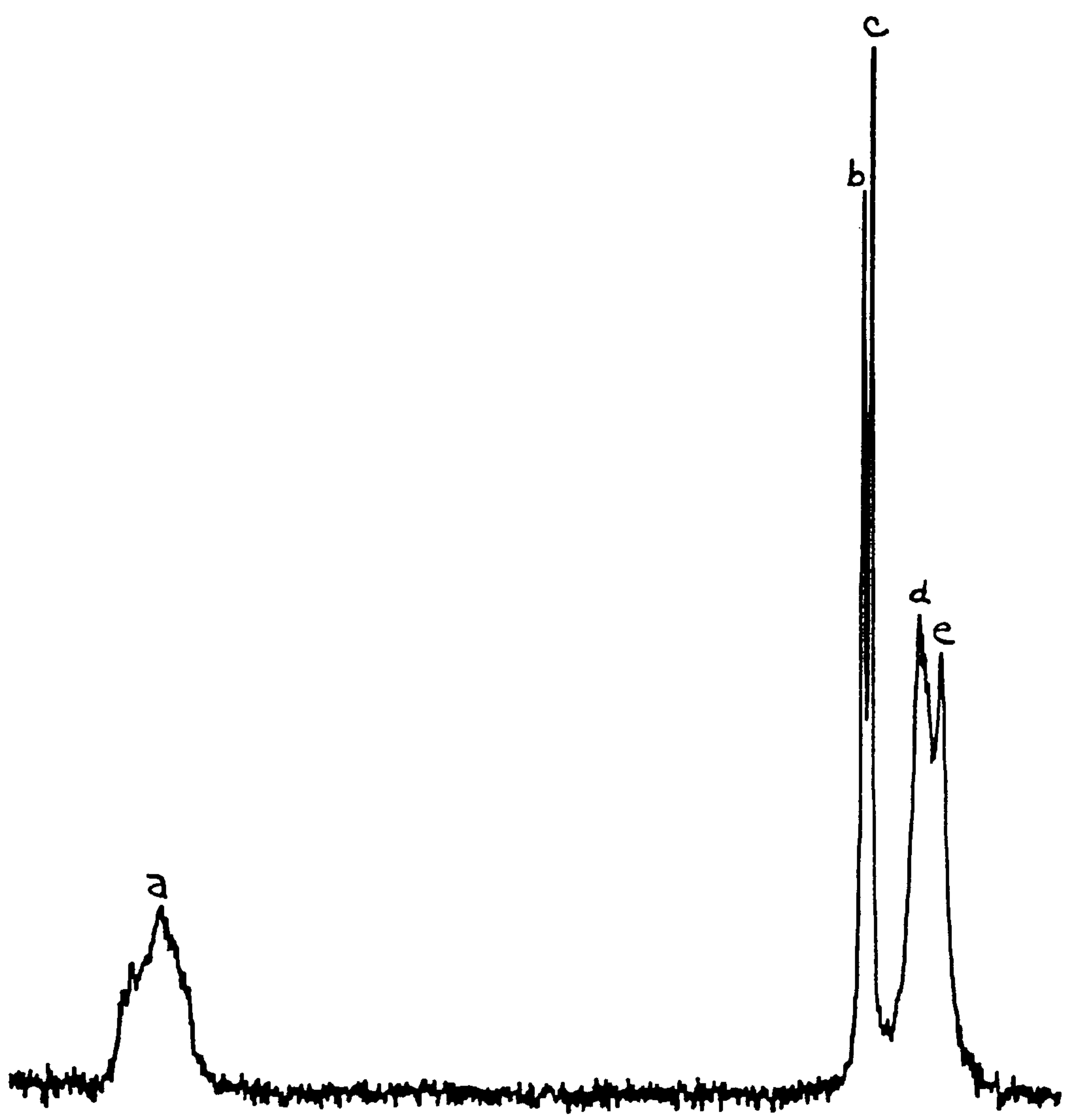

Figure 6.14: ^{13}C CP/MAS spectrum of compound (52). SF=50.3227 MHz. RD=10 s; PD=5 μs; CT=5 ms. ν_r=3985 Hz; NT=212. δ_C (a) 72.5, (b) 17.2, (c) 16.6, (d) 12.8, (e) 11.0 ppm.

hydrogen bonded acid proton at 12.3 ppm. This compares with 14.5 and 11.0 for HEDP.

It should be noted that the results here (both ^{31}P and ^{1}H) are significantly different from that of HEDP of which this compound is the phosphinic acid analogue. It is clear that the presence of the methyl group has both a steric effect and an influence on the overall hydrogen bonding structure of the crystal.

```
          P° P°
          |  |
(53) Bu^t-CH-CH    1-t-Butylethane-P,P',P''-trimethyl-1,2,2-
             |            trisphosphinic acid
             P°
```

The phosphorus CP/MAS spectrum of this compound consists of a singlet and two incompletely resolved resonances, the shapes of which suggest unresolved AB doublets. The integration of the three lines over the spinning sideband manifold is 1:1:1. It is felt that the case here is similar to that of phosphonic acids (30), (31), and (32), one of which (31) is the analogue of this compound. Here, as in the phosphonic acids, there is a single-molecule asymmetric unit. This is confirmed by the ^{13}C NQS spectrum. The two ^{31}P lines, which are to low frequency, are broadened by unresolved P-P scalar coupling. Again, a single type of strong hydrogen bond is indicated in the ^{1}H results.

```
       P° P°
       |  |
(54) Ø-CH-CH    1-Phenylethane-P,P',P''-trimethyl-1,2,2-
          |            trisphosphinic acid
          P°
```

The ^{31}P spectrum of this phosphinic acid is, at the moment, quite confusing. The centreband consists of a singlet and what appears to be a triplet in an approximate 1.1:1 intensity ratio. As yet, there is no explanation for the unusual shape or integral. The compound appears pure by solution-state ^{31}P NMR. The sample was also run at higher field (7 Tesla), but this gave no further information.

(55) $P^{\bullet}-CH_2-CH_2-P^{\bullet}$ Ethane-P,P'-diphenyl-1,2-diphosphinic acid

Note that this compound is a phenylphosphinic acid.

The centreband phosphorus spectrum of compound (41) is a single, narrow resonance. A single-molecule asymmetric unit with the phosphorus atoms related by symmetry is indicated. The ^1H spectrum has a single acid proton resonance in the region associated with strong hydrogen bonding.

6.3 Chemical Shift Considerations

6.3.a General Comments

The theoretical background for the chemical shifts of the phosphonic and phosphinic acids are beyond the scope of this thesis. The reader is referred to the work of Crutchfield, Dungan, Letcher, Mark and Van Wazer[23] for a discussion of general phosphorus chemical shift theory. It is noted, however, that the general trends for the phosphonic acids follow observations for alkyl diphosphonic acids in solution made by Moedritzer and Irani[7]. They observed a general shielding effect for neighbouring alkyl-PO_3H_2 groups and showed that this effect decreased with the intervening number of CH_2 groups. They also noted the general shielding effects upon Na_2 and Na_4 salt formation for the straight-chain alkyl-diphosphonic acids.

It will be further seen from comparison of Tables 6.1 and 6.5 that the trends for the phosphinic acids follow that of the phosphonic acids. The former, however, exhibit a general shift of +20-30 ppm from their phosphonic acid analogues. This shift will be seen to be a direct result of the replacement of the oxygen by the CH_3 group. Such deshielding effects for phosphorus have been discussed by Van Wazer *et al.*[24]

Table 6.8
Comparison of Solid- and Solution-State
Phosphorus Chemical Shifts for the Phosphonic Acids

Compound	Solid-state δ_P/ppm	Solution-state δ_P/ppm
(15) P*-CH_2-P*	26.2 24.7	22.4[a]
(16) P*-CH_2-P* Na_2 salt	22.3 14.4	15.2[a]
(18) P*-CH_2-CH_2-P*	32.7	28.83[c]
(19) P*-CH_2-CH_2-P* Na_2 salt •$4H_2O$	29.3	23.3[a]
(20) P*-CH_2-CH_2-P* Na4 salt	24.8	22.4[a]
(21) P*-CH_2-CH-P*$_2$	28.7 19.9	26.39 20.04
(22) P*$_2$-CH-CH-P*$_2$ $[(NH_2)_3C]^+{}_6$ salt•$6H_2O$	19.9 18.3	19.47 15.36[b]
(23) P*$_2$-CH-CH-P*$_2$ anhydride Na_6 salt•$11H_2O$	19.3 16.1	18.25 13.90[c]
(24) P* CH_3-C-OH •$1H_2O$ (HEDP) P*	25.3 18.7	19.8[a]
(29) P* P* Ø-CH-CH_2	32.3 (broad)	27.57 25.8[d]
(32) P* P* Ø-CH-CH P*	26.7[d] 21.5 20.0	25.46 20.59 18.01[d]
(33) P*$_2$-CH-CH_2-CH-P*$_2$	29.3 26.2 24.1 21.4	21.68[c]
(35) 1-phenyl-trans-1,4-tetralin-bisphosphonic acid	37.5 36.5	30.47 29.88[c]
(36) 1-phenyl-cis-1,4-tetralin-bisphosphonic acid	35.1 31.7	26.56 23.7[c]
(37) Compound III	4.9 -0.5	2.41 0.23
(38) C_6H_5-P*	21.0	18.5[a]

Estimated error for solid-state data: δ_P ± 0.1 ppm.
a = reference 23 b = reference 10
c = reference 17 d = reference 16

6.3.b Comparison of Solid- and Solution-State Results

A comparison of solution- and solid-state phosphorus chemical shifts may be found in Tables 6.8 and 6.9. The solution-state values included in these tables represents work from a number of references as well as several from this study. (It should be noted that a potential source of shift difference here will be variation in referencing procedure.) As can be seen, the solid-state phosphorus shifts are comparable to those noted in solution. Differences may be attributed to medium effects (including the influence of surrounding molecules in the solid state) and the small changes in bond length and angle between solution and solid.

Table 6.9
Comparison of Solid- and Solution-State
Phosphorus Chemical Shifts for the Phosphinic Acids

R	Compound	Solid-State δ_P/ppm	Solution-State δ_P/ppm
(49) CH_3	$P^{\circ}\text{-}CH_2\text{-}CH_2\text{-}P^{\circ}$	61.9 60.8	56.00[a]
(50) CH_3	$P^{\circ}\text{-}CH_2\text{-}CH\text{-}P^{\circ}_2$	54.4 52.8 39.0	54.5 50.06[b]
(51) CH_3	$P^{\circ}_2\text{-}CH\text{-}CH\text{-}P^{\circ}_2$	54.3 39.9 39.0	48.21[b]
(54) CH_3	P° P° Ø-CH-CH P°	58.0 50.5 48.1 46.1	50.6 47.9 41.0

Estimated error for solid-state data: $\delta_P \pm 0.1$ ppm.
a = reference 10. b = reference 17.

6.4 Shielding Tensor Considerations

For the MAS spectra of the phosphonic and phosphinic acid compounds in which the lines were sufficiently resolved, calculations of the principal components of the chemical shielding tensors were done. Initial calculations were made using the method

Table 6.10 Shielding Tensor Data
for the Phosphonic and Phosphinic Acids

Compound	Shielding Tensor Components					
	σ_{iso}	δ	η	σ_{11}	σ_{22}	σ_{33}
	Phosphonic Acids					
(15) P*-CH_2-P*	-26.2	53.1	0.794	-73.7	-31.8	26.9
	-24.7	54.2	0.720	-71.3	-32.3	29.5
(17) HOOC-CH_2-P*	-17.1	68.6	0.389	-64.7	-38.1	51.5
(18) P*-CH_2-CH_2-P*	-32.7	48.2	0.241	-62.6	-51.0	15.5
(19) P*-CH_2-CH_2-P* Na_2 salt •$4H_2O$	-29.3	-61.3	0.857	27.6	-24.9	-90.6
(20) P*-CH_2-CH_2-P* Na4 salt	-24.8	-59.6	0.185*	10.5	-0.513	-84.4
(25) HEDP Na_2 salt •$4H_2O$	-23.8	-74.5	0.885	46.4	-19.5	-98.3
	-22.5	-71.7	0.858	44.1	-17.4	-94.2
(26) HEDP Na_3 salt •$6H_2O$	-27.8	-66.6	0.967	37.7	-26.7	-94.4
	-18.4	-73.6	0.389	32.7	4.1	-92.4
(33) $P*_2$-CH-CH_2-CH-$P*_2$	-29.3	45.7	0.545	-64.6	-39.7	16.4
	-26.2	49.2	0.594	-65.4	-36.2	23.0
	-24.1	60.6	0.602	-72.6	-36.1	36.5
	-21.4	46.3	0.799	-63.0	-26.1	24.9
(37) Compound III	-4.9	-82.9	0.992	77.7	-4.5	-87.8
	0.5	-88.4	0.901	84.5	4.9	-87.9
(38) C_6H_5-P*	-21.0	49.3	0.947	-69.0	-22.3	28.3
	Aminophosphonic Acids					
(39) H_2N-CH_2-P*	-18.3	82.2	0.930	-97.4	-20.9	64.1
(40) H_2N-CH_2-CH_2-P*	-19.1	68.5	0.906	-84.4	-22.3	49.4
(41) H_2N-CH_2-CH_2-CH_2-P*	-25.2	58.4	0.969	-82.7	-26.1	33.2
(42) $(CH_3)_2N$-C(P*)(P*)-H	-9.1	-71.1	0.711	69.9	19.4	-62.0
	-2.0	73.9	0.900	-72.2	-5.70	71.9

(continued)

Shielding Tensor Data for the
Phosphonic and Phosphinic Acids (continued)

Compound	Shielding Tensor Components					
	σ_{iso}	δ	η	σ_{11}	σ_{22}	σ_{33}
(43) $H_2N-CH_2-CH_2-C(P^*)_2-OH$	-15.9	-66.8	0.709	41.2	-6.2	-82.7
	-12.8	67.2	0.904	-76.8	-16.0	54.4
(45) $N(CH_2-P^*)_3$	-12.1	-65.4	0.955	51.8	-10.6	-77.5
(46) AHP	-17.8	-53.2	0.837	31.1	-13.5	-71.0
	-8.4	-65.5	0.860	52.5	-3.8	-73.9
(47) AHP Na_2 salt	-28.1	-64.9	0.913	33.9	-25.3	-93.0
	-23.9	73.2	0.831	-90.9	-30.1	49.3
Methylphosphinic Acids						
(49) $P^{\circ}-CH_2-CH_2-P^{\circ}$	-61.9	39.5	0.899	-99.4	-63.9	-22.4
	-60.8	38.6	0.990	-99.2	-61.0	-22.2
(50) $P^{\circ}-CH_2-CH-P^{\circ}_2$	-54.4	58.2	0.921	-110.3	-56.7	3.8
	-52.8	57.1	0.934	-108.0	-54.7	4.3
	-39.0	-67.0	0.934	25.8	-36.8	-106.0
Phenylphosphinic Acids						
(55) $P^{\circ}-CH_2-CH_2-P^{\circ}$	-44.0	-65.9	0.962	20.6	-42.7	-109.9

*Actually, axially symmetric within experimental error.
Note: The shielding tensor values for compounds (**17**, **19**, **20**, **39**, **40** and **41**) were determined from static spectra and are thus quoted to ±2 ppm. All other values were obtained by spinning-sideband analysis and are given to ±5 ppm. A discussion of the errors may be found in Chapter 4.

of moments analysis of Maricq and Waugh. In all cases, the results were further refined using the sideband fitting routine SBFIT. Additionally, for several of the compounds where there was a single phosphorus environment, static spectra were run and the tensor values determined from a fit of the static bandshape. The results of these calculations are reported in Table 6.10.

There are, at present, very few reports in the literature of shielding tensor values for the derivatives of phosphonic and phosphinic acids. Those which are reported are mainly for the phosphonic acid esters[25] or aminophosphonic acids[26]. No values were found for any of the compounds in this work.

The anisotropy (δ) values range in magnitude for the phosphonic acids from 46.3 to 82.2 ppm, for the aminophosphonic acids from 53.2 to 82.2 ppm, and the phosphinic acids from 38.6 to 67 ppm. The spread for both types of compound is smaller than that reported for the inorganic phosphates which have magnitudes of approximately 69 to 156 ppm[12,13]. This, however, is most likely due to the fact that the present study has not covered a particularly wide range of phosphonic or phosphinic acid salts. It is generally these salts with their associated hydration, deprotonation, and cation charge and electronegativity factors, which have a significant effect on the range of the shielding environments in the inorganic phosphates.

It will be noted from examination of Table 6.10 that the asymmetry values for the phosphonic and phosphinic acids are consistent and generally indicate an asymmetric shielding environment. These results are consistent with the strong hydrogen bonding nature of these compounds and suggest that there is clearly a double-bonded oxygen present. Where η deviates significantly from asymmetric, an explanation is usually clear. The axially symmetric bandshape of compound (20) has been discussed already and may be seen to result from complete deprotonation of the acid. For compound (23), in which three of the four acid protons have been removed, it is clear that one of the phosphonic acid groups has been deprotonated while the other retains a proton (probably in the form of a hydrogen bond). The cause of the low asymmetry value for compounds (17) and (18) is less clear.

As with the diphosphine disulphide compounds, attempts were made to correlate the shielding tensor properties of these acids with various structural features from known diffraction studies. (See Table 6.3. Note that there were no crystal structures found for any of the phosphinic acids in Table 6.6). With one exception, no good correlations were found. A general discussion of the problems involved in such correlation studies may be found in Chapter 5. For these compounds, though, one would not expect the residual dipolar interaction to be a major source of errors, as there are no directly bonded phosphorus atoms. The nearest intramolecular P-P distances occur in methylene diphosphonic acid (3.586Å)[5] and in HEDP (3.098Å)[11]. These distances correspond to P-P dipolar interactions of 642 Hz and 995 Hz respectively as calculated for the isolated cases.

As noted above, one clear empirical correlation was evident. For the aminophosphonic acids with known crystal structures, there was a linear correspondence between the P-O distance for the π-bonded oxygen and the largest shielding tensor, σ_{33}. The relationship may be given as $\sigma_{33} = -2582r_{P-O} + 3937$, where r_{P-O} is given in Angstroms. A correlation coefficient of 0.99 was determined for the least-squares fit. Linear correspondence between the π-bonded P-O distance and $\bar{\sigma}$ has been reported by several authors[27,28] as is noted in section 5.5. Such correlations may be explained by the fact that increasing π-bond character will correlate with increasing shielding in the bond direction.

6.5 CRAMPS Results - Hydrogen Bonding

6.5.a Introduction

It has been shown by several X-ray diffraction studies (see references in Table 6.3) that the solid-state structure of the phosphonic acids consists of a network of hydrogen-bonded molecules. Indeed, it is evident from an examination of the results of these studies that the networks may be quite intricate. There are no diffraction studies published for the phosphinic acids; however, one would expect similar hydrogen-bonded structures for these types of molecules as well. It is certainly clear from the known structural investigations that characterization of the hydrogen-bonding is required if one is to properly understand the solid-state structure of these compounds.

A further impetus for the study of hydrogen bonding in these acids is found in the examination of the chelation properties of the phosphonic acids. A number of gem-diphosphonates have been found to have effective alkaline earth ion sequestration properties[1]. HEDP (**24**), in particular, has been demonstrated to be an effective inhibitor of calcium hydroxyapatite crystal growth *in vitro* and to inhibit pathological calcification *in vivo*[2]. The importance of hydrogen bonding in the resulting calcium complexes has been demonstrated[29].

While X-ray or neutron diffraction studies may provide useful information about hydrogen bonding, both of these methods are difficult and time-consuming. In addition, the lack of suitable crystals may further limit their application. However, proton CRAMPS may be used effectively in the study of hydrogen bonding in solids. Such methods may be applicable to the investigation of phosphinic and phosphonic acids. After a short review of the literature, proton CRAMPS results for these systems will be presented.

Several relevant NMR studies of hydrogen bonding in solids may be found in the literature. Berglund and Vaughan[30] used multiple-pulse techniques to characterize the hydrogen bonding in a number of static organic and inorganic acid samples. This study compared the oxygen-oxygen distance of the hydrogen bond (as determined by X-ray diffraction techniques) to the proton chemical shift and anisotropy. A correlation between the isotropic proton shift and the $r_{O...O}$ was found. The correlation curve used by Berglund and Vaughan may be seen as the solid line of Figure 6.16. The curve has been offset to account for the overall difference between theoretically and experimentally derived shifts. It will be seen that there is relative deshielding as the $r_{O...O}$ distance decreases (i.e. as the hydrogen-bond strength increases). The authors have attributed the source of the proton shift to two factors: 1) the loss of electron density of the proton upon hydrogen bond formation and 2) the deshielding effect of the bond magnetic susceptibility anisotropy of the acceptor oxygen.

Further work in this area has been carried out by Rolfing *et al.*[31] and by Jeffrey and Yeon[32]. The former study relates *ab initio* calculations of ^{1}H shielding tensor and hydrogen-bond geometry. In the work of Jeffrey and Yeon, the isotropic ^{1}H shift is related to the proton-to-acceptor distance $r_{O...H}$. A linear correlation of proton shift increasing with bond strength was determined. Unfortunately, accurate proton positions are required for this correlation. Proton positions of such accuracy can only be determined[32] by neutron diffraction analysis or by normalizing the covalent O-H distance to a standard neutron diffraction value of 0.97Å. The latter method may introduce further inaccuracies, though, as no account is taken of the possible non-linearity of the hydrogen bond.

Finally, a recent study by Harris and Jackson[33] has extended this work. In a study of ca. 60 compounds, the correlations of $r_{O...O}$ and $r_{O...H}$ with the isotropic ^{1}H shift were further confirmed and refined.

6.5.b ^{1}H CRAMPS Results and Discussion

Proton CRAMPS spectra were run on all of the phosphonic and phosphinic acids. The pulse sequence used has been described in Chapter 3. Spinning speeds of ca. 3.5 kHz were used for all CRAMPS spectra. The results are presented in Tables 6.2, 6.7 and 6.11. The latter table contains a comparison between proton shifts and oxygen-oxygen bond distances as determined by X-ray diffraction techniques. As expected, the CRAMPS technique did not provide resolution sufficient to resolve the protons in the carbon backbone of these molecules. It was, however, found to be useful in determining the characteristics of the hydrogen bonding present in these systems. One can, in general, deduce the number of different types of hydrogen bond present in the system as well as get some idea of their relative strengths. A correlation between bond length and isotropic proton chemical shift similar to that reported above has been noted.

6.5.b.1 Example Spectra

An instructive example of the type of information obtained from CRAMPS spectra may be found by examining the spectrum of Figure 6.15A in light of the published X-ray crystal data[22]. The compound is nitrilotrimethylenetriphosphonic acid, $N(-CH_2-PO_3)_3$. The diffraction study shows the material to exist as a zwitterion with six intramolecular hydrogen bonds in the structure. The lengths of these from reference 22 are noted below. NMR assignment was made with due consideration to the trends described in the literature:

Bond	$r_{O...O}$/Å	Assigned resonance/ppm
O(1)...O(2)	2.532	12.5
O(6)...O(7)	2.602	12.5
O(5)...O(8)	2.551	12.5
O(6)...O(9)	2.524	12.5
O(3)...O(4)	2.458	16.3
N(1)...O(1)	2.842	9.2

The remaining peak at ca. 4.5 ppm arises from the methylene protons.

There have been a number of considerations in assigning this spectrum. Firstly, the resonances at 16.3 and 12.5 ppm are roughly of the ratio 1:4, though this is difficult to measure in this type of spectrum.

Secondly, it will be seen that the hydrogen bond at 2.602 Å

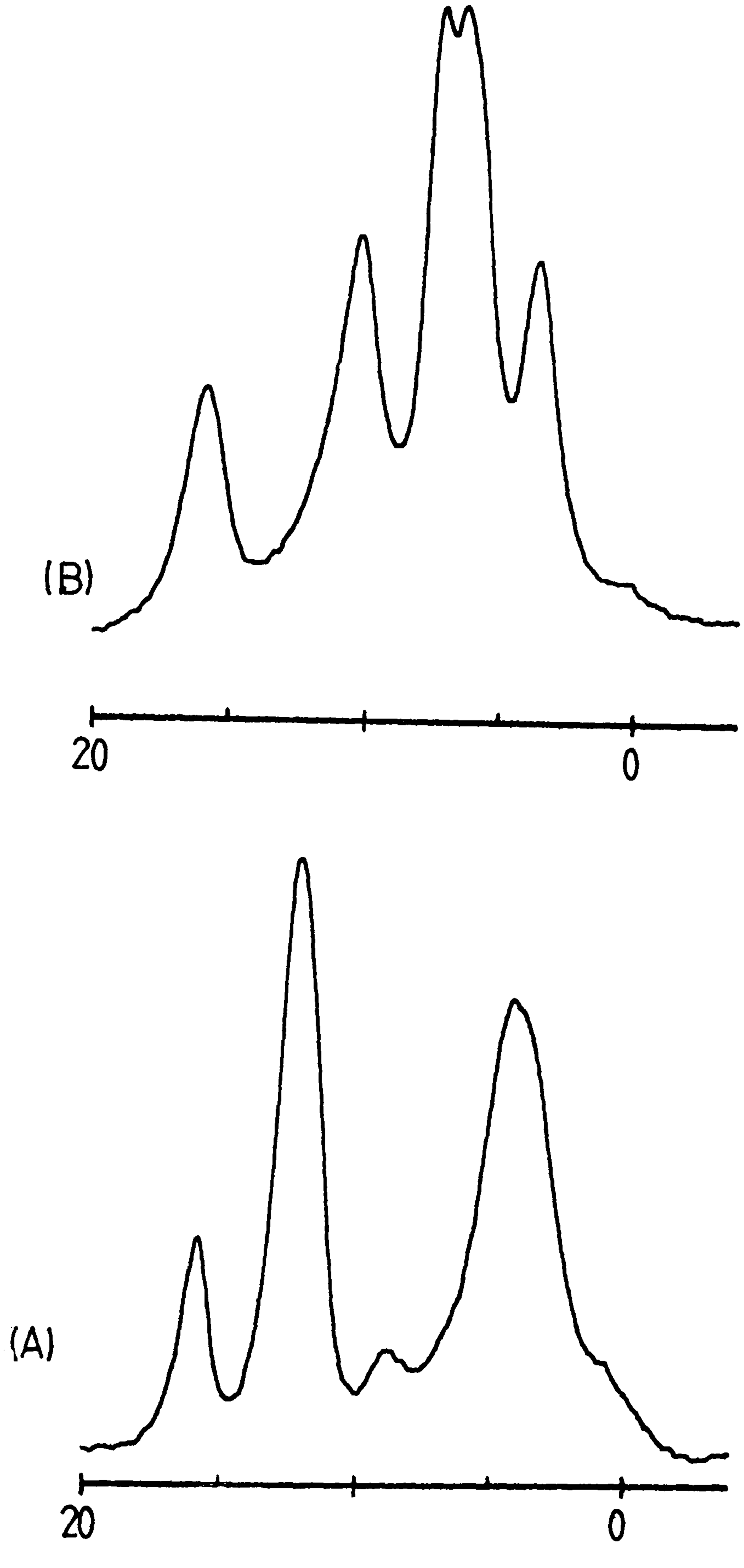

Figure 6.15: ^{1}H CRAMPS spectra. SF=200.13 MHz. (A) Compound (**45**) $N(CH_2-PO_3H_2)_3$. RD=10 s; PD=2 μs; NT=32. δ_H = 16.3, 12.5, 9.2 and 4.5 ppm. See text for assignment. (B) Compound (**32**). RD=20 s; PD=2 μs; NT=20. δ_H = 15.9, 10.3, 7.3, 6.4 and 3.6 ppm. See text for assignment. The scales are in ppm.

might easily have been expected to be a separate resonance, as the other three bonds assigned to the line at 12.5 ppm are fairly close in length. The probable explanation for this is as follows: Examination of the X-ray data shows this hydrogen bond, O(6)..O(7), to have O(6) as the acceptor. This oxygen is attached to the PO_3 group determined in the crystal structure to be the ^1H donor to the zwitterion. This PO_3 group, therefore, has a net negative charge. The effect of this negative charge will be to shift the resonance for the hydrogen bond ~1-2 ppm to high frequency, where it is unresolved from the resonances arising from the other three, shorter hydrogen bonds assigned to 12.5 ppm.

A similar argument applies to the single hydrogen-bond of 2.458 Å. The shift of 16.3 ppm seems higher than one would expect for this length bond if one considers the data in Table 6.11 and Figure 6.16. Again, the acceptor oxygen is shown to be on the PO_3^- group.

Further, it will be noted that the resonance at 9.2 ppm assigned to the N..H-O hydrogen bond may be of lower intensity compared to the other resonances in the spectrum. The primary reason for this is that there are spinning sidebands associated with this line which are not shown in the figure. A second possible reason is incomplete removal of direct $^1H-^{14}N$ dipolar coupling by magic-angle spinning[8]. Such broadening is common for ^{13}C in solids and is a result of the fact that ^{14}N is a quadrupolar nucleus.

Finally, the proton which is involved in the zwitterion formation may be assigned to the broad underlying component in the spectrum. The breadth of this resonance will most probably result from a combination of the quadrupolar effect noted above and rapid exchange processes. If such exchange processes have correlation times of the order of the multiple-pulse cycle times, complete averaging of the dipolar interaction will not take place.

A second example spectrum which gives a general idea of the overall resolution of the CRAMPS technique, may be found in Figure 6.15.B. The compound here is 1-phenyl-ethane-1,2,2-trisphosphonic acid (**32**). There is no crystal structure published. There appear to be two distinct types of hydrogen bond present in a 1:1 ratio, represented by the lines at 15.9 and 10.3 ppm. The aromatic protons are assigned the resonances at 7.3 and 6.4 ppm and the aliphatic protons may be found at 3.6 ppm.

6.5.b.2 Correlation Study

Using known hydrogen bond distances from X-ray crystal structure studies, an attempt was made to correlate oxygen-oxygen bond distances with proton chemical shift. The results are presented in Table 6.11 and Figure 6.16. While it is clear from the graph that the general trend of the Berglund and Vaughan paper seems to be followed, there is by no means an exacting quantitative correlation between ^1H shift and $r_{O...O}$ as determined by crystallographic methods. The discrepancies here can be related to a number of factors: 1) Chemical shift referencing in CRAMPS work is complicated by the scaling of the shift by the pulse sequence, by broad linewidths and difficulties in phasing. As a result, shifts can only be reported to ±0.5 ppm. 2) The use of the oxygen-oxygen bond distance assumes that the hydrogen bond is linear which may not be the case. The more accurate correlation of proton-to-acceptor oxygen ($r_{O...H}$) used by Jeffrey and Yeon may not be used here because only two diffraction studies of the compounds in this study give O...H distances to sufficient accuracy (if at all). 3) Some hydrogen bonds are not of fixed length but rather quite mobile (e.g those involving H_2O). 4) There is a general lack of X-ray data which, of course, limits the number of points on the curve.

Regardless of these problems, it is considered that the ^1H CRAMPS spectra give a reasonable indication of the number and relative strength of the hydrogen bonding in these materials. In the light of recent results for carboxylic acids[33], the results here are very encouraging and suggest an area of work which could provide a great deal of useful information.

Table 6.11: Solid-State ^1H Shifts Compared with Oxygen-Oxygen Bond Distances from Crystallographic Data for Phosphonic Acids

Compound	δ_H/ppm of Hydrogen Bonded Acid Protons	$r_{O...O}$/Å	Reference
(15) $P^*-CH_2-P^*$	11.9 10.3	2.570† 2.677	5
(23) $P^*_2-CH-CH-P^*_2$ anhydride Na_5 salt $\cdot 11H_2O$	17.2	2.439	10
(24) $CH_3-C(P^*)_2-OH$ $\cdot 1H_2O$ (HEDP)	14.5 11.0	2.465‡ 2.642†	11
(25) HEDP Na_2 salt $\cdot 4H_2O$	11.9	2.610	14
(38) $C_6H_5-P^*$	11.9	2.581‡	18
Aminophosphonic Acids			
(39) $H_2N-CH_2-P^*$	11.9	2.570	19
(40) $H_2N-CH_2-CH_2-P^*$	12.4	2.546	20
(41) $H_2N-CH_2-CH_2-CH_2-P^*$	12.2	2.522	21
(45) $N(CH_2-P^*)_3$	16.3 12.5	2.458 2.552§	22

Estimated error: $\delta_H \pm 0.5$ ppm.
† = average of three values.
‡ = Average of two values.
§ = Average of four values.

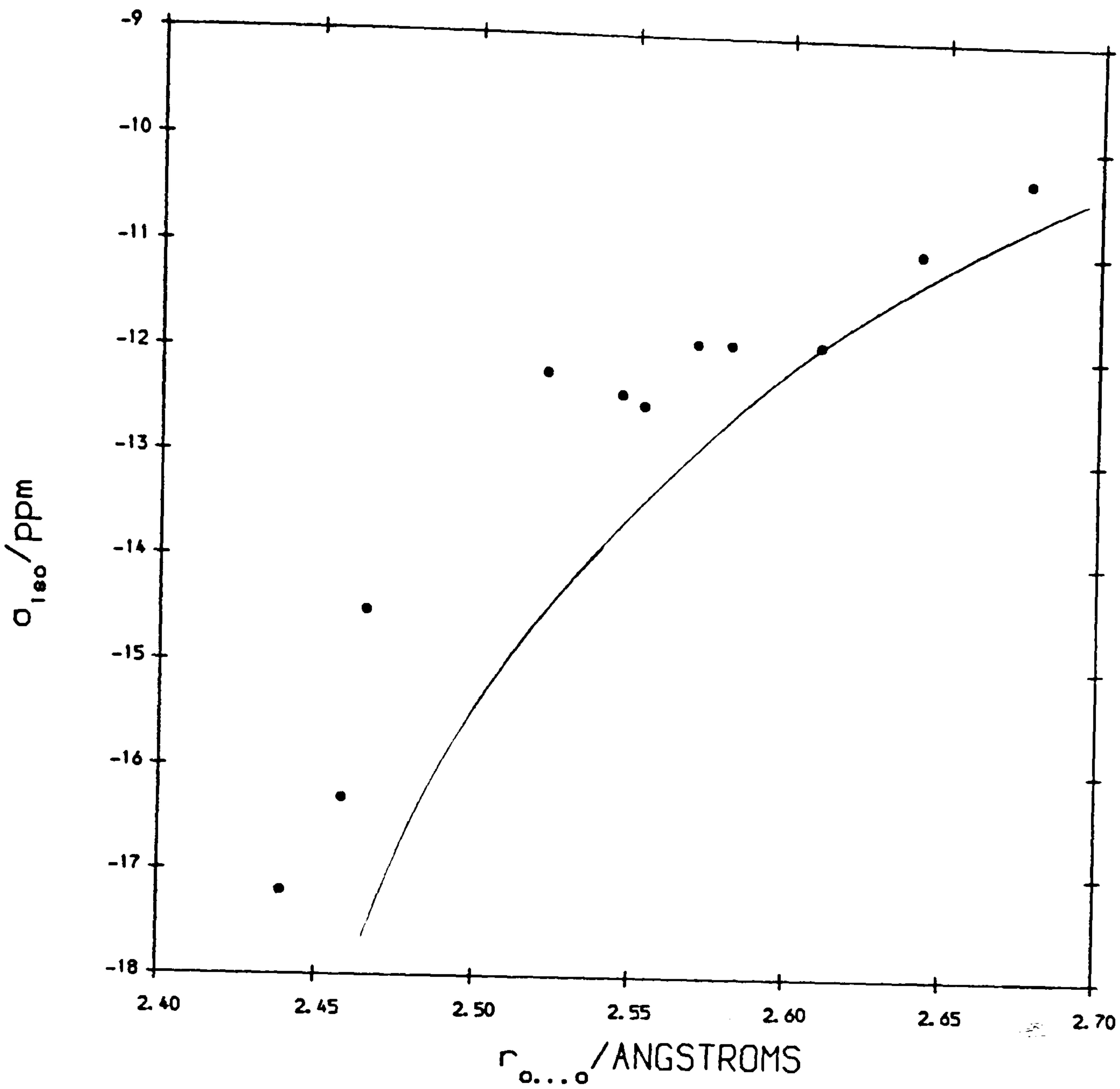

Figure 6.16: Plot of [1]H isotropic shielding versus the oxygen-oxygen bond distance, $r_{O\ldots O}$, for hydrogen bonds in a series of phosphonic acids. The individual points relate CRAMPS data from this study to oxygen-oxygen bond distances from diffraction studies (see Table 6.11). The solid curve represents the results of theoretical calculations made on the $(H_2O)_2$ dimer from reference 30, and has been offset to higher frequency by 6 ppm.

6.5.c Comparison of ^{1}H CRAMPS Results for Phosphonic and Phosphinic Acids

Examination of The ^{1}H CRAMPS results in Tables 6.2 and 6.7 show two general trends when comparing analogous phosphonic and phosphinic acids. First of all, there are obviously fewer types of hydrogen bond in the phosphinic acid as there are less acid protons available for bonding. Secondly, if there are two types of hydrogen bond present in the phosphonic acid, it will be found that the phosphinic acid hydrogen bond will have a shift that is in the middle ground between the two (compare the following pairs of compounds: (**10**) and (**38**), (**17**) and (**39**), (**18**) and (**40**)). It may be postulated that a balance is reached between forming the strongest hydrogen bond possible and the steric considerations of keeping the methyl groups as far apart as possible.

References

1. C.F. Callis, A.F. Kerst and J.W. Lyons, "Coordination Chemistry", S. Kirschner, Ed., Plenum Publishing Co., New York (1969) pp 223-247.

2. M.D. Francis, R.G.G. Russell and H. Fleisch, *Science* **169**, 1264 (1969).

3. U. Fischer and G. Hägele, *Z. Naturforsch.* **40b**, 1152 (1985).

4. D. DeLamatter, J.J. McCullough and C.Calvo, *J. Phys. Chem.* **77**, 1146 (1973).

5. S.W. Peterson, E. Gebert, A.H. Reis,jr., M.E. Druyan, G.W. Mason and D.F.Peppard, *J. Phys. Chem.* **81**, 466 (1977).

6. G. Hägele, private communications.

7. K. Moedritzer and R.I. Irani, *J. Inorg. Nucl. Chem.* **22**, 297 (1961).

8. B.C. Gerstein and C.R. Dybowski, "Transient Techniques in NMR of Solids: An Introduction to Theory and Practice", Academic Press, Inc., New York (1985).

9. R.J. Kirkpatrick, R.A. Kinsey, K.A. Smith, D.M. Henderson and E. Oldfield, *American Mineralogist* **70**, 106 (1985).

10. G. Hägele, unpublished results.

11. V.A. Uchtman and R.A. Gloss, *J. Phys. Chem.* **76**, 1298 (1972).

12. T.M. Duncan and D.C. Douglass, *Chem. Phys.* **87**, 339 (1984).

13. L. Griffiths, A. Root, R.K. Harris, K.J. Packer, A.M. Chippendale and F.R. Tromans, *J. Chem. Soc., Dalton Trans.*, 2247 (1986).

14. B.L. Barnett and L.C. Strickland, *Acta Cryst.* **B35**, 1212 (1979).

15. D.G. Gorenstein, *Prog. NMR Spectrosc.* **16**, 1 (1984).

16. U.Fischer, thesis, University of Düsseldorf (1986).

17. A. Gaedcke, thesis, University of Düsseldorf (1986).

18. T.J.R. Weakley, *Acta Cryst.* **B32**, 2889 (1976).

19. M. Darriet, J. Darriet, A. Cassaigne and E. Neuzil, *Acta Cryst.* **B31**, 469 (1975).

20. Y. Okaya, *Acta Cryst.* **20**, 712 (1966).

21. T. Glowiak and W. Sawka-Dobrowolska, *Acta Cryst.* **B36**, 961 (1980).

22. J.J. Daley and P.J. Weatley, *J. Chem. Soc. (A)*, 212 (1967).

23. M.M. Crutchfield, C.H. Dungan, J.H. Letcher, V. Mark and J.R. Van Wazer, "^{31}P Nuclear Magnetic Resonance", Interscience Publishers, New York (1967).

24. J.R. Van Wazer, C.F. Callis, J.N. S hoolery and R.C. Jones, *J. Amer. Chem. Soc.* **78**, 5715 (1956).

25. G. Klose, L. Trahms and A. Möps, *Chem. Phys Lett.* **122**, 545 (1985).

26. F.F. Kizbullin, B.P. Strumin and E.I. Maslennikov, *Zh. Strukt. Khim.* **27**, 60 (1986).

27. A.R. Grimmer, *Spectrochemica Acta* **34A**, 941 (1978).

28. G.L. Turner, K.A. Smith, R.J. Kirkpatrick and E. Oldfield, *J. Magn. Reson.* **70**, 408 (1986).

29. V.A. Uchtman, *J. Phys. Chem.* **76**, 1304 (1972).

30. B. Berglund and R.W. Vaughan, *J. Chem. Phys.* **73**, 2037 (1980).

31. C.M. Rohlfing, L.C. Allen and R. Ditchfield, *J. Chem. Phys.* **79**, 4958 (1983).

32. G.A. Jeffrey and Y. Yeon, *Acta Cryst.* **B42**, 410 (1986).

33. R.K. Harris and P. Jackson, submitted for publication.

CHAPTER SEVEN - SOLID-STATE NITROGEN-15 NMR

7.1 Introduction

In this chapter the applicability of CP/MAS NMR techniques to the study of ^{15}N at natural abundance in solids will be examined. It will be seen from the literature survey that a rather limited amount of work has been done in this area. This is more a reflection of the difficulties inherent in nitrogen NMR than it is of the importance of the chemical and structural information available. CP/MAS techniques have provided significant information in the study of proteins, DNA, plant and cell metabolism, and adsorption on silica and alumina surfaces (*vide infra*). In such complex cases, ^{15}N enrichment is an absolute necessity. However, the literature shows very few CP/MAS solid-state studies of relatively smaller molecules or pure chemical systems. The comparative simplicity and proportionately larger percentage of nitrogen in such systems suggest that they may provide ^{15}N spectra with a reasonable utilization of spectrometer time and without the necessity of costly enrichment. To such ends, the literature of solid-state nitrogen NMR will be reviewed. Nitrogen-15 NMR at natural abundance at two fields will be reported and the associated difficulties discussed. Examples of the types of systems examined and the representative times to acquire useful spectra will be related. Suggestions for further work have been made.

As may be seen in Table 7.1, there are two stable isotopes of nitrogen available for study by NMR methods. Unfortunately, each of these has its associated difficulties. Nitrogen-14, with a high natural abundance and relative receptivity may be easily detected; however, ^{14}N has a spin $I=1$ and as such a quadrupolar moment. Linewidths for ^{14}N in solids may be as large as several megahertz. Information regarding isotropic chemical shifts and crystallographic inequivalence is generally unavailable due to the dominance of the quadrupolar interaction.

Table 7.1

NMR-Related Properties of Nitrogen Isotopes[1]

	^{14}N	^{15}N
Spin	1	1/2
Relative abundance (%)	99.635	0.365
Gyromagnetic Ratio ($\gamma \times 10^{-7}$ /rad T^{-1} s^{-1})	1.9338	-2.712
Quadrupole moment (10^{28} Q/m^2)	1×10^{-2}	-
Relative receptivity (^{13}C)	5.69	2.19×10^{-2}
NMR frequency⁺ Ξ/MHz	7.228	10.136

⁺The resonance frequency for a field in which the protons of TMS would resonate at exactly 100.00 MHz.

The other isotope of interest, nitrogen-15, is spin I=1/2. Though the fact that it is an I=½ nucleus is encouraging for high-resolution work, there are several drawbacks here also. Nitrogen-15 has a natural abundance of only 0.365% and also a low magnetogyric ratio. Consequently, this nucleus has a very low receptivity. In addition, ^{15}N has a negative magnetogyric ratio resulting in a negative nuclear Overhauser enhancement (NOE). All is not in vain however. The low magnetogyric ratio suggests the possibility of up to a theoretical enhancement factor of 9.8 in the cross-polarization (CP) experiment. Furthermore, in the CP experiment NOE is not observed. These factors, combined with the utilization of modern high-field instrumentation and pulse techniques suggest that solid-state ^{15}N NMR at natural abundance may be reasonably possible for certain systems.

7.1.a Nitrogen Chemical Shifts and Chemical Shift Referencing

One of the most attractive aspects of NMR studies of nitrogen is the large chemical shift range which spans about 1000 ppm[1].

Comparison with carbon, which has a range of ca. 250 ppm, shows high-resolution nitrogen NMR to be well suited for structural studies. Nitrogen is also directly involved in hydrogen bonding and, as will be noted below, has large shifts in such circumstances. A general discussion of nitrogen chemical shifts is beyond the scope of this work. Such information as is available for solids may be found in the references of the literature review below. For solution-state NMR, several compilations of nitrogen shifts are available[2,3,4].

The fact that there are two NMR-active isotopes of nitrogen suggests the possibility of a primary isotope effect causing two different chemical shifts. It has been determined by Becker *et al.* that the difference in chemical shifts between ^{14}N and ^{15}N is zero within experimental error[5]. Chemical shifts for the isotopes of nitrogen may therefore be used interchangeably.

A reference compound for solid nitrogen chemical shifts has not yet been fixed. In the literature reviewed, it was found that ammonium sulphate and ammonium nitrate (ammonium resonance) were used as the predominant shift reference compounds. Ammonium chloride, the nitrate resonance of ammonium nitrate, external liquid ammonia or liquid nitromethane were also used. Ratcliffe and co-workers[6] have examined the relationship between the chemical shift of the ammonium ^{15}N resonance and the choice of counterion for various ^{15}N enriched ammoniun salts in the CP/MAS experiment. This work has shown there to be significant differences in chemical shifts depending upon the anion involved. The range of shifts runs from 16.5 to -24.1 ppm, measured with ammonium chloride as the zero ppm point. Some shifts of interest for the ammonium salts are noted in Table 2.

There appears to be no clear cut choice in the selection of solid reference compounds. The use of the nitrate resonance of ammonium nitrate would be in line with the use of nitromethane and the nitrate ion as shift references in liquids as suggested by Harris and Mann[1] and by Martin, Martin and Gouesnard[2]. However, this has the disadvantage that most shifts would be negative in sign. The use of the ammonium resonance would solve that problem

Table 7.2

Observed ^{15}N Chemical Shifts in Ammonium Salts

(Relative to $^{15}NH_4Cl$)[6]

Salt	Chemical Shift δ_N (±0.1 ppm)
NH_4I	16.5
NH_4Br	2.1
NH_4Cl	0.0
NH_4SCN	-5.1
$(NH_4)_2SO_4$	-14.7
NH_4NO_3	-17.4
$NH_4{}^{15}\underline{NO_3}$	+336.0

but create another in that it falls within the range of the chemical shifts of many amines. Thus, it may interfere with resonances of interest if used as an internal standard. In support of the use of the ammonium resonance, however, Levy and Lichter[4] report all liquid shifts with respect to external liquid ammonia. Although this has obvious practical difficulties, there is the advantage that liquid ammonia is the maximum shielding case, and all shifts could be reported in positive ppm.

As noted in Chapter 3 all shifts in this work will be reported with respect to the nitrate resonance of solid ammonium nitrate at $\delta_N = 0.0$ ppm. Factors to convert between the various solution-state reference compounds may be found in Martin *et al*[2].

7.2 Literature Survey for ^{14}N and ^{15}N NMR of Solids

7.2.a Nitrogen-14

Although the use of nitrogen-14 NMR has been limited by the problems associated with its quadrupole moment, it will be seen that ^{14}N is a nucleus that can provide useful information about bond distances and molecular motion in solids of both single-crystal and powder form. In all cases, however, systems are restricted to those in which the nitrogen-14 is in an environment of sufficient symmetry that quadrupolar broadening effects are limited[7].

Griffin and co-workers[8] used single crystals of ammonium hydrogen oxalate hemihydrate to demonstrate that ^{14}N in single-crystal solids could be observed directly. Essentially they used dipolar decoupling to sharpen the ^{14}N resonance lines to a width of about 300 Hz. Well-resolved spectra were obtained in one minute. From the spectra, two ^{14}N electric field gradient tensors were obtained. These corresponded to two inequivalent NH_4^+ ions in the solid. The analysis indicated that the inequivalence arises from distortion of the N-H bond distances produced by the lattice.

If in the NMR experiment proton decoupling is omitted, N-H dipolar splittings arise. Although associated line broadening results in an order of magnitude loss in resolution, useful information may still be obtained. From a study of the dipolar splittings and associated dipolar tensors, it may be possible to derive N-H bond distances and orientations in both single crystals[9-16] and powders[7, 17-19].

Stark *et al.*[9] have used ^{14}N NMR of single crystal n-acetyl-dl-valine to determine the N-H bond distance in dl-valine. Well-resolved N-H dipolar splittings were observed in less than one minute.

Bodenhausen *et al.*[10] have proposed techniques to separate overlapping resonances caused by proton-nitrogen dipolar coupling in single-crystal ^{14}N spectra. It is likely that in large peptide systems, the lines of the proton coupled ^{14}N spectra could overlap, thus obscuring the determination of the dipolar tensors and the structural information which they provide. A two-dimensional technique was developed, which essentially separates the quadrupolar and dipolar spectra into orthogonal frequency dimensions. Single crystals of the amino acid L-histidine hydrochloride monohydrate (L-His•HCl•H_2O) were used as a model system in this work. (L-His•HCl•H_2O) yields a proton-coupled spectrum where overlap of the resonances prevents determination of the dipolar tensors. Use of the pulse technique described provided a clearly resolved 2-D spectrum from which the pertinent information could be obtained.

Haberkorn and co-workers[11] have used a combination of ^{13}C and ^{14}N NMR to characterize single crystals of glycine. They have reported C-C and C-N bond distances as well as C-C-N bond angles for this simple amino acid. The quadrupole coupling tensors were reported for the two inequivalent nitrogens in the unit cell, and a nuclear quadrupole coupling constant of $e^2qQ/h = 1.182 \pm 0.010$ MHz was determined. The advantages of ^{14}N NMR of single crystals were also discussed.

There is one report of the use of cross-polarization in single-crystal ^{14}N NQR. Grechishkin[12] has used CP with multiple contacts to study single crystals of urea at 77 K.

Tycko *et al.*[13,14,15] and Stewart *et al.*[16] have used both single-crystal and powder ^{14}N NMR to determine the orientation of peptide planes. Using both fundamental and overtone ^{14}N NMR, orientation-dependent parameters such as quadrupolar splitting, chemical shift, dipolar splitting and nutation frequency were measured. The angles between the interaction tensors of the parameters were related to the orientation of a particular chemical species. The orientation of a peptide plane can be determined by two independant angular measurements.

Work on the ^{14}N NMR of powders has been published by a number ofauthors. Wasylishen and Pettitt[17] have determined the T_1 of ^{13}C and ^{14}N in triethylenediamine and have used the information to describe molecular motion in the solid phase of the molecule.

Similar motional information has been elucidated for methylammonium nitrate by Wasylishen[18], who used ^{2}H, ^{14}N and ^{17}O to study its high-temperature plastic phase. Pratum and Klein have used quadrupolar echo[7] and cross-polarization[19] methods to describe the quadrupole coupling parameters, and thus molecular structure and motion, in various tetraalkylammonium compounds. The use of cross polarization, although not quite as straightforward as in the case of spin $I=½$ nuclei, was shown to be quite effective in the observation of ^{14}N powder patterns.

7.2.b Nitrogen-15

7.2.b.1 Systems of Biological Interest

In the paper "Strategy of Nitrogen NMR of Biopolymers"[20], Cross and co-workers have presented a strong case for the attractiveness of nitrogen NMR for biopolymers and, by extrapolation, for nitrogen-containing chemical systems in general. There are relatively few nitrogens in biopolymers compared to ^{1}H or ^{13}C, thus simplifying assignment. The nitrogens are active in hydrogen bonding and show large chemical shift differences under such circumstances. Furthermore, the nitrogens are often located in sites of specific interest, such as the bases of RNA and DNA, the peptide backbone of proteins and active enzyme residues. Finally, the enrichment of ^{15}N in biopolymers does not have the problem of homonuclear coupling as seen with uniform ^{13}C enrichment, since in biopolymers there are no nitrogens directly bonded to other nitrogens.

This paper goes on to report the structure of the DNA in ^{15}N-enriched bacteriophage fd. A ^{15}N NMR spectrum was obtained in 4000 transients (cycle time not given). Resonances for thirteen of the fourteen nitrogen sites of the DNA were observed with many of the chemical shifts for the nucleotides within 2 ppm of their solution values. Resolution of resonances of the single proline residue in this strand indicates that resolution of a specific single atomic site is possible. Furthermore, as the resonances of the nitrogen in the protein coat of the phage have little overlap with the DNA resonances, both sample preparation and spectra are simplified.

Further ^{15}N NMR work on DNA has been carried out by DiVerdi and Opella[21]. Although the location and dynamics of interstrand hydrogen bonding is very important in understanding DNA, little is known about it because of limitations in X-ray diffraction techniques. Two-dimensional, separated local field/MAS spectroscopy was used to determine N-H bond lengths in uniformly ^{15}N-labelled B form DNA. The location and length of several direct and hydrogen-bonded N-H bonds were determined.

The use of two-dimensional nitrogen-15 NMR techniques for ^{15}N-enriched biopolymers has also been reported in several other papers. Munowitz[22] and co-workers have used a two-dimensional, dipolar-shift pulse sequence to determine the orientation and values of the N-H dipolar coupling and chemical shift tensors. The work was applied to structural aspects of the dipeptide glycylglycine hydrochloride monohydrate (Gly•Gly•HCl•H_2O). Cross and Opella[23] have used similar methods to determine the orientation of the single tryptophan residue in bacteriophage fd coat protein. The position and geometry of the tryptophan residue were determined from the 2-D separated local field spectra of the oriented protein sample. Finally, Aue *et al.*[24] have used the ^{15}N resonances of the glycine and Gly•Gly•HCl•H_2O systems in the evaluation of uniform chemical shift scaling pulse sequences for MAS experiments.

Munowitz *et al.*[25,26] have used high-resolution ^{15}N CP/MAS techniques to study the acid-base tautomeric equilibria of solid histidine and imidazole. The "pH" of the solid was shifted by lyophilizing the 95% ^{15}N-enriched amino acid from solutions of varying pH. A similar treatment was used for the model compound, imidazole. As the exchange processes in these molecules are slower in solids than in liquids, separate ^{15}N NMR resonances were found for the various tautomeric and ionic forms of the molecule. Results indicated the preferred tautomeric structure as well as the extent of hydrogen bonding between the alpha-amino nitrogen and the ring nitrogen.

Several groups have used solid-state NMR in structural investigations of polypeptides, enzymes and proteins. Huang and co-workers[27] have used ^{15}N-labelled histidine segments in α-lytic protease to examine the structure of this enzyme and to compare structures in the solid- and solution-states. Information was obtained regarding structure, preferred tautomeric equilibria, and the nature of hydrogen bonding present. Frey *et al.*[28] used a number of nuclei in a study of the structure and dynamics of several ^{15}N-labelled cyclic pentapeptide model compounds. The structures were found to be stabilized by two intramolecular hydrogen bonds. The bond length for these was determined from ^{15}N separated local field/MAS 2-D experiments. Smith and co-workers[29] have used solid-state ^{15}N NMR to examine the structure of the protein environment of the retinal chromophore and the protonation site of tyrosine in bacteriorhodopsin. The ^{15}N-labelled Schiff base of this material was determined to be protonated and weakly hydrogen bound.

Mackenzie *et al.*[30] have shown solid-state ^{15}N NMR to be useful in the determination of enzyme mechanism. Carboxypeptidase-Aα was complexed with the slow (pseudo) substrate glycyl tyrosine which had been labelled at the scissile amide bond. ^{15}N CP/MAS spectra of crystals taken from the reaction mixture were useful in determining the extent of cleavage of the peptide bond as well as the binding between the product and enzyme. The technique provided a very useful correlation between X-ray data, the geometry of the substrate undergoing slow catalysis, and corresponding NMR shifts in the enriched substrate.

Protein backbone dynamics have been studied by Bogusky and co-workers using a combination of solution- and solid-state ^{15}N NMR[31]. A specific bacterial coat protein was examined in its membrane bound state. Solution-state NOE measurements were used to characterize motions in the 10^9 Hz region. Solid-state shielding tensor results allowed the monitoring of motions in the 10^4 Hz range.

Solid-state ^{15}N NMR has also been used by several groups[32-35] to characterize metabolism in bacteria. The specific organism of interest was grown on a medium containing a ^{15}N enriched amino acid. The cells were then lyophylized and ^{15}N CP/MAS spectra were run. Information may be obtained regarding nitrogen fixation, cell wall structure, the mechanism of antibiotics such as penicillin, and the site of incorporation in the cell of a specific amino acid.

The Maillard reaction has been studied by several groups using ^{15}N CP/MAS techniques[36,37]. The influence of reaction time, temperature and reactant composition on the end products has been characterized.

In related work, two groups have used ^{15}N CP/MAS NMR to examine the processes of composting and peat formation. Ripmeester and co-workers[38] have used ^{15}N-labelled glycine in an incubated sample to determine the the fate of this amino acid upon humification. This group has also been involved in a natural abundance ^{15}N NMR study of a proposed composting system for scrap from a fish cannery[39]. The technique was used to monitor the composting process and to characterize products. In both studies, it was possible to characterise the reaction by noting the classes of nitrogen-containing compounds produced (amines, primary and secondary amides, ammonium ions and pyrrole type compounds).

7.2.b.2 Double-Cross-Polarization

Schaefer and his co-workers[40] have proposed a double-cross-polarization (DCP) pulse sequence for ^{15}N NMR. This is based upon the standard cross-polarization experiment[41] but with a second polarization transfer. The procedure consists of consecutive Hartmann-Hahn[42] spin-lock cross-polarization transfers from either ^{1}H to ^{13}C, and then from ^{13}C to ^{15}N; or from ^{1}H to ^{15}N, and then from ^{15}N to ^{13}C[40]. The pulse sequence can provide detailed information about ^{15}N-^{13}C coupling. As such, it may be used to determine the ratio of ^{13}C-^{15}N to ^{12}C-^{15}N pairs in a partially labelled solid, to follow a specifically double labelled ^{13}C-^{15}N bond, or to aid in ^{13}C spectral assignment.

Of the two variations of the double-cross-polarization experiment noted above, the one preferred by Schaefer *et al.* is that of transfer from ^{1}H to ^{15}N followed by a ^{15}N to ^{13}C "drain" and observation of the ^{15}N signal. The effect of the ^{15}N-^{13}C contact is to remove magnetization from those ^{15}N nuclei directly bound to ^{13}C. By alternating the "hold" and "drain" pulse sequences, and alternately adding and subtracting the signal, a spectrum of only those ^{15}N directly bound to a ^{13}C is obtained[43]. (In the hold sequence the ^{13}C transmitter is on but is tuned off-resonance from the Hartmann-Hahn condition; thus, no magnetization is transferred from ^{15}N. This is done to ensure equivalent sample heating.)

The double-cross-polarization technique has been used by this group to follow the amino acid and protein metabolism in various parts of the soybean plant[44-47]. In these studies, the ability to follow a specific double-labelled bond provided new information about the metabolism and fate of specific amino acids. Well-resolved cross-polarization spectra of ^{15}N-enriched samples were obtained in less than one hour[44]. Double-cross-polarization difference spectra required from 12 to 24 hours of data collection[46].

Recently, papers by Schaefer and Stejskal have indicated refinements in the DCP experiment[43,48]. Analysis of cross-polarization rates in model compounds and a better understanding of the experiment have resulted in a method for the quantitative determination of ^{13}C-^{15}N bonds in enriched samples. Analysis of the results show that the fraction of enrichment can be measured to within ten percent. These measurements, however, require a spectrometer with closely controlled MAS spinning speeds and RF fields.

7.2.b.3 Organic and Inorganic Systems

One of the few papers published on the ^{15}N CP/MAS NMR of small inorganic chemical systems is that of Ratcliffe and co-workers[6] on the chemical shifts of solid NH_4^+ salts. (Some of the results of this work have already been presented in Table 7.2 in the chemical shift referencing section.) The shifts of a number of solid ammonium salts were determined and *ab initio* calculations relating geometry and nitrogen shielding were done. The range of chemical shifts was explained by changes in NH_4^+ geometry and anion environment.

The oxides of silicon and aluminium are very important materials as catalysts and have been studied extensively. Of importance to the chemist are such factors as the geometry of the substrate sites, the type of bonding which occurs between substrate and adsorbate, and the molecular dynamics of the absorbed species. ^{15}N NMR is shown to be a significant tool for use in these investigations[49].

Initial work in the use of ^{15}N NMR to study adsorbed species was done by Michel *et al.*[49] and by Bernstein *et al*[50]. In both of these studies only conventional solution-state Fourier-transform NMR techniques were used. To maintain reasonably narrow linewidths, high temperatures or high surface coverage factors were used. (High surface coverage promotes rapid exchange, thus simulating solution conditions.)

Despite these two drawbacks, these initial studies demonstrated that ^{15}N NMR is a powerful tool for the examination of surface phenomena. It was shown[49] that resonance shifts depend very strongly on the nature of adsorption sites and on the type of bonding involved (much more so than the corresponding ^{13}C spectra). In addition, a suitable choice of adsorbate (e.g. ammonia, acetonitrile, pyridine) should enable a selective study of the various active sites in a particular type of adsorbent.

The full range of CP/MAS ^{13}C and ^{15}N solid-state techniques was used by Maciel *et al.*[51] in the study of pyridine adsorbed on silica-alumina. Pyridine was the adsorbate choice because the ^{15}N chemical shift is strongly solvent dependent and should thus be a sensitive probe of surface sites. Thirty percent nitrogen-15 enriched pyridine was used in this study. Data collection times varied greatly due to the amount of pyridine loading on the silica;

well-resolved spectra were obtained using one second repetition times and 8000, 16,000 and 50,000 transients (2, 4.5, and 14 hours respectively).

The results of the work provided a fairly detailed study of the pyridine/silica-alumina system. At low loading levels, the Lewis acid-base complex was shown to be the primary mode of adsorption, while at higher levels (greater than 0.5 monolayer) hydrogen bonding was seen as the significant interaction. At the high loading levels, pyridine was found to be highly mobile. A complex overall motion was postulated with rotation about the C_2 axis being a major component. For HCl-pretreated silica-alumina samples, two discrete forms of protonated pyridine were found. The structure of these was discussed briefly, but the exact form of the complex was not postulated. Finally, it is suggested in the work that ^{15}N-enrichment studies currently underway have shown additional, low-intensity peaks which may correspond to slowly exchanging Brønsted complexes.

A number of adsorption studies similar to those detailed above have also been carried out and similar sorts of information reported. Ripmeester[52] and Majors and Ellis[53] have used ^{15}N-labelled pyridine as the adsorbate in studies of the surface sites of γ-alumina. Pyridine was also the adsorbate of choice in a NMR/CNDO study of silica by Bernstein and Pfeifer[54] and in the study of the surface oxidation of coal by Ripmeester and co-workers[55]. Bosacek *et al.*[56] have applied these techniques to HY zeolite using adsorbed acetonitrile, and Earl *et al.*[57] have examined Y zeolite using ammonia and trimethylamine as the absorbates. In all of these studies, the adsorbate was ^{15}N enriched.

Wasylishen *et al.*[58] have used ^{14}N and ^{15}N NMR to study the motion of the nitrate ions in the solid I and solid II phases of ammonium nitrate. In phase I (405°K) the nitrate ion showed a sharp ^{15}N resonance indicating rapid isotropic motion. In the phase II solid, the lack of a ^{15}N nitrate resonance implied more hindered movement. This was noted to be consistent with suggestions that motions are restricted to in-plane C_3 rotations.

Nitrogen-14 T_1 measurements (inversion recovery) are used to quantify nitrate ion rotation in the solid I phase.

Further phase studies of ammonium nitrate have been carried out by Marina and Bulusu[59]. MAS techniques were used to measure the shielding anisotropy for the phase IV to III transition. Energies of activation for both ions in the room-temperature phase were determined.

The first ^{15}N solid-state NMR study of nitrogen-containing ligands in a metal complex was reported by Mason *et al*[60]. ^{15}N CP/MAS NMR was used to examine the nitrosyl ligands of the complex $[RuCl(NO)_2(PPh_3)_2](BF_4)$. Changes in isotropic chemical shift and in the principal shielding tensor components were used to characterize the nitrosyl ligand geometry. A ^{15}N-enriched sample was used.

Opella and co-workers[61] have examined the P-Au-N bonding in triethylphosphine-gold-(^{15}N)-phthalimide using solid-state nitrogen-15 NMR. Solid- and solution-state spectra were shown to compare favourably and ^{31}P-^{15}N scalar couplings were determined. Gold triphosphines are proposed as a probe of ^{15}N-labelled proteins, as $^3J_{PN}$ coupling may be used to characterize the Au binding sites.

Nitrogen-15 NMR has been used by Limbach to study the proton transfer kinetics of solid ^{15}N-enriched porphines[62] and related compounds[63,64]. CP/MAS techniques were used to compare the behavior of meso-tetra-phenylporphine (TPP) and meso-tetra-p-tolylporphine (TTP) in the temperature range 210° - 302°K. At the lower temperature each compound showed two resonances corresponding to the two tautomeric forms. At higher temperatures the lines for TTP coalesce, indicating that proton transfer becomes rapid on the NMR timescale. At the same temperature, the resonance lines for TPP remain well resolved indicating relatively slow migration. The reason for the differing behaviours is related to the induction of a more symmetric crystal environment of the TTP.

Chuang *et al.*[65] have used solid-state NMR to characterize cured urea-formaldehyde resins. ^{15}N CP/MAS and NQS/MAS methods were used in an attempt to correlate the molecular structure of the resin with its macroscopic properties. The study, however, did not provide straightforward information. This was mainly due to lack of resolution in the amide region of the nitrogen spectrum. It is suggested that a comprehensive and systematic ^{15}N and ^{13}C NMR study with varying urea/formaldehyde ratio and cure time might provide more definitive answers. ^{15}N-enriched materials were used here for all but a few simple model compounds.

A more conclusive ^{15}N and ^{13}C CP/MAS study of a resin system is that of Maciel and Hatfield[66]. Solid-state NMR techniques were used to examine the curing of phenolic resis by ^{15}N enriched hexamethylenetetramine. Various intermediates were determined and the modes of cross linking were characterized. A strong case for multinuclear NMR studies of such systems was made.

Bulusu[67,68,69] has used solid-state ^{15}N NMR to characterize explosive and propellant mixtures. Materials including nitrocellulose, nitroguanidine, HMX and RDX were examined using CP/MAS NMR. Information on structure and the degree of chemical interaction between the components in the mixtures was obtained.

Finally, Schaefer *et al.* have reported several nitrogen-15 studies of solids from reactions intended to model conditions on earth prior to the existence of life. The purpose of these experiments was to create primitive heteropolypeptides from reactions of various combinations of hydrogen cyanide, water, ammonia and methane. One of the studies[70] used unenriched starting material (taking 56 hours to acquire the spectrum!) while the other two[71,72] used ^{15}N enriched HCN. A number of nitrogen functionalities were detected in the reaction mixtures. The results suggest that primitive heteropolypeptides may have been formed without the intervening formation of α-amino acids.

7.3 Experimental Results and Discussion

7.3.a Introduction

As was seen in the review of the literature, nitrogen-15 NMR is a powerful and sensitive tool in many applications. However, most reports found in the literature were either for quite complex systems, such as those of biological interest, or investigations where the overall amount of nitrogen present was quite small, as in the absorption studies. In either case, ^{15}N enrichment was absolutely necessary to the experiment. In general, however, there seemed a lack of investigations into reasonably straightforward nitrogen-containing chemical systems which might possibly be accessible without the need for expensive and possibly difficult enrichment. An investigation into the feasibility of running ^{15}N CP/MAS NMR at natural abundance was undertaken.

An initial overview of the situation revealed three factors which seemed to be in our favour. The first of these is the absence of the nuclear Overhauser effect (NOE) in most solid-state NMR experiments[20]. The NOE, as observed in solution-state NMR, is essentially a change in X nucleus population which is driven by heteronuclear proton decoupling. The maximum value of the NOE is $NOE=1+(\gamma_H/2\gamma_X)$, and the total effect of the NOE on the spin population is proportional to the ratio of the dipolar component of the spin-lattice relaxation rate (T_{1dd}^{-1}) to the total spin-lattice relaxation rate (T_1^{-1}). For nuclei with negative magnetogyric ratios, such as ^{15}N, if this ratio is of the order of $\gamma_H/2\gamma_X$, then the resonance will have an intensity near to zero. A null signal will thus result. While such a situation is certainly possible in the solution-state, in solids the use of cross-polarization will preclude any nuclear Overhauser effects.

The second encouraging factor involved is the sensitivity increase associated with cross-polarization. The general advantages and use of CP are well known[73]. It remains here to emphasize the property of cross polarization which is the enchancement of the rare spin signal by the ratio of the γ's. That is to say, the intensity of the rare-spin signal will be increased by a theoretical maximum factor of γ_H/γ_X over the intensity for a situation where the magnetization is generated under normal equilibrium conditions in the static B_o field. In the case of nitrogen, this ratio is 9.8. Thus, given optimum conditions, one should expect CP to give an order of magnitude increase in relative sensitivity. This is still at least an order of magnitude less than carbon-13; however, the fact is encouraging.

It should also be noted for CP that repetition times will depend on $T_1(H)$ and not $T_1(N)$. This will generally circumvent the problem of long ^{15}N T_1 relaxation times.

The final positive factor involved here is that of high-field instrumentation. It is well known that signal intensity is proportional to $B_o^{3/2}$. The routinely available fields of today's spectrometer systems should make ^{15}N more accessible that previously possible.

7.3.b Initial Experiments at 4.7 Tesla - CXP-200

The initial experiments in this work were carried out on the Bruker CXP-200. A double-bearing CP/MAS probe which tuned to the nitrogen frequency, 20.2868 MHz, was used. The initial test sample was ammonium nitrate 20% enriched in ^{15}N in both nitrogen positions. While such a sample should give cross-polarization sensitivity at least comparable to that of ^{13}C, at least one week was spent looking for a nitrogen signal to no avail. The probe tuning, matching and electronics were checked and found to be in working order. The system was also checked by running ^{35}Cl (19.61 MHz) and ^{10}B (21.50 MHz) spectra of a saturated NaCl solution and solid $NaBH_4$ respectively. Reasonable spectra were found in both cases. The ammonium nitrate sample was also checked for enrichment by mass spectroscopy. Although an accurate determination of the percentage of enrichment was not possible due to interfering factors, it was clear that the sample was indeed enriched to

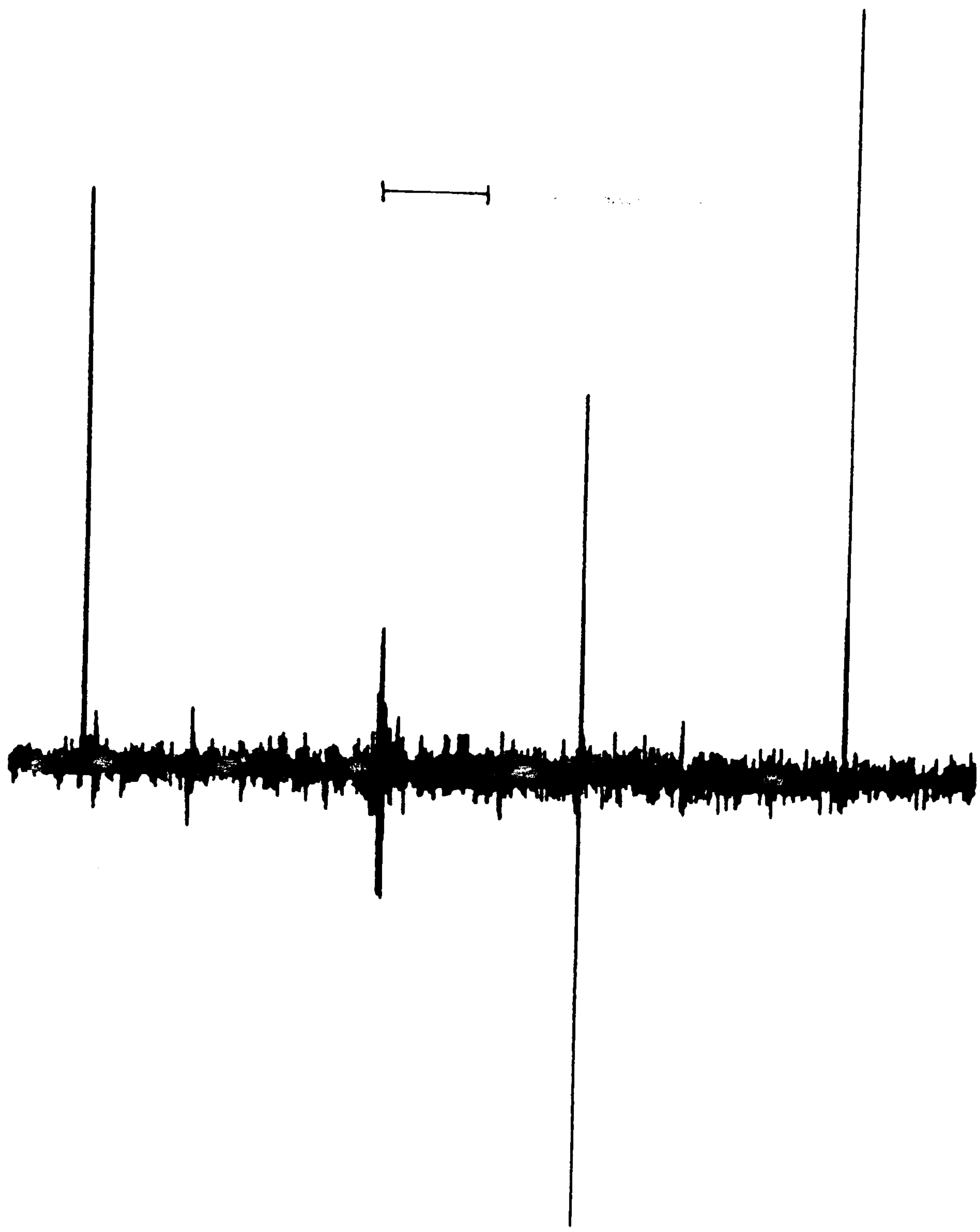

Figure 7.1: CXP-200 ^{15}N CP/MAS spectrum of 20% enriched $^{15}NH_4{}^{15}NO_3$. The outer lines are the nitrate and ammonium resonances at δ_N = 0.0 and -353.1 ppm respectively. The central, unphased spikes are radio-frequency interference. SF=20.2868 MHz. PD=5 μs. CT=10 ms. NT=1. ν_r=2945 Hz. The bar represents 1 kHz.

approximately the specified level. It appeared that the main problem with obtaining a ^{15}N Hartman-Hahn match was that there was a great deal of radio frequency (RF) noise in the 20 MHz region which prevented us from seeing and/or optimising an FID.

For the next attempts at finding a Hartmann-Hahn match, a sample of ammonium nitrate enriched 95% at the ammonium position was obtained. A CP match was found almost immediately and optimised for recycle delay, contact time and spectrometer frequency. Because of the RF interference, it was not possible to optimise the match by observing single acquisition FID's. Rather, this process was carried out by optimizing on the FID of sixteen acquisitions.

This sample was then replaced with the twenty percent enriched material. A single-acquisition CP/MAS spectrum of this may be seen in Figure 7.1. Signal-to-noise in this spectrum is very poor. The most prominent feature of the spectrum is a spike approximately midway between the two resonances. This spike is the RF interference which was causing the initial difficulties in finding the match.

The source of the interference has been traced to a 20 MHz oscillator clock on an interface board in the CXP's Aspect 2000 computer[74]. Because of the source and strength of the interference, it is considered[75] almost impossible to exclude it by using any type of Faraday shielding.

Attempts to exclude the interference from the spectra by the use of narrow spectral and filter widths were not sucessful. The interference is strong throughout the 19-21 MHz region and will fold even into the most narrow of practical filter bandwidths. Furthermore, it is sufficiently phase coherent, such that it is not averaged by multiple acquisitions as is random noise. Figure 7.2, the natural abundance ^{15}N spectrum of glycine, shows the interference to be quite strong despite a relatively narrow spectrum width of 5000 Hz and averaging over 688 acquisitions. It is clear from this spectrum that this RF interference will pose almost insurmountable problems.

To conclude this section, the presence of the strong RF

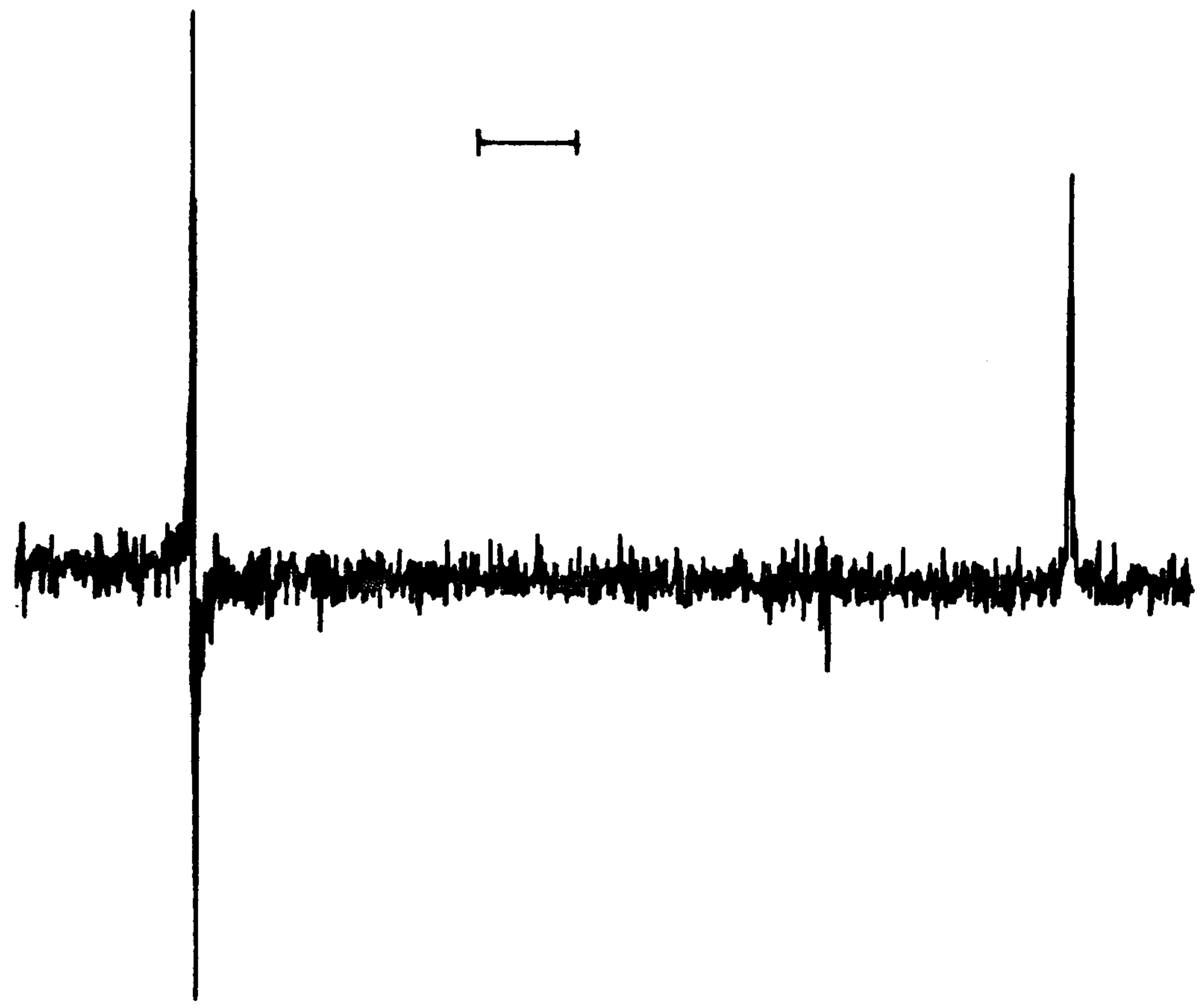

Figure 7.2: CXP-200 ^{15}N CP/MAS spectrum of glycine, H_2N-CH_2-COOH. The unphased spike to the left of the spectrum is RF interference. SF=20.2868 MHz. PD=5 μs. CT=2 ms. NT=688. RD=5 s. ν_r=2.6 kHz. δ_N = −342.5 ppm. The bar represents 250 Hz.

interference combined with the low comparative sensitivity (*vide infra*) of the 200 MHz (4.7 Tesla) field has essentially precluded the use of the CXP-200 from natural abundance ^{15}N studies.

7.3.c 7 Tesla Results - VXR-300

Considering the results above, the next step was to move to the 7.0 Tesla VXR-300 system which had become operational after the above work was completed. There were two advantages to be gained here. Firstly, the nitrogen frequency of this system is 30.405 MHz. This is well away from the 20 MHz oscillator clock frequency, and thus interference from these types of sources should be avoided. Secondly, this spectrometer represents a 50% increase in field strength over the CXP-200. A theoretical sensitivity increase proportional to $B_o^{3/2}$ should, therefore, be expected.

In this case, our somewhat high expectations were confirmed. Setting the Hartmann-Hahn match on the 20% enriched sample of ammonium nitrate proved to be straightforward. The single-acquisition spectrum of this material is shown in Figure 7.3. As can be seen, signal-to-noise is excellent as compared with Figure 7.1 and there is no evidence of any RF interference. Furthermore, the ammonium nitrate proved to be a good set-up sample in that the spinning sidebands of the nitrate resonance were found to be very sensitive to magic-angle mis-set. Very small deviations in the angle caused this resonance and its sidebands to broaden appreciably. The method was clearly more sensitive than the standard KBr technique generally used to set the angle.

Further evidence of the sensitivity advantage of working at 7 Tesla may be found by examining Figure 7.4. Displayed are natural abundance spectra of glycine obtained on the CXP-200 and VXR-300 under similar conditions. (Glycine is 18.7 wt% nitrogen.) The striking difference here is the time required to acquire spectra of similar signal-to-noise. The CXP spectrum took 57 minutes while the VXR spectrum took only eight. All of this difference, however, cannot be attributed solely to the difference in fields. Other

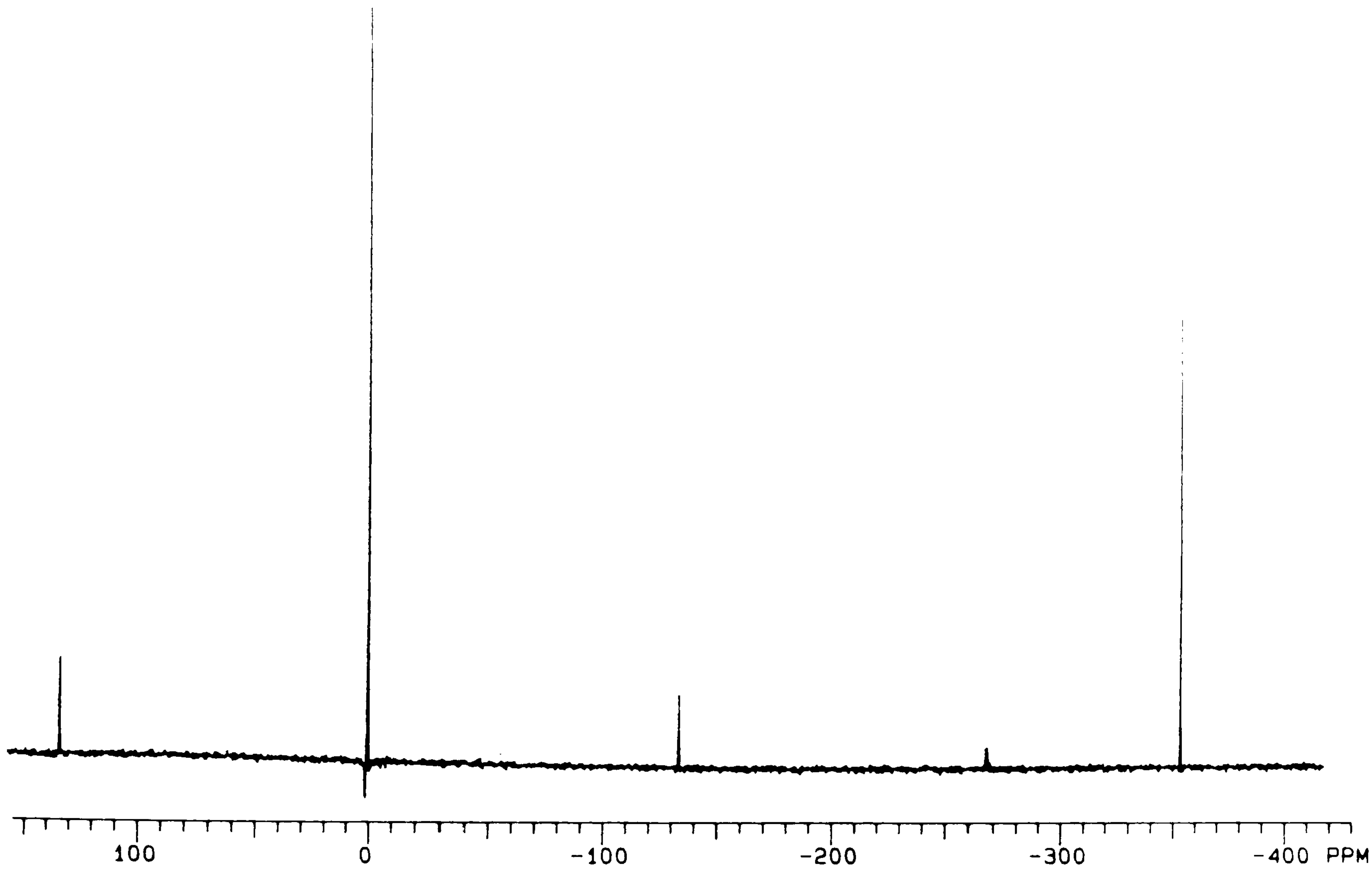

Figure 7.3: VXR-300 ^{15}N CP/MAS spectrum of 20% enriched $^{15}NH_4{}^{15}NO_3$.
SF=30.405 MHz. RD=5 s; PD=11 μs; CT=10 ms; ν_r=4067 kHz; NT=1.
NO_3^-: δ_N = 0.0 ppm. NH_4^+: δ_N = -353.4 ppm

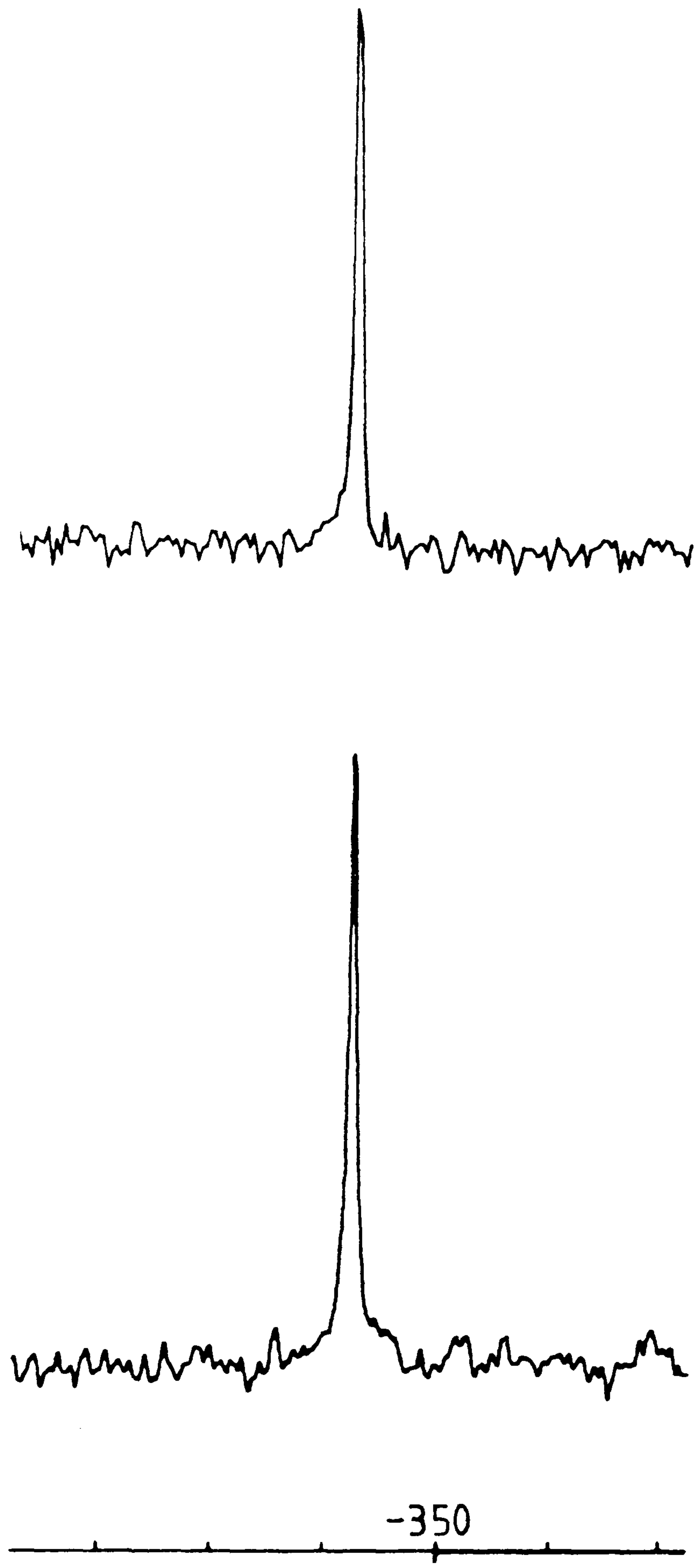

Figure 7.4: Natural abundance ^{15}N CP/MAS spectra of glycine.
Top: VXR-300; SF=30.405 MHz; RD=5 s; CT=2 ms; ν_r=4.0 kHz; NT=100.
Bottom: CXP-200; SF=20.2868 MHz; RD=5 s; CT=2 ms; ν_r=2.6 kHz; NT=688. Scale equals 10 ppm per division.

factors probably include variations in rotor volume, filling factor, Hartmann-Hahn match and, of course, reduction/elimination of the strong RF interference. Regardless, the advantage of the higher field instrument is clear.

Let us now examine the spectra of Figure 7.5. These are natural-abundance ^{15}N spectra of two aminophosphonic acids. The compounds represent systems which are both lower in overall nitrogen content (5-6%) than glycine and which also are of interest to other work in this thesis. (It should be noted that a reasonably good idea of the proton and CP parameters for these compounds was determined while running ^{13}C and ^{31}P spectra before the ^{15}N work was started. Such information should be obtained wherever possible, so that one can work with the appropriate contact times and recycle delays.) The spectrum of dimethylamino-methanediphosphonic acid (Figure 7.5.a) required just under 2 hours to acquire, while that of the 3-amino-1-hydroxy-propane-1,1-diphosphonic acid (Figure 7.5.b) required only 30 minutes. Both spectra show good signal-to-noise. Given that the percentage of nitrogen is essentially equivalent in the two compounds, the difference in the time needed to acquire spectra of similar S/N may most probably be attributed to proton relaxation characteristics and efficiency of cross-polarization. It is clear from these spectra and the glycine spectrum that, given reasonable proton relaxation characteristics (i.e. the sample is not a highly rigid system with very long proton T_1's), ^{15}N spectra at natural abundance of comparatively small molecules may be obtained in relatively short amounts of time.

We next wanted to examine a fairly complex molecule which possibly might have crystallographic splittings and which would be representative of the largest molecular weight chemical system that would seem reasonable for a natural-abundance study. The cephalosporin derivative cefuroxime E47 ester, which exists in several crystallographic forms, was chosen. Two different crystalline samples were obtained, samples 8AII and 9BII. They were described to us only as two pure diastereomer forms (A and B) of the material. The structure of cefuroxime E47 ester is shown in

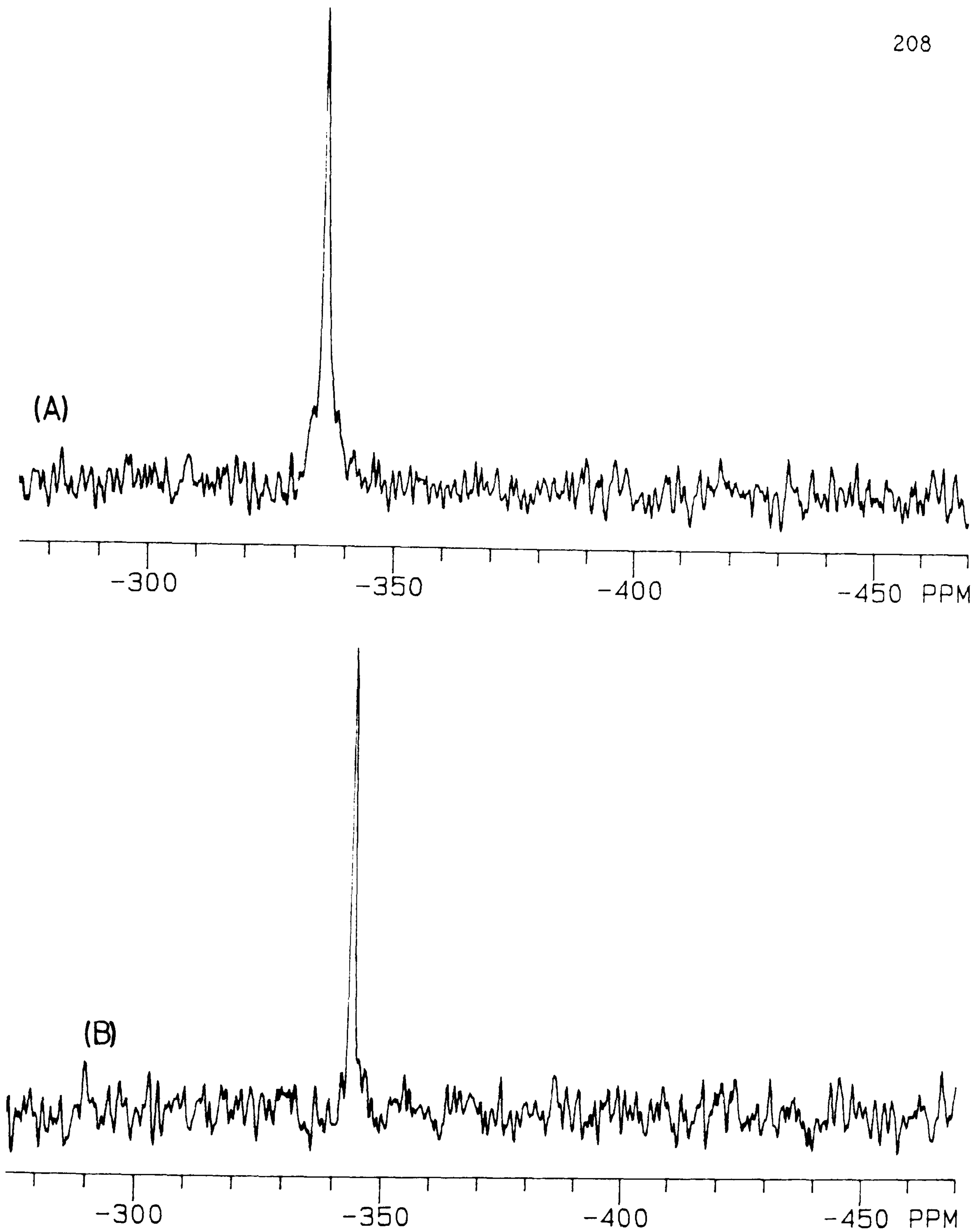

Figure 7.5: ^{15}N CP/MAS spectra. (A) N,N'-dimethylaminomethanebisphosphonic acid (**42**). SF=30.405 MHz; RD=15 s; PD=11 μs; CT=1 ms; v_r=3.5 kHz; NT=464. δ_N = -355.7 ppm. (B) 3-amino-1,1-propanebisphosphonic acid (**44**). SF=30.405 MHz; RD=10 s; PD=11 μs; CT=1 ms; v_r=3.5 kHz; NT=180. δ_N = -343.6 ppm.

Figure 7.6. Note that there are two carbon chiral centres.

Cefuroxime E47 ester was chosen for a number of reasons: A) The compound contains four chemically-distinct nitrogen environments. B) The sample has a reasonably high molecular weight of 510. C) Considering that each nitrogen will have a distinct resonance, the weight percent of each is 2.8%. D) Previous ^{13}C CP/MAS work[76] on the 9BII diastereomer had shown the possibility of crystallographic inequivalences but had been inconclusive.

Figure 7.6 shows the CP/MAS and NQS/MAS spectra of the 8AII diastereomer of cefuroxime E47 ester. The CP experiment ran overnight (15 hours); the NQS spectrum was obtained in five hours. Both spectra have reasonable S/N. In the CP/MAS experiment, the four different nitrogen environments are well resolved. Assignment was made by using the NQS data and by comparison with published solution-state results for the related compound cephalosporin[77,78]. The chemical shift values are noted on the spectrum and are assigned from left to right as follows: oxime, ring tertiary amine, amide, terminal NH_2. It is clear from the spectrum that a single crystalline environment is present.

It is interesting to note in the NQS spectrum (40 μs delay)of 8AII that the amide nitrogen has remained. A similar effect was seen in the NQS spectrum of 9BII where the window width was increased to 70 μs. This perhaps implies that there is some delocalization of the proton attached to this nitrogen, that the N-H bond distance is unusually long, or that there is rapid motion in the system.

Figure 7.7 is the ^{15}N CP/MAS spectrum of the 9BII sample. This was again an overnight run. The spectrum may be assigned in the same manner as sample 8AII. Chemical shift differences between the resonances of the two samples vary between one and four ppm and can be attributed to crystallographic effects. The most important feature of this spectrum is that there appear to be two different crystallographic forms present. The splittings are most distinct in the resonances of the oxime and amide nitrogens. This result corroborates and confirms those of the previous carbon-13 work[76].

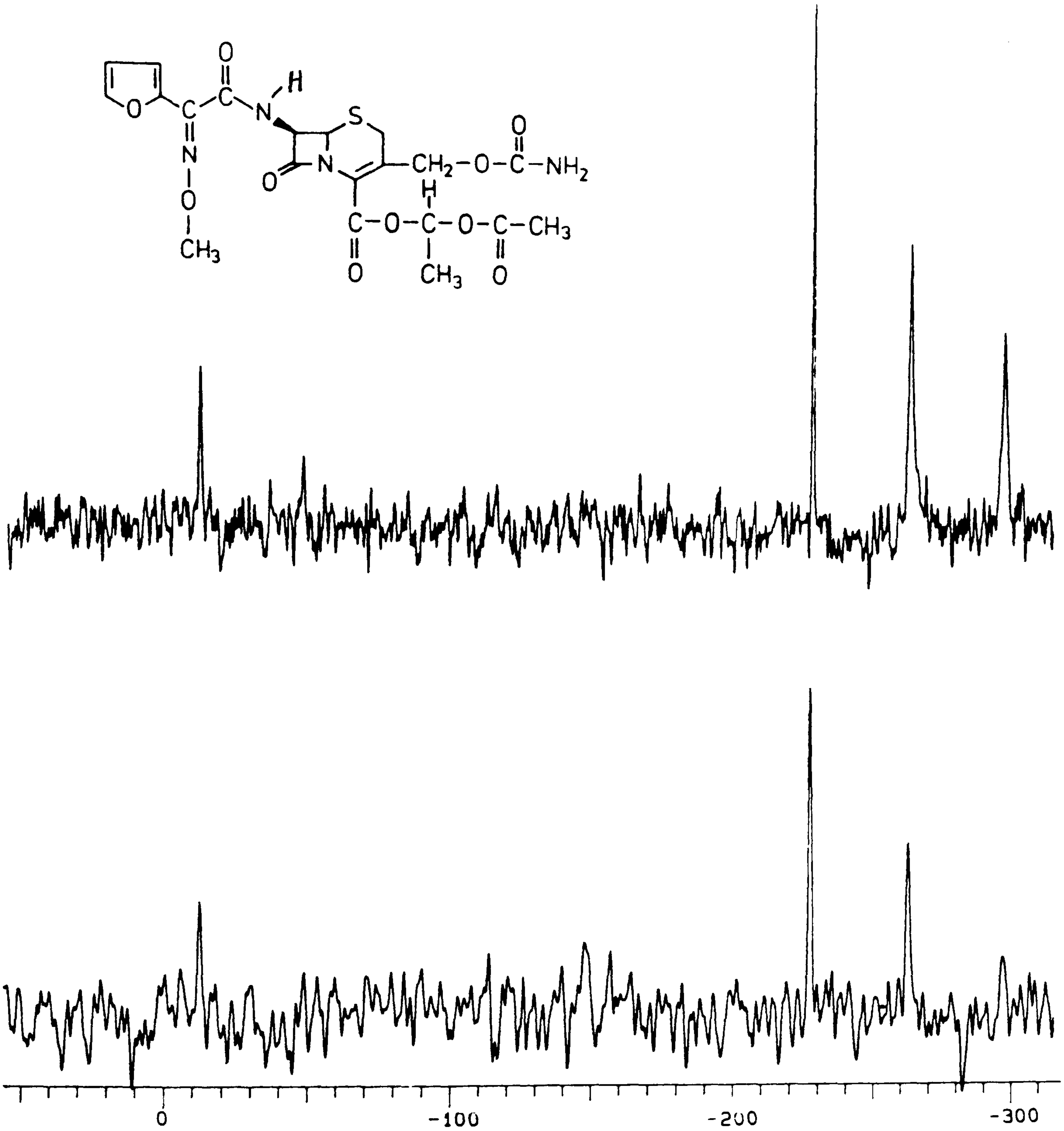

Figure 7.6: ^{15}N spectra of Cefuroxime E47 Ester 8AII.
SF=30.405 MHz. Top: CP/MAS; RD=15 s; PD=11 μs; CT=3 ms; NT=3600;
ν_r=4.2 kHz; δ_N = -12.8, -227.7, -263.0 and -296.7 ppm.
Bottom: NQS/MAS; RD=15 s; PD=11 μs; CT=3 ms; DA=40 μs; NT=1280;
ν_r=4.2 kHz; δ_N = -12.8, -227.7 and -263.0 ppm.

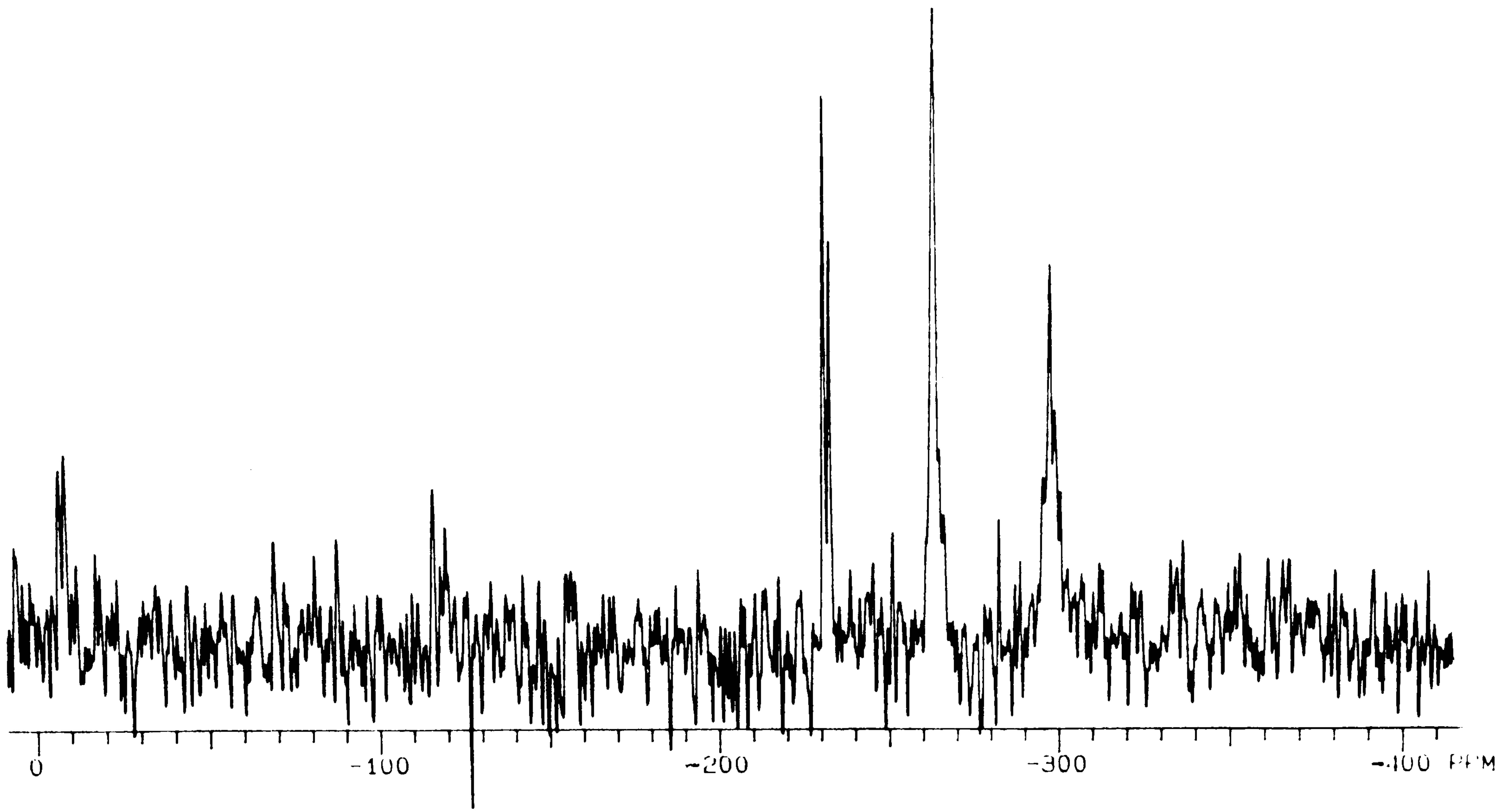

Figure 7.6: ^{15}N CP/MAS spectrum of Cefuroxime E47 Ester 9BII. SF=30.405 MHz. RD=15 s; PD=11 μs; CT=3 ms; NT=3600; ν_r=4.5 kHz; δ_N = -7.3, -9.0, -230.9, -232.8, -263.3 and-297.7 ppm.

7.3.d Comments and Recommendations

There are two matters concerning the current operations on the VXR-300 spectrometer system which are important to the results of this chapter. The first of these was known when the results were obtained, but the second has only recently come to light. Firstly, for technical reasons, it has not been possible to implement a cross-polarization pulse sequence which incorporates flip-back (see Chapter 3) on the VXR. For situations where both T_1 and $T_{1\rho}$ are long, the use of flip-back would make the CP process more efficient by reducing the necessary recycle delay. Secondly, it has recently been discovered that there may be some phase instability in the VXR proton channel. Such phase instability means that the protons do not remain properly spin-locked. If that is the case, the cross-polarization efficiency (and hence the enhancement factor) will be reduced. The most efficient utilization of spectrometer time for nitrogen, or indeed any nucleus, will require that these two situations be corrected.

In conclusion, the literature review has shown solid-state nitrogen-15 NMR to be a powerful technique in a great variety of applications. The large range of nitrogen chemical shifts and the sensitivity of nitrogen shifts to chemical environment (e.g. hydrogen bonding) make it a very powerful probe of structure. Its use, however, has been limited by its low natural abundance and subsequent low sensitivity. In the work presented here, solid-state natural abundance nitrogen-15 NMR has been shown to be viable for reasonably-sized molecules in chemical systems. It is clear that a large range of inorganic and organic chemical systems as well as such compounds as pharmaceuticals could benefit from solid-state ^{15}N NMR study. Given current CP/MAS techniques and a spectrometer of reasonably high field (i.e. probably at least 7 T), such studies should be possible without the use of excessive spectrometer time or expensive ^{15}N isotopic enrichment.

References

1. R.K. Harris and B.E. Mann, "NMR and the Periodic Table", Academic Press, London (1978) P. 96.

2. G.J. Martin, M.L. Martin and J.P. Gouesnard, "^{15}N-NMR Spectroscopy", Springer-Verlag, Berlin (1981).

3. M. Witanowski and G.A. Webb, "Nitrogen NMR", Plenum Publishing, London (1973).

4. G.C. Levy and R.L. Lichter, "Nitrogen-15 Nuclear Magnetic Resonance Spectroscopy", John Wiley & Sons, New York (1979).

5. E.D. Becker, R.B. Bradley and T. Axenrod, *J. Magn. Reson.* **4**, 136 (1971).

6. C.I. Ratcliffe, J.A. Ripmeester and J.S. Tse, *Chem. Phys Lett.* **99**, 177 (1983).

7. T.K. Pratum and M.P. Klein, *J. Magn. Reson.* **53**, 473 (1983).

8. E.K. Wolff, R.G. Griffin and C. Watson, *J. Chem. Phys.* **66**, 5433 (1977).

9. R.E. Stark, R.A. Haberkorn and R.G. Griffin, *J. Chem. Phys.* **68**, 1996 (1978).

10. G. Bodenhausen, R.E. Stark, D.J. Reuben and R.G. Griffin, *Chem. Phys Lett.* **67**, 424 (1979).

11. R.A. Haberkorn, R.E. Stark H. van Willigen and R.G. Griffin, *J. Amer. Chem. Soc.* **103**, 2534 (1981).

12. V.S Grechishkin, *Fiz. Tverd. Tela. (Leningrad)* **27**, 3425 (1985).

13. R. Tycko and S.J. Opella, *J. Amer. Chem. Soc.* **108**, 3531 (1986).

14. R. Tycko, P.L. Stewart and S.J. Opella, *J. Amer. Chem. Soc.* **108**, 5419 (1986).

15. R. Tycko and S.J. Opella, *J. Chem. Phys.* **86**, 1761 (1987).

16. P.L. Stewart, K.G. Valentine and S.J. Opella, *J. Magn. Reson.* **71**, 45 (1987).

17. R.E. Wasylishen, B.A. Pettitt and R.Y. Dong, *J. Chem. Soc., Faraday Trans. II* **76** 571 (1980).

18. R.E. Wasylishen, *Canad. J. Chem.* **64**, 773 (1986).

19. T.K. Pratum and M.P. Klein, *J. Magn. Reson.* **55**, 421 (1983).

20. T.A. Cross, J.A. DiVerdi and S.J. Opella, *J. Amer. Chem. Soc.* **104**, 1759 (1982).

21. J.A. DiVerdi and S.J. Opella, *J. Amer. Chem. Soc.* **104**, 1761 (1982).

22. M. Munowitz, W.P. Aue and R.G. Griffin, *J. Chem. Phys.* **77**, 1686 (1982).

23. T.A. Cross and S.J. Opella, *J. Amer. Chem. Soc.* **105**, 306 (1983).

24. W.P. Aue, D.J. Reuben and R.G. Griffin, *J. Chem. Phys.* **80**, 1729 (1984).

25. M. Munowitz, W.W. Bachovchin, J. Herzfeld, C.M. Dobson and R.G. Griffin, *J. Amer. Chem. Soc.* **104**, 1192 (1982).

26. M. Munowitz, T.H. Huang, C.M. Dobson and R.G. Griffin, *J. Magn. Reson.* **57**, 56 (1984).

27. T.-H. Huang, W.W. Bachovchin, R.G. Griffin and C.M. Dobson, Biochemistry **23**, 5933 (1984).

28. M.H. Frey, S.J. Opella, A.L. Rockwell and L.M. Gierasch, *J. Amer. Chem. Soc.* **107**, 1946 (1985).

29. S.O. Smith, G.S. Harbinson, D.P. Raleigh, J.E. Roberts, J.A. Pardown, S.K. Dasgupta, R.A. Mathies, J. Lugtenberg, J. Herzfeld and R.G. Griffin, *Proc. 2nd Int. Symp. Synthesis and Applications of Isotopically Labelled Compounds*, 239 (1985).

30. N.E. MacKenzie, P.E. Fagerness and A.I. Scott, *J. Chem. Soc., Chem. Commun.*, 635 (1985).

31. M.J. Bogusky, R.A. Schiksnis, G.C. Leo, and S.J. Opella, *J. Magn. Reson.* **72**, 186 (1987).

32. G.E. Wilson , G.S. Jacob, and J. Schaefer, *Biochem. Biophys. Res. Comm.* **126**, 1006 (1985).

33. J. Schaefer, J.R. Garbow, G.S. Jacob, T.M. Forrest and G.E. Wilson, *Biochem. Biophys. Res. Comm.* **137**, 736 (1986).

34. B.-S. Choi, J.E. Roberts, J.N.S. Evans and M.F. Roberts *Biochemistry* **25**, 2243 (1986).

35. G.S. Jacob, J. Schaefer, J.R. Garbow and E.O. Stejskal, *J. Biol. Chem.* **262**, 254 (1987).

36. F. Hayse, S.B. Kim and H. Kato, *Agric. Biol. Chem.* **50**, 1951 (1986).

37. L.M. Benzing-Purdie and C.I. Ratcliffe, *Dev. Food Sci.* **13**, 193 (1986).

38. L.M. Benzing-Purdie, M.V. Cheshire, B.L. Williams, G.P. Sparling, C.I. Ratcliffe and J.A. Ripmeester, *J. Agric. Food Chem.* **34**, 170 (1986).

39. C.M. Preston, J. A. Ripmeester, S.P. Mathur and M. Levesque, *Canad. J. Spect.* **31**, 63 (1986).

40. J. Schaefer, R.A. McKay and E.O. Stejskal, *J. Magn. Reson.* **34**, 443 (1979).

41. A. Pines M.G. Gibby and J.S. Waugh, *J. Chem. Phys.* **59**, 569 (1973).

42. S.R. Hartmann and E.L. Hahn, *Phys. Rev.* **128**, 2042 (1962).

43. E.O. Stejskal, J. Schaefer and R.A. McKay, *J. Magn. Reson.* **57**, 471 (1984).

44. J. Schaefer, E.O. Stejskal and R.A. McKay, *Biochem. Biophys. Res. Comm.* **88**, 274 (1979).

45. J. Schaefer, E.O. Stejskal, M.D. Sefcik and R.A. McKay, *Phil. Trans. Royal Soc. London* **A299**, 593 (1981).

46. J. Schaefer, T.A. Skokut, E.O. Stejskal, R.A. McKay and J.E. Varner, *J. Biol. Chem.* **256**, 11574 (1981).

47. J. Schaefer, T.A. Skokut, E.O. Stejskal, R.A. McKay and J.E. Varner, *Proc. Nat. Acad. Sci. USA* **78**, 5978 (1981).

48. J. Schaefer, E.O. Stejskal, J.R. Garbow and R.A. McKay, *J. Magn. Reson.* **59**, 150 (1984).

49. D. Michel, A. Germanus and H. Pfeifer, *J. Chem. Soc., Faraday Trans. I* **78**, 237 (1982).

50. T. Bernstein, L. Kitaev, D. Michel and H. Pfeifer, *J. Chem. Soc., Faraday Trans. I* **78**, 761 (1982).

51. G.E. Maciel, J.F. Haw, I.S. Chuang, B.L. Hawkins, T.A. Early, D.R. McKay and L. Petrakis *J. Amer. Chem. Soc.* **105**, 5529 (1983).

52. J.A. Ripmeester, *J. Amer. Chem. Soc.* **105**, 2925 (1983).

53. P. Majors and P.D. Ellis, *J. Amer. Chem. Soc.* **109**, 1648 (1987).

54. T. Bernstein and H. Pfeifer, *Z. Phys. Chem (Leipzig)* **266**, 94 (1985).

55. J.A. Ripmeester, R.E. Hawkins, J.A. McPhee and B.N. Nandi, *Fuel* **65**, 740 (1986).

56. V. Bosacek, D. Freude, W. Gruender, W. Meiler and H. Pfeifer, *Z. Phys. Chem (Leipzig)* **265**, 241 (1984).

57. W.L. Earl, P.O. Fritz, A.A.V. Gibson and J.H. Lunsford, *J. Phys. Chem.* **91**, 2091 (1987).

58. R.E. Waslyishen, *Spectrochemica Acta* **40A**, 115 (1984).

59. R.A. Marino and S. Bulusu, *J. Energ. Mater.* **3**, 57 (1985).

60. J. Mason, D.M.P. Mingos, J. Schaefer, D. Sherman and E.O. Stejskal, *J. Chem. Soc., Chem. Commun.*, **444** (1985).

61. S.J. Berners-Price, M. Morden, S.J. Opella and P.J. Sadler, *Magn. Reson. Chem.* **24**, 734 (1986).

62. H.H. Limbach, J. Henning, R.D. Kendrick and C.S. Yannoni, *J. Amer. Chem. Soc.* **106**, 4059 (1984).

63. H.H. Limbach, B. Wehrle, H. Zimmerman and R.D. Zimmerman, *Angew. Chem.* **99**, 241 (1987).

64. H.H. Limbach, B. Wehrle, H. Zimmerman, R.D. Zimmerman and C.S. Yannoni, *J. Amer. Chem. Soc.* **109**, 929 (1987).

65. I.S. Chuang, B.L. Hawkins, G.E. Maciel and G.E. Meyers, *Macromolecules* **18**, 1482 (1985).

66. G.R. Hatfield and G.E. Maciel, *Macromolecules* **20**, 608 (1987).

67. S. Bulusu, *Proc. Sagamore Army Mater. Res. Conf., 1984*, 479 (1986).

68. S. Bulusu, *Proc. Sagamore Army Mater. Res. Conf., 1984*, 487 (1986).

69. S. Bulusu, R.L. Dudley and J.R. Autera, *Magn. Reson. Chem.* **25**, 234 (1987).

70. J. Schaefer, E.O. Stejskal, G. Jacob and R.A. McKay, *Applied Spectroscopy* **36**, 179 (1982).

71. C.N. Matthews, R. Lucicky, J. Schaefer, E.O. Stejskal and R.A. McKay, *Origins Life* **14**, 243 (1984).

72. J.R. Garbow, J. Schaefer, R. Ludicky and C.N. Matthews, *Macromolecules* **20**, 305 (1987).

73. C.A. Fyfe, "Solid State NMR for Chemists", C.F.C. Press, Guelph (1983).

74. Bruker GmbH, "Aspect 2000 Computer Diagrams: Disk Interface Board, Print Number: 76502, Drawing Number: Z3-152963d.

75. B.J. Say, Private communication.

76. A. Kenwright, Unpublished results.

77. G.C. Levy and R.L. Lichter, Ref.4, page 64.

78. G.J. Martin, M.L. Martin and J.P. Gouesnard, Ref.2, p. 144.

APPENDIX ONE: EXPANSION OF EQUATION 4.19

Equation 4.19 requires further expansion before it may be numerically evaluated:

$$g(t) = \sum_{\alpha}\sum_{\beta}\sum_{\gamma} \exp[\,i\omega_0\delta\int_0^t \xi(\alpha,\beta,\gamma,t')dt'\,]. \qquad \text{A-1}$$

$\xi(t)$ has the form noted below:

$$\xi(t) = C_1\cos(\omega_r t) + S_1\sin(\omega_r t) + C_2\cos(2\omega_r t) + S_2\sin(2\omega_r t) \qquad \text{A-2}$$

where:

$$C_1 = \tfrac{1}{2}\sin2\theta\sin\beta[\cos\beta(\eta\cos2\gamma - 3)\cos\alpha - \eta\sin2\gamma\sin\alpha]$$

$$S_1 = \tfrac{1}{2}\sin2\theta\sin\beta[\cos\beta(3 - \eta\cos2\gamma)\sin\alpha - \eta\sin2\gamma\cos\alpha]$$

$$C_2 = \tfrac{1}{2}\sin^2\theta\{[3/2\sin^2\beta + (\eta/2)\cos2\gamma(1 + \cos^2\beta)]\cos2\alpha - \eta\cos\beta\sin2\gamma\sin2\alpha\}$$

$$S_2 = \tfrac{1}{2}\sin^2\theta\{-[3/2\sin^2\beta + (\eta/2)\cos2\gamma(1 + \cos^2\beta)]\sin2\alpha - \eta\cos\beta\sin2\gamma\cos2\alpha\}.$$

α, β and γ are the Euler angles, ω_0 is the larmour frequency, δ is the anisotropy, η is the asymmetry, θ is the magic angle and ω_r is the angular spinning speed.

The evaluation requires the expansion of the integral in the first expression. From equation A-2 it is clear that this may be done term-by-term. Noting that the terms C_1, C_2, S_1 and S_2 are invariant with respect to t and evaluating each integral over 0 to t, the resulting expressions for the integral of the terms of $\xi(t)$ are:

$$\int C_1\cos(\omega_r t)dt = C_1[\sin(\omega_r t)]/\omega_r$$

$$\int S_1\sin(\omega_r t)dt = -S_1[\cos(\omega_r t)]/\omega_r$$

$$\int C_2\cos(2\omega_r t) = C_2[\sin(2\omega_r t)]/2\omega_r$$

$$\int S_2\sin(2\omega_r t) = -S_2[\cos(2\omega_r t) - 1]/2\omega_r$$

Collecting the terms:

$$\int_0^t \xi(\alpha,\beta,\gamma,t')dt' = 1/\omega_r[S_1 + \tfrac{1}{2}S_2 + C_1\sin(\omega_r t) - S_1\cos(\omega_r t)$$
$$+ \tfrac{1}{2}(C_2\sin(2\omega_r t) - S_2\cos(2\omega_r t))].$$

As noted in Chapter 4, this integral must be numerically evaluated over all permutations of α, β and γ. For each (α,β,γ), the integral over t becomes a sum over the limits of the integral which are 0 to $2\pi/\omega_r$. The mesh for this sum is $N(\omega_r/2\pi)$ as explained in Chapter 4. (Each point in the mesh is equivalent to a point in the FID.) The complete free induction decay for the spectrum is thus:

$$g(t) = \sum_\alpha \sum_\beta \sum_\gamma \exp\{i[\omega_0\delta \sum_{t=0}^{t=(2\pi/\omega_r)} \xi(\alpha,\beta,\gamma,t)]\}. \qquad \text{A-3}$$

Representing the term in square brackets as Δ, and remembering that

$$\exp[i\Omega] = \cos\Omega + i\sin\Omega,$$

for each of the N points of the sum on t in equation A-3 the complete FID is accumulated into variable arrays for the real and imaginary components represented by R(N) and I(N) respectively:

$$\text{FID} = \sum_\alpha \sum_\beta \sum_\gamma \{R(N) + \cos[\Delta(\alpha,\beta,\gamma,t)],\quad I(N) + \sin[\Delta(\alpha,\beta,\gamma,t)]\}.$$

The result of this is two arrays of dimension N, one array containing the real components of the FID and one containing the imaginary part of the FID. The Fourier transform routine (Chapter 4, reference 22) will manipulate these data to give the frequency domain spectrum.

APPENDIX TWO - SPINNING SIDEBAND SIMULATION PROGRAM

```
C     Program SBSIM.2 - Simulates a spinning sideband pattern
C     Lawrence H. Merwin, Dept. of Chemistry, University of Durham
C     Version 2, 2 July 1987
C     Ref: M.Maricq and J. Waugh, J. Chem. Phys. 70, 3300 (1979)
C
      PROGRAM SBSIM
C
      IMPLICIT REAL*8 (A-H,O-Z)
      DIMENSION SPC(-25:25)
      COMMON /EXPI/ NSB,IH,IL
      COMMON /EXPR/ WR,VR,SF
      COMMON /PAR/ DELP,EETA,SISO
      COMMON /ERR/ IFAIL2
      IFAIL2=0
      CALL INSET
      CALL OUTPUT
      STOP
      END
C
C     ************************************************************************
C
      SUBROUTINE INSET
C
C
C     Input experimental data and set up arrays and tables
C
      IMPLICIT REAL*8 (A-H,O-Z)
      DIMENSION ST(0:90),CT(0:90)
      CHARACTER*80 TITL
      COMMON /EXPI/ NSB,IH,IL
      COMMON /EXPR/ WR,VR,SF
      COMMON /CHAR/ TITL
      COMMON /TABLE/ ST,CT
      COMMON /PAR/ DELP,EETA,SISO
      DATA NOR,TWOPI,PI /30,6.283185307,3.141592653/
C
C     Data Input Section ------------------------------------------
C     Read in: title, spinning speed (Hz), number of sidebands, delta (ppm)
C     eta, and isotropic sigma (ppm)
C
      READ(5,100) TITL
  100 FORMAT(A80)
      READ(5,*) VR,SF
      READ(5,*) NSB
      READ(5,*) DELP,EETA,SISO
      S11=SISO-0.5*DELP*(1.0+EETA)
      S22=SISO-0.5*DELP*(1.0-EETA)
      S33=SISO+DELP
C
C     Output starting parameters to unit 6 ------------
C
      WRITE(6,150)
  150 FORMAT(6X,'PROGRAM SBSIM: DATA AND RESULTS',///,1X)
      WRITE(6,200) TITL
  200 FORMAT(1X,A80,//,1X)
      WRITE(6,250) VR,SF
  250 FORMAT(1X,'ROTOR SPEED= ',F8.2,' Hz     SPECTROMETER FREQUENCY= ',
     1F9.4,' MHz',//,1X)
      WRITE(6,350) DELP,EETA,SISO
  350 FORMAT(1X,'ANISOTROPY= ',F9.3,' ppm',3X,'ASYMMETRY= ',F8.5,
```

```
     13X,'SIGMA(iso)= ',F9.3,//,1X)
      WRITE(6,400) S11,S22,S33
  400 FORMAT(1X,'CORRESPONDING TO SHIELDING TENSOR VALUES OF: ',
     13(1X,F9.3),///,1X)
C
C     Calculate angular spinning speed
C     Calculate sin and cos look-up tables
C
      IH=-(NSB/2)
      IL=(NSB/2-1)
      WR=VR*TWOPI
      DO 30 I=0,NOR
          ARG=I*PI/NOR
          ST(I)=DSIN(ARG)
          CT(I)=DCOS(ARG)
   30 CONTINUE
      RETURN
      END
C
C     ****************************************************************
C
      SUBROUTINE SPECT(DELT,ETA,SPC)
C
C     Calculate spectrum by summing over molecular orientations
C
      IMPLICIT REAL*8 (A-H,O-Z)
      DIMENSION SPC(-25:25),X(50),Y(50),WORK(50),TEMP(50)
      DIMENSION ST(0:90),CT(0:90)
      REAL*8 NORC
      COMMON /EXPI/ NSB,IH,IL
      COMMON /EXPR/ WR,VR,SF
      COMMON /TABLE/ ST,CT
      COMMON /ERR/ IFAIL2
      DATA NOR /30/
      DATA THD,TWOPI /0.333333333,6.283185306/
C
C     Zero arrays - Calculate spectrum over Euler angles and rotor period
C
      RP=1.0/(NSB*VR)
      DO 100 I=1,50
          X(I)=0.0
          Y(I)=0.0
  100 CONTINUE
      DO 140 I=0, NOR
        SINA=ST(I)
        COSA=CT(I)
        SIN2A=2.0*ST(I)*CT(I)
        COS2A=CT(I)*CT(I)-ST(I)*ST(I)
        DO 130 J=0, NOR
          SINB=ST(J)
          COSB=CT(J)
          SSQB=SINB*SINB
          CO1=0.4714045*SINB
          CSQB=COSB*COSB
          DO 120 K=0, NOR
            SIN2C=2.0*ST(K)*CT(K)
            COS2C=CT(K)*CT(K)-ST(K)*ST(K)
C
            CO2=ETA*COS2C
```

```
      CO3=(1.5*SSQB+(ETA/2)*COS2C*(1+CSQB))
      C1=CO1*(COSB*(CO2-3)*COSA-ETA*SIN2C*SINA)
      S1=CO1*(COSB*(3-CO2)*SINA-ETA*SIN2C*COSA)
      C2=THD*(CO3*COS2A-ETA*COSB*SIN2C*SIN2A)
      S2=-THD*(CO3*SIN2A+ETA*COSB*SIN2C*COS2A)
      DO 110 L=1,NSB
        T=(L-1)*RP
        AN=WR*T
        AN2=2.0*AN
        XI=(1.0/WR)*(S1+0.5*S2+C1*DSIN(AN)-S1*DCOS(AN)
     1  +0.5*(C2*DSIN(AN2)-S2*DCOS(AN2)))
        PT=XI*DELT*SF*TWOPI
        X(L)=X(L)+DCOS(PT)
        Y(L)=Y(L)+DSIN(PT)
  110   CONTINUE
  120 CONTINUE
  130 CONTINUE
  140 CONTINUE
C     Normalize FID - Do the FT - Normalize real SSB spectrum
      NORC=0.0
      DO 150 I=1,NSB
        NORC=NORC+X(I)*X(I)+Y(I)*Y(I)
  150 CONTINUE
      NORC=DSQRT(NORC)
      DO 160 I=1,NSB
        X(I)=X(I)/NORC
        Y(I)=Y(I)/NORC
  160 CONTINUE
      CALL C06FCF(X,Y,NSB,WORK,IFAIL2)
      NORC=0.0
      DO 170 I=1,NSB
        NORC=NORC+X(I)
  170 CONTINUE
      DO 180 I=1,NSB
        X(I)=(X(I)*100.0)/NORC
  180 CONTINUE
C
C     Place SSB's in the proper order
C
      CUT=NSB/2
      START=CUT+1
      IJ=1
      DO 190 I=START,NSB
        TEMP(IJ)=X(I)
        IJ=IJ+1
  190 CONTINUE
      DO 200 I=1,CUT
        TEMP(IJ)=X(I)
        IJ=IJ+1
  200 CONTINUE
      J=1
      DO 210 I=IH,IL
        SPC(I)=TEMP(J)
        J=J+1
  210 CONTINUE
      RETURN
      END
C
```

```
C     ********************************************************************
C
      SUBROUTINE OUTPUT
C
C     Produce output of calculated parameters and normalized
C     SSB intensities.  Plot SSB patterns.
C
      IMPLICIT REAL*8 (A-H,O-Z)
      DIMENSION SPC(-25:25)
      REAL*8 MXY
      REAL*4 PXLL,PXRL,MY,P,PT2,PDELT,PETA,DY,PDY
      CHARACTER*80 TITL
      COMMON /EXPI/ NSB,IH,IL
      COMMON /EXPR/ WR,VR,SF
      COMMON /PAR/ DELP,EETA,SISO
      COMMON /CHAR/ TITL
      COMMON /ERR/ IFAIL2
C
      IF (IFAIL2.EQ.1) GOTO 110
      IF (IFAIL2.EQ.2) GOTO 130
      IF (IFAIL2.EQ.3) GOTO 150
      GOTO 300
  110 WRITE(6,120)
  120 FORMAT(1X,'THE FT ROUTINE HAS FAILED: A PRIME FACTOR OF NSB IS > 1
     19',//1X)
      RETURN
  130 WRITE(6,140)
  140 FORMAT(1X,'FT ROUTINE HAS FAILED: NSB HAS MORE THAN 20 FACTORS',
     1//1X)
      RETURN
  150 WRITE(6,160)
  160 FORMAT(1X,'THE FT ROUTINE HAS FAILED: NSB < 1',//1X)
      RETURN
C
  300 DO 888 I=IH,IL
        SPC(I)=0.0
  888 CONTINUE
      CALL SPECT(DELP,EETA,SPC)
      WRITE(6,350)
  350 FORMAT (18X,'SIDEBAND INTENSITIES',//,1X,'SIDEBAND',6X,
     1'CALCULATED'//)
      DO 370 I=IH,IL
        WRITE(6,360) I,SPC(I)
  360   FORMAT(3X,I3,10X,F9.6)
  370 CONTINUE
C
C     Plotting section ---------------------------------------------
C
C     Note that REAL*8 variables have been used to this point
C     because of the requirements of NAG on the MTS mainframe.
C     For the GHOST-80 plot routines, REAL*4 variables must be used
C     See type statements for a list of REAL*4 plotting variables.
C
      PXLL=IH-1
      PXRL=IL+1
      MXY=0.0
      DO 400 I=IH,IL
        MXY=DMAX1(MXY,SPC(I))
  400 CONTINUE
      MY=MXY*1.10
```

```
      CALL PAPER(1)
      CALL PSPACE(0.10,0.95,0.20,0.80)
      CALL MAP(PXLL,PXRL,0.0,MY)
      CALL BLKPEN
      CALL BORDER
      PINC=0.02*(PXRL-PXLL)
      CALL CTRMAG(20)
      DO 420 I=IH,IL
        P=I
        PT2=SPC(I)
        CALL FULL
        CALL POSITN(P,0.0)
        CALL JOIN(P,PT2)
        IF (I .NE. 0) GOTO 420
        DY=PT2/20
        PDY=PT2+DY
        CALL PLOTNC(P,PDY,225)
420   CONTINUE
      CALL CSPACE(0.05,0.99,0.05,0.99)
      CALL CTRMAG(20)
      CALL PLACE(5,9)
      CALL CTRFNT(2)
      CALL TYPENC(100)
      CALL TYPENC(164)
      PDELT=DELP
      PETA=EETA
      CALL TYPENF(PDELT,3)
      CALL PLACE(5,10)
      CALL TYPENC(106)
      CALL TYPENC(164)
      CALL TYPENF(PETA,4)
      CALL PLACE(5,11)
      CALL TYPENC(110)
      CALL CTRFNT(1)
      CALL TYPENC(114)
      CALL TYPENC(164)
      CALL TYPENF(VR,2)
      CALL CTRMAG(15)
      CALL PLACE(5,8)
      CALL TYPECS(TITL)
      CALL GREND
      RETURN
      END
```

APPENDIX THREE

SPINNING-SIDEBAND SPECTRUM FITTING PROGRAM

```
C     Program SBFIT - Iteratively fits a spinning sideband pattern
C     Lawrence H. Merwin, Dept. of Chemistry, University of Durham
C     Version 2, 11 August 1987
C     Ref: M.Maricq and J. Waugh, J. Chem. Phys. 70, 3300 (1979)
C
      PROGRAM SBFIT
C
      IMPLICIT REAL*8 (A-H,O-Z)
      DIMENSION SPI(-25:25),SPN(-25:25),Z(2),W1(2),W2(2),W3(2),W4(2)
      DIMENSION W5(3),W6(3,3)
      INTEGER LLIM,RLIM
      COMMON Z
      COMMON /EXPI/ NSB,IH,IL,LLIM,RLIM
      COMMON /EXPR/ WR,VR,SF
      COMMON /SPEC/ SPN,SPI
      COMMON /PAR/ DELP,EETA,SISO
      COMMON /ERR/ IFAIL1,IFAIL2
      EXTERNAL FUNCT,MONIT
      DATA N,IW,MAXCAL /2,3,100/
C
      IFAIL1=0
      IFAIL2=0
      XAF=X02AAF(R)
      TOL=DSQRT(XAF)
      CALL INSET
      CALL E04CCF(N,Z,F,TOL,IW,W1,W2,W3,W4,W5,W6,FUNCT,MONIT,
     1MAXCAL,IFAIL1)
      CALL OUTPUT
      STOP
      END
C
C     ******************************************************************
C
      SUBROUTINE INSET
C
C
C     Input experimental data and set up arrays and tables
C
      IMPLICIT REAL*8 (A-H,O-Z)
      DIMENSION SPI(-25:25), SPN(-25:25), Z(2), SPX(-25:25)
      DIMENSION ST(0:90),CT(0:90)
      INTEGER LLIM,RLIM
      CHARACTER*80 TITL
      COMMON Z
      COMMON /EXPI/ NSB,IH,IL,LLIM,RLIM
      COMMON /EXPR/ WR,VR,SF
      COMMON /SPEC/ SPN,SPI
      COMMON /CHAR/ TITL
      COMMON /TABLE/ ST,CT
      COMMON /PAR/ DELP,EETA,SISO
      COMMON /SCALE/ FSCAL
      COMMON /LIMS/ IUL,ILL
      DATA NOR,TWOPI,PI /20,6.283185307,3.141592653/
C
C     Data Input Section ------------------------------------------
C     Read in sidebands and experimental parameters
C     Normalize sidebands and calculate delta and eta
C
      READ(5,100) TITL
  100 FORMAT(A80)
```

```
      READ(5,*) VR,SF
      READ(5,*) NSB,IH,IL
      READ(5,*) LLIM,RLIM
      SNRM=0.0
      READ(5,*) (SPI(I), I=IH,IL)
      DO 10 I=IH,IL
         SNRM=SNRM+SPI(I)
   10 CONTINUE
      DO 20 I=IH,IL
         SPN(I)=(SPI(I)*100.0)/SNRM
   20 CONTINUE
      READ(5,*) DELP,EETA,SISO
      S11=SISO-0.5*DELP*(1.0+EETA)
      S22=SISO-0.5*DELP*(1.0-EETA)
      S33=SISO+DELP
C
C     Output starting parameters and spectrum to unit 6 ------------
C
      WRITE(6,150)
  150 FORMAT(6X,'PROGRAM SBFIT:DATA AND RESULTS',///,1X)
      WRITE(6,200) TITL
  200 FORMAT(1X,A80,//,1X)
      WRITE(6,250) VR,SF
  250 FORMAT(1X,'ROTOR SPEED= ',F8.2,' Hz     SPECTROMETER FREQUENCY= ',
     1F9.4,' MHz',//,1X)
      WRITE (6,300)
  300 FORMAT(10X,'STARTING PARAMETERS',//,1X)
      WRITE(6,350) DELP,EETA,SISO
  350 FORMAT(1X,'ANISOTROPY= ',F9.3,' ppm',3X,'ASYMMETRY= ',F8.5,
     13X,'SIGMA(iso)= ',F9.3,//,1X)
      WRITE(6,400) S11,S22,S33
  400 FORMAT(1X,'CORRESPONDING TO SHIELDING TENSOR VALUES OF: ',
     13(1X,F9.3),//,1X)
      WRITE(6,500) LLIM,RLIM
  500 FORMAT(1X,'FITTING OVER SIDEBAND RANGE: ',I3,' TO',I3,///1X)
C
C     Calculate angular spinning speed, initialize fitting arrays
C     Calculate sin and cos look-up tables
C
      ILL=(NSB/2-1)
      IUL=-(NSB/2)
      WR=VR*TWOPI
      Z(1)=1.0
      Z(2)=EETA
      DO 30 I=0,NOR
         ARG=I*PI/NOR
         ST(I)=DSIN(ARG)
         CT(I)=DCOS(ARG)
   30 CONTINUE
      CALL SPECT(DELP,EETA,SPX)
      FSCAL=0.0
      DO 40 I=LLIM,RLIM
        FSCAL=FSCAL+(SPN(I)-SPX(I))**2
   40 CONTINUE
      FSCAL=1.0/FSCAL
      RETURN
      END
C
C     ****************************************************************
C
```

```
      SUBROUTINE SPECT(DELT,ETA,SPC)
C
C     Calculate spectrum by summing over molecular orientations
C
      IMPLICIT REAL*8 (A-H,O-Z)
      DIMENSION SPC(-25:25),X(50),Y(50),WORK(50),TEMP(50)
      DIMENSION ST(0:90),CT(0:90)
      INTEGER LLIM,RLIM
      REAL*8 NORC
      COMMON /EXPI/ NSB,IH,IL,LLIM,RLIM
      COMMON /EXPR/ WR,VR,SF
      COMMON /TABLE/ ST,CT
      COMMON /ERR/ IFAIL1,IFAIL2
      COMMON /LIMS/ IUL,ILL
      DATA NOR /20/
      DATA THD,TWOPI /0.333333333,6.283185306/
C
C     Zero arrays - Calculate spectrum over Euler angles and rotor period
C
      RP=1.0/(NSB*VR)
      DO 100 I=1,50
         X(I)=0.0
         Y(I)=0.0
  100 CONTINUE
      DO 140 I=1, NOR
        SINA=ST(I)
        COSA=CT(I)
        SIN2A=2.0*ST(I)*CT(I)
        COS2A=CT(I)*CT(I)-ST(I)*ST(I)
        DO 130 J=1, NOR
          SINB=ST(J)
          COSB=CT(J)
          SSQB=SINB*SINB
          CO1=0.4714045*SINB
          CSQB=COSB*COSB
          DO 120 K=1, NOR
            SIN2C=2.0*ST(K)*CT(K)
            COS2C=CT(K)*CT(K)-ST(K)*ST(K)
C
            CO2=ETA*COS2C
            CO3=(1.5*SSQB+(ETA/2)*COS2C*(1+CSQB))
            C1=CO1*(COSB*(CO2-3)*COSA-ETA*SIN2C*SINA)
            S1=CO1*(COSB*(3-CO2)*SINA-ETA*SIN2C*COSA)
            C2=THD*(CO3*COS2A-ETA*COSB*SIN2C*SIN2A)
            S2=-THD*(CO3*SIN2A+ETA*COSB*SIN2C*COS2A)
            DO 110 L=1,NSB
              T=(L-1)*RP
              AN=WR*T
              AN2=2.0*AN
              XI=(1.0/WR)*(S1+0.5*S2+C1*DSIN(AN)-S1*DCOS(AN)
     1        +0.5*(C2*DSIN(AN2)-S2*DCOS(AN2)))
              PT=XI*DELT*SF*TWOPI
              X(L)=X(L)+DCOS(PT)
              Y(L)=Y(L)+DSIN(PT)
  110       CONTINUE
  120     CONTINUE
  130   CONTINUE
  140 CONTINUE
```

```
C     Normalize FID - Do the FT - Normalize real SSB spectrum
      JORC=0.0
      DO 150 I=1,NSB
        NORC=NORC+X(I)*X(I)+Y(I)*Y(I)
  150 CONTINUE
      NORC=DSQRT(NORC)
      DO 160 I=1,NSB
        X(I)=X(I)/NORC
        Y(I)=Y(I)/NORC
  160 CONTINUE
      CALL C06FCF(X,Y,NSB,WORK,IFAIL2)
      NORC=0.0
      DO 170 I=1,NSB
        NORC=NORC+X(I)
  170 CONTINUE
      DO 180 I=1,NSB
        X(I)=(X(I)*100.0)/NORC
  180 CONTINUE
C
C     Place SSB's in the proper order
C
      CUT=NSB/2
      START=CUT+1
      IJ=1
      DO 190 I=START,NSB
        TEMP(IJ)=X(I)
        IJ=IJ+1
  190 CONTINUE
      DO 200 I=1,CUT
        TEMP(IJ)=X(I)
        IJ=IJ+1
  200 CONTINUE
      J=1
      DO 210 I=IUL,ILL
        SPC(I)=TEMP(J)
        J=J+1
  210 CONTINUE
      RETURN
      END
C
C     ************************************************************
C
      SUBROUTINE FUNCT(N,XC,FC)
C
C     Routine called from E04CCF calculates sum squared difference
C     between real and calculated SSB patterns over chosen range
C
      IMPLICIT REAL*8 (A-H,O-Z)
      DIMENSION XC(N),SPN(-25:25),SPC(-25:25),SPI(-25:25)
      INTEGER N,LLIM,RLIM
      COMMON /PAR/ DELP,EETA,SISO
      COMMON /EXPI/ NSB,IH,IL,LLIM,RLIM
      COMMON /SPEC/ SPN,SPI
      COMMON /SCALE/ FSCAL
      CDELT=XC(1)*DELP
      CETA=XC(2)
      FC=0
      CALL SPECT(CDELT,CETA,SPC)
      DO 10 I=LLIM,RLIM
```

```
      FC=FC+(SPN(I)-SPC(I))**2
   10 CONTINUE
      FC=FC*FSCAL
      RETURN
      END
C
C     *****************************************************************
C
      SUBROUTINE MONIT (FMIN,FMAX,SIM,N,IS,NCALL)
C
C     Subroutine to produce monitor output for the fitting routine E04CCF
C     output to unit 7
C
      REAL*8 MIN,FMAX,SIM(IS,N)
      INTEGER IS,N,NCALL
      WRITE(7,100) NCALL,FMIN
  100 FORMAT (2X,'AFTER',I4,' FUNCTION CALLS, THE VALUE IS ',E14.7,
     1' WITH SIMPLEX:',/,1X)
      WRITE (7,200)((SIM(I,J), J=1,N),I=1,IS)
  200 FORMAT(3(2F12.4/))
      RETURN
      END
C
C     *****************************************************************
C
      SUBROUTINE OUTPUT
C
C     Produce output of experimental and calculated parameters and
C     normalized SSB intensities.  Plot SSB patterns.
C
      IMPLICIT REAL*8 (A-H,O-Z)
      DIMENSION SPN(-25:25),SPC(-25:25),SPI(-25:25),Z(2)
      REAL*8 MXY
      REAL*4 PXLL,PXRL,MY,P,P2,PT1,PT2,PINC,PDELT,PETA
      INTEGER LLIM,RLIM
      CHARACTER*80 TITL
      COMMON Z
      COMMON /EXPI/ NSB,IH,IL,LLIM,RLIM
      COMMON /EXPR/ WR,VR,SF
      COMMON /SPEC/ SPN,SPI
      COMMON /PAR/ DELP,EETA,SISO
      COMMON /CHAR/ TITL
      COMMON /ERR/ IFAIL1,IFAIL2
C
      WRITE(6,100)
  100 FORMAT(////,1X)
      IF (IFAIL2.EQ.1) GOTO 110
      IF (IFAIL2.EQ.2) GOTO 130
      IF (IFAIL2.EQ.3) GOTO 150
      GOTO 170
  110 WRITE(6,120)
  120 FORMAT(1X,'THE FT ROUTINE HAS FAILED: A PRIME FACTOR OF NSB IS > 1
     19',//1X)
      RETURN
  130 WRITE(6,140)
  140 FORMAT(1X,'FT ROUTINE HAS FAILED: NSB HAS MORE THAN 20 FACTORS',
     1//1X)
      RETURN
  150 WRITE(6,160)
  160 FORMAT(1X,'THE FT ROUTINE HAS FAILED: NSB < 1',//1X)
```

```
      RETURN
170   IF(IFAIL1.EQ.2) GOTO 180
      IF (IFAIL1.EQ.1) GOTO 200
      GOTO 300
180   WRITE(6,190)
190   FORMAT(1X,'THE ROUTINE (EO4CCF) HAS REACHED THE MAXIMUM NUMBER',/,
     11X,'OF FUNCTION CALLS WITHOUT REACHING THE SPECIFIED TOLERANCE:'/,
     21X,'THE RESULTS OF THE LAST ITERATION ARE NOTED BELOW',///,1X)
      GOTO 300
200   WRITE(6,210)
210   FORMAT(1X,'ONE OR MORE OF THE PARAMETERS FOR ROUTINE EO4CCF IS',
     1/,1X,'OUTSIDE OF THE SPECIFIED RANGE: SEE OUTPUT IN I/O UNIT 7',
     2////,1X)
      RETURN
C
300   CDELT=Z(1)*DELP
      CETA=Z(2)
      DO 888 I=IH,IL
        SPC(I)=0.0
888   CONTINUE
      CALL SPECT(CDELT,CETA,SPC)
      S11=SISO-0.5*CDELT*(1.0+CETA)
      S22=SISO-0.5*CDELT*(1.0-CETA)
      S33=SISO+CDELT
      WRITE(6,310)
310   FORMAT(1X,'SBFIT HAS FIT THE SIDEBAND PATTERN TO THE SPECIFIED
     1 TOLERANCE ',//,1X)
      WRITE(6,320) CDELT,CETA
320   FORMAT(1X,' ANISOTROPY= ',F9.3,' ppm',3X,'ASYMMETRY= ',F8.5,//1X)
      WRITE (6,340) S11,S22,S33
340   FORMAT (1X,'THE CORRESPONDING SHIELDING TENSORS ARE:', 3(3X,F9.3),
     1///1X)
      WRITE(6,350)
350   FORMAT (18X,'SIDEBAND INTENSITIES',//,1X,'SIDEBAND',4X,'ENTERED',
     19X,'NORMALIZED',4X,'CALCULATED (NORMALIZED)',//)
      SDF=0.0
      DO 370 I=IH,IL
        WRITE(6,360) I,SPI(I),SPN(I),SPC(I)
        SDFF=SPN(I)-SPC(I)
        SDF=SDF+(SDFF*SDFF)
360     FORMAT(3X,I3,3X,F11.2,9X,F9.6,8X,F9.6)
370   CONTINUE
      WRITE(6,371) SDF
371   FORMAT(1X,/,1X,'SUM OF DIFFERENCES SQUARED = ',1PE12.5)
C
C     Plotting section =============================================
C
C     Note that REAL*8 variables have been used to this point
C     because of the requirements of NAG on the MTS mainframe.
C     For the GHOST-80 plot routines, REAL*4 variables must be used
C     See type statements for a list of REAL*4 plotting variables.
C
      PXLL=IH-1
      PXRL=IL+1
      MXY=0.0
      DO 400 I=IH,IL
        MXY=DMAX1(MXY,SPN(I),SPC(I))
400   CONTINUE
      MY=MXY*1.02
      CALL PAPER(1)
```

```
      CALL PSPACE(0.10,0.95,0.20,0.80)
      CALL MAP(PXLL,PXRL,0.0,MY)
      CALL BLKPEN
      CALL BORDER
      PINC=0.02*(PXRL-PXLL)
      DO 420 I=IH,IL
        P=I
        P2=I+PINC
        PT1=SPN(I)
        PT2=SPC(I)
        CALL FULL
        CALL POSITN(P,0,0)
        CALL JOIN(P,PT1)
        CALL BROKEN(5,5,5,5)
        CALL POSITN(P2,0,0)
        CALL JOIN(P2,PT2)
420   CONTINUE
      CALL CSPACE(0.05,0.99,0.05,0.99)
      CALL CTRMAG(20)
      CALL PLACE(5,9)
      CALL CTRFNT(2)
      CALL TYPENC(100)
      CALL TYPENC(164)
      PDELT=CDELT
      PETA=CETA
      CALL TYPENF(PDELT,3)
      CALL PLACE(5,10)
      CALL TYPENC(106)
      CALL TYPENC(164)
      CALL TYPENF(PETA,4)
      CALL PLACE(5,11)
      CALL TYPENC(110)
      CALL CTRFNT(1)
      CALL TYPENC(114)
      CALL TYPENC(164)
      CALL TYPENF(VR,2)
      CALL CTRMAG(15)
      CALL PLACE(5,8)
      CALL TYPECS(TITL)
      CALL GREND
      RETURN
      END
```

APPENDIX FOUR

The Board of Studies in Chemistry requires that each postgraduate research thesis contains an appendix which lists:

A) all research colloquia, research seminars and lectures arranged by the Department of Chemistry and the Durham University Chemical Society during the period of the author's residence as a postgraduate student;

B) all research conferences attended and papers presented by the author during the same period;

C) details of the postgraduate induction course.

UNIVERSITY OF DURHAM

Board of Studies in Chemistry

COLLOQUIA, LECTURES AND SEMINARS GIVEN BY INVITED SPEAKERS: 1st AUGUST 1984 to 31st JULY 1985

* ATKINS, Dr. P.W. (University of Oxford) — 7th March 1985
'Magnetic Reactions'

AYLETT, Prof. B.J. (Queen Mary College, University of London) — 1st November 1984
'Silicon - Dead Common or Refined'

* BELTON, Dr. P.S. (Food Research Institute, Norwich) — 4th June 1985
'Analytical Photoacoustic Spectroscopy'

BROWN, Dr. C. (IBM San Jose) — 19th September 1984
'New Superbase Reactions - Organic Compounds'

* BROWN, Prof. I.D. (Institute for Materials Research, McMaster University, Canada) — 17th May 1985
'Bond Valence as a Model for Inorganic Chemistry'

* CHAMBERS, Prof. R.D. (University of Durham) — 6th December 1984
'The Unusual World of Fluorine'

CLARK, Prof. D.T. (ICI New Science Group) — 22nd November 1984
'Structure, Bonding, Reactivity and Synthesis as Revealed by ESCA'

* COATES, Prof. G.E. (formerly of University of Wyoming, U.S.A.) — 7th May 1985
'Chemical Education in Britain and America: Successes and Deficiencies'

COVINGTON, Dr. A.K. (University of Newcastle-upon-Tyne) — 24th January 1985
'Chemistry with Chips'

* DILLON, Dr. K.B. (University of Durham) — 12th December 1984
'^{31}P NMR Studies of Some Anionic Phosphorus Complexes'

* EVERALL, Mr. N. (University of Durham) — 21st November 1984
'Picosecond Pulsed Laser Raman Spectroscopy'

* FEAST, Dr. W.J. (University of Durham) — 25th October 1984
'Syntheses of Conjugated Polymers. Why and How?'

* FEAST, Dr. W.J. (University of Durham) — 27th November 1984
'A Plain Man's Guide to Polymeric Organic Metals'

FLEET, Dr. G.W.J. (University of Oxford) — 13th February 1985
'Syntheses of some Alkaloids from Carbohydrates'

GERMAIN, Dr. A. (Université du Languedoc, Montpellier) — 19th October 1984
'Anodic Oxidation of Perfluoro Organic Compounds in Perfluoroalkane Sulphonic Acids'

GIBSON, Dr. H.W. (Signal UOP Research Centre, Des Plaines, Illinois) — 21st September 1984
'Isomerization of Polyacetylene'

GOLDING, Prof. B.T. (University of Newcastle-upon-Tyne) — 15th November 1984
'The Vitamin B_{12} Mystery'

*GREEN, Dr. M.L.H. (University of Oxford) — 31st January 1985
'Naked Atoms and Negligée Ligands'

GRIMMETT, Dr. R. (University of Otago, Dunedin, New Zealand) — 22nd May 1985
'Some Aspects of Nucleophilic Substitution in Imidazoles'

GROSSEL, Dr. M.C. (Bedford College, University of London) — 24th April 1985
'Hydroxypyridone Dyes - Bleachable One-Dimensional Metals?'

*HARRIS, Prof. R.K. (University of Durham) — 24th October 1984
'NMR of Solid Polymers'

*HARRIS, Prof. R.K. (University of Durham) — 9th May 1985
'Chemistry in a Spin: Nuclear Magnetic Resonance'

HUDLICKY, Dr. M. (Virginia State University, Blacksburg) — 22nd May 1985
'Preferential Elimination of Hydrogen Fluoride from Vicinal Bromofluorocompounds'

*KATRITZKY, Prof. A.R., FRS (University of Florida) — 14th March 1985
'Some Adventures in Heterocyclic Chemistry'

LAALI, Dr. K. (Hydrocarbon Research Institute, University of Southern California) — 12th July 1985
'Recent Developments in Superacid Chemistry and Mechanistic Considerations in Electrophilic Aromatic Substitutions; a Progress Report'

LEDWITH, Prof. A. (Pilkington Bros.) — 7th February 1985
'Glass as a High Technology Material'

*LOGAN, Dr. N. (University of Nottingham) — 18th October 1984
'N_2O_4 and Rocket Fuels'

*LUX, Mr. P.J. (University of Durham) — 5th December 1984
'IR and GC Studies of the Interaction of CH_3OH with High Silica Zeolites'

MAITLIS, Prof. P.M., FRS (University of Sheffield) — 21st February 1985
'What Use is Rhodium?'

*MINCHER, Dr. D.J. (University of Durham) — 19th February 1985
'Stereoselective Syntheses of Some Novel Anthracyclinones Related to the Anti-Cancer Drug Adriamycin and to the Steffimycin Antibiotics'

*MITCHELL, Dr. T.N. (University of Dortmund) — 19th June 1985
'Some Synthetic and NMR-Spectroscopic Studies of Organotin Compounds'

MULVEY, Dr. R.E. (University of Durham) — 27th February 1985
'Some Unusual Lithium Complexes'

*MUNRO, Dr. H.S. (University of Durham) — 7th November 1984
'New Information from ESCA Data'

PACKER, Dr. J.E. (University of Auckland, New Zealand) — 15th May 1985
'Studies of Free Radical Reactions in Aqueous Solution Using Ionising Radiation'

*PACKER, Prof. K.J. (B.P. Research Centre) — 12th March 1985
'NMR Investigations of the Structure of Solid Polymers'

*PARKER, Dr. D. (ICI plc, Petrochemical & Plastics Division, Wilton) — 1st May 1985
'Applications of Radioisotopes in Industrial Research'

*PASSMORE, Prof. J. (University of New Brunswick) — 14th May 1985
'The Synthesis and Characterisation of some Novel Selenium-Iodine Cations. Aided by ^{77}Se NMR Spectroscopy'

*POLIAKOFF, Dr. M. (University of Nottingham) — 21st March 1985
'New Methods for Detecting Organometallic Intermediates in Solution'

*PORTERFIELD, Prof. W.W. (Hampden-Sydney College, U.S.A.) — 7th November 1984
'There is No Borane Chemistry (Only Geometry)'

RAPPOPORT, Prof. Z. (The Hebrew University, Jerusalem) — 14th June 1985
'The Rich Mechanistic World of Nucleophilic Vinylic Substitution'

*RINGSDORF, Prof. H. (Organic Chemistry Institute, University of Mainz) — 28th March 1985
'Polymeric Liposomes as Models for Biomembranes and Cells?'

RODGERS, Dr. P.J. (ICI plc, Agricultural Division, Billingham) — 7th March 1985
'Industrial Polymers from Bacteria'

*SALTHOUSE, Dr. J.A. (University of Manchester) — 14th February 1985
'Son et Lumiere' (A Chemical Energy Show)

SHAW, Prof. G. (University of Bradford) — 26th June 1985
'Synthetic Studies on Imidazole Nucleosides and the Antibiotic Coformycin'

STEPHENSON, Dr. T.A. (University of Edinburgh) — 28th November 1984
'Some Recent Studies in Platinum Metals Chemistry'

*STIRLING, Prof. C.J.M. (University College of North Wales) — 29th November 1984
'Molecules Taking the Strain'

SUSCHITZKY, Emeritus Prof. H. (University of Salford) — 11th January 1985
'Fruitful Fissions of Benzofuroxanes and Isobenzimadazoles (umpolung of *o*-phenylenediamine)'

TUCK, Prof. D. (University of Windsor, Ontario) — 8th May 1985
'Lower Oxidation State Chemistry of Indium'

*WILLIAMS, Dr. D.L.H. (University of Durham) — 21st May 1985
'Chemistry in Colour'

*WILLIAMS, Prof. G. (University College of Wales, Aberystwyth) — 8th May 1985
'Liquid Crystalline Polymers'

*WOOLLINS, Dr. D. (Imperial College, University of London) — 13th June 1985
'Metal-Sulphur-Nitrogen Complexes'

UNIVERSITY OF DURHAM

Board of Studies in Chemistry

COLLOQUIA, LECTURES AND SEMINARS GIVEN BY INVITED SPEAKERS: 1st AUGUST 1985 to 31st JULY 1986

* BARNARD, Dr. C.J.F. (Johnson Matthey Group) 'Platinum Anti-Cancer Drug Development'	20th February 1986
BROWN, Dr. J.M. (University of Oxford) 'Chelate Control in Homogeneous Catalysis'	12th March 1986
* CLARK, Dr. B.A.J. (Kodak Ltd.) 'Chemistry and Principles of Colour Photography'	28th November 1985
CLARK, Dr. J.H. (University of York) 'Novel Fluoride Ion Reagents'	29th January 1986
DAVIES, Dr. S.G. (University of Oxford) 'Chirality Control and Molecular Recognition'	14th November 1985
* DEWING, Dr. J. (U.M.I.S.T.) 'Zeolites - Small Holes, Big Opportunities'	24th October 1985
ERTL, Prof. G. (University of Munich) 'Heterogeneous Catalysis'	7th November 1985
* GRIGG, Prof. R. (Queen's University, Belfast) 'Thermal Generation of 1,3-Dipoles"	13th February 1986
* HARRIS, Prof. R.K. (University of Durham) 'The Magic of Solid State NMR'	27th February 1986
HATHWAY, Dr. D. (University of Durham) 'Herbicide Selectivity'	5th March 1986
IDDON, Dr. B. (University of Salford) 'The Magic of Chemistry'	6th March 1986
* JACK, Prof. K.H. (University of Newcastle) 'Chemistry of Si-Al-O-N Engineering Ceramics'	21st November 1985
LANGRIDGE-SMITH, Dr. P.R.R. (University of Edinburgh) 'Naked Metal Clusters - Synthesis, Characterisation and Chemistry'	14th May 1986
* LEWIS, Prof. Sir Jack (University of Cambridge) 'Some more Recent Aspects in the Cluster Chemistry of Ruthenium and Osmium Carbonyls'	23rd January 1986
* LUDMAN, Dr. C.J. (University of Durham) 'Some Thermochemical Aspects of Explosions'	17th October 1985
MACBRIDE, Dr. J.A.H. (Sunderland Polytechnic) 'A Heterocyclic Tour on a Distorted Tricycle - Biphenylene'	20th November 1985

O'DONNELL, Prof. M.J. (Indiana-Purdue University) 5th November 1985
'New Methodology for the Synthesis of Amino Acids'

PARMAR, Dr. V.S. (University of Delhi) 13th September 1985
'Enzyme Assisted ERC Synthesis'

PHILLIPS, Dr. N.J. (University of Technology, Loughborough) 30th January 1986
'Laser Holography'

PROCTER, Prof. G. (University of Salford) 19th February 1986
'Approaches to the Synthesis of some Natural Products'

* SCHMUTZLER, Prof. R. (University of Braunschweig) 9th June 1986
'Mixed Valence Diphosphorous Compounds'

SCHRODER, Dr. M. (University of Edinburgh) 5th March 1986
'Studies on Macrocycle Complexes'

* SHEPPARD, Prof. N. (University of East Anglia) 15th January 1986
'Vibrational and Spectroscopic Determinations of the Structures of Molecules Chemisorbed on Metal Surfaces'

TEE, Prof. O.S. (Concordia University, Montreal) 12th February 1986
'Bromination of Phenols'

TILL, Miss C. (University of Durham) 26th February 1986
'ESCA and Optical Emission Studies of the Plasma Polymerisation of Perfluoroaromatics'

* TIMMS, Dr. P. (University of Bristol) 31st October 1985
'Some Chemistry of Fireworks'

WADDINGTON, Prof. D.J. (University of York) 28th November 1985
'Resources for the Chemistry Teacher'

WHITTLETON, Dr. S.N. (University of Durham) 30th October 1985
'An Investigation of a Reaction Window'

* WILDE, Prof. R.E. (Texas Technical University) 23rd June 1986
'Molecular Dynamic Processes from Vibrational Bandshapes'

* YARWOOD, Dr. J. (University of Durham) 12th February 1986
'The Structure of Water in Liquid Crystals'

UNIVERSITY OF DURHAM

Board of Studies in Chemistry

COLLOQUIA, LECTURES AND SEMINARS GIVEN BY INVITED SPEAKERS
1ST AUGUST 1986 TO 31ST JULY 1987

* ALLEN, Prof. Sir G. (Unilever Research) Biotechnology and the Future of the Chemical Industry	13th November 1986
* BARTSCH, Dr. R. (University of Sussex) Low Co-ordinated Phosphorus Compounds	6th May 1987
* BLACKBURN, Dr. M. (University of Sheffield) Phosphonates as Analogues of Biological Phosphate Esters	27th May 1987
BORDWELL, Prof. F.G. (Northeastern University, U.S.A.) Carbon Anions, Radicals, Radical Anions and Radical Cations	9th March 1987
* CANNING, Dr. N.D.S. (University of Durham) Surface Adsorption Studies of Relevance to Heterogeneous Ammonia Synthesis	26th November 1986
* CANNON, Dr. R.D. (University of East Anglia) Electron Transfer in Polynuclear Complexes	11th March 1987
CLEGG, Dr. W. (University of Newcastle-upon-Tyne) Carboxylate Complexes of Zinc; Charting a Structural Jungle	28th January 1987
DÖPP, Prof. D. (University of Duisburg) Cyclo-additions and Cyclo-reversions Involving Captodative Alkenes	5th November 1986
DORFMÜLLER, Prof. T. (University of Bielefeld) Rotational Dynamics in Liquids and Polymers	8th December 1986
* GOODGER, Dr. E.M. (Cranfield Institute of Technology) Alternative Fuels for Transport	12th March 1987
GREENWOOD, Prof. N.N. (University of Leeds) Glorious Gaffes in Chemistry	16th October 1986
* HARMER, Dr. M. (I.C.I. Chemicals & Polymer Group) The Role of Organometallics in Advanced Materials	7th May 1987
HUBBERSTEY, Dr. P. (University of Nottingham) Demonstration Lecture on Various Aspects of Alkali Metal Chemistry	5th February 1987
* HUDSON, Prof. R.F. (University of Kent) Aspects of Organophosphorus Chemistry	17th March 1987
HUDSON, Prof. R.F. (University of Kent) Homolytic Rearrangements of Free Radical Stability	18th March 1987

Conferences Attended:

1. Bruker CXP Users Meeting, November, 1985.

2. British Radiofrequency Spectroscopy Group, High Resolution NMR in Solids, University of Oxford, April, 1986.

3. NATO Advanced Study Institute, Physical Properties and Thermodynamic Behaviour of Minerals, NMR Section, August, 1987.

Papers Presented:

"The Principles of High Resolution Solid-State NMR" Presented to a seminar at the Institute for Inorganic Chemistry, University of Düsseldorf, October, 1985.

Postgraduate Induction Course, October, 1984:

1. Departmental organization
2. Safety matters
3. Electrical appliances and infrared spectroscopy
4. Chromatography and microanalysis
5. Atomic absorptiometry and inorganic analysis
6. Library facilities
7. Mass spectroscopy
8. Nuclear magnetic resonance spectroscopy
9. Glassblowing technique

JARMAN, Dr. M. (Institute of Cancer Research) 19th February 1987
The Design of Anti Cancer Drugs

KRESPAN, Dr. C. (E.I. Dupont de Nemours) 26th June 1987
Nickel(0) and Iron(0) as Reagents in Organofluorine Chemistry

* KROTO, Prof. H.W. (University of Sussex) 23rd October 1986
Chemistry in Stars, between Stars and in the Laboratory

* LEY, Prof. S.V. (Imperial College) 5th March 1987
Fact and Fantasy in Organic Synthesis

* MILLER, Dr. J. (Dupont Central Research, U.S.A.) 3rd December 1986
Molecular Ferromagnets; Chemistry and Physical Properties

MILNE/CHRISTIE, Dr. A./Mr. S. (International Paints) 20th November 1986
Chemical Serendipity - A Real Life Case Study

* NEWMAN, Dr. R. (University of Oxford) 4th March 1987
Change and Decay: A Carbon-13 CP/MAS NMR Study of Humification and Coalification Processes

OTTEWILL, Prof. R.H. (University of Bristol) 22nd January 1987
Colloid Science a Challenging Subject

PASYNKIEWICZ, Prof. S. (Technical University, Warsaw) 11th May 1987
Thermal Decomposition of Methyl Copper and its Reactions with Trialkylaluminium

* ROBERTS, Prof. S.M. (University of Exeter) 24th June 1987
Synthesis of Novel Antiviral Agents

RODGERS, Dr. P.J. (I.C.I. Billingham) 12th February 1987
Industrial Polymers from Bacteria

SCROWSTON, Dr. R.M. (University of Hull) 6th November 1986
From Myth and Magic to Modern Medicine

SHEPHERD, Dr. T. (University of Durham) 11th February 1987
Pteridine Natural Products; Synthesis and Use in Chemotherapy

* THOMSON, Prof. A. (University of East Anglia) 4th February 1987
Metalloproteins and Magnetooptics

* WILLIAMS, Prof. R.L. (Metropolitan Police Forensic Science) 27th November 1987
Science and Crime

* WONG, Prof. E.H. (University of New Hampshire, U.S.A.) 29th October 1986
Coordination Chemistry of P-O-P Ligands

* WONG, Prof. E.H. (University of New Hampshire, U.S.A.) 17th February 1987
Symmetrical Shapes from Molecules to Art and Nature